# THE USE OF HPMA COPOLYMER CONJUGATES FOR THE INTRACELLULAR TARGETING OF ANTICANCER DRUGS

by

Jon Doyle Callahan

A dissertation submitted to the faculty of
The University of Utah
in partial fulfillment of the requirements for the degree of

Doctor of Philosophy

Department of Bioengineering

The University of Utah

August 2017

**The University of Utah Graduate School**

# STATEMENT OF DISSERTATION APPROVAL

The dissertation of **Jon Doyle Callahan**

has been approved by the following supervisory committee members:

| | | |
|---|---|---|
| **Jindřich Kopeček** | , Chair | **May 12, 2017** Date Approved |
| **James Herron** | , Member | **May 12, 2017** Date Approved |
| **Katherine Ullman** | , Member | **May 12, 2017** Date Approved |
| **Hamid Ghandehari** | , Member | **May 12, 2017** Date Approved |
| **Vladimir Hlady** | , Member | **May 12, 2017** Date Approved |

and by **David Grainger** , Chair/Dean of

the Department of **Bioengineering**

and by David B. Kieda, Dean of The Graduate School.

# ABSTRACT

The work presented here represents three separate research projects. Each explores different approaches to the same problem: how can artificial macromolecules be used to target specific intracellular sites in living organisms, and how may that technology be exploited to treat different disease states? Here, the copolymers based on pHPMA [poly *N*-(2-hydroxypropyl)methacrylamide)] were used to demonstrate cellular and subcellular targeting in a cancer model. Used as carriers for low molecular weight drugs, pHPMA copolymers may possess great potential for increasing the efficacy of drugs, while also decreasing side effects resulting from drug exposure to healthy tissues and cells.

In the first project, antibody Fab' fragments were dimerized using a multifunctionalized PEG (poly(ethylene glycol)) crosslinker to create a targeting module for pHPMA/drug carriers. The linker was semitrifunctional, able to crosslink 2 Fab' antibody fragments, which could then be attached to an HPMA-doxorubicin anticancer drug carrier. Monoclonal antibody Fab' fragments were chosen that target ovarian carcinoma cells. Using this strategy, the conjugates are selectively uptaken by cancer cells, whereby free doxorubicin is released.

In the second project, HPMA copolymers were created with a terminal mitochondriotropic chemical moiety, TPP (triphenylphosphonium). Lipophilic cations are used to traffic low molecular weight drugs to mitochondria. Studies had reported that terminal TPP can also traffic high molecular weight, uncharged, linear macromolecules

into mitochondria, and enable delivery to the cytosol via direct transduction through the plasma membrane. Semitelechelic TPP-HPMA copolymers were synthesized to determine if this effect could be applied to HPMA copolymer drug conjugates.

In the third project, the flexibility of HPMA polymerization chemistry was exploited to create a large “library” or array of different HPMA copolymers with a wide range of chemical properties. Copolymers were made incorporating a variety of cationic, anionic, and hydrophobic sidechains. This array of copolymers was incubated and microinjected directly into the cytoplasm of living cells. The resulting uptake and/or intracellular distribution was observed using time-lapse confocal microscopy and flow cytometry. Using HPMA copolymers as a model, this work functioned as a general survey for cellular uptake, and the intracellular distribution/trafficking that can be expected when artificial macromolecules are internalized into living cells.

This work was dedicated to Jill.

TABLE OF CONTENTS

ABSTRACT ..... iii

LIST OF TABLES ..... x

LIST OF FIGURES ..... xi

LIST OF ABBREVIATIONS ..... xv

ACKNOWLEDGEMENTS ..... xxi

Chapters

1. INTRODUCTION ..... 1

1.1 Engineered Materials in Medicine ..... 1
1.1.1 Natural vs. Synthetic Polymers ..... 2
1.1.2 Synthetic Polymers in Medicine ..... 3
1.1.3 Polymer Conjugates ..... 4
1.1.4 PEGylation ..... 5
1.2 Polymer-Drug Conjugates for the Treatment of Cancer ..... 7
1.2.1 The EPR Effect and Passive Tumor Tissue Targeting ..... 8
1.3 Macromolecular Drug Carriers and Barriers to Cell Entry ..... 9
1.3.1 Lysosomotropic Drug Carriers and Cell Targeting ..... 10
1.3.2 Macromolecular Delivery to the Cytoplasm ..... 11
1.3.4 Gene Therapy and Direct Cytoplasmic Delivery ..... 13
1.4 Antibodies for Cellular Targeting ..... 14
1.4.1 Bispecific Antibodies and Cell Targeting ..... 15
1.4.2 Early Approaches to Fab' Chemical Conjugates ..... 16
1.5 PEG-Dimerized Fab' Fragments for Targeting Ovarian Carcinoma Cells ..... 18
1.6 Mitochondrial Targeting of HPMA Copolymers ..... 20
1.6.1 Rationale ..... 20
1.6.2 Mitochondria Targeting Peptides ..... 21
1.6.3 Lipophilic Cations ..... 22
1.6.4 Mitochondriotropic Semitelechelic TPP-HPMA Copolymers ..... 25
1.7 A Large Polymer Array – a Synthetic Polymer Library ..... 27
1.7.1 An HPMA Copolymer Array ..... 28
1.7.2 Nuclear Entry ..... 29
1.8 References ..... 31

2. PEG-DIMERIZED Fab' CONJUGATES FOR THE TARGETING OF HPMA COPOLYMER-DRUG CONJUGATES ..... 52

2.1 Introduction ..... 52
2.1.1 Bispecific Targeting for Cancer Cells ..... 53
2.2.2 Research Plan ..... 54
2.2.3 Monoclonal Antibodies ..... 57
2.2.4 $(Fab')_2$ Production-IgG2a Subclass Antibodies ..... 57
2.2.5 Fab' Dimerization ..... 59
2.2 Materials ..... 60
2.3 Methods ..... 60
2.3.1 Trifunctional Bismalemide PEG Linker ..... 60
2.3.2 Maleimide and Vinyl Sulfone Assays ..... 61
2.3.3 Cell Lines ..... 62
2.3.4 Monoclonal Antibody Production ..... 63
2.3.5 $(Fab')_2$ Production from IgG1 Antibodies ..... 64
2.3.6 $(Fab')_2$ from IgG2a Antibodies Via Lysyl Endopeptidase Digestion ..... 64
2.3.7 Preparation of Fab' ..... 65
2.3.8 Preparation and Characterization of PEG-dimerized OV-TL16 ..... 66
2.3.9 Preparation and Characterization of Bispecific (Fab'OV-TL16)-PEG-(Fab'anti-EGFR) ..... 66
2.3.10 Binding Constant Determination ..... 67
2.3.11 Determination of Fab'-PEG-Fab' Uptake by Confocal Microscopy ..... 68
2.4 Results and Discussion ..... 69
2.4.1 Preparation of $(Fab')_2$ from IgG2a Antibodies ..... 69
2.4.2 Dimerization of OV-TL16 Fab' ..... 70
2.4.3 Bispecific $Fab'_{OV\text{-}TL16}$-PEG-$Fab'_{anti\text{-}EGFR}$ (preliminary) ..... 73
2.5 Conclusion ..... 74
2.6 References ..... 76

3. SEMITELECHELIC HPMA COPOLYMERS FUNCTIONALIZED WITH TRIPHENYLPHOSPHONIUM AS DRUG CARRIERS FOR MEMBRANE TRANSDUCTION AND MITOCHONDRIAL LOCALIZATION ..... 93

3.1 Abstract ..... 93
3.2 Introduction ..... 94
3.3 Experimental ..... 97
3.3.1 Materials ..... 97
3.3.2 Synthesis of the Chain Transfer Agent Thiobutyltriphenylphosphonium Bromide ..... 97
3.3.3 Triphenylphosphonium-BODIPY® FL ..... 99
3.3.4 MA-GG-BODIPY® FL Monomer ..... 100
3.3.5 Semitelechelic HPMA Polymers: Synthesis and Characterization ..... 100
3.3.6 Octanol : H2O Partition Coefficient Determinations ..... 101

3.3.7 Size-exclusion Chromatography ..... 101
3.3.8 Mass Spectrometry ..... 102
3.3.9 TPP-HPMA-FITC Copolymers ..... 102
3.3.10 TPP-HPMA-BODIPY® FL Copolymers ..... 103
3.3.11 Polymers for Uptake and Localization Experiments ..... 104
3.3.12 Uptake of TPP-HPMAs by Isolated Mitochondria ..... 104
3.3.13 Whole Cell Incubation ..... 106
3.3.14 Microinjection ..... 107
3.4 Results ..... 107
3.4.1 Synthesis and Characterization of Semitelechelic TPP-HPMA Copolymers ..... 107
3.4.2 Partition Coefficients ..... 110
3.4.3 Fluorescence Quenching Analyses with Isolated Mitochondria ..... 110
3.4.4 Cell Uptake and Localization Studies ..... 112
3.5 Discussion ..... 113
3.5.1 Polymer Synthesis and Characterization ..... 113
3.5.2 Biological Activity ..... 114
3.6 References ..... 120

4. INTRACELLULAR TRAFFICKING AND SUBCELLULAR DISTRIBUTION OF A LARGE ARRAY OF HPMA COPOLYMERS ..... 133

4.1 Abstract ..... 133
4.2 Introduction ..... 134
4.3 Experimental Methods ..... 138
4.3.1 Monomers ..... 138
4.3.2 Polymer Chemistry ..... 139
4.3.3 Texas Red-labeled HPMA Copolymer ..... 140
4.3.4 Copolymer Characterization ..... 141
4.3.5 Copolymer Fractionation ..... 142
4.3.6 Cell Culture ..... 143
4.3.7 Live Cell Imaging ..... 143
4.3.8 Incubation of MDAH Cells with Copolymers Dissolved in Media ..... 144
4.3.9 Microinjection ..... 144
4.3.10 Intracellular Distribution of Copolymer Fractions ..... 144
4.3.11 Rates of Nuclear Entry/Time Lapse Imaging ..... 145
4.3.12 Fluorescence Recovery After Photobleaching (FRAP) ..... 146
4.3.13 Coinjection of FG Peptide Copolymers and Nuclear Exclusion Markers ..... 147
4.4 Results and Discussion ..... 147

4.4.1 Design and Characterization of an HPMA Copolymer Array .....147
4.4.2 Endocytosis and Subcellular Trafficking of Polymers from Media .....149
4.4.3 Cytosolic Microinjection of HPMA Copolymers .....149
4.3.4 Short-Term Intracellular Distribution .....150
4.3.5 Long-term Intracellular Distribution.....151
4.3.6 Kinetics of Nuclear Entry of Copolymers .....152
4.3.7 Nuclear Transport Modulation with FG-peptide Copolymers.....158
4.3.8 Polymer Coinjections.....158
4.4 Conclusions.....162
4.5 References.....165

5. AFTERWORD.....180

5.1 Bispecific Fab' Conjugates for the Targeting of HPMA Copolymers .....180
5.1.1 PEG Dimerized Fab' Fragments.....182
5.1.2 Drug-free Therapeutic Polymers.....184
5.1.3 Bispecific Targeting for Cancer.....185
5.2 Mitochondrial Targeting Using TPP.....185
5.2.1 Conclusions on Mitochondrial Targeting with TPP .....187
5.3. Large Polymer Array .....188
5.3.1 Endocytosis.....188
5.3.2 Microinjection.....193
5.3.3 Other Work Citing Array Copolymers .....195
5.4 Final Observations .....196
5.5 References.....199

LIST OF TABLES

2.1. Summary of results of Scatchard analysis of OV-TL16 IgG, Fab', and Fab'-PEG-Fab' binding constant determinations.....91

3.1 Summary of polymers used for mitochondrial uptake, cell incubation and microinjection studies .....128

4.1. Characterization of microinjected HPMA copolymers .....171

4.2. Characterization of FG-containing and exclusion marker HPMA copolymers...171

5.1. Selected list of bispecific antibody constructs that are undergoing clinical testing or have been approved for clinical use .....206

5.2. Endocytic pathway selective inhibitors and concentrations used. .....206

LIST OF FIGURES

1.1. Summary of the cell surface and intracellular targets for drug carriers and the pathways to cell uptake ..... 43

1.2. Schematic model of targetable polymer drug conjugates with degradable drug linkers ..... 43

1.3. Depictions of the basic structure of the IgG protein ..... 44

1.4. General scheme to produce Fab' fragments from IgG antibodies ..... 45

1.5. Structures of thiol crosslinkers used in early protein conjugation studies ..... 46

1.6. General method to dimerize bispecific Fab' fragments ..... 47

1.7. General synthesis of TPP-functionalized semitelechelic HPMA copolymers ..... 48

1.8. Comonomers used for the large array of the HPMA copolymers ..... 49

1.9. Summary of polymer reaction used for large copolymer array ..... 50

1.10. Representation of the chemical characteristics of the HPMA copolymers in the large polymer array ..... 51

2.1. Depictions of the basic structure of the IgG protein. ..... 79

2.2. General structure of IgG1 antibody ..... 80

2.3. General scheme to produce Fab' fragments from IgG antibodies ..... 81

2.4. Two types of thiol-specific PEG crosslinkers used in study ..... 82

2.5. General method to dimerize homospecific Fab' fragments using a bismaleimide PEG crosslinker ..... 83

2.6. General method to dimerize bispecific Fab' fragments using a bismaleimide PEG crosslinker ..... 84

2.7. Scheme to produce hemitrifunctional linker for Fab' dimerization using heterobifunctional PEG linker coupled to lysine .....85

2.8. Schematic for the addition of Fab'-PEG-Fab' module to HPMA doxorubicin copolymer .....86

2.9. General structure for proposed HPMA drug conjugates targeted with bispecific Fab'-PEG-Fab' .....87

2.10. SDS-PAGE analysis of: **(A)** anti-P-gp IgG2a**, (B)** the digestion mixture of anti-Pgp IgG2a, (**C**) purified Fc fragment, (**D**) purified anti-P-gp $(Fab')_2$ fragment, (**E**) molecular weight ladder. .....88

2.11. SDS-PAGE analysis of: **(A)** anti-fluorescyl BDC1 IgG2a**, (B)** purified anti-P-gp $(Fab')_2$ fragment, (**C**) purified $F_c$ fragment .....88

2.12. Analytical size exclusion chromatography (SEC Superdex 200) profile of OV-TL 16 Fab' conjugation reaction with MAL-$PEG_{3400}$-MAL crosslinker .....89

2.13. Size exclusion chromatography profiles for the purification of dimerized OV-TL 16 Fab'-PEG-Fab' .....90

2.14. Scatchard plot analysis of OV-TL16 Fab'-PEG-Fab' binding kinetics to OVCAR-3 cells .....91

2.15. Results of confocal microscopy of OVCAR-3 cells incubated with Fab'-PEG-Fab'-FITC for 1 h (left), and OV-TL16-FITC antibody for 4 h (right) .....92

3.1. Synthetic scheme for TPP-functionalized semitelechelic HPMA copolymer incorporating the fluorescent moiety BODIPY® FL .....125

3.2 Synthesis of TPP chain transfer agent thiolbutyltriphenylphosphonium .....126

3.3. Synthesis of the control fluorescent probe TPP-BODIPY® FL by the conjugation of TBTP and BODIPY® FL N-(2-aminoethyl) maleimide .....127

3.4. Synthetic scheme for the comonomer MA-GG-BODIPY® FL by the conjugation of BODIPY® FL EDA and MA-GG-ONp .....127

3.5. Summary of semitelechelic TPP-HPMA molecular weight vs. feed chain-transfer agent concentration to monomer concentration .....128

3.6. Typical MALDI-TOF mass spectrum of semitelechelic TPP-HPMA copolymer 129

3.7. Typical MALDI-TOF mass spectrum of semitelechelic TPP-HPMA/MA-FITC copolymer .....129

3.8. Typical MALDI-TOF mass spectrum of semitelechelic TPP-HPMA/MA-GG-BODIPY® FL copolymer .....130

3.9. Timeline profiles of fluorescence quenching by mitochondria. .....130

3.10. Confocal laser scanning fluorescent microscopy (40x mag.) of MDAH2774 ovarian carcinoma cells after incubation with fluorescently-labeled polymers.....131

3.11 Confocal laser scanning fluorescent microscopy of MDAH2774 cells after microinjection with fluorescently-labeled polymers. .....132

4.1. General synthetic scheme for HPMA copolymers .....170

4.2. Structures of the monomers used to create the array of copolymers.....170

4.3. Example of the structure of an array HPMA copolymer. 5% MATC-P: HPMA, MATC, MA-FITC copolymer .....172

4.4. Size-exclusion chromatography profiles for fractionated 5% MAA-P with average Mw indicated for each fraction.....172

4.5. Confocal images of MDAH2774 after 24 h incubation with 0.5 mg/ml F9 fractions of HPMA copolymers .....173

4.6. Typical images from confocal laser scanning fluorescent microscopy of live ovarian carcinoma cells after microinjection with FITC-labeled polymers .....174

4.7. Example of time-lapse imaging from FRAP .....175

4.8. Typical images of fixed MDAH2774 cells after microinjection with strongly cationic copolymer 20% MATC-P-F4.....176

4.9. Time series of a single z-slice of MDAH2774 ovarian carcinoma cells microinjected with 5% GFLG-P-F7.....177

4.10 Nuclear Uptake Kinetics for Copolymer Injected Cells .....178

4.11. Summary of the nuclear uptake kinetics of co-microinjected TR-P-F6.....179

5.1. Structures and general reaction schemes for thiol-reactive disulfide bridging functional groups .....205

5.2. Endocytosis and quantification of uptake of HPMA copolymers .....207

5.3. Quantification of uptake of copolymers by flow cytometry .....208

5.4. Molecular weight dependence of uptake of HPMA copolymers .....208

5.5. Illustration of NPC models.....209

# LIST OF ABBREVIATIONS

| | |
|---|---|
| AIBN | Azobisisobutyronitrile |
| ANTP | Antennapedia |
| aTBTP | Acylated thiolbutyltriphenylphosphonium bromide |
| BCA | Bicinchoninic acid |
| BiAb | Bispecific antibody |
| BMH | *N*,*N'* Bismaleimidohexane |
| BMME | *N*,*N'*Bis-maleimidomethyl ether (BMME), |
| BMP | Bis(3-maleimidopropionyl)-2-hydroxyl-1,3-propanediamine |
| BOC | Butyloxycarbonyl |
| BODIPY FL | 4,4-Difluoro-5,7-dimethyl-4-bora-3a,4a-diaza-s-indacene |
| Chol | Cholesterol |
| CPP | Cell penetrating peptides |
| CTA | Chain transfer agent |
| DBNT | 5,5'-Disulfanediylbis(2-nitrobenzoic acid) |
| DEMA | 2-(*N*,*N*-Dimethylamino)ethyl methacrylate |
| DEMA-P | Copolymer of HPMA and DEMA |
| DIPEA | *N*,*N*-Diisopropylethylamine |
| DMF | Dimethylformamide |
| DMSO | Dimethylsulfoxide |

| | |
|---|---|
| DNA | Deoxyribonucleic acid |
| DPBS | Dulbecco's phosphate-buffered saline |
| EAU | Experimental autoimmune uveoretinitis |
| EDMA | Ethylene dimethacrylate |
| EDTA | Ethylenediaminetetraacetic acid |
| EGFR | Epithelial growth factor receptor |
| EGTA | Ethylene glycol-bis(β-aminoethyl ether)-*N*,*N*,*N'*,*N'*-tetraacetic acid |
| ESI | Electrospray ionization |
| ESI-MS | Electrospray ionization mass spectroscopy |
| Fab | Fragment of antibody |
| Fab-PEG-Fab (FpF) | Two Fab fragments linked by a PEG spacer |
| Fab'-PEG-Fab' | Two Fab' fragments linked by a PEG spacer |
| FBS | Fetal bovine serum |
| Fc | Crystallizable fragment |
| FCCP | Carbonyl cyanide-4-(trifluoromethoxy)phenylhydrazone |
| FDA | Food and drug administration |
| FG | Phenylalanine-glycine |
| FITC | Fluorescein isothiocyanate |
| FPLC | Fast protein liquid chromatography |
| FPLC | Fast protein liquid chromatography |
| FR | Folate receptor |
| FRAP | Fluorescence recovery after photobleaching |
| Fv | Variable fragment |

| | |
|---|---|
| GFLG | Glycine - phenylalanine - leucine - glycine |
| GFP | Green fluorescent protein |
| GGFG-P | Copolymer of HPMA and MA-GGLG |
| GGLFG-P | Copolymer of HPMA and MA-GGLFG |
| GPCR | G-protein coupled receptors |
| H-SFM | Hybridoma serum-free media |
| HABA | 2,4-Hydroxy-3,5-dimethoxyphenyl)acrylic acid |
| HEMA | 2-Hydroxyethyl methacrylate |
| HEPES | (4-(2-Hydroxyethyl)-1-piperazineethanesulfonic acid) |
| HER-2 | Human epidermal growth factor receptor-2 |
| HMW | High molecular weight |
| HPa | Hectopascal |
| HPLC | High performance liquid chromatography |
| HPMA | *N*-(2-Hydroxypropyl)methacrylamide |
| Ig | Immunoglobulin |
| iRNA | Informational RNA |
| kDA | Kilodaltons |
| $k_a$ | Association rate |
| $K_D$ | Equilibrium disassociation constant |
| $k_d$ | Disassociation rate |
| iRNA | Informational RNA |
| kDA | Kilodaltons |
| MA-FITC | *N*-Methacrylolyaminopropyl fluorescein thiourea |

| | |
|---|---|
| MA-GF | *N*-Methacryloylglycylphenylalanine |
| MA-GF-P | Copolymer of HPMA and MA-GG |
| MA-GFLG | *N*-Methacryloylglycylphenylalanylleucylglycine |
| MA-GFLG-P | Copolymer of HPMA and MA-GFLG |
| MA-GG | *N*-Methacryloylglycylglycine |
| MA-GG-BODIPY FL | *N*-Methacryloylglycylglycyl 4,4 difluoro-5,7-dimethyl-4-bora-3a,4a-diaza-s-indacene |
| MA-GGFG-NH2 | *N*-Methacryloylglycylglycylphenylalanylglycine amide |
| MA-GGLFG-$NH_2$ | *N*- Methacryloylglycylglycylleucylphenylalanylglycine amide |
| MAA | Methacrylic acid |
| mAb | Monoclonal antibody |
| MAL | Maleimide |
| MALDI-TOF MS | Matrix assisted laser desorption ionization-time of flight mass spectrometry |
| MATC | *N*-Methacryloyloxyethyl trimethylammonium chloride |
| MATC-P | Copolymer of HPMA and MATC |
| MES | 2-(*N*-Morpholino)ethanesulfonic acid |
| MLS | Mitochondria localization sequence |
| mMDH | Mitochondrial malate dehydrogenase |
| Mn | Number average molecular weight |
| MSF | Mitochondrial import stimulation factor |
| MT | Microtubule |
| mtDNA | Mitiochondrial DNA |

| | |
|---|---|
| $M_w$ | Weight average molecular weight |
| MWCO | Molecular weight cut-off |
| NES | Nuclear export sequence |
| NHS | *N*-Hydroxysuccinimide ester |
| NMR | Nuclear magnetic resonance |
| NPC | Nuclear pore complex |
| NTR | Nuclear transport receptor |
| Nups | Nucleoporins |
| *o*-PDA | *o*-Phthaldialdehyde |
| OA3 | Ovarian Cancer Antigen 3 |
| PAMAM | Poly(amidoamine) |
| PBS | Phosphate buffered saline |
| PC | Lecithin |
| PDM | *N*,*N'* Phenylene dimaleimide |
| PEG | Poly(ethylene glycol) |
| PEI | polyethylenimine |
| pHPMA | Poly(*N*-(2-hydroxypropyl)methacrylamide) |
| pHPMA-FITC | Copolymer of HPMA and MA-FITC |
| PNA | Peptide nucleic acid |
| PTD | Peptide transduction domain |
| PVP | Poly(2-vinylpyrrolidone) |
| RES | Reticuloendothelium system |
| RNA | Ribonucleic acid |

| | |
|---|---|
| RP | Reverse phase |
| rpm | Revolutions per minute |
| scFv | Single-chain Fv fragment |
| SDS_PAGE | Sodium dodecyl sulfate polyacrylamide gel electrophoresis |
| SEC | Size exclusion chromatography |
| SEMA | 2-Sulfoethyl methacrylate |
| SEMA-P | Copolymer of HPMA and SEMA |
| SMA | Styrene-maleic anhydride copolymer |
| SMCC | Succinimidyl-4-(*N*-maleimidomethyl)cyclohexane-1-carboxylate |
| SPDP | Succinimidyl-3(2-pyridyl-dithiol)-propionate |
| STPP | Stearyltriphenylphosphonium bromide |
| TAT | Transactivator of transcription |
| TBTP | Thiobutyltriphenylphosphonium |
| TCEP | Tris(2-carboxyethyl)phosphine hydrochloride |
| TFA | Trifluoroacetic acid |
| TLC | Thin layer chromatrograophy |
| TLCK | $N^a$-tosyl-L-lysyl chloromethyl ketone |
| TNF-$\alpha$ | Tumor necrosis factor alpha |
| TPP-HPMA | Semitelechelic pHPMA with terminal TPP moiety |
| TPP-HPMA-BODIPY FL | TPP semitelechelic copolymer of HPMA and MA-GG-BODIPY FL |
| TPP-HPMA-FITC | TPP semitelechelic copolymer of HPMA and MA-FITC |
| TR-P | pHPMA labeled with Texas Red |
| UV | Ultraviolet |

# ACKNOWLEDGEMENTS

Foremost, I would like to thank my advisor, Dr. Jindřich Kopeček, for his guidance, wisdom, kindness, and most of all, patience for allowing me to continue and complete this work. My special thanks also to Dr. Pavlá Kopečková for her assistance, instructions, and suggestions for my work. I would also like to thank my committee members, Dr. Vladimir Hlady, Dr. James Herron, Dr. Katherine Ullman, and Dr. Hamid Ghandehari for all their help over these years. And special thanks to all my past coworkers in the Kopeček Lab for their comradery and support during good times and bad, including Kirk, Jihua, Monika, ZR, Songqi, Russell, Monica, Pad, Vaikunth, Aijun, Sasha, Claudia, Aparna, Ayelet, Keith, Jane, Susan, Chun, Dong, Chunyu, Tamara, Jarunee, Hui, Weiwei, Thomas, Kuangshi, Nicole, Boris, and Michal. Special thanks also to Chris Rodesch, for his invaluable assistance in the Cell Imaging Facility.

Finally, I would like to thank my parents and my wife Wendy for all their support over the years, and all they did that made finishing this work possible.

# CHAPTER 1

# INTRODUCTION

## 1.1 Engineered Materials in Medicine

The role of biomaterials in medicine has expanded greatly over the past century. Our ability to replace, replicate or augment biological functions using engineered materials has grown in line with our greater understanding of biological systems and the requirements necessary to make materials biocompatible and functional in living systems. In all complex organisms, a fundamental obstacle to engineered materials is the myriad of biological recognition systems in place to detect the presence of foreign or altered materials, i.e., the recognition of self from nonself. These include the many familiar pathways involved in the immune, complement, and blood coagulation systems. These responses have evolved to detect physical damage or to help defend living things from toxins, intrusions, parasites, or biological invaders. However, these same systems represent the fundamental barrier restricting the application of synthetic or engineered materials for medicinal uses.

Understanding what makes a material or chemical compound *biocompatible* has been a slow process of trial and error and innovation, evolving over many decades. This has required a deep understanding of biological systems or how they respond to a variety of stimuli. For example, the on-going refinement of implants for orthopedic,

cardiovascular, or dental applications are representative of the type of progress that has been made possible by the refinement of biomaterials. A great deal has also been accomplished via biotechnology, which is essentially the production of natural proteins and nucleic acids through the artificial manipulation of biological systems. In the emerging fields of nanotechnology and nanomedicines, synthetic materials have been shown to be increasingly useful for biological applications.

### 1.1.1 Natural vs. Synthetic Polymers

Proteins, polysaccharides and nucleic acids play central roles in all organisms, and are basic building blocks of all living systems. The use of *artificial* polymers in medicine has been spurred by the possibility of expanding our ability to create engineered materials that are not restricted by the chemical and physical limitations of naturally occurring chemicals and polymers. Engineered natural polymers face an array of natural biological hurdles when used as medicines, such as the array of enzymes and endogenous physical conditions, such as low pH, that may degrade their physical structures and break them down. Further, the immune system is specifically adapted to detect natural polymers and possesses a myriad of responses that recognize, neutralize, remove, or degrade natural polymers. Part of the utility of synthetic polymers is the ability to overcome many of these barriers.

The research described in this document is focused on what are now termed “nanomedicines”, engineered macromolecules introduced (typically via the vasculature) into organisms for therapeutic applications. As this technology advances, they can be generalized as chemical conjugates of both natural and artificial polymers, which are

further able to form a myriad of possible aggregates and other superstructures, and possess nearly limitless potential functions. Overall, however, the type of constructs to be discussed here are engineered “nanoparticles” that function in many of the same roles of as natural, free circulating proteins, analogous to *blood plasma proteins*.

### 1.1.2 Synthetic Polymers in Medicine

The root of polymeric nanomedicines can be traced back to the first medical applications of wholly synthetic polymers. Early examples were demonstrated by polymers used as blood plasma expanders during World War II. To maintain osmotic pressure after trauma, the synthetic polymer PVP [poly(2-vinylpyrrolidone)] was used as a blood plasma expander after traumatic blood loss (1). This essentially replaced the function of albumin, the most prevalent protein in blood, thereby maintaining osmotic pressure within the vasculature. It was found that PVP, HPMA (*N*-(2-hydroxypropyl)methacrylamide) and other hydrophilic polymers used as plasma expanders were nonimmunogenic, and high molecular weight polymers could be retained in circulation for periods of time much longer compared to most endogenous plasma proteins (2).

Polymers that form hydrogels were the basis of the first gas-permeable contact lens. Notably, hydrogels made from copolymers of HEMA (2-hydroxyethyl methacrylate) and EDMA (ethylene dimethacrylate) were one of the first materials used (3, 4). These materials were not only useful due to their optical properties, hydrogel polymers were noted early on for their long-term biocompatibility, specifically the lack of inflammation or other immune responses they elicited when exposed to living tissue for extended periods of time.

These homopolymers maintain a structural free random coil structure and most have a large hydrodynamic volume disproportionate to their molecular weight as compared to proteins. Albumin has a molecular weight of 66 kDa and represents the upper limit for glomeruli filtration, a pore size of about 7 nm. Synthetic polymers with a hydrodynamic radius below the renal threshold of 3.8 nm are rapidly cleared from circulation. However, polymers and other nanoparticles above 7 nm are maintained in circulation until removed via complement and the RES (reticuloendothelium system), also known as the mononuclear phagocytic system. They can also be removed by the phagocytic Kuffer cells in the liver (5).

### 1.1.3 Polymer Conjugates

The most successful uses of water-soluble, synthetic polymers to date has been to create simple conjugates to modify the properties of therapeutically active compounds, proteins, or nucleic acids. The flexibility inherent in polymer synthesis has been proven to be useful when combined with other types of biological agents. These hybrid constructs have included polymer-drug conjugates, polymer-protein conjugates, polymeric micelles, and polymer-nucleic acid polyplexes. In each of these cases, polymers are employed to greatly enhance the existing biological activities and/or the transport characteristics of the given therapeutic agent and have been used to greatly enhance the biocompatibility (6), pharmacokinetics (7, 8), nonimmunogenicity (9), and cell targetability (9-11) of these agents, while reducing their toxicity toward nontargeted tissues.

### 1.1.4 PEGylation

The invisibility of many synthetic polymers from biological systems has been the rationale for the creation of some of the most useful polymer-based conjugates. PEG (poly(ethylene glycol)) has long been used for its “stealth” properties and its ability to confer these properties when they are conjugated to proteins and other materials. “PEGylated” proteins are produced by the covalent attachment of functionalized polymers, where one end of the polymer chain possesses a reactive functional group that can react with a specific amino acid side chain on a protein. Compared to the unaltered protein, the polymer conjugate is typically more soluble and stable, and possesses a longer intravascular half- life after injection. This approach was first demonstrated in the 1970s when Abuchowski et al. PEGylated bovine serum albumin and bovine liver catalase. It was found that the PEGylated proteins possessed improved stability, greatly increased circulation time, and a sharply reduced immunological response compared to the unmodified proteins (12, 13).

The hydrodynamic volume of PEG is disproportionately large for a given molecular weight, and the increased volume of the protein conjugate can be used to exclude it from filtration and removal from circulation by the glomulerus. As a surface polymer, it protects the protein from proteolytic degradation in plasma or tissue interstitium and inhibits removal from circulation by the RES. The immunogenicity of the protein is also reduced by protecting the protein from interaction with various components of the immune system, such as antibodies that would recognize unmodified proteins.

PEGylated proteins represent the most common and successful medicinal applications of synthetic polymers and several types of these conjugates have been

approved by the FDA for clinical use. Included are: PEG–asparaginase (Oncaspar®) for the treatment of acute lymphoblastic leukemia (14, 15), PEG–adenosine deaminase (Adagen®) for severe combined immunodeficiency disease (SCID)(16), PEG–interferon α2a (Pegasys®) for renal cell carcinoma and hepatitis C,(17, 18) PEG–interferon α2b (PEG–Intron®) for hepatitis C, several types of cancer, multiple sclerosis, and HIV/AIDS,(19) PEG–granulocyte-colony stimulating factor (Pegfilgrastim, Neulasta®) for neutropenia during chemotherapy (20), PEG-interferon β1a (Plegridy®) for multiple sclerosis (21), mPEG-epoetin β (Mircera®) for anemia due to chonic kidney disease (22), PEG-uricase (Krystexxa) for gout (23), PEG-antihemophilic factor VIII (Adynovate®) for hemophilia A (24), and PEG–growth hormone receptor antagonist (Pegvisomant, Somavert®) for the treatment of acromegaly (25).

The appeal of PEG has traditionally been drawn from its simplicity, low cost of synthesis, and its presumed lack of biorecognition and immunogenicity. More recent studies, however, have shown PEG is not as biologically inert as originally thought. Under certain conditions PEG and PEG conjugates can generate several types of immune responses. Some conjugates have been found to cause complement activation in certain circumstances (21, 26-29). Rapid clearance of PEGylated liposomes can occur after repeated injections due to immune recognition (30). PEG can also be chemically altered by peroxidation, which has been shown to cause several negative effects in biological systems (31-33).

The limitations of PEG as a component of nanomedicine conjugates has driven renewed interest into research in other synthetic alternatives.(34, 35) HPMA copolymers, for example, continue to be of interest due to their biocompatibility and the predictability

of copolymer synthesis with a variety of other monomers. One of the reasons HPMA was initially selected was due to the hydrolytic stability of the amide bond connecting the 2-hydroxlypropyl sidechain (36). Copolymers of HPMA are also easier to synthesize with the use of other methacrlyates and methacryamide monomers. The composition of the resulting copolymers is relatively easy to predict and multiple types of comonomer can be incorporated in the same copolymer.

## 1.2 Polymer-Drug Conjugates for the Treatment of Cancer

An example of a more direct approach to using synthetic polymers to create therapeutics has been the development of polymer-drug conjugates. Here, polymer conjugates are created with traditional chemotherapy drugs covalently attached to them via degradable spacers. The use of the polymeric carrier introduces many advantages for the treatment of disease.

The current standard of care for the treatment of most types of cancer usually includes the use of chemotherapy agents. These cytotoxic drugs are traditionally low molecular weight hydrophobic compounds that induce apoptosis by the inhibition of DNA replication or microtubule spindle functions in mitotic cells. They selectively destroy tumor cells by triggering apoptosis in rapidly dividing cells in a dose-dependent manner. Dosages used therapeutically, however, are limited by their toxicity to rapidly dividing normal cells. These include bone marrow cells, and the epithelial cells of the kidney and gastrointestinal tract. The effectiveness of chemotherapy drugs is also limited due to their susceptibility to enzymatic alterations in the body and their rapid clearance from the vasculature via glomerular filtration.

To overcome these limitations, chemotherapy drugs have been conjugated to high molecular weight, hydrophilic polymer carriers. Carriers used have included natural polymers such as dextran (6), and albumin (37); and synthetic polymers including: poly(ethylene glycol) (PEG) (38), styrene-maleic anhydride copolymer (SMA) (9), and *N*-(2-hydroxypropyl)methacrylamide (HPMA) copolymer (8, 10). Water-soluble macromolecular drug conjugates have been demonstrated to possess a greater intravascular half-life, a lower specific toxicity, able to avoid traditional multidrug resistance mechanisms, and possess the potential to be more precise and effective than free antitumor drugs.

### 1.2.1 The EPR Effect and Passive Tumor Tissue Targeting

Cancer was a natural subject for some of the first polymer-drug conjugates due to the "EPR (enhanced permeability and retention) effect" (1). Early research with soluble polymers showed that circulating macromolecules passively concentrated in tumor tissues over time. For intravenous applications, extravasion through the endothelium is a barrier that typically limits all macromolecules (biological or nonbiological) greater than ~50 kDa from escaping the vasculature. The accumulation of macromolecules was attributed to the higher rates of macromolecular extravasation that occur in the neovasculature typically produced by solid tumors. Because lymphatic drainage is also often impaired, the EPR effect allows long-circulating macromolecules to be concentrated in the local interstitium surrounding tumors (9).

For these reasons, macromolecular drug carriers were capable of passive targeting of tumor tissues. Early attempts to exploit the EPR effect via polymer-drug conjugates were

limited by the fact that the active component remains covalently attached to the polymeric carrier. Most LMW drugs require internalization by the cancer cells and, typically, subcellular localization to the active site in the nucleus or mitochondria. This spurred the development of polymer-drug conjugates where the drug was attached via a degradable bond hydrolyzed selectively after reaching the tumor cell, whereby the drug would enter cells by simple diffusion.

Much of the recent history of polymer-drug conjugate development has been devoted to the design of better methods to deliver high enough concentrations of drugs to an active site within cells to produce their therapeutic effect. This effort has entailed methods to actively target the cells, and strategies to better concentrate the bioactive ingredient to the required subcellular target.

## 1.3 Macromolecular Drug Carriers and Barriers to Cell Entry

To improve the cellular uptake and specificity of drugs possible by diffusion, numerous approaches have been developed to use polymeric carriers for cell uptake. Macromolecules are naturally excluded from the outer plasma and various subcellular membranes. Notable membrane-excluded intracellular organelles include endosomes, lysosomes, the nucleus, and mitochondria. Therefore, two general approaches have been used to overcome these barriers: 1) direct membrane transduction, or 2) co-opting of the active endocytotic pathways, enzyme activities, and subcellular trafficking mechanisms of the cell. Figure 1.1. summarizes some of the targets of drug delivery in the cell and the possible pathways to them.

### 1.3.1 Lysosomotropic Drug Carriers and Cell Targeting

Many polymer-drug conjugates developed are lysosomotropic, that is, conjugates designed to be internalized by cells via endocytosis and trafficked to the lysosomal compartment (8). There, the lowered pH and/or presence of lysosome-specific enzymes would cleave the bond used to attach the drug to the conjugate. The LMW drug would then be free to diffuse out of the lysosome and reach its active site within the cell.

This paradigm of the targetable lysosomotropic HPMA copolymer-drug conjugates is represented in Figure 1.2. The basic structural features are of a hydrophilic polymer "decorated" with low molecular weight drug. These are attached by covalent linkers which are selectively degradable at the target site. These are typically hydrolysable bonds that are cleaved due to lowered pH or specific redox conditions, or are enzyme-specific peptide bonds. Also attached is a targeting moiety or other selective binding construct that is designed to specifically bind to surface receptors on target cells. The objective in this model is to deliver high concentrations of drug with a long biological half-life to specific cell types, without significant toxicity to normal cells (39). The HPMA backbone and pendant linkers are hydrolytically and enzymatically stable in the vasculature and the interstitium, that have been shown to retain most of their biological activity (40). Subcellular localization of intact polymer-drug conjugates raises the possibility of trafficking and stably maintaining the drug at the location of the drug's biological target.

### 1.3.2 Macromolecular Delivery to the Cytoplasm

More recent work has been devoted to the development of methods to deliver intact macromolecules to the cytoplasm of living cells that avoid trafficking to the lysosomal compartment. These can be divided into two categories, peptidic and nonpeptidic factors. In each of these pathways, a compound is internalized into the cell by either endocytosis, or by nonendocytotic, direct transduction into the cytosol. The transduction factor then destabilizes the internalizing vesicle by some method that allows the release of the compound into the cytoplasm. Peptide transduction domains (PTDs) or cell penetrating peptides (CPPs) were originally thought to directly penetrate the plasma membrane by a nonenergetic physical mechanism. However, more recent work has disputed this hypothesis and they are now thought to be rapidly internalized by fluid-phase lipid raft-dependent macropinocytosis, a specialized form of endocytosis (41). The peptide then destabilizes the vesicle to release their contents into the cytoplasm. Subcellular targeting represents another potential layer of control in targeted drug delivery.

Quantum dots are semiconductor nanoparticles that have been successfully used as stable fluorescent particles for labeling and tracking subcellular structures in live cells. For targeting the cytosol, quantum dots up to 30 nm in diameter and coated with PEG-grafted PEI were shown to be rapidly endocytosed, and then slowly released in the cytoplasm of live Hela cells (42). Alternately, quantum dots coated with PEG and conjugated to NLS or MLS peptides have been shown to efficiently localize to the mitochondria or nuclei, respectively, of live 3T3 fibroblast cells after electroporation or transfection agents (43).

For peptidic factors, the homeotic transcription factor ANTP peptide (RRMKWKK) from *drosophilia* and the TAT protein peptide (GRKKRRQRRR) from the

HIV-1 virus are prototypical CPPs. In initial studies to modulate the uptake of macromolecules, TAT peptide was chemically added to several proteins such as horseradish peroxidase and beta-galactosidase to mediate delivery (44). Since then, TAT peptide has been used to enhance the uptake of a variety of proteins, nucleic acids, polymers, and nanoparticles (45-49). More recently, TAT peptide was combined with the pH-sensitive fusogenic peptide HA2 to create an internalization module that greatly enhanced the uptake, endosomal release and cytoplasmic delivery of macromolecules. Using this, escape from macropinosomes was dramatically enhanced for a transducible TAT-Cre recombinase reporter assay on live cells (50).

Alternately, polymeric and dendritic carriers with weakly cationic charges may be transduced into the cytoplasm via the so-called "proton sponge effect," whereby lysis of endosomes can be induced before fusion with lysosomes (51). By this hypothesis, lowering of the pH in endosomes causes the polymer to build up $H^+$ ions. The ions raise the membrane potential of the vesicle causing the concentration of $Cl^-$ ions to increase also. The combination increases the osmotic pressure in the endosome until it bursts, releasing its contents into the cytosol (52). For example, polyethylenimine (PEI) has been used extensively as a nonviral vector for nucleic acid transfections, in vitro and in vivo (53, 54). By this method polyanionic DNA or RNA is condensed with PEI to form a stable polyplex that is *endosomolytic*. The polyplex is then uptaken by endocytosis, but avoids degradation in the lysosome, as the nucleic acid is released from endosomes into the cytoplasm intact.

### 1.3.4 Gene Therapy and Direct Cytoplasmic Delivery

To place the role of drug delivery with macromolecular carriers in perspective, many of the issues related to the development of therapeutic macromolecules have been illustrated in the field of gene therapy. There are many aspects to this field. However, the most typical goal of this work is to develop methods whereby a nucleic acid encoding an entire gene (or RNAi) is internalized by targeted cells. Transfecting genomic DNA with a new gene can be thought of as macromolecular drug transport problem where the ideal vector: 1) delivers an intact nucleic acid to a targeted organ, tissue, or cell type; 2) permits the binding and uptake by cells in a way that avoids degradation in the lysosomal compartment; 3) allows subcellular transit through the cytoplasm and/or uptake into the nucleus.

From this perspective, the virus is a nanodevice, able to reprogram a cell with a payload of genes, and can efficiently perform several functions at the same time, including protecting nucleic acid from enzymatic degradation during transport through the organism, biorecognition and binding to a target cell, direct transduction of nucleic acids through the plasma membrane, and directing the intracellular trafficking of the nucleic acid to the targeted subcellular compartment. The development of man-made materials as drug carriers can be interpreted as the initial stage of development of a nanotechnology that mimic the transport and molecular functions of viruses while avoiding their biological limitations.

## 1.4 Antibodies for Cellular Targeting

Antibodies are globular proteins produced in blood plasma and are the body's mainline defense against pathological foreign organisms. They are divided into 5 main specialized classes: IgG, IgA, IgM, IgD and IgE, with IgG the most abundant. IgGs consist of 4 protein components, 2 50kDa heavy chains and 2 25kDa lights chains, which form a tetrameric quaternary structure. The heavy chains consist of 3 constant domains ($C_H1$, $C_H2$, $C_H3$) and a variable domain ($V_H$). The light chains have 1 constant domain ($C_L$) and a variable domain ($V_L$). The heavy chains are connected to each other and the light chains are connected to the heavy chains via disulfide bonds and form the protein into a general Y-shape. The connector point in the middle is referred to as the hinge region. The "trunk" of the antibody is the C-terminal domain of the heavy chains and is referred to as the Fc region for "fragment crystallizable". The N-terminal "arms" of the antibody each contain an antigen binding region and are referred to as the Fab fragments for "fragments antigen binding" (Figure 1.3.).

To chemically isolate the Fab from the IgG proteins, there are two general approaches using proteolytic enzymes. If IgG1 is digested with papain, the open hinge region of the antibody is completely digested leaving Fab' fragments containing a single interchain disulfide bond. If IgG1 is digested with pepsin, however, the hinge region can be partially digested leaving a $(Fab')_2$ fragment, where the two Fab' fragments remain connected by a portion of the hinge region. If the cysteine bonds of the $(Fab')_2$ fragment are then selectively reduced to disassociate the fragments, the Fab arms with the remaining pieces of the hinge region are referred to as Fab' fragments. (Figure 1.4.) The active thiol groups of Fab' fragments are useful in synthetic chemistry for site-specific thiol-selective

conjugation chemistries (55).

There are small differences in structure between the subtypes of IgG antibodies (56). (Figure 1.3.) In experiments described in Chapter 2, the U1C2 hybridoma for anti-P-glycoprotein (anti-P-gp) was used to produce Fab' for conjugate chemistries. However, the U1C2 antibody is of the IgG2a subtype, which has a slightly different structure from IgG1, particularly with respect to the hinge region and the number of interchain disulfide bonds. Digestion of IgG2a antibodies was found to produce a heterogeneous mixture of fragments, so a new protocol was developed using lysyl endopeptide as the protease. This protocol development is described in detail in Fowers et al. (2001) (57).

### 1.4.1 Bispecific Antibodies and Cell Targeting

The development of bispecific antibodies (BiAbs) and other bispecific targeting constructs is a rapidly expanding field with numerous applications for drug development, diagnosis, and imaging (58-62). Many strategies have been developed using BiAbs. These include, redirection of lymphatic cells, dual targeting and pretargeting strategies, intravasculature half-life extension, and delivery through biological barriers, such as the blood-brain barrier (63-65). Bispecific antibodies are used for a variety of diseases, including cancer, chronic inflammatory diseases, autoimmune, neurodegeneration, bleeding disorders, and infections (66-69).

Bispecific monoclonal antibodies (BsAbs) and multivalent Fab' (or Fv') conjugates have been explored more recently to further expand the capabilities of immunotherapy. These constructs have been developed to bring together disparate cell and/or molecular species or to increase binding efficacy. Currently, the creation of BsAbs to mediate the

recruitment of cytotoxic T cells to tumor cells is one of the most promising approaches for the treatment of a variety of cancers (70, 71).

Many methods have been developed for bispecific or multispecific targeting using the antigen-binding domains of antibodies. These include hybridoma fusion lines (triomas or quadromas), a wide array of genetically engineered constructs (such minibodies and diabodies), and chemical conjugation (72-78). Quadromas and genetic constructs are efficient sources of bispecific targeting agents once they are isolated. However, both require a great deal of time, money and expertise to initially produce. Further, their effectiveness can't be easily predicted before they are constructed, synthesized and purified. Chemical conjugation allows any existing pair of mAbs to be used to screen their feasibility for bispecific targeting. Chemical conjugation of antibody proteins would logically be the most straightforward method to rapidly test bispecific targeting constructs, but this approach was long limited for several reasons. Purified antibodies and antibody fragments are often instable in solution, particularly when undergoing chemical modification reactions. The disulfide bridges in the proteins are particularly prone to breaking or swapping. Low molecular weight chemical crosslinking agents were hard to target and were inefficient due to steric factors. Separation and purification of the antibody products was difficult, requiring multiple steps. All these factors resulted in low yields.

### 1.4.2 Early Approaches to Fab' Chemical Conjugates

In most early synthetic procedures, purified IgG was first digested in the hinge region with the enzyme pepsin to obtain the $(Fab')_2$ fragment. This was especially convenient using IgG1 antibodies since the Fc portion of the antibody is completely

degraded into small fragments which were easily removed by gel filtration. $(Fab')_2$ is then reduced to yield two Fab' fragments. The free thiol groups are then used to site-specifically crosslink fragments for two different antigens. (Figure 1.4.)

Two types of reactions initially used to conjugate Fab' fragments that produced useful bispecific products were: 1) thiol activation and exchange and 2) maleimide crosslinking.

The thiol exchange method was demonstrated via activation with 5,5'-disulfanediylbis(2-nitrobenzoic acid) (DBNT–Ellman's reagent) (79) and 4,4'-dipyridyl disulfide (Figure 1.5. **A**) (80). For both, one Fab' is activated and the unreacted activator is then removed by gel filtration. The second Fab' is then allowed to react with the activated conjugate which is thereby coupled by simple disulfide bonds. Yields of BsAb up to 50% were reported. The reagent succinimidyl-3(2-pyridyl-dithiol)-propionate (SPDP) had also been described. However, it produced random crosslinks and the resulting products were too heterogeneous for further characterization (Figure 1.5. **A**) (81).

Low molecular weight bismaleimide conjugates were later developed to improve synthetic yields. Quadri et al. assessed three bismaleimide linkers to stabilize a homospecific antiferritin $(Fab')_2$ fragment in vivo (Figure 1.5. **B**): bis-maleimidomethyl ether (BMME), N,N' p-phenylene dimaleimide (p-PDM), and N,N' bismaleimidohexane (BMH) (82). The small size of these linkers was putatively intended to reduce possibility of linker derived immune recognition of the conjugate. All three conjugates here were found to be nonimmunogenic and to remain in circulation longer than unmodified $(Fab')_2$. Other chemically linked BsAbs cited in the literature during this time often used σ-PDM (83-86). Using σ-PDM, final yields of BsAb were no more than 15% or less. In studies of

the hydrolytic stability of chemically conjugated Fab' fragments, Quadri et al. used solid phase synthesis of BsAbs to simplify synthesis and showed that low yields are largely the result of inefficient coupling of the second Fab' fragment to the Fab'-PDM conjugate (87). This was likely due to steric hindrance.

A larger bismaleimide crosslinker, *N,N'*-bis(3-maleimidopropionyl)-2-hydroxyl-1,3-propanediamine (BMP), was used to create chimeric Fab'/Fc conjugates (% yields not reported). Bispecific minibodies have been synthesized using peptide linkers capped with Nε-maleimidocaproyl amino acids to conjugate scFv' fragments (Figure 1.5. **B**.) (88).

Maleimide and polyoxime-based linkers were custom-synthesized by several research groups to produce trivalent and tetravalant Fab' conjugates (89, 90). These linkers require several reactions to produce and do not lend themselves to the production of multi-specific conjugates. Yields using these linkers were reported to range from 4 to 18%.

## 1.5 PEG-Dimerized Fab' Fragments for Targeting Ovarian Carcinoma Cells

Chapter 2 describes the development of PEG-crosslinked Fab' fragments as targeting modules for HPMA copolymer drug conjugates. This work explored use of short PEG polymers that possessed two thiol-specific terminal functional groups to dimerize Fab' fragments isolated from monoclonal antibodies. Antibodies chosen were specific for surface antigens commonly expressed on ovarian, and many other, carcinoma cells.

Previously, polymer-drug conjugates had been developed that employed a single monoclonal antibody, a single Fab' fragment, or used multiple Fab' fragments in a heterogeneous manner (91-96). These were shown to possess selective binding and uptake

by cultured carcinoma cells. However, the resulting drug conjugate did not demonstrate significantly higher chemotherapeutic effectiveness compared to nontargeted conjugates. The work here explores the use of well-defined targeting modules consisting of dimerized Fab' fragments created with PEG linkers. The goal of this approach was to develop an efficient and well-defined synthetic method to couple antibody fragments in a manner that would also provide for the bispecific targeting of carcinoma cells.

The basic structure of the proposed targeting moiety would consist of two Fab' fragments derived from monoclonal antibodies specific for epitopes on two different antigens found on ovarian carcinoma cells, each bound to an end of a branched PEG linker (Figure 1.6.). The Fab' fragments have a relatively low affinity to their corresponding receptor proteins but since the Fab' fragments are covalently linked, it was hypothesized that the binding of one would result in the cooperative binding of the other. The length of the linker would be large enough to span the average distance between two membrane proteins on a cell, but small enough to present the membrane surface to both fragments at the same time. Ideally, binding to a nontarget cell with only one target epitope would be reversible and would release the conjugate before it is endocytosed into the cell. It was proposed that the binding kinetics to cells that present both target epitopes would uptake conjugate via receptor-mediated endocytosis in concentrations orders of magnitude higher than cells that possessed only one surface epitope.

The use of two affinity moieties connected by a flexible linker was intended to achieve several effects at once. First, the availability of two antigen proteins presents many possible combinations for targets on cancer cells. Second, bispecific targeting doesn't require the presence of a unique epitope on the targeted cell. This is especially important

since most carcinoma cells are phenotypically diverse and the presence of a unique and universal oncoprotein or other antigen on the cells would be unusual. Third, the use of long flexible PEG linkers to tether the antibody fragments would theoretically increase the affinity of the conjugate to cells as well as decrease the time required to diffuse to the cell. This would result from reduced steric hindrance of the antigen binding site from the rest of the conjugate and from increased translational and rotational mobility of the fragments. Antibody/antigen interactions require a specific orientation for binding, and increased freedom of movement would, hypothetically, increase conjugate binding kinetics to targeted cells

## 1.6 Mitochondrial Targeting of HPMA Copolymers

### 1.6.1 Rationale

Chapter 3 describes the synthesis and characterization of HPMA copolymers designed to target mitochondria. Mitochondria possess a variety of factors desirable for drug targeting. The organelles have been increasingly recognized to have important roles in functions aside from glycolysis and ATP production for the cell, and are a logical focus for anticancer treatments as they are crucial for execution of apoptosis (programmed cells death). In addition, mitochondria dysfunction has been shown to contribute to a growing number of disease states, including cancer, neuronal degeneration, obesity, diabetes and ischemia-reperfusion injury (97, 98). Most of these diseases are associated with excess oxidative damage resulting from mitochondrial dysfunction. For this reason, the development of mitochondriotropic antioxidants has been a focus for drug discovery. Changes in mitochondrial function and mutations in mitochondrondial DNA have emerged

as pivotal events in the development of cancer. For example, BCL-2 family proteins have become active targets for the design of anticancer drugs (99). These proteins are integral regulators of apoptotic cell death located at the mitochondrial outer membrane. Numerous mitochondriotropic compounds are in development and clinical testing as cancer treatments. These include antisense agents to knock out protein expression (100), and several small molecule antagonists (101).

### 1.6.2 Mitochondria Targeting Peptides

Precursor proteins that are trafficked to mitochondria depend on an MLS (mitochondrial localization sequence) or MTS (mitochondrial-targeting sequence) peptide region located on their N-termini. These peptides control the active import of the mitochondrial protein code in the cells' genomic DNA. They are recognized by the cytoplasmic molecular chaperone, MSF, and then by Tom70 and Tom20 of the mitochondrial outer membrane receptor complex. For intramitochondrial localization, MLS's possess a multirole sorting sequence that specifically interact with various components of the mitochondrial protein import pathway.

MLS sequences have been successfully conjugated with various proteins, polymers and other macromolecules to render them mitochondriotropic (as noted for quantum dots, previously). For this purpose, MLS peptide leader sequences MSVLTPLLLRGLTGSARRLPVPRAKIH (27 aa) from cytochrome-*c* oxidase VIII (COX-8) subunit (102) and MLSALARPVGAALRRSFSTSAQNN (24 aa) mitochondrial malate dehydrogenase (mMDH) (103) have both been used. For example, a mMDH peptide conjugate with a GFP-tat fusion protein was shown to localize to and remain in

mitochondria in several cells types (104).

### 1.6.3 Lipophilic Cations

Nonpeptidic cationic functional groups have also been used as targeting moieties to traffic conjugates to the mitochondrial compartment. Most small molecule mitochondriotropic compounds are lipophilic cations and include rhodamine-123(105, 106), oligoguanidinium (107, 108), triarylmethane (109-111), and triphenylphosphonium (TPP)(112-114). Each of these consists of cationic charges that are highly delocalized in a multiple aromatic ring structure. These moieties possess a net positive charge that is shielded in a “cage” of hydrophobic rings that prevent the approach of counter ions. Mitochondrial localization is thereby generated by the attraction of the delocalized cation for the negative transmembrane electrostatic potential (Δpsi) in mitochondria created during respiration during oxidative phosphorylation (115, 116). The mix of cationic and hydrophobic properties of the cations also greatly enhances their diffusion across lipid bilayers. In this model, the cations have a high affinity for the surface anionic charge of biological membranes, which enhances the initial adsorption to the bilayer. In the outer plasma membrane and mitochondrial membrane, the transmembrane potential creates a driving force to pull the cation across the bilayer while the net hydrophobicity of the moiety structure minimizes the energy barrier that would normally block the diffusion of cations.

Lipophilic cations have also been incorporated into the bipolar lipid dequalinium that have been used to form mitochondriotropic vesicles or “DQAsomes” (117, 118). DQAsomes have been used as vectors for drug and nucleic acids to the mitochondria of living cells. In this delivery system, the vesicles are not destabilized when in contact with

anionic lipid membranes but release their payload after trafficking and adsorption with the cardiolipin-rich mitochondrial membrane. DQAsomes loaded with MLS-plasmid conjugates were shown to colocalize intact DNA with mitochondria in living cells in contrast with MLS-plasmid alone (119, 120).

1.6.3.1 Triphenylphosphonium (TPP)

TPP has been used to create an entire class of low molecular weight mitochondria localizing drugs, largely through the work of Michael Murphy now at the MRC Dunn Human Nutrition Unit, Cambridge, UK. For instance, TPP has been used to make antioxidants mitochondriotropic in conjugation with vitamin E ("Mito Vit E"), ebselen ("MitoPeroxidase") and ubiquinol ("MitoQ") to enhance the ability of the compound to protect cells from oxidative damage (121-125). Cells incubated with micromolar concentrations of Mito Vit E were found to have levels of the drug in their mitochondria 80-fold higher compared to those incubated with unmodified vitamin E (121).

MitoQ compounds were synthesized by attaching TPP to ubiquinone using an alkyl spacer. In isolated cells, it was found that the compounds were localized to mitochondria in concentrations several hundred-fold higher than that expected with ubiquinone. Furthermore, when the length of the alkyl spacer was altered between C3 and C15, the degree of association with the inner mitochondrial membrane could be regulated, as determined by a lipid peroxidation assay (126). In vivo, rats fed MitoQ showed improved heart function compared to control animals after ischemic injury to their heart tissue (97). MitoPeroxidase was developed as an antioxidant to prevent degradation of phospholipids by hydroperoxides. It consisted of TPP covalently conjugated to an ebselen moiety. In

RBL-2H3 rats, basophilic leukemia cells stressed using 2-deoxyglucose or $H_2O_2$, both MitoPeroxidase and ebselen were found to decrease caspase 3 activity and the likelihood of apoptosis (122). TPP has also been used to create mitochondriotropic compounds for other purposes. Thiobutyltriphenylphosphonium bromide was successfully used to specifically label thiol proteins in mitochondria via Western blotting using an anti-TPP monoclonal antibody as a probe. An mtDNA-specific alkylating agent was created incorporating TPP in the compound [4-((11aS)-7-methoxy-1,2,3,11a-tetrahydro-5H-pyrrolo[2,1-c][1,4]benzodiazepin-5-on-8-oxy)butyl]-triphenylphosphonium iodide to derivatize guanidine bases. However, this compound failed to alter the mtDNA in living cells (127).

1.6.3.2 TPP: Membrane Transduction and Trafficking of Macromolecules

TPP caught the attention of those working on polymeric drug carriers when, in 2001, it was successfully used to target macromolecules to mitochondria. Murphy et al. found that terminally functionalized TPP targeted antisense PNAs (peptide nucleic acids) localized within isolated mitochondria and co-localized in the mitochondria of whole cells in vitro (116). Furthermore, it was reported that TPP-PNA conjugates as large as 4 kDa incubated with live cells were directly transduced through the plasma membrane, trafficked through the cytosol, and passed through the inner and outer membranes of mitochondria in high concentrations. It was hypothesized that the terminal TPP cation destabilized the structure of lipid bilayers sufficiently to allow a large, linear, uncharged macromolecule to be inserted into and pulled through the plasma membrane and mitochondrial membrane due to the electrostatic force produced by transmembrane potential.

In the initial paper, TPP-PNA conjugates were created that contained an antisense sequence specific for the point mutation in mtDNA that causes the 'myoclonic epilepsy and ragged red fibres' (MERRF) phenotype in cultured cells. Mitochondrial localization was confirmed in living cells using a TPP-specific electrode, anti-TPP immunoblotting after subcellular fractionation, confocal microscopy, immunogold SEM, and by crosslinking to mitochondrial matrix proteins. Although PCR probing of mRNA expression indicated antisense activity in cell-free systems, the conjugate failed to block the expression of the mutated gene. Direct plasma membrane penetration was further supported using TPP-PNAs where the TPP moiety was attached using a linker containing a disulfide bond. The compound was designed to allow the TPP moiety to be released upon transduction to the cytosol after reduction by the glutathione activity found in cytoplasm. Cytosol-specific delivery was demonstrated in mouse P388 cells incubated with conjugates containing antisense PNAs for the Pax2 protein. It was found that the expression of the Pax2 protein decreased by 85-90% (115).

### 1.6.4 Mitochondriotropic Semitelechelic TPP-HPMA Copolymers

Like PNAs, HPMA homopolymers are also linear, uncharged, hydrophilic macromolecular polymers. Indeed, the balance of hydrophilicity/hydrophobicity of PNA and pHPMA is very similar (128). It was therefore hypothesized that pHPMA polymer chains with a single terminal TPP cation end-group would possess the same membrane transduction and mitochondriotropic properties observed using TPP-PNA. Since either one of these properties could be exploited for variety of possible drug carrier applications, a series of “TPP-HPMA” copolymers were synthesized, characterized and tested for their

membrane transduction and mitochondria-localization properties.

The TPP-HPMA copolymers synthesized were semitelechelic HPMA copolymers possessing a single TPP end group on one terminus. Polymerizing semitelechelic TPP-HPMA polymers was performed in single step via the use of a thiol chain transfer agent containing TPP, thereby creating low-molecular weight polymer chains each possessing single cation fixed on one terminus of the final polymer (Figure 1.7.). The use of a chain transfer agent also allowed for more control over the molecular weight of the resulting polymers, yielding lower molecular weight with low polydispersity.

For trafficking experiments, semitelechelic TPP-HPMA copolymers were created using methacroylylated monomers containing either fluorescein or BODIPY® FL (4,4-difluoro-5,7-dimethyl-4-bora-3a,4a-diaza-s-indacene) to act as drug models and to allow for microscopic visualization of the polymers in vitro and in vivo (128). Since it was unknown how sensitive the activity of TPP cation's function would be to the single carboxylate negative charge on fluorescein, uncharged fluorescent marker BODIPY® FL was included to ensure that the resulting copolymers attached to TPP were electrically neutral. Mitochondrial localization was characterized incubating cultured ovarian carcinoma cells in media containing the copolymers, by measuring copolymer binding to isolated mitochondria from mouse liver, and by microinjection of TPP-HPMA copolymer solutions into live cells. Cell uptake and intracellular trafficking of the copolymers was characterized by confocal microscopy using cultured carcinoma cells.

This study represented an initial feasibility study on the use of the lipophilic cation TPP to targeted HPMA copolymers to mitochondria in living cells. It was also an evaluation of the limits of the membrane transduction potential of TPP. If successful, many

diseases could hypothetically be treated using mitochondriotropic drug carriers. Further, proof of direct transduction through the cell's plasma membrane would represent an entirely new method carrying drugs to the cytosol that didn't rely on active uptake by endocytosis pathways.

## 1.7 A Large Polymer Array – a Synthetic Polymer Library

Since the development of simple polymer conjugates, many new polymers for drug delivery have been developed that employ a huge array of functions that control biodistribution, bioavailability, biodegradability, cell targeting, and subcellular trafficking. Polymers of different types are incorporated into these nanocarriers that include micelles, polymersomes, dendrimers, nanohydrogels, nanoparticles and nanotubules (129). However, these innovations are still in their infancy and basic knowledge of how these materials interact with living organisms, and how to control the various biological functions of these materials remains lacking. The motivation of the work described in Chapter 4 was to gain a systematic understanding of how cells can interact with a variety of synthetic materials.

A review of contemporary literature revealed that there are large gaps in our understanding of how synthetic macromolecules interact with living cells. Experiments designed to directly transduce HPMA copolymers into the cytoplasm of living cells was difficult to evaluate since little is known about how basic physio-chemical characteristics of synthetic materials affect the distribution and transport of nanoparticles within cells. Basic information, such as the diffusivity of synthetic polymers through cytoplasm, was unknown or incomplete. Other general characterizations were also incomplete. Little was

known regarding how charge, molecular weight, and relative hydrophilicity affect binding to cell membranes, cell uptake, intracellular trafficking, membrane transduction, cell toxicity, intracellular distribution and fate.

### 1.7.1 An HPMA Copolymer Array

HPMA copolymers are extremely versatile for incorporating monomers containing various other chemical moieties and functional groups. In contrast with PEG, the incorporation of methacryloylated comonomers is straightforward and the contents of the resulting copolymers is predictable based on the ratios of the feed monomers. Given this flexibility, a large array of HPMA copolymers was created that possessed a very wide range of different charges, charge densities and hydrophilicities (Figure 1.8.). The comonomers used included weak and strong acids, weak and strong bases, and methacryoylated (MA) peptide monomers with varying numbers of hydrophobic amino acids. The general reaction scheme is shown in Figure 1.9. Each polymer was fractionated based on molecular weight using identical size-exclusion chromatography protocols to create parallel “ladders” of copolymer molecular weight standards.

This work represents a systematic approach to characterizing how the physio-chemical features of water soluble polymers interact with the cell. In one experimental series, each of the polymers was microinjected in live cultured cells and the distribution of the cells over time was monitored in detail using time-lapse confocal microscopy (130). In the other experimental series, live cells were incubated in media containing each copolymer and the differences in cell uptake and trafficking were observed by flow cytometry and by confocal microscopy. Details of the differences in the endocytic pathways taken by each

copolymer in this array were studied by Liu et al., and are summarized in Chapter 5 (131).

### 1.7.2 Nuclear Entry

Special interest was devoted to the rates of entry into the nucleus. Initial microinjection experiments using array copolymers revealed significant differences in the rates of polymer diffusion into the nuclei. Cytoplasmic macromolecules are typically excluded from entering membrane-limited organelles, such as mitochondria, lysosomes, the ER, in a nonspecific manner. The exception to this is the nucleus whose membrane possesses channels that allow the passive uptake of intermediate-sized macromolecules. The NPC (nuclear pore complex) of the nuclear envelope is composed of about 30 different nucleoporin proteins and is the conduit for both nuclear import and export of macromolecules, such as proteins and nucleic acids. In active transport, cargos as large as 40 nm possessing NLS (nuclear localization sequence) or NES (nuclear export sequence) signaling peptides are guided through the channel after binding to NTR (nuclear transport receptor) proteins (132). For smaller macromolecules below 10 nm, however, NPCs have been shown to act as nonspecific pores that allow exchange between the nucleus and cytoplasm by diffusion (133). As a conduit for nonbiological macromolecules, the NPCs have been shown to transmit PEG-coated gold colloid particles 4-7 nm in diameter (134). In contrast, 27 nm and 39 nm PEG-gold particles and 25 nm quantum dot particles conjugated with NLS peptide sequences have been shown to require the active nuclear import mechanism for uptake by the nucleus (132, 134, 135).

Dynamic structural modeling of several of the nucleoporins in the core of the NPC has been used to explain the dual size selection of active vs. passive nuclear transport

selection. The structure of several nucleoporins notably contains natively unfolded domains containing hydrophobic FG (phenylalanine-glycine) domains, consisting of FG, GFLG, and FXFG peptide repeats. Several different models are currently under debate to account for the dynamics of NPC transport. Ribbeck et al. (136, 137) proposed that the FG domains form a polymer brush conformation in the NPC channel that excludes larger solutes by entropic hydrophobic repulsion. Frey et al. suggested that nucleoporins form an unstructured hydrogel mesh in the core of the NPC channel through reversible crosslinks of FG peptide repeats that they possess (138). Nuclear transport receptors have been shown to possess a number of hydrophobic regions that specifically bind to nucleoporins in their FG repeat regions and have been proposed to disassociate interchain crosslinks. The pore proteins, thereby, form a 3-dimensional mesh with a simple molecular weight permeability cut-off when crosslinked. In this model of active transport, NTRs are able to open the nucleoporin mesh by "melting" the hydrogel structure and guide large macromolecules in or out of the nuclear compartment (139). Alternately, Melčák et al. proposed an interface between the α-helical regions of nucleoporins that selectively slide circumferentially to dilate the NPC pore opening after NTR binding (140).

Since this work was done, many models have been proposed for the structure and function of the NPC. However, the subject currently remains an active area of contention (141-145). Models developed since the time of this research will be discussed in detail in Chapter 5.

## 1.8 References


1. Seeley SF & Pulaski EJ (1953) The plasma substitutes: Progress report. *The American Journal of Surgery* 85(3):382-385.

2. Kopeček J, Šprincl L, & Lím D (1973) New types of synthetic infusion solutions. I. Investigation of the effect of solutions of some hydrophilic polymers on blood. *Journal of Biomedical Materials Research* 7(2):179-191.

3. Kopeček J (2009) Hydrogels from soft contact lenses and implants to self-assembled nanomaterials. *Journal of Polymer Science. Part A, Polymer chemistry* 47(22):5929-5946.

4. Kopeček J & Kopečková P (2010) HPMA copolymers: Origins, early developments, present, and future. *Advanced Drug Delivery Reviews* 62(2):122-149.

5. Frank MM & Fries LF (1991) The role of complement in inflammation and phagocytosis. *Immunology Today* 12(9):322-326.

6. Molteni L (1985) Dextran and inulin conjugates as drug carriers. *Methods in Enzymology* 112:285-298.

7. Maeda H, Ueda M, Morinaga T, & Matsumoto T (1985) Conjugation of poly(styrene-co-maleic acid) derivatives to the antitumor protein neocarzinostatin: Pronounced improvements in pharmacological properties. *Journal of Medicinal Chemistry* 28(4):455-461.

8. Kopeček J, Rejmanová P, Duncan R, & Lloyd JB (1985) Controlled release of drug model from *N*-(2-hydroxypropyl)-methacrylamide copolymers. *Annals of the New York Academy of Sciences* 446:93-104.

9. Maeda H, Seymour LW, & Miyamoto Y (1992) Conjugates of anticancer agents and polymers: Advantages of macromolecular therapeutics in vivo. *Bioconjugate Chemistry* 3(5):351-362.

10. Peterson CM, *et al.* (1996) Combination chemotherapy and photodynamic therapy with N-(2-hydroxypropyl) methacrylamide copolymer-bound anticancer drugs inhibit human ovarian carcinoma heterotransplanted in nude mice. *Cancer Research* 56(17):3980-3985.

11. Duncan R, *et al.* (1986) Fate of N-(2-hydroxypropyl)methacrylamide copolymers with pendent galactosamine residues after intravenous administration to rats. *Biochimica et Biophysica Acta* 880(1):62-71.

12. Abuchowski A, McCoy JR, Palczuk NC, van Es T, & Davis FF (1977) Effect of covalent attachment of polyethylene glycol on immunogenicity and circulating life of bovine liver catalase. *Journal of Biological Chemistry* 252(11):3582-3586.

13. Abuchowski A, Van Es T, Palczuk N, & Davis F (1977) Alteration of immunological properties of bovine serum albumin by covalent attachment of polyethylene glycol. *Journal of Biological Chemistry* 252(11):3578-3581.

14. Graham ML (2003) Pegaspargase: A review of clinical studies. *Advanced Drug Delivery Reviews* 55(10):1293-1302.

15. Graham ML, *et al.* (1998) Toxicity, pharmacology and feasibility of administration of PEG-L-asparaginase as consolidation therapy in patients undergoing bone marrow transplantation for acute lymphoblastic leukemia. *Bone Marrow Transplantation* 21(9):879-885.

16. Levy Y, *et al.* (1988) Adenosine deaminase deficiency with late onset of recurrent infections: Response to treatment with polyethylene glycol-modified adenosine deaminase. *The Journal of Pediatrics* 113(2):312-317.

17. Choueiri TK, Hutson TE, & Bukowski RM (2003) Evolving role of pegylated interferons in metastatic renal cell carcinoma. *Expert Review of Anticancer Therapy* 3(6):823-829.

18. Bailon P, *et al.* (2001) Rational design of a potent, long-lasting form of interferon: a 40 kDa branched polyethylene glycol-conjugated interferon alpha-2a for the treatment of hepatitis C. *Bioconjugate Chemistry* 12(2):195-202.

19. Wang YS, *et al.* (2002) Structural and biological characterization of pegylated recombinant interferon alpha-2b and its therapeutic implications. *Advanced Drug Delivery Reviews* 54(4):547-570.

20. Kinstler OB, *et al.* (1996) Characterization and stability of N-terminally PEGylated rhG-CSF. *Pharmaceutical Research* 13(7):996-1002.

21. Kieseier BC, *et al.* (2015) Peginterferon beta-1a in multiple sclerosis: 2-year results from ADVANCE. *Multiple Sclerosis (Houndmills, Basingstoke, England)* 21(8):1025-1035.

22. Carrera F, *et al.* (2010) Maintenance treatment of renal anaemia in haemodialysis patients with methoxy polyethylene glycol-epoetin beta versus darbepoetin alfa administered monthly: A randomized comparative trial. *Nephrology, Dialysis, Transplantation : Official Publication of the European Dialysis and Transplant Association - European Renal Association* 25(12):4009-4017.

23. Sundy JS, *et al.* (2011) Efficacy and tolerability of pegloticase for the treatment of chronic gout in patients refractory to conventional treatment: Two randomized controlled trials. *The Journal of the American Medical Association* 306(7):711-720.

24. Stidl R, *et al.* (2016) Safety of PEGylated recombinant human full-length coagulation factor VIII (BAX 855) in the overall context of PEG and PEG conjugates. *Haemophilia* 22(1):54-64.

25. Trainer PJ, *et al.* (2000) Treatment of acromegaly with the growth hormone-receptor antagonist pegvisomant. *The New England Journal of Medicine* 342(16):1171-1177.

26. Hamad I, Hunter AC, Szebeni J, & Moghimi SM (2008) Poly(ethylene glycol)s generate complement activation products in human serum through increased alternative pathway turnover and a MASP-2-dependent process. *Molecular Immunology* 46(2):225-232.

27. Moein Moghimi S, *et al.* (2006) Activation of the human complement system by cholesterol-rich and PEGylated liposomes-modulation of cholesterol-rich liposome-mediated complement activation by elevated serum LDL and HDL levels. *Journal of Liposome Research* 16(3):167-174.

28. Moghimi SM, *et al.* (2010) Complement activation cascade triggered by PEG-PL engineered nanomedicines and carbon nanotubes: The challenges ahead. *Journal of Controlled Release* 146(2):175-181.

29. Moghimi SM, *et al.* (2004) Causative factors behind poloxamer 188 (Pluronic F68, Flocor)-induced complement activation in human sera. A protective role against poloxamer-mediated complement activation by elevated serum lipoprotein levels. *Biochimica et Biophysica Acta* 1689(2):103-113.

30. Knop K, Hoogenboom R, Fischer D, & Schubert US (2010) Poly(ethylene glycol) in drug delivery: Pros and cons as well as potential alternatives. *Angewandte Chemie International Edition* 49(36):6288-6308.

31. Kumar V & Kalonia DS (2006) Removal of peroxides in polyethylene glycols by vacuum drying: Implications in the stability of biotech and pharmaceutical formulations. *AAPS PharmSciTech* 7(3):62.

32. Sung H-J, *et al.* (2010) Poly(ethylene glycol) as a sensitive regulator of cell survival fate on polymeric biomaterials: The interplay of cell adhesion and pro-oxidant signaling mechanisms. *Soft Matter* 6(20):5196-5205.

33. Sung HJ, *et al.* (2009) Synthetic polymeric substrates as potent pro-oxidant versus anti-oxidant regulators of cytoskeletal remodeling and cell apoptosis. *Journal of Cellular Physiology* 218(3):549-557.

34. Barz M, Luxenhofer R, Zentel R, & Vicent MJ (2011) Overcoming the PEG-addiction: Well-defined alternatives to PEG, from structure-property relationships to better defined therapeutics. *Polymer Chemistry* 2(9):1900-1918.

35. Venditto VJ & Szoka FC, Jr. (2013) Cancer nanomedicines: So many papers and so few drugs! *Advanced Drug Delivery Reviews* 65(1):80-88.

36. Kopeček J (1981) Soluble polymers in medicine. *Systemic Aspects of Biocompatibility* 2:159-180.

37. Trouet A, Masquelier M, Baurain R, & Deprez-De Campeneere D (1982) A covalent linkage between daunorubicin and proteins that is stable in serum and reversible by lysosomal hydrolases, as required for a lysosomotropic drug-carrier conjugate: In vitro and in vivo studies. *Proceedings of the National Academy of Sciences* 79(2):626-629.

38. Ashihara Y, Kono T, Yamazaki S, & Inada Y (1978) Modification of E. coli L-asparaginase with polyethylene glycol: Disappearance of binding ability to anti-asparaginase serum. *Biochemical and Biophysical Research Communications* 83(2):385-391.

39. Cartlidge SA, Duncan R, Lloyd JB, Kopečková—Rejmanová P, & Kopeček J (1987) Soluble, crosslinked *N*-(2-hydroxypropyl)methacrylamide copolymers as potential drug carriers: 3. Targeting by incorporation of galactosamine residues. Effect of route of administration. *Journal of Controlled Release* 4(4):265-278.

40. Wang D, *et al.* (2002) Inhibition of cathepsin K with lysosomotropic macromolecular inhibitors. *Biochemistry* 41(28):8849-8859.

41. Kaplan IM, Wadia JS, & Dowdy SF (2005) Cationic TAT peptide transduction domain enters cells by macropinocytosis. *Journal of Controlled Release* 102(1):247-253.

42. Duan H & Nie S (2007) Cell-penetrating quantum dots based on multivalent and endosome-disrupting surface coatings. *Journal of the American Chemical Society* 129(11):3333-3338.

43. Derfus AM, Chan WCW, & Bhatia SN (2004) Intracellular delivery of quantum dots for live cell labeling and organelle tracking. *Advanced Materials* 16(12):961-966.

44. Fawell S, *et al.* (1994) Tat-mediated delivery of heterologous proteins into cells. *Proceedings of the National Academy of Sciences* 91(2):664-668.

45. Astriab-Fisher A, Sergueev DS, Fisher M, Shaw BR, & Juliano RL (2000) Antisense inhibition of P-glycoprotein expression using peptide-oligonucleotide conjugates. *Biochemical Pharmacology* 60(1):83-90.

46. Nori A, Jensen KD, Tijerina M, Kopečková P, & Kopeček J (2003) Subcellular trafficking of HPMA copolymer-Tat conjugates in human ovarian carcinoma cells. *Journal of Controlled Release* 91(1-2):53-59.

47. Shokolenko IN, Alexeyev MF, LeDoux SP, & Wilson GL (2005) TAT-mediated protein transduction and targeted delivery of fusion proteins into mitochondria of breast cancer cells. *DNA Repair (Amst)* 4(4):511-518.

48. Tkachenko AG, *et al.* (2004) Cellular trajectories of peptide-modified gold particle complexes: Comparison of nuclear localization signals and peptide transduction domains. *Bioconjugate Chemistry* 15(3):482-490.

49. Wadia JS & Dowdy SF (2005) Transmembrane delivery of protein and peptide drugs by TAT-mediated transduction in the treatment of cancer. *Advanced Drug Delivery Reviews* 57(4):579-596.

50. Wadia JS, Stan RV, & Dowdy SF (2004) Transducible TAT-HA fusogenic peptide enhances escape of TAT-fusion proteins after lipid raft macropinocytosis. *Nature Medicine* 10(3):310-315.

51. Behr J-P (1997) The proton sponge: A trick to enter cells the viruses did not exploit. *CHIMIA International Journal for Chemistry* 51(1-2):34-36.

52. Freeman EC, Weiland LM, & Meng WS (2013) Modeling the proton sponge hypothesis: Examining proton sponge effectiveness for enhancing intracellular gene delivery through multiscale modeling. *Journal of Biomaterials Science. Polymer Edition* 24(4):398-416.

53. Sawant RR, *et al.* (2012) Polyethyleneimine-lipid conjugate-based pH-sensitive micellar carrier for gene delivery. *Biomaterials* 33(15):3942-3951.

54. Zhang Y, Satterlee A, & Huang L (2012) In vivo gene delivery by nonviral vectors: overcoming hurdles? *Molecular Therapy* 20(7):1298-1304.

55. Parham P (1983) On the fragmentation of monoclonal IgG1, IgG2a, and IgG2b from BALB/c mice. *Journal of Immunology* 131(6):2895-2902.

56. Liu H & May K (2012) Disulfide bond structures of IgG molecules: Structural variations, chemical modifications and possible impacts to stability and biological function. *mAbs* 4(1):17-23.

57. Fowers KD, Callahan J, Byron P, & Kopeček J (2001) Preparation of Fab' from murine IgG2a for thiol reactive conjugation. *Journal of Drug Targeting* 9(4):281-294.

58. de Gast GC, van de Winkel JG, & Bast BE (1997) Clinical perspectives of bispecific antibodies in cancer. *Cancer Immunology, Immunotherapy* 45(3-4):121-123.

59. van Spriel AB, van Ojik HH, & van De Winkel JG (2000) Immunotherapeutic perspective for bispecific antibodies. *Immunology Today* 21(8):391-397.

60. Kamta J, Chaar M, Ande A, Altomare DA, & Ait-Oudhia S (2017) Advancing cancer therapy with present and emerging immuno-oncology approaches. *Frontiers in Oncology* 7:64.

61. Yuraszeck T, Kasichayanula S, & Benjamin JE (2017) Translation and clinical development of bispecific t-cell engaging antibodies for cancer treatment. *Clinical Pharmacology and Therapeutics* 101(5):634-645.

62. Zhang X, Yang Y, Fan D, & Xiong D (2017) The development of bispecific antibodies and their applications in tumor immune escape. *Experimental Hematology & Oncology* 6:12.

63. Zhukovsky EA, Morse RJ, & Maus MV (2016) Bispecific antibodies and CARs: Generalized immunotherapeutics harnessing T cell redirection. *Current Opinion in Immunology* 40:24-35.

64. Kontermann RE (2011) Strategies for extended serum half-life of protein therapeutics. *Current Opinion in Biotechnology* 22(6):868-876.

65. Niewoehner J, *et al.* (2014) Increased brain penetration and potency of a therapeutic antibody using a monovalent molecular shuttle. *Neuron* 81(1):49-60.

66. Kontermann RE (2012) Dual targeting strategies with bispecific antibodies. *mAbs* 4(2):182-197.

67. Chames P & Baty D (2009) Bispecific antibodies for cancer therapy: The light at the end of the tunnel? *mAbs* 1(6):539-547.

68. Byrne H, Conroy PJ, Whisstock JC, & O'Kennedy RJ (2013) A tale of two specificities: Bispecific antibodies for therapeutic and diagnostic applications. *Trends in Biotechnology* 31(11):621-632.

69. Nogami K (2016) Bispecific antibody mimicking factor VIII. *Thrombosis Research* 141 Suppl 2:S34-35.

70. Fanger MW, Shen L, Graziano RF, & Guyre PM (1989) Cytotoxicity mediated by human Fc receptors for IgG. *Immunology Today* 10(3):92-99.

71. Fan G, Wang Z, Hao M, & Li J (2015) Bispecific antibodies and their applications. *Journal of Hematology & Oncology* 8(1):130.

72. Kreutz FT, Wishart DS, & Suresh MR (1998) Efficient bispecific monoclonal antibody purification using gradient thiophilic affinity chromatography. *Journal of Chromatography. B, Biomedical Sciences and Applications* 714(2):161-170.

73. Brinkmann U & Kontermann RE (2017) The making of bispecific antibodies. *mAbs* 9(2):182-212.

74. Xu Y, *et al.* (2015) Production of bispecific antibodies in “knobs-into-holes” using a cell-free expression system. *mAbs* 7(1):231-242.

75. Hu S, *et al.* (1996) Minibody: A novel engineered anti-carcinoembryonic antigen antibody fragment (single-chain Fv-CH3) which exhibits rapid, high-level targeting of xenografts. *Cancer Research* 56(13):3055-3061.

76. Kostelny SA, Cole MS, & Tso JY (1992) Formation of a bispecific antibody by the use of leucine zippers. *The Journal of Immunology* 148(5):1547-1553.

77. Muller KM, Arndt KM, & Pluckthun A (1998) A dimeric bispecific miniantibody combines two specificities with avidity. *FEBS Letters* 432(1-2):45-49.

78. De Jonge J, *et al.* (1995) Production and characterization of bispecific single-chain antibody fragments. *Molecular Immunology* 32(17-18):1405-1412.

79. Brennan M, Davison PF, & Paulus H (1985) Preparation of bispecific antibodies by chemical recombination of monoclonal immunoglobulin G1 fragments. *Science (New York, N.Y.)* 229(4708):81-83.

80. Hamblin TJ, *et al.* (1987) Initial experience in treating human lymphoma with a chimeric univalent derivative of monoclonal anti-idiotype antibody. *Blood* 69(3):790-797.

81. Segal DM & Snider DP (1989) Targeting and activation of cytotoxic lymphocytes. *Chemical Immunology* 47:179-213.

82. Quadri SM, Lai J, Mohammadpour H, Vriesendorp HM, & Williams JR (1993) Assessment of radiolabeled stabilized $F(ab')_2$ fragments of monoclonal antiferritin in nude mouse model. *Journal of Nuclear Medicine* 34(12):2152-2159.

83. Glennie MJ, McBride HM, Worth AT, & Stevenson GT (1987) Preparation and performance of bispecific F(ab' gamma)2 antibody containing thioether-linked Fab' gamma fragments. *The Journal of Immunology* 139(7):2367-2375.

84. Stalteri MA & Mather SJ (1995) A cross-linked monoclonal antibody fragment for improved tumor targeting. *Bioconjugate Chemistry* 6(2):179-186.

85. Stevenson GT, Anderson VA, Kan KS, & Worth AT (1997) Conjugation of human Fc gamma in closed-hinge or open-hinge configuration to Fab'gamma and analogous ligands. *The Journal of Immunology* 158(5):2242-2250.

86. Tutt A, Stevenson GT, & Glennie MJ (1991) Trispecific F(ab')3 derivatives that use cooperative signaling via the TCR/CD3 complex and CD2 to activate and redirect resting cytotoxic T cells. *The Journal of Immunology* 147(1):60-69.

87. DeSilva BS & Wilson GS (1995) Solid phase synthesis of bifunctional antibodies. *Journal of Immunological Methods* 188(1):9-19.

88. Adams GP, *et al.* (1993) Highly specific in vivo tumor targeting by monovalent and divalent forms of 741F8 anti-c-erbB-2 single-chain Fv. *Cancer Research* 53(17):4026-4034.

89. Schott ME, Frazier KA, Pollock DK, & Verbanac KM (1993) Preparation, characterization, and in vivo biodistribution properties of synthetically cross-linked multivalent antitumor antibody fragments. *Bioconjugate Chemistry* 4(2):153-165.

90. Werlen RC, *et al.* (1996) Preparation of a trivalent antigen-binding construct using polyoxime chemistry: Improved biodistribution and potential for therapeutic application. *Cancer Research* 56(4):809-815.

91. Liu J, *et al.* (2012) Prostate-cancer-targeted *N*-(2-hydroxypropyl)methacrylamide copolymer/docetaxel conjugates. *Macromolecular Bioscience* 12(3):412-422.

92. Seymour LW, *et al.* (1991) Synthetic polymers conjugated to monoclonal antibodies: Vehicles for tumour-targeted drug delivery. *Selective Cancer Therapeutics* 7(2):59-73.

93. Lu ZR, Kopečková P, & Kopeček J (1999) Polymerizable Fab' antibody fragments for targeting of anticancer drugs. *Nature Biotechnology*17(11):1101-1104.

94. Johnson RN, Kopečková P, & Kopeček J (2009) Synthesis and evaluation of multivalent branched HPMA copolymer-Fab' conjugates targeted to the B-cell antigen CD20. *Bioconjugate Chemistry* 20(1):129-137.

95. Johnson RN, Kopečková P, & Kopeček J (2012) Biological activity of anti-CD20 multivalent HPMA copolymer-Fab' conjugates. *Biomacromolecules* 13(3):727-735.

96. Chu TW, Yang J, & Kopeček J (2012) Anti-CD20 multivalent HPMA copolymer-Fab' conjugates for the direct induction of apoptosis. *Biomaterials* 33(29):7174-7181.

97. Adlam VJ, *et al.* (2005) Targeting an antioxidant to mitochondria decreases cardiac ischemia-reperfusion injury. *FASEB Journal : Official Publication of the Federation of American Societies for Experimental Biology* 19(9):1088-1095.

98. Armstrong JS (2006) Mitochondria: A target for cancer therapy. *British Journal Of Pharmacology* 147(3):239-248.

99. Manion MK & Hockenbery DM (2003) Targeting BCL-2-related proteins in cancer therapy. *Cancer Biology & Therapy* 2(4 Suppl 1):S105-114.

100. Webb A, *et al.* (1997) BCL-2 antisense therapy in patients with non-Hodgkin lymphoma. *Lancet (London, England)* 349(9059):1137-1141.

101. Manion MK, Fry J, Schwartz PS, & Hockenbery DM (2006) Small-molecule inhibitors of Bcl-2. *Current Opinion in Investigational Drugs (London, England : 2000)* 7(12):1077-1084.

102. Manfredi G, *et al.* (2003) BCL-2 improves oxidative phosphorylation and modulates adenine nucleotide translocation in mitochondria of cells harboring mutant mtDNA. *The Journal of Biological Chemistry* 278(8):5639-5645.

103. Bohni PC, Daum G, & Schatz G (1983) Import of proteins into mitochondria. Partial purification of a matrix-located protease involved in cleavage of mitochondrial precursor polypeptides. *The Journal of Biological Chemistry* 258(8):4937-4943.

104. Del Gaizo V & Payne RM (2003) A novel TAT-mitochondrial signal sequence fusion protein is processed, stays in mitochondria, and crosses the placenta. *Molecular Therapy* 7(6):720-730.

105. Johnson LV, Walsh ML, & Chen LB (1980) Localization of mitochondria in living cells with rhodamine 123. *Proceedings of the National Academy of Sciences* 77(2):990-994.

106. Wu FS (1987) Localization of mitochondria in plant cells by vital staining with rhodamine 123. *Planta* 171(3):346-357.

107. Fernandez-Carneado J, *et al.* (2005) Highly efficient, nonpeptidic oligoguanidinium vectors that selectively internalize into mitochondria. *The Journal of the American Chemical Society* 127(3):869-874.

108. Goun EA, Pillow TH, Jones LR, Rothbard JB, & Wender PA (2006) Molecular transporters: Synthesis of oligoguanidinium transporters and their application to drug delivery and real-time imaging. *Chembiochem : A European Journal of Chemical Biology* 7(10):1497-1515.

109. Kandela IK, Lee W, & Indig GL (2003) Effect of the lipophilic/hydrophilic character of cationic triarylmethane dyes on their selective phototoxicity toward tumor cells. *Biotechnic & Histochemistry : Official Publication of the Biological Stain Commission* 78(3-4):157-169.

110. Kowaltowski AJ, Turin J, Indig GL, & Vercesi AE (1999) Mitochondrial effects of triarylmethane dyes. *Journal of Bioenergetics and Biomembranes* 31(6):581-590.

111. Modica-Napolitano JS, Joyal JL, Ara G, Oseroff AR, & Aprille JR (1990) Mitochondrial toxicity of cationic photosensitizers for photochemotherapy. *Cancer Research* 50(24):7876-7881.

112. Reily C, *et al.* (2013) Mitochondrially targeted compounds and their impact on cellular bioenergetics. *Redox Biology* 1(1):86-93.

113. Finichiu PG, *et al.* (2015) A mitochondria-targeted derivative of ascorbate: MitoC. *Free Radical Biology & Medicine* 89:668-678.

114. Modica-Napolitano JS & Aprille JR (2001) Delocalized lipophilic cations selectively target the mitochondria of carcinoma cells. *Advanced Drug Delivery Reviews* 49(1-2):63-70.

115. Filipovska A, Eccles MR, Smith RA, & Murphy MP (2004) Delivery of antisense peptide nucleic acids (PNAs) to the cytosol by disulphide conjugation to a lipophilic cation. *FEBS Letters* 556(1-3):180-186.

116. Muratovska A, *et al.* (2001) Targeting peptide nucleic acid (PNA) oligomers to mitochondria within cells by conjugation to lipophilic cations: Implications for mitochondrial DNA replication, expression and disease. *Nucleic Acids Research* 29(9):1852-1863.

117. Weissig V, *et al.* (1998) DQAsomes: A novel potential drug and gene delivery system made from dequalinium. *Pharmaceutical Research* 15(2):334-337.

118. Weissig V & Torchilin VP (2000) Mitochondriotropic cationic vesicles: A strategy towards mitochondrial gene therapy. *Current Pharmaceutical Biotechnology* 1(4):325-346.

119. D'Souza GG, Boddapati SV, & Weissig V (2005) Mitochondrial leader sequence--plasmid DNA conjugates delivered into mammalian cells by DQAsomes co-localize with mitochondria. *Mitochondrion* 5(5):352-358.

120. D'Souza GG, Rammohan R, Cheng SM, Torchilin VP, & Weissig V (2003) DQAsome-mediated delivery of plasmid DNA toward mitochondria in living cells. *Journal of Controlled Release* 92(1-2):189-197.

121. Smith RA, Porteous CM, Coulter CV, & Murphy MP (1999) Selective targeting of an antioxidant to mitochondria. *European Journal of Biochemistry* 263(3):709-716.

122. Filipovska A, *et al.* (2005) Synthesis and characterization of a triphenylphosphonium-conjugated peroxidase mimetic. Insights into the interaction of ebselen with mitochondria. *The Journal of Biological Chemistry* 280(25):24113-24126.

123. Kelso GF, *et al.* (2001) Selective targeting of a redox-active ubiquinone to mitochondria within cells: Antioxidant and antiapoptotic properties. *The Journal of Biological Chemistry* 276(7):4588-4596.

124. Alleva R, *et al.* (2001) Coenzyme Q blocks biochemical but not receptor-mediated apoptosis by increasing mitochondrial antioxidant protection. *FEBS Letters* 503(1):46-50.

125. Coulter CV, Kelso GF, Lin TK, Smith RA, & Murphy MP (2000) Mitochondrially targeted antioxidants and thiol reagents. *Free Radical Biology & Medicine* 28(10):1547-1554.

126. Asin-Cayuela J, Manas AR, James AM, Smith RA, & Murphy MP (2004) Fine-tuning the hydrophobicity of a mitochondria-targeted antioxidant. *FEBS Letters* 571(1-3):9-16.

127. Burns RJ & Murphy MP (1997) Labeling of mitochondrial proteins in living cells by the thiol probe thiobutyltriphenylphosphonium bromide. *Archives of Biochemistry and Biophysics* 339(1):33-39.

128. Callahan J & Kopeček J (2006) Semitelechelic HPMA copolymers functionalized with triphenylphosphonium as drug carriers for membrane transduction and mitochondrial localization. *Biomacromolecules* 7(8):2347-2356.

129. Bamrungsap S, *et al.* (2012) Nanotechnology in therapeutics: A focus on nanoparticles as a drug delivery system. *Nanomedicine (Lond)* 7(8):1253-1271.

130. Callahan J, Kopečková P, & Kopeček J (2009) Intracellular trafficking and subcellular distribution of a large array of HPMA copolymers. *Biomacromolecules* 10(7):1704-1714.

131. Liu J, *et al.* (2010) Endocytic uptake of a large array of HPMA copolymers: Elucidation into the dependence on the physicochemical characteristics. *Journal of Controlled Release* 143(1):71-79.

132. Pante N & Kann M (2002) Nuclear pore complex is able to transport macromolecules with diameters of about 39 nm. *Molecular Biology of the Cell* 13(2):425-434.

133. Paine PL, Moore LC, & Horowitz SB (1975) Nuclear envelope permeability. *Nature* 254(5496):109-114.

134. Feldherr CM & Akin D (1997) The location of the transport gate in the nuclear pore complex. *Journal of Cell Science* 110 (Pt 24):3065-3070.

135. Chen AA, Derfus AM, Khetani SR, & Bhatia SN (2005) Quantum dots to monitor RNAi delivery and improve gene silencing. *Nucleic Acids Research* 33(22):e190.

136. Ribbeck K & Görlich D (2001) Kinetic analysis of translocation through nuclear pore complexes. *EMBO* 20(6):1320-1330.

137. Ribbeck K & Görlich D (2002) The permeability barrier of nuclear pore complexes appears to operate via hydrophobic exclusion. *EMBO* 21(11):2664-2671.

138. Frey S, Richter RP, & Görlich D (2006) FG-rich repeats of nuclear pore proteins form a three-dimensional meshwork with hydrogel-like properties. *Science (New York, N.Y.)* 314(5800):815-817.

139. Bickel T & Bruinsma R (2002) The nuclear pore complex mystery and anomalous diffusion in reversible gels. *Biophysical Journal* 83(6):3079-3087.

140. Melčák I, Hoelz A, & Blobel G (2007) Structure of Nup58/45 suggests flexible nuclear pore diameter by intermolecular sliding. *Science (New York, N.Y.)* 315(5819):1729-1732.

141. Alber F, *et al.* (2007) The molecular architecture of the nuclear pore complex. *Nature* 450(7170):695-701.

142. Ando D & Gopinathan A (2017) Cooperative interactions between different classes of disordered proteins play a functional role in the nuclear pore complex of baker's yeast. *PloS one* 12(1):e0169455.

143. Ando D, *et al.* (2014) Nuclear pore complex protein sequences determine overall copolymer brush structure and function. *Biophysical Journal* 106(9):1997-2007.

144. Beck M & Medalia O (2008) Structural and functional insights into nucleocytoplasmic transport. *Histology and Histopathology* 23(8):1025-1033.

145. Yang W & Musser SM (2006) Nuclear import time and transport efficiency depend on importin beta concentration. *The Journal of Cell Biology* 174(7):951-961.

146. Klein JS & Bjorkman PJ (2010) Few and far between: How HIV may be evading antibody avidity. *PLoS Pathogens* 6(5):e1000908.

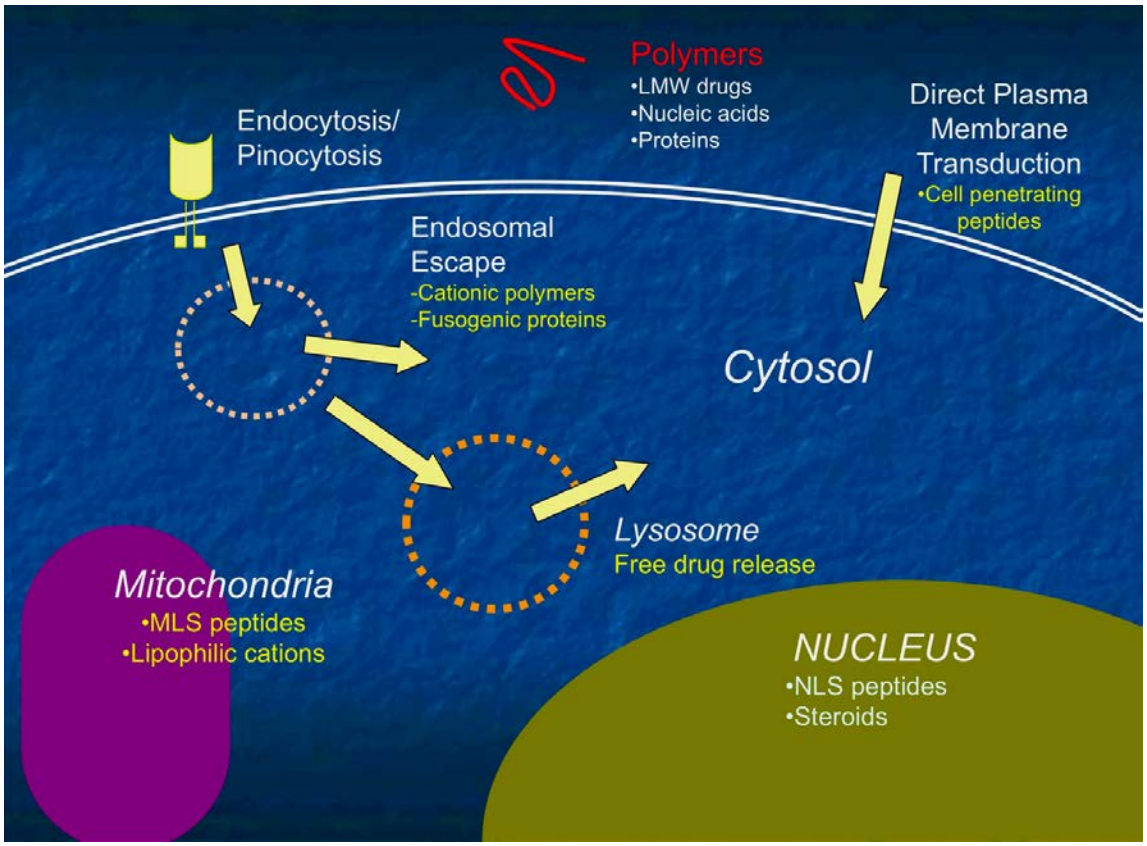


Figure 1.1. Summary of the cell surface and intracellular targets for drug carriers and the pathways to cell uptake

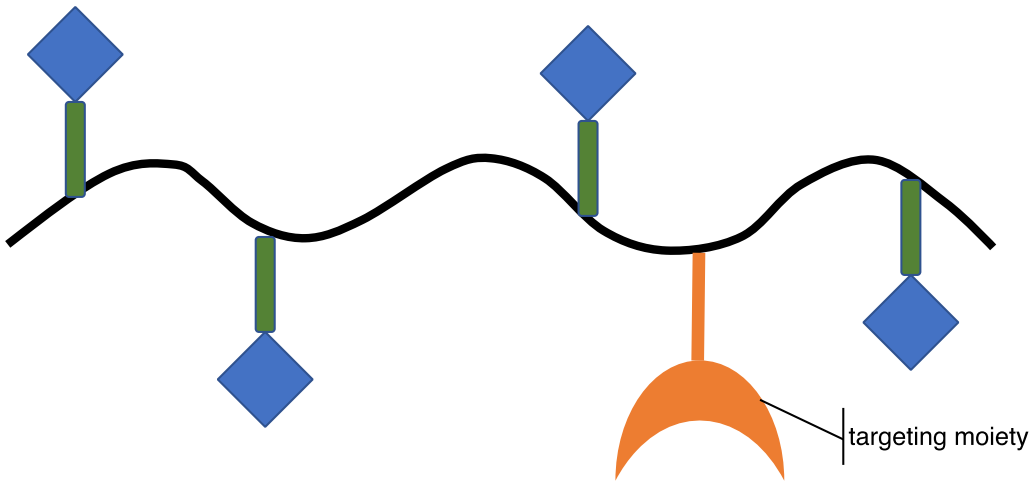


Figure 1.2. Schematic model of targetable polymer drug conjugates with degradable drug linkers

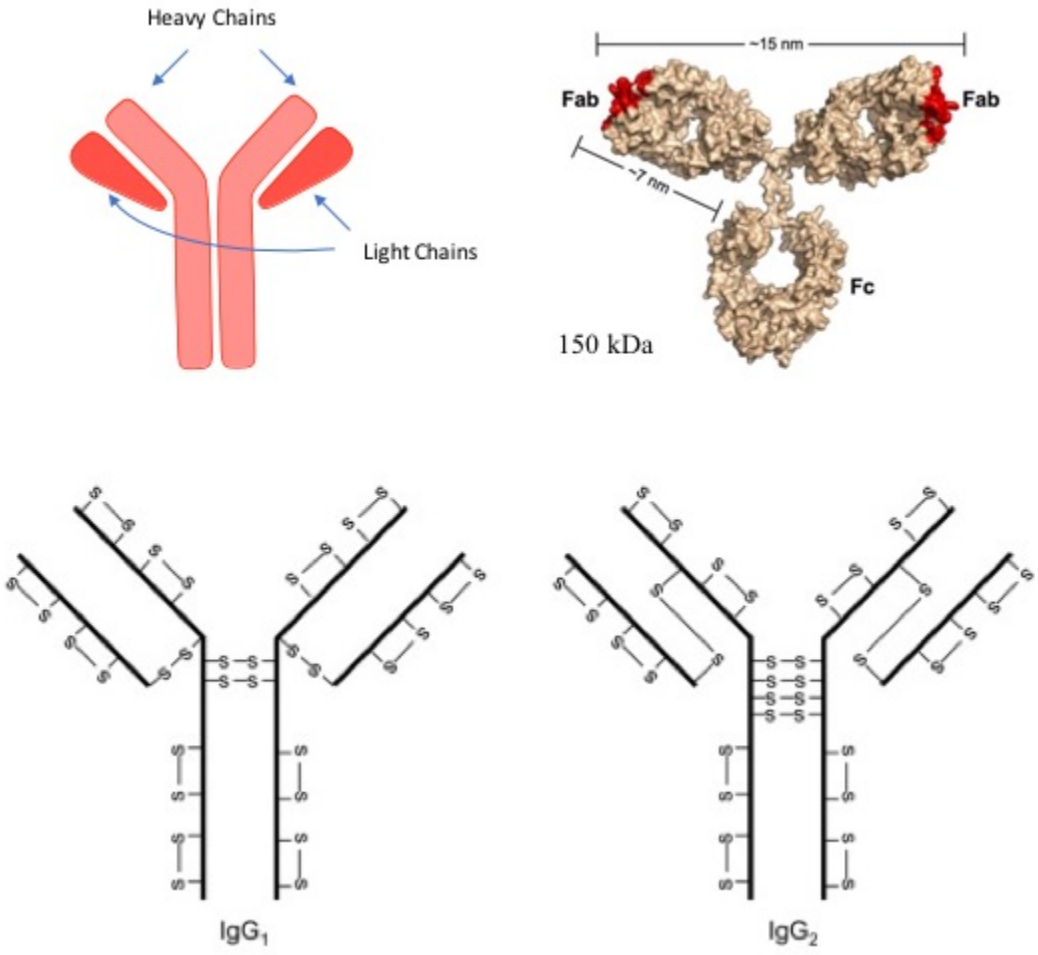


Figure 1.3. Depictions of the basic structure of the IgG protein. Lower half illustrates the differences in disulfide bridging between IgG1 and IgG2 isotype antibodies. Adapted from (146)

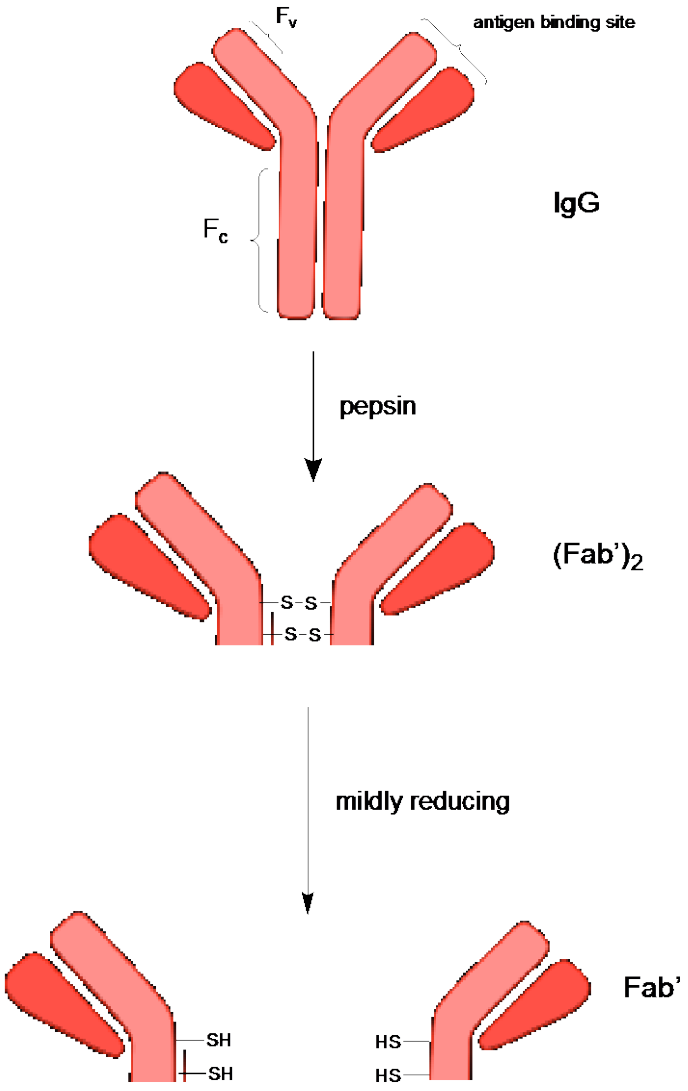


Figure 1.4. General scheme to produce Fab' fragments from IgG antibodies

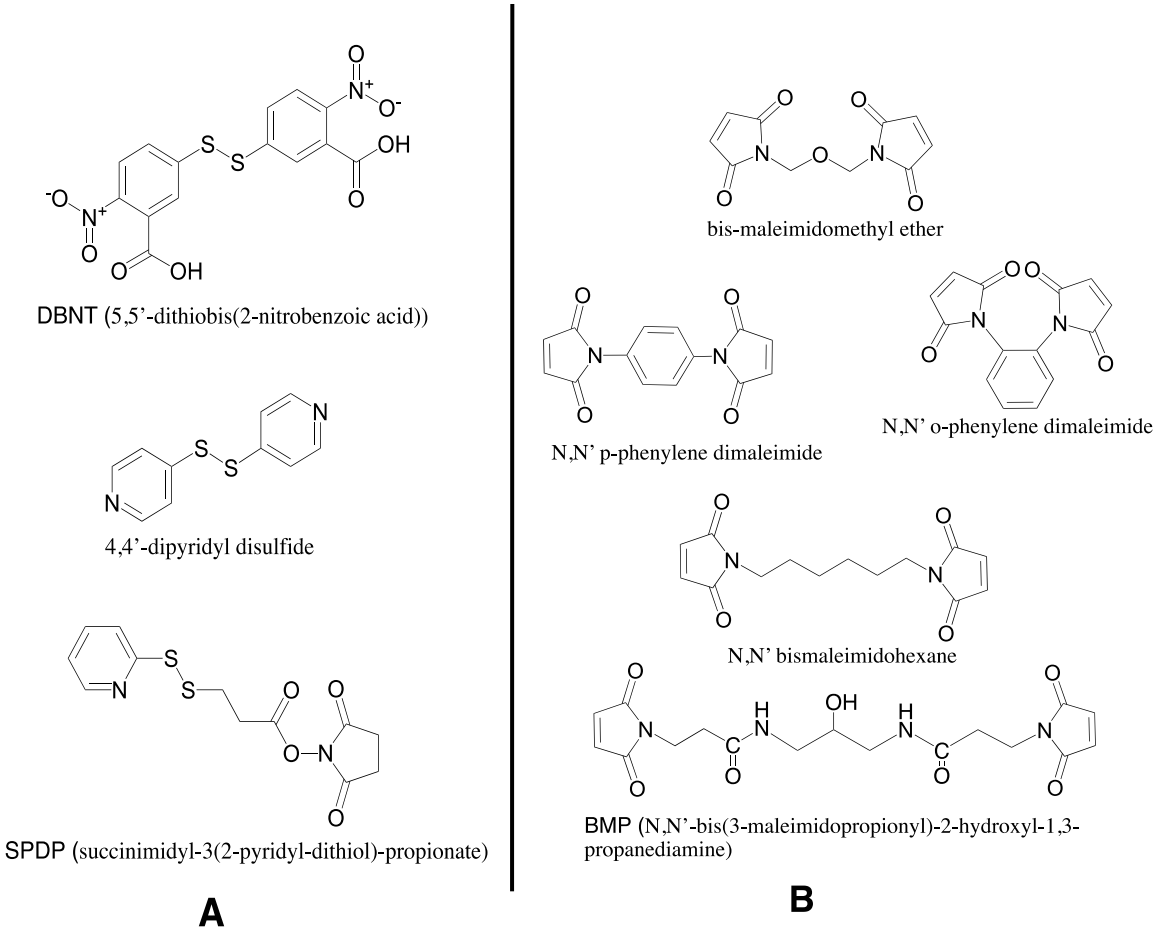


Figure 1.5. Structures of thiol crosslinkers used in early protein conjugation studies. A) Disulfide crosslinkers based on thiol exchange; B) Structures of bismaleimide thiol crosslinkers

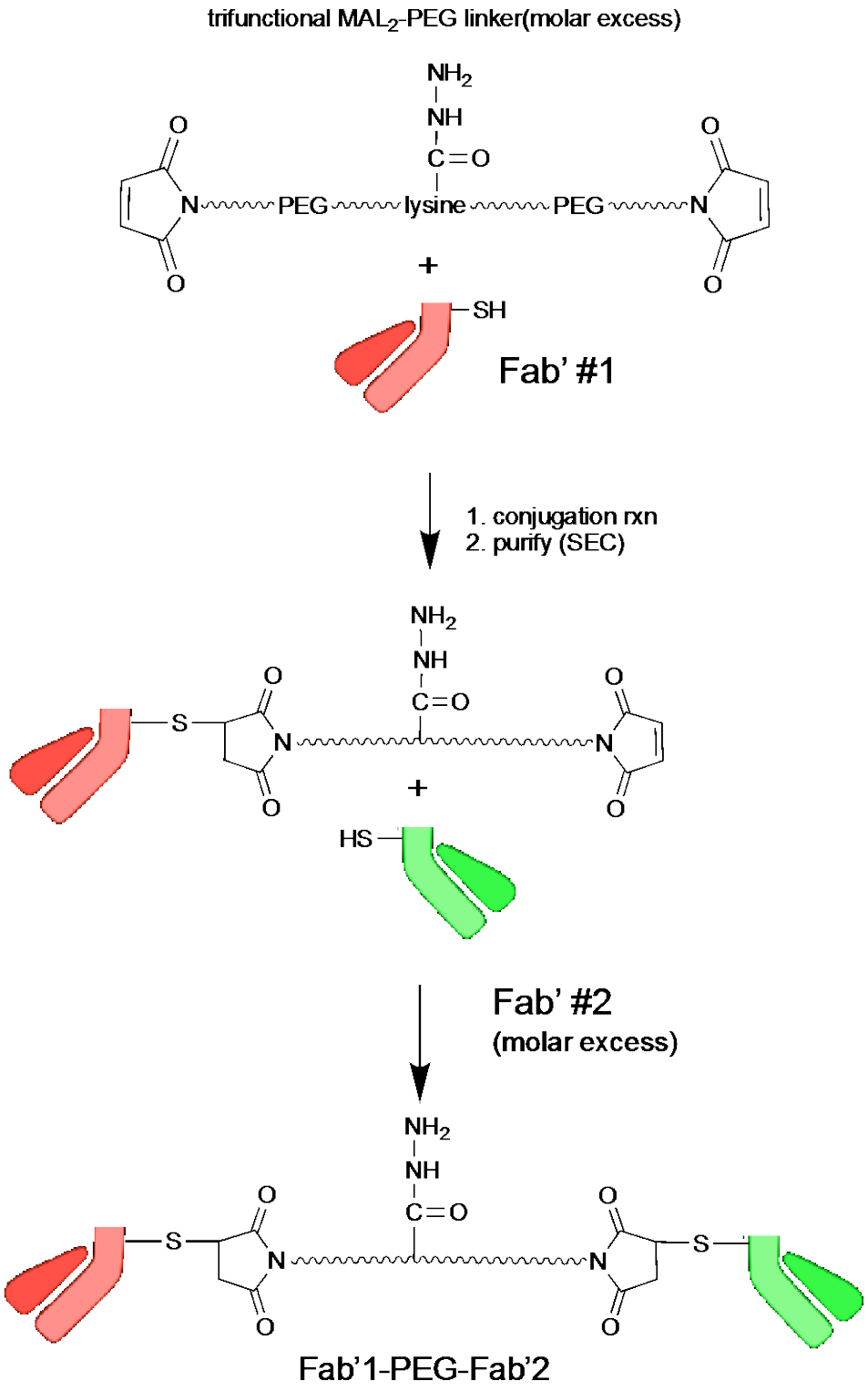


Figure 1.6. General method to dimerize bispecific Fab' fragments using a bismaleimide PEG crosslinker with a central acyl hydrazide functional group

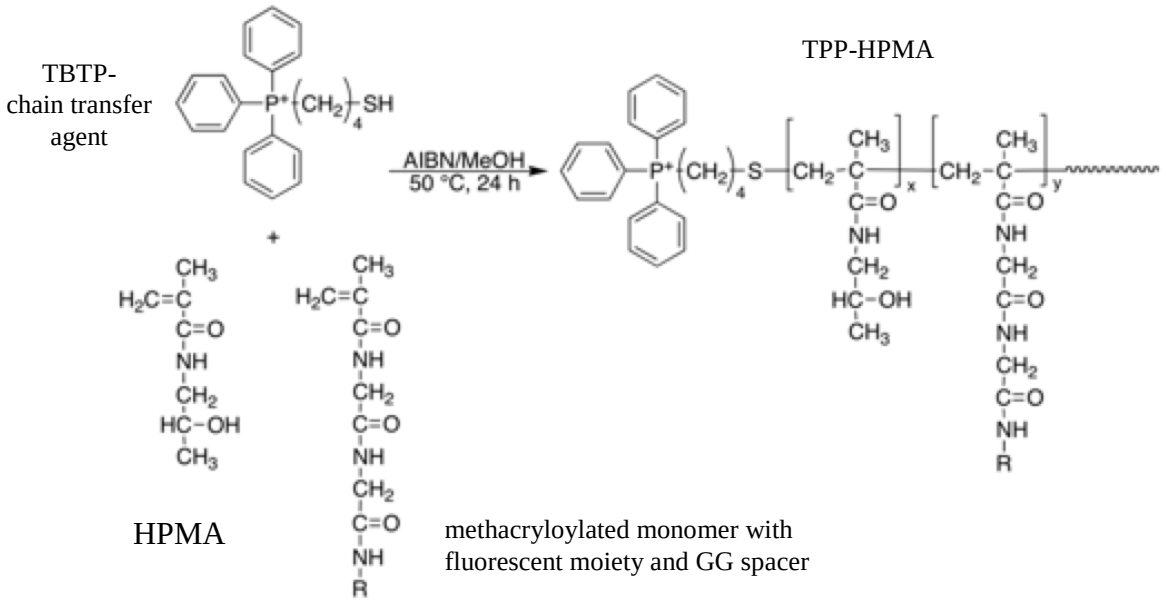


Figure 1.7. General synthesis of TPP-functionalized semitelechelic HPMA copolymers.

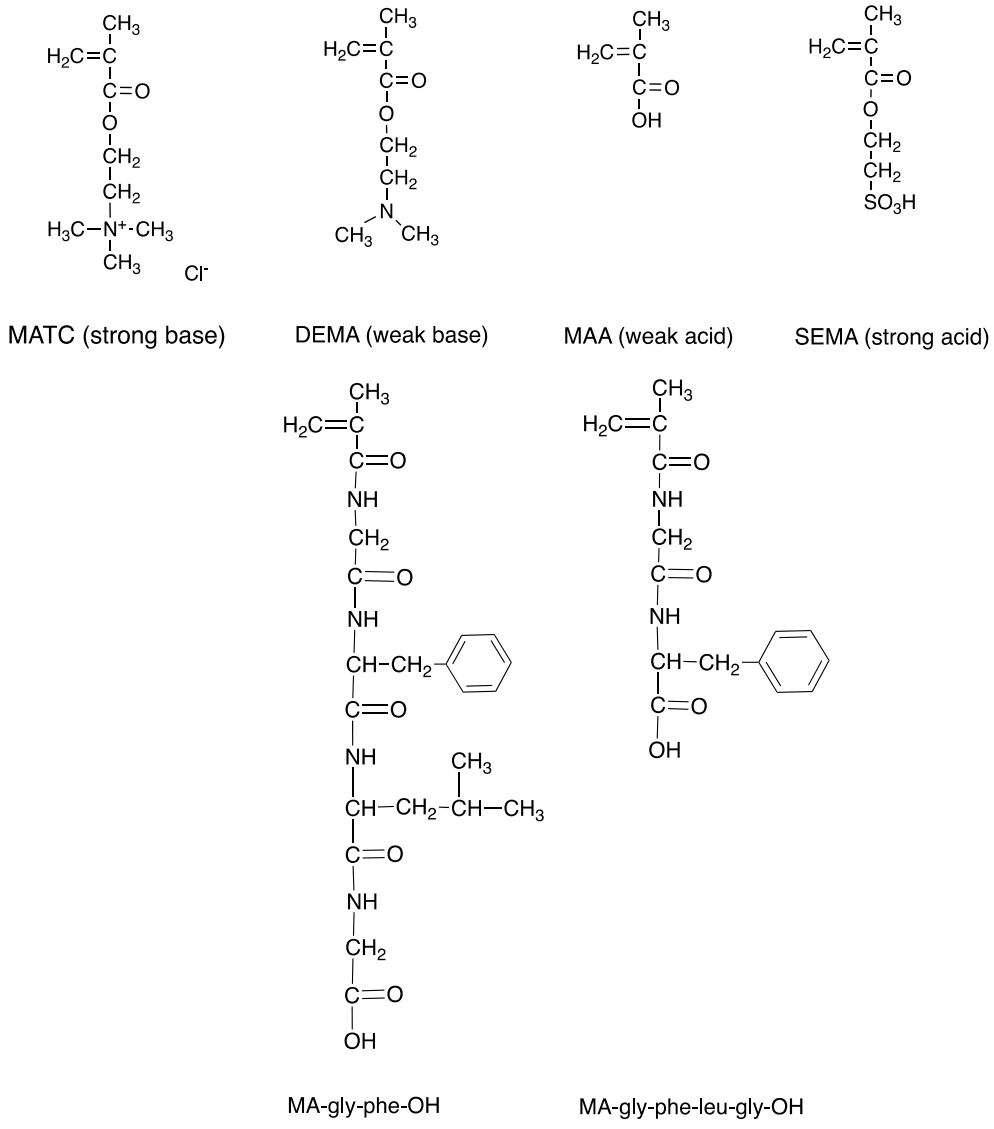


Figure 1.8. Comonomers used for the large array of the HPMA copolymers

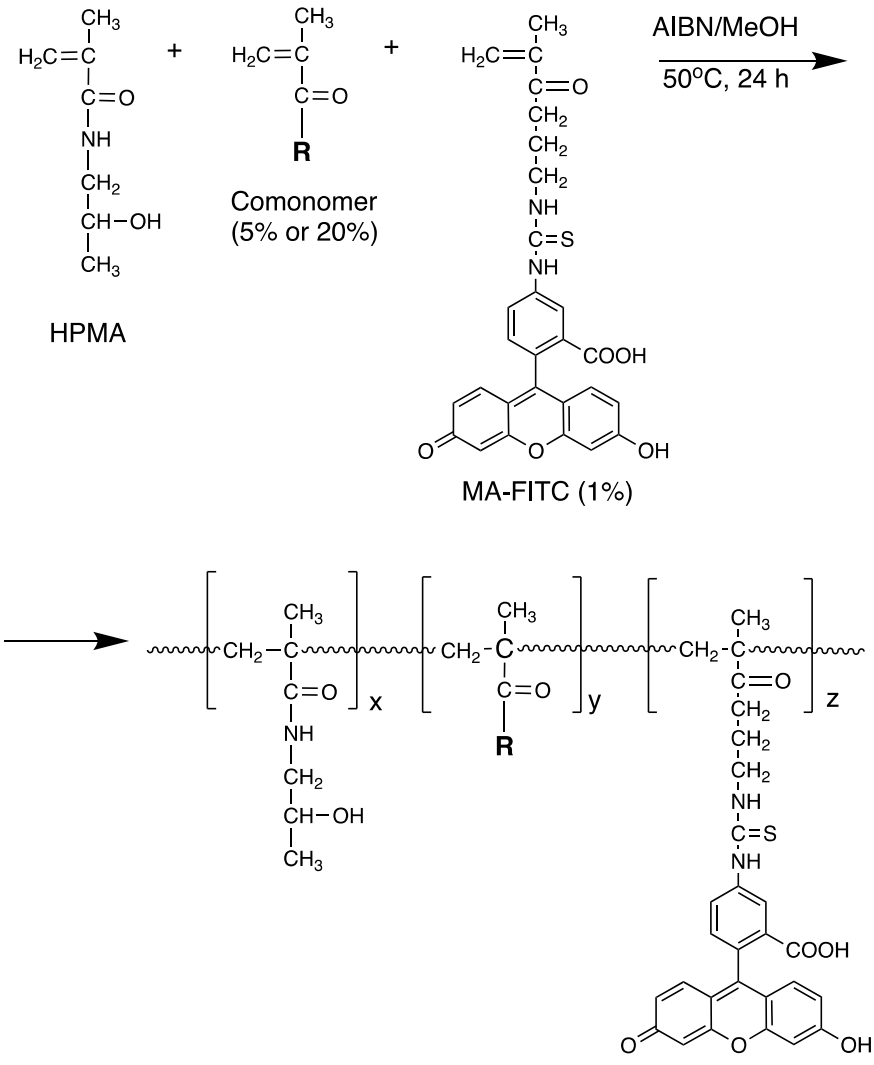


Figure 1.9. Summary of polymer reaction used for large copolymer array

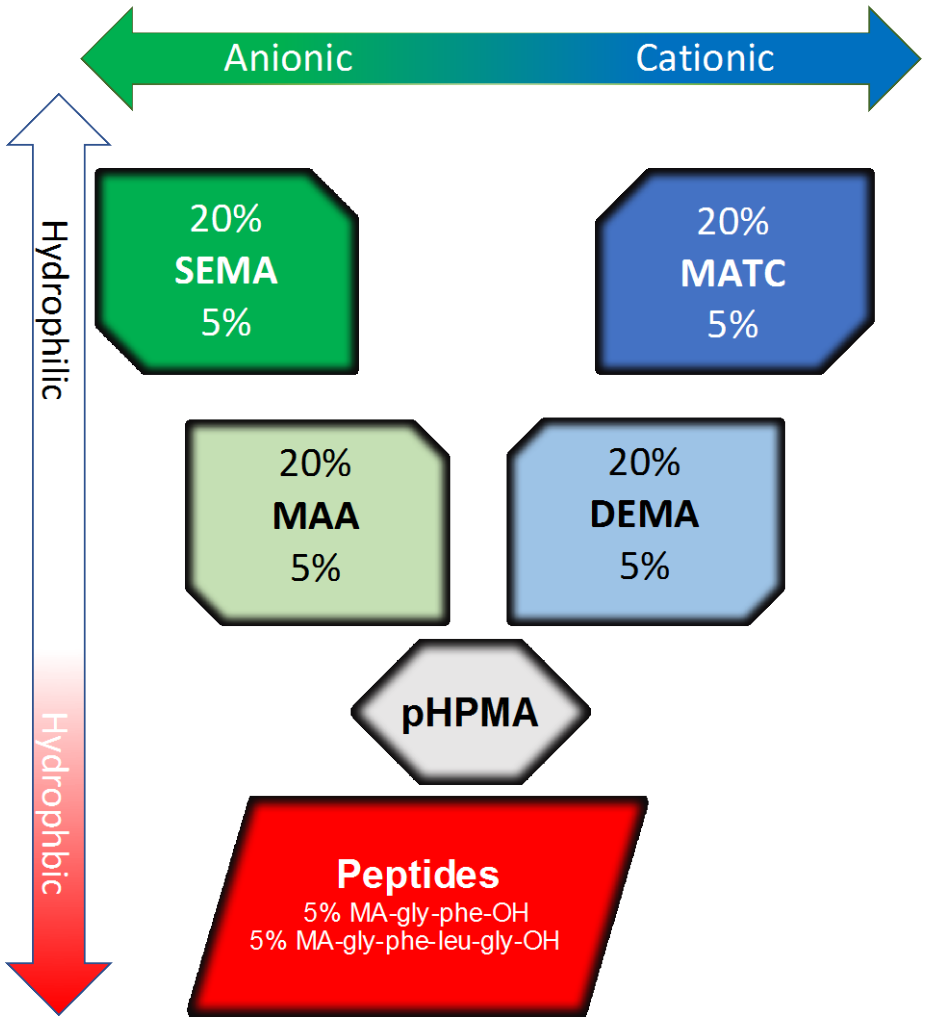


Figure 1.10. Representation of the chemical characteristics of the HPMA copolymers in the large polymer array

# CHAPTER 2

# PEG-DIMERIZED Fab' CONJUGATES FOR THE TARGETING OF HPMA COPOLYMER-DRUG CONJUGATES

## 2.1 Introduction

Monoclonal antibodies and Fab' antibody fragments previously have been incorporated into drug-polymer conjugates to selectively target drug delivery to cancer cells(1-3). Antibodies bind very specifically and avidly to cell surface antigens, but their high-molecular weight and interactions between lymphocytes and the Fc of the whole antibody often limits their usefulness for conjugate targeting. To avoid these issues, isolated Fab' fragments have been used. However, they possess much lower binding affinities and yield less effective cell uptake rates as a result. When antibodies or antibody fragments are attached to polymers via nonspecific conjugation reactions, it has been shown that there is often significant loss of antibody affinity to the corresponding epitope. This loss of affinity can be attributed to several sources, including chemical alteration of the antibody antigen binding site, reduction in the translational and rotational diffusivity of the polymer-coupled antibody, and steric hindrance of the antigen binding site by the polymer backbone.

In this chapter, chemically dimerized Fab' fragments were investigated as possible targeting modules for polymer-drug conjugates. These modules were created by

the site-specific attachment of Fab' fragments using extended PEG linkers possessing two terminal thiol-specific moieties. It was hypothesized that these modules would be ideal for targeting cancer cells and would enhance cellular uptake of conjugates. PEG was used, as opposed to low molecular weight crosslinkers, to improve synthetic yields, and to possibly increase yields for a subsequent site-directed attachment of the PEG linker to HPMA-drug conjugates. Expected higher synthetic yields were hypothesized to result from the high degrees of freedom imparted to the functionalized termini of the PEG linker, and due to the lack of steric interference between the crosslinked protein fragments (4, 5). In addition, the fragments would not require a specific orientation towards each for crosslinking to occur.

An efficient chemical crosslinking method for antibody fragments was sought to create a direct and efficient method to create *bispecific* $(Fab')_2$ constructs (6). By this theoretical approach, existing monoclonal antibodies could be "mixed and matched" in any bispecific combination, thereby creating a method to quickly screen the effectiveness of bispecific approaches, and avoid the time-consuming trial and error process required for genetically engineered constructs, such as diabodies.

### 2.1.1 Bispecific Targeting for Cancer Cells

Although many surface features have been identified that can be used to target tumor cells, a general difficulty in developing targeted conjugates is the identification of antigens that are specific for tumor cells. Specific surface features of tumors cells may include the translational products of specific oncogenes and other proteins expressed on many tumor cells, such as the products of the MDR1 gene, P-glycoprotein (1). These

products, however, are usually not unique to tumor cells, but are rather overexpressed in comparison to normal cells. With targeted binding using monospecific, high-avidity antibodies, a large majority of the drug-conjugates may bind to nontumor cells with low densities of the target epitope since the number of these cells is typically much greater than tumor cells (and correspondingly, the total number of potential binding sites).

The cell surface antigens that tumor cells typically present are not only often non-specific, they are also highly variable due to the genomic and phenotypic instability of most cancer cells (7, 8). In general, most receptor proteins that tumor cells present are characteristic of the type of tissue to which oncogenesis first occurred. As the cancer progresses, however, these receptor proteins can change as the cells become more poorly differentiated. Changes in cell phenotype can also occur in response to environmental conditions, such as the selective response to various chemotherapy drugs. The design of targeted conjugates for the treatment of cancer requires not only that different targeting moieties be used for different types of cancer, but that the targets are critical to the proliferation of the cancer cells. Bispecific targeting allows the targeting of cancer cell surface antigens that are not only overexpressed, but presented in combined pairs that aren't typically found on any normal cells in the body.

### 2.2.2 Research Plan

The conjugates described here are based on targeted HPMA conjugates previously described for use against tumor cells derived from human ovarian epithelial cells. These conjugates consisted of a HPMA backbone with a fraction of sidechains substituted with either a drug (doxorubicin or mesochlorin $e_6$) or an antibody-derived targeting moiety.

The substituted chemicals are covalently bound to the backbone with a gly-phe-leu-gly tetrapeptide linker. This linker has been shown to be specifically cleaved from the conjugate by cathepsin B and to only release the conjugated drug in the lysosomal compartment (9).

Rather than use a targeting moiety based on a single monoclonal antibody, however, the goal of this research was to investigate the possibility of the use of a bi- or multispecific targeting moiety. The basic structure of the proposed targeting moiety would consist of two Fab' fragments derived from monoclonal antibodies specific for epitopes on two different proteins found on the tumor cell, connected to each end of a branched PEG linker. Single Fab' fragments have a relatively low affinity to their corresponding receptor proteins, but it was hypothesized that a bifunctional Fab' construct connected with an extended polymer linker would have a high affinity for targeted tumor cells. Since the antibody fragments are covalently linked, the binding of one should result in the cooperative binding to cell surface receptors. It was proposed that the polymeric linker possessing many degrees of conformational freedom would be long enough to span the average distance between two membrane proteins on the cell, but small enough to present the membrane surface to both fragments at the same time. It was also suggested that binding to a nontarget cell with only one target epitope would be reversible and would release the conjugate before it is endocytosed into the cell. Only cells that present both target epitopes would result in the binding of the conjugate to allow receptor-mediated endocytosis to take place and, therefore, greatly increase the uptake of the polymer-drug conjugate.

For this research, several hybridoma cell lines were obtained that produce

monoclonal IgG antibodies that specifically bind cell surface proteins known to be expressed on ovarian carcinoma cells, including P-glycoprotein, CD44/OA3, HER-2, and EGFR. Using in vitro bioreactors, hybridomas were grown at scales large enough to produce antibodies in amounts suitable for laboratory-scale synthetic chemistry. Antibodies were purified and concentrated using preparative–scale affinity chromatography. $(Fab')_2$ antibody fragments were obtained by partial enzymatic digestion of the protein in their relative open hinge regions (Figure 2.1. and Figure 2.2.). Fab' fragments were produced for site-specific attachment to polymers via free cysteine thiol groups in their hinge region (Figure 2.3.).

For proof of concept, commercially available bifunctional PEG crosslinkers were used to dimerize antibody fragments via site-specific attachment to the free thiol in the hinge region of Fab'. PEG linkers possessing maleimide or vinyl sulfone terminal moieties were used to create PEG crosslinked Fab' fragments (Figure 2.4.). Both monospecific and bispecific Fab' dimers were created (Figure 2.5. and Figure 2.6.). The effect of the PEG crosslinking on binding kinetics and uptake of the constructs by cultured ovarian carcinoma cells were compared to that of unmodified IgG antibodies.

Hemitrifunctional bismaleimide-PEG crosslinkers were synthesized to dimerize Fab' fragments via a linker that could subsequently be selectively attached to HPMA copolymer-drug conjugates. This was accomplished by coupling two heterobifunctional PEGs possessing terminal amine-specific succinimide and thiol-specific maleimide moieties (Figure 2.7.). This created a bifunctional maleimide PEG linker possessing a central carboxylate that could be subsequently functionalized with a hydrazide moiety for site-specific attachment to HPMA-doxorubicin copolymer-drug conjugate containing side

chains functionalized with a reactive p-nitrophenyl ester group (Figure 2.8.). The end goal of this work was to, in effect, create engineered bispecific antibodies with an “Fc fragment” removed and replaced with a polymer-drug conjugate, while also replacing the hinge region with a synthetic, extended PEG polymer. Different Fab’ fragments were used to create bispecific $(Fab')_2$ constructs linked by PEG hinges and the biological activity of the coupled antibody fragments was investigated.

### 2.2.3 Monoclonal Antibodies

For this work, four types of monoclonal antibodies were produced for targeting ovarian carcinoma cell lines: OV-TL16, which produces an IgG1 subclass antibody against the CD44/OA3 tumor marker; anti-EGFR (anti-epithelial growth factor receptor); anti-HER2 (anti- human epidermal growth factor receptor 2); and UIC2, an IgG2a subclass antibody against p-glycoprotein (anti-P-gp), the product of the MDR1 gene (multidrug resistance) that is frequently over-expressed in drug-resistant cancer cell lines.

### 2.2.4 $(Fab')_2$ Production-IgG2a Subclass Antibodies

Since the enzymatic cleavage methods that produce Fab’ fragments from IgG1 type antibodies is not optimizable for IgG2a antibodies, a new method to produce Fab’ from IgG2a antibodies was required to obtain Fab’ fragments from the U1C2 anti-P-gp monoclonal antibody. Extensive work was required to develop and optimize a simplified method using the enzyme lysyl endopeptidase (LE) to create IgG2a Fab’ fragments (10).

When preparing $(Fab')_2$ fragments, the IgG subclass is important in the choice of digestive enzyme (11, 12). Pepsin, lysyl endopeptidase (LE), clostripain, and

mercuripapain, among others, have been investigated to optimize preparation of $(Fab')_2$ from the mouse IgG2a subclass (12-14). LE cleavage of IgG2a has been shown to provide stable $(Fab')_2$ and Fc fragments (12). Lysyl endopeptidase has an optimal activity pH range between 8.5 and 10.7 (15), but it does retain sufficient enzymatic activity at physiological pH. Pepsin also produces stable $(Fab')_2$ fragments from IgG2a, although pepsin cleavage may result in a heterogeneous product due to broader substrate specificity (16-18).

A simple and efficient method for preparation of Fab' fragments from murine IgG2a was developed that would allow conjugation to an *N*-(2-hydroxypropyl)methacrylamide (HPMA) copolymer-drug conjugate for targeting the P-glycoprotein-expressing cell line, A2780/AD. Due to the difficulties encountered with preparation of Fab' fragments from murine IgG2a, purification of the $(Fab')_2$ fragment was carried out to prevent LE cleavage in the hinge region above the two remaining disulfide bonds. Previous literature detailing digestion with LE did not show cleavage at the secondary site following purification of $(Fab')_2$ using Protein A and ion exchange chromatography (12). Proteolytic cleavage sites in the hinge region, however, may be affected by alterations in the conformation of the protein, i.e., antigen binding, reduction of disulfide bonds, or acid pretreatment (17, 19). Select antibodies may show an increased susceptibility to proteolytic cleavage, and require optimization of the substrate to enzyme ratio, and a more thorough washing procedure to remove residual enzyme, i.e., LE.

A Protein G affinity chromatography purification procedure was developed based on known differences in avidity and the number of components in the digestion

preparation, i.e., $(Fab')_2$ and Fc fragments for LE digestion or undigested IgG2a, $(Fab')_2$, and Fab fragments for pepsin digestion (20-22). With LE enzymatic affinity in mind, a washing procedure following binding to a protein G affinity column was developed to remove residual LE following digestion to prevent further proteolytic cleavage of the $(Fab')_2$ to Fab' fragment.

### 2.2.5 Fab' Dimerization

In the first experiments, Fab' fragments derived from the OV-TL16 monoclonal antibody were first dimerized using the commercially available (Shearwater/Nektar) thiol-specific crosslinker MAL-$PEG_{3400}$-MAL, a linear PEG polymer with both termini functionalized with maleimide moieties. The binding affinity constant of the constructs was determined using OVCAR-3 ovarian carcinoma cell lines. The in vitro binding and relative rate of uptake by cancer cells was investigated using confocal fluorescence microscopy and flow cytometry. Binding constants were determined by Scatchard analysis via the binding of $^{125}$I-iodinated cells to live OVCAR-3 cells that express the CD44/OA3 receptor protein that possesses the epitope for OV-TL16.

Subsequent experiments used mAbs that recognize P-glycoprotein (UIC2), HER-2 (ATCC #11602), and EGFR (ATCC #C225) to produce Fab' fragments for dimerization. Commercially available MAL-$PEG_{3400}$-MAL, and later, a bisvinylsulfone PEG linker (VS-$PEG_{5000}$-VS) were used for Fab' dimerization experiments.

## 2.2 Materials

RPMI-1640 medium, DMEM medium, Dubelco's phosphate buffered saline (DPBS), insulin, fetal bovine serum, Boc-Val-Leu-Lys-7-amido 4-methyl coumarin, $N^{\alpha}$-tosyl-L-lysyl chloromethyl ketone, 3-(4,5-dimethylthiazol-2-yl)-2,5-diphenyltetrazolium bromide (MTT), and pepsin were purchased from Sigma (St. Louis, MO). Protein G Sepharose 4 Fast Flow column, DEAE cellulose, protein A Sepharose chromatography resins, and PD-10 columns were purchased from Pharmacia (Peapack, NJ). Lysyl endopeptidase was purchased from Wako Bioproducts (Richmond, VA). Spectra/Por 2 dialysis tubing MWCO 12-14 kDa was purchased from Spectrum Laboratories (Rancho Dominguez, CA). 4-(Maleimidomethyl)-cyclohexanecarboxylic acid N-hydroxysuccinimide ester was purchased from Aldrich (Milwaukee, WI). Bicinchoninic acid (BCA) assay was purchased from Pierce (Rockford, IL). All other chemicals were obtained commercially as reagent grade products.

## 2.3 Methods

### 2.3.1 Trifunctional Bismalemide PEG Linker

The trifunctionalized PEG linker proposed for the dimerization of Fab' fragments for the Fab'-PEG-Fab' targeting complex was synthesized by reacting L-lysine with a 10% molar excess of the heterobifunctional PEG linker MAL-$PEG_{2000}$-NHS (2 kDa molecular weight PEG end-functionalized with maleimide and *N*-hydroxysuccinimide ester moieties (Shearwater/Nektar). The reactants were first dissolved in a minimal volume of PBS, pH 5. While stirring, the pH of the reaction was raised to pH 7.5 over the course of 2 h using 0.1 N NaOH. The reaction was then continued for another 8 h. When

complete, low MW components were removed by applying to a PD-10 column equilibrated with PBS, pH 7.5. The resulting trifunctional linker (MAL-$PEG_{2000}$-lysine-$PEG_{2000}$-MAL) was purified from unreacted PEG linker using SEC (Superdex75). The SEC fractions containing the conjugate were combined and then dialyzed against water using 6-8 kDa cutoff dialysis tubing (Spectra). The product solution was then frozen and the trifunctional PEG conjugate was isolated by freeze-drying. The identity of the conjugate was confirmed using SEC retention time. The final yield was approximately 20%.

In subsequent syntheses, trifunctional linker made from heterobifunctional linkers possessing vinyl sulfone moieties, instead of maleimide, were performed using the same protocol. The reaction yield of the dimerized bisvinylsulfone trifunctional linker (VS-$PEG_{3400}$-lysine-$PEG_{3400}$-VS) was 50%. However, SAMSA thiol conjugation assays of the thiol reactivity of these conjugates showed that more than 50% of the vinyl sulfone functional groups were lost during the procedure.

### 2.3.2 Maleimide and Vinyl Sulfone Assays

The content of maleimide and vinyl sulfone functional groups in the bismaleimide and bisvinyl sulfone PEG linkers was determined by conjugation with the fluorescent marker SAMSA fluorescein [5-((2-(and-3)-S-(acetylmercapto)succinoyl)amino) fluorescein] (Fisher). In a small glass tube covered with foil, 1.3 mg of SAMSA fluorescein was activated by dissolving in 0.5 ml 0.1 M NaOH. and incubated at room temperature for 15 min. This removed the acetyl protecting group. Following activation of SAMSA FL, the solution was neutralized with ~3 μL of 6 M HCl and buffered with

approximately 0.1 ml of 0.5 M sodium phosphate at pH 7.

For the conjugation reaction, a 5-fold molar excess of SAMSA-FL was reacted with bismal-PEG in phosphate buffer. The PEG conjugate was first dissolved in 0.1 M sodium phosphate/1 mM EDTA and then combined with the activated SAMSA-FL solution. The reaction proceeded at room temperature for 2.5 h with gentle shaking. The unreacted dye was then removed by applying the reaction mixture to a PD-10 column and eluting in 0.1 M borate buffer, pH 8.3. The degree of labeling could then be determined from the absorbance of the labeled conjugate at 495 nm. The extinction coefficient of SAMSA fluorescein is 80,000 $cm^{-1}M^{-1}$ at 495 nm.

### 2.3.3 Cell Lines

The human ovarian carcinoma cell lines OVCAR-3, ES-2 and MDAH 2780 were purchased from ATCC (Rockville, MD). Ovarian carcinoma cell lines A2780, A2780/AD (doxorubicin resistant), were obtained from Dr. T.C. Hamilton (Fox Chase Cancer Center, PA). OVCAR-3 cell lines transfected with the MDR1 genes were a gift from Dr. Mikhail Slinkin. All ovarian carcinoma cells lines were cultured in RPMI-40 medium containing 10 μg/ml insulin and supplemented with 10% fetal bovine serum.

The hybridoma cell lines OV-TL16 for anti-OA3 IgG1 mAb, and UIC2 for the IgG2a against P-gp (anti-P-gp), and hybridomas for anti-EGFR and anti-HER2 were purchased from ATCC (Rockville, MD). Anti-fluorescein IgG2a antibodies from the hybridoma cell lines BDC-1 and 4-4-20 were a gift of Dr. James Herron (University of Utah) (23). All cells were cultured at 37°C in a humidified atmosphere containing 5% $CO_2$ (v/v).

### 2.3.4 Monoclonal Antibody Production

The hybridoma cells were initially cultured in DMEM medium supplemented with 10% fetal bovine serum. The amount of serum in their media was gradually reduced over a period of 2 to 3 weeks to adapt them to serum-free hybridoma medium, H-SFM (Gibco Life Sciences), prior to either producing ascites in mice or seeding the cells into a Cellco Bioreactor system.

Antibodies obtained from mouse ascites fluid were precipitated in saturated ammonium sulfate prior to being dissolved in 0.01 M $Na_2HPO_4$, 0.15 M NaCl, 0.01 M EDTA pH 7.0 buffer (buffer A). The protein solution was then filtered through a 0.2 μM filter prior to applying it to a Protein G Sepharose 4 Fast Flow column at a flow rate of 1 ml/min.

Antibody-containing hybridoma media from the bioreactors were subjected to centrifugation at 3500 rpm for 10 min and the supernatant was removed. The hybridoma media was filtered sequentially through a glass fiber, 0.45 μm, and 0.2 μm filters prior to applying it directly to the protein G affinity chromatography column. The Protein G affinity chromatography column was washed with buffer A until the absorbance at 280 nm returned to baseline. Purified IgG was eluted using 0.5 M acetate pH 3.0 buffer (buffer B). Fractions containing IgG were neutralized with 3M Tris and stored at 4°C.

Antibody purity was assessed by SDS-PAGE analysis. The specificity of fluorescently-labeled antibodies was confirmed by flow cytometry using cell lines that possessed the receptor specific to the antibody (24). The specificity of the antifluorescyl antibodies was measured against fluorescein directly.

### 2.3.5 $(Fab')_2$ Production from IgG1 Antibodies

For OV-TL16 and anti-EGFR antibodies, antibodies were digested with 10% pepsin (wt/wt) in 0.1 M citric buffer pH 4.0 at 37°C for 8 h to give $(Fab')_2$. The protein was purified using PD-10 columns equilibrated in the particular buffer used to reduce the fragment to Fab'.

### 2.3.6 $(Fab')_2$ from IgG2a Antibodies Via Lysyl Endopeptidase Digestion

Buffer A: 0.01 M $Na_2HPO_4$, 0.15 M NaCl, 0.01 M EDTA pH 7.0; Buffer B: 0.5 M acetate pH 3.0 buffer. IgG2a antibodies at a concentration of 2-10 mg/ml were incubated with LE for 4 h at 37°C in 50 mM Tris-HCl pH 8.5 (12). The optimal molar ratio of anti-Pgp to LE, as determined using titration experiments to obtain complete digestion of IgG2a to $(Fab')_2$ and Fc, without over-digestion was 500:1 (data not shown). LE activity was inhibited by excess addition of a stoichometric inhibitor $N^{\alpha}$-tosyl-L-lysyl chloromethyl ketone (TLCK) (12). The digestion mixture was applied to a protein G column equilibrated in buffer A. The UV absorbance was monitored at 280 nm until the absorbance returned to baseline.

The elution of LE was performed by washing the column with 200 mM L-lysine in buffer A until the LE activity was negligible. LE activity was measured during elution using a fluorogenic assay and the substrate Boc-Val-Leu-Lys-7-amido 4-methyl coumarin (BOC-Val-Leu-Lys-AMC) (25, 26). The absence of LE in the eluted Fc and $(Fab')_2$ fractions was confirmed by assaying the elution peaks in buffer B; the samples were neutralized by dilution 1:10 (v/v) with 0.2 M Tris-HCl pH 9.0 prior to assay.

The $(Fab')_2$ and Fc fragments were eluted from the column by two methods. The

first method involved two step changes in the pH/ionic strength. Once the absorbance reached baseline, a solution of buffer A and buffer B, 75:25 (v/v), pH = 4.5, was applied to the column until the Fc peak was fully eluted. $(Fab')_2$ was eluted using a step change to 100% buffer B. An alternative method was performed with a gradient elution for the Fc peak, and elution of the $(Fab')_2$ peak with a step change to 100% buffer B. The linear gradient was changed from 0% to 27% buffer B over a 15 min period to elute the Fc fragment, at which point a step change to 100% B elutes the $(Fab')_2$ fragment. Continuation of the gradient following elution of the Fc peak elutes the $(Fab')_2$ in a broad peak consisting of a 5-10-fold higher volume. The $(Fab')_2$ fragment was eluted in a much sharper peak if a step change to 100% buffer B is utilized following elution of the Fc peak. The gradient was performed using a FPLC system (Pharmacia) with buffers A and B.

### 2.3.7 Preparation of Fab'

For IgG1 antibodies, $(Fab')_2$ was reduced to Fab' with 20 mM cysteine for 1 h at 37°C, pH 8. Excess cysteine was removed using a Sephadex G-25 spin column (Pharmacia) equilibrated with MES buffer, pH 6.3, to collect Fab' in crosslinking buffer.

For IgG2 antibodies, $(Fab')_2$ from LE digestion was reduced to Fab' using 1 mM β-mercaptoethanol in 20 mM $NaH_2PO_4$ pH 8.0 buffer containing 5 mM EDTA at 37°C for 1 h.(14, 27) Free β-mercaptoethanol was removed by passing the Fab' product solution twice over a PD-10 column equilibrated in 0.1 M $Na_2PO_4$ pH 7.4 buffer containing 1 mM EDTA. The purity of the products was confirmed using SDS-PAGE (Phastsystem).

### 2.3.8 Preparation and Characterization of PEG-dimerized OV-TL16

Fab' was conjugated with MAL-$PEG_{3400}$-MAL (bismaleimide PEG, MW = 3,431g/mol, Shearwater) by mixing 30 mg of active Fab' at a 2.5-molar excess to MAL-$PEG_{3400}$-MAL in MES buffer (pH 6.3) at room temperature for 30 h. The PEG linker was added in aliquots over a period of 12 h. The progress of the reaction was monitored every few hours by SEC (Superdex 200, analytical FPLC column). In the final reaction mixture, measured by SEC, peak area indicated yields typically 35-45% Fab'-PEG-Fab', 50-60% Fab'-PEG, with 2-5% free Fab' remaining. (Figure 2.10) Monosubstituted Fab'-PEG and dimerized OV-TL16 Fab'-PEG-Fab' were separated and purified using 2 rounds of SEC (Superdex 75 column, preparative FPLC system). One ml fractions were collected during SEC, pooled as shown in Figure 2.11., and product purity was determined by SDS-PAGE. The identity of the products was assigned by SEC retention time and SDS-PAGE migration distance. Fractions containing pure dimerized Fab'-PEG-Fab' were pooled and concentrated using ultrafiltration (Amicon). The final yield after all purifications steps was typically 20-40%. The final product was then used for binding kinetic analysis, and in vitro cell uptake analysis.

### 2.3.9 Preparation and Characterization of Bispecific (Fab'$_{OV\text{-}TL16}$)-PEG-(Fab'$_{anti\text{-}EGFR}$)

Bispecific (Fab'$_{OV\text{-}TL16}$)-PEG-(Fab'$_{anti\text{-}EGFR}$) was synthesized using Fab' fragments from OV-TL16 and anti-EGFR antibodies. The final method reacted freshly reduced OV-TL16 Fab' with a 5-fold molar excess of VS-$PEG_{5000}$-VS (bisvinyl sulfone PEG, MW = 5048 Da, Shearwater/Nektar) in phosphate buffer, pH 8.3, for 3 h. Monosubstituted Fab'-

PEG was then purified by SEC (Superose 12) to remove the unreacted PEG crosslinker and any unreacted Fab'$_{OV\text{-}TL16}$. The isolated fractions pooled, concentrated and then exchanged with phosphate buffer, pH 8.7 by ultrafiltration (Amicon). Freshly reduced anti-EGFR Fab' was then added to monosubstituted Fab'-PEG. The reaction solution was divided in two equal halves: in one a 3-fold molar excess of anti-EGFR Fab' was added, in the other, a 2-fold excess was added. In both cases, roughly equivalent amounts of bispecific (Fab'$_{OV\text{-}TL16}$)-PEG-(Fab'$_{anti\text{-}EGFR}$) was produced. After two rounds of SEC purification, approximately 1 mg of product was obtained. Product identity and purity was confirmed by SEC retention time, SDS-PAGE, and by mass spectroscopy (MALDI-TOF).

### 2.3.10 Binding Constant Determination

By the method described previously (1), OV-TL16 Fab'-PEG-Fab' and OV-TL16 Ab were radiolabeled with $^{125}$I using the Iodo-gen iodination reagent (Pierce). Known concentrations of $^{125}$I-Fab'-PEG-Fab' and $^{125}$I-OV-TL16 IgG were incubated with $10^6$ suspended OVCAR-3 cells for 6 h at 4°C. The cells were then pelleted and concentrations of bound and free construct/antibody in the pellet and supernatant were calculated using a scintillation counter. Scatchard plot analysis was then used to determine their binding kinetics. Binding data was plotted using Prism 7 software. Isotherm data were used to determine dissociation constants and standard errors using least-square fitting of the data.

### 2.3.11 Determination of Fab'-PEG-Fab' Uptake by Confocal Microscopy

#### 2.3.11.1 Fluorescent Labeling

Approximately 1 mg each of homospecific OV-TL16 Fab'-PEG-Fab' and OV-TL16 IgG were FITC-labeled using the Alexa Fluor 488 Protein labeling kit (Molecular Probes) (28). Approximately 500 µg of Fab'$_{OV\text{-}TL16}$-PEG-Fab'$_{anti\text{-}EGFR}$ and 1 mg of anti-EGFR IgG were fluorescently labeled using Texas Red using the Texas Red Protein Labeling kit (Molecular Probes) to produce "(Fab'$_{OV\text{-}TL16}$)-PEG-(Fab'$_{anti\text{-}EGFR}$)–TR" and "anti-EGFR-TR".

#### 2.3.11.2 Uptake of Homospecific OV-TL16 Fab'-PEG-Fab'

OVCAR-3 cells seeded on glass coverslips were incubated using RPMI media containing 10 µg/ml of FITC-labeled Fab'-PEG-Fab' or OV-TL16 (37°C). At 1, 4 and 24 h, slide samples were washed with PBS and fixed with paraformaldehyde. The slides were then mounted and examined using laser scanning confocal microscopy (Zeiss) at 100x magnification. For fluorescence measurements, an excitation wavelength of 488 nm was used and a long pass filter cutoff wavelength of 505 nm was used for detection.

#### 2.3.11.3 Uptake of Bispecific (Fab'$_{OV\text{-}TL16}$)-PEG-(Fab'$_{anti\text{-}EGFR}$)

OVCAR-3 cells mounted on coverslips were incubated in RPMI media containing 1µg/ml bispecific (Fab'$_{OV\text{-}TL16}$)-PEG-(Fab'$_{anti\text{-}EGFR}$)-TR, OV-TL16-FITC, or anti-EGFR-TR at 37°C for up to 24 h. At times 1, 3, 5, and 24 h, samples from each incubation series were fixed with paraformaldehyde and mounted on slides. The slides were then examined by confocal microscopy using fluorescence filters appropriate to each of the labels used.

## 2.4 Results and Discussion

### 2.4.1 Preparation of $(Fab')_2$ from IgG2a Antibodies

The use of IgG2a monoclonal antibodies for this study required the development of a new method of $(Fab')_2$ preparation to provide sufficient quantities for synthetic-scale conjugation chemistry. Traditional pepsin digestion of IgG2a subtype antibodies typically results in undigested whole IgG2a, and overdigestion, producing free Fab fragments LE digestion of the three monoclonal IgG2a antibodies, was shown to produce similar cleavage products. The optimal molar ratio of LE to IgG2a was 500:1 for anti-P-gp and anti-fluorescyl-IgG2a (BDC1 and 4-4-20). The identity of the two peaks, 100 and 50 kDa, was confirmed by SDS-PAGE as the $(Fab')_2$ and Fc fragments, respectively.

The new method used protein G affinity chromatography after LE proteolytic cleavage of IgG2a (12). This allows for purification of $(Fab')_2$, in a single step, rather than the multiple steps previously used, which involved protein A affinity chromatography and size exclusion chromatography. This separation procedure took advantage of the differing avidities of IgG2a, $(Fab')_2$, and Fc for Protein G, and allows separation and purification of the individual components by use of changes in the pH/ionic strength of the chromatographic mobile phase.

To prevent enzymatic damage to the $(Fab')_2$ fragment, and to the protein G column itself, 200 mM L-lysine in buffer A was required to fully elute LE from the column during the washing procedure. To ensure this during method development, enzyme activity was monitored using a fluorogenic substrate for LE. The $(Fab')_2$ was stable for at least 8 months, once residual LE activity was eliminated

Following digestion with LE, isolation of both the Fc and $(Fab')_2$ fragments from

the Protein G column resulted in a highly purified and concentrated preparation, as assessed by SDS-PAGE. This procedure for IgG2a allowed for a simpler procedure for isolation of the $(Fab')_2$ fragment, and produced much higher yields compared to $(Fab')_2$ purified after pepsin digestion.

The anti-P-gp antibody proved to be difficult to work with due to its structural and colloidal stability. SDS-PAGE analysis of the UIC2 IgG2a and it $(Fab')_2$ fragments frequently showed smeared bands, perhaps indicating heterogeneity due to post-translational modifications or degradation (Figure 2.10.). The lane with the U1C2 $(Fab')_2$ product was typically monodisperse, but doubt still remained about the stability of the UIC2 IgG2a. After ensuring that the procedure was not damaging the protein by LE overdigestion or other conditions in the procedures, the same protocol was repeated using the BDC1 anti-fluorescyl IgG2a. Figure 2.11. shows the resulting SDS-PAGE analysis, and whole IgG2a, Fc, and $(Fab')_2$ proteins are in sharp bands. This was done to ensure that the protocol used was applicable for typical IgG2a antibodies and that remaining problems with U1C2 Fab' fragments and with conjugation chemistries were issues derived from the choice of anti-P-gp monoclonal antibody.

### 2.4.2 Dimerization of OV-TL16 Fab'

#### 2.4.2.1 Purification and Characterization

Conjugation reactions of Fab' with the MAL-PEG-MAL linker typically yielded a mixture of 30% Fab'-PEG-Fab', 50% Fab'-PEG and 20% unconjugated Fab'. As shown by the size-exclusion chromatography profile in Figure 2.12., these synthetic yields compare favorably to early Fab' dimerization experiments using low molecular weight

linkers, which typically ranged from 5 to 10% (6). Two rounds of purification using preparative SEC were required to separate Fab'-PEG from dimerized Fab'-PEG-Fab' (Figure 2.13.). The purity of isolated Fab'-PEG-Fab' dimer was confirmed using analytical SEC (Figure 2.13. **C**) and by SDS-PAGE (data not shown). In later experiments dimerizing OV-TL16 Fab' using Shearwater's MAL-PEG-MAL crosslinker, yields of Fab'-PEG-Fab' over 50% were typical.

2.4.2.2 Determination of Binding Constants

The Scatchard plot dissociation constant determinations of the OV-TL16 Fab'-PEG-Fab' construct, as shown in Figure 2.14., indicated an overall binding affinity to CD44/OA3 on OVCAR-3 cells of $K_D$=20 nM. This was somewhat lower than that of unmodified OV-TL16 antibody (2.0 nM), but significantly higher than that of monomeric OV-TL16 Fab' (83 nM). Furthermore, the Scatchard plot of the construct is *biphasic*, with a low affinity component (30 nM), and a high affinity component (5 nM) that was comparable to that of the unmodified antibody (Table 2.1). The biphasic kinetic results for the construct may be the result of binding to two different types of surface receptor antigens on OVCAR-3, or may represent two modes of construct binding to cell surface antigens. This may be an effect of the extended PEG linker since the two Fab' fragment can either bind independently or cooperatively, depending on the relative concentration of Fab' vs. CD44/OA3 antigens on the cells.

As reported in 2013, Khali et al. created monospecific PEG linked Fab' fragments derived from the commercially available therapeutic mAbs bevacizumab (anti-VEGF) and trastuzumab (anti-HER2), as well as the therapeutic Fab fragment ranibizumab (anti-

VEGF). (29, 30) PEG linkers of 6, 10, and 20 kDa were used for each. Using plasmon surface resonance to measure binding kinetics, they found that, although the conjugates had lower $K_D$ and $k_a$ constants, the measured $k_d$ values were approximately 5-fold higher than the $k_d$ values of the unmodified antibody proteins. In vitro assays of the activity of the anti-VEGF constructs revealed antiangiogenic activities comparable to or better than whole bevacizumab IgG. These results are consistent with the results found for the Fab'-PEG-Fab' construct in this study.

2.4.2.3 Uptake of Homospecific OV-TL 16 Fab'-PEG-Fab' by Live Cells

In Figure 2.15., the results of the confocal imaging show the binding of the OV-TL16 Fab'-PEG-Fab' construct and the OV-TL16 antibody to the plasma membrane via cell surface receptors, and showed the presence of each internalized by the cells. The distribution of fluorescence showed high concentrations of antibody/construct in the lysosomes after incubation times of 1 and 4 h. At t=24 h, most of the fluorescence intensity appeared to be distributed throughout the cytosol of the cells. This observation can be best explained by initial endocytosis of the antibody/construct followed by release of free label into the cytosol as the proteins are degraded in the lysosomal compartment. In the images shown, the relative concentration of internalized OV-TL16 Fab'-PEG-Fab' in the cells was significantly greater at 1 h. At 4 h, the apparent concentration of internalized antibody appeared approximately the same. Based on fluorescence intensity and flow cytometry (data not shown), the relative concentration of surface bound antibody was about twice that of Fab'-PEG-Fab' at all incubation times measured.

OV-TL16 has been shown to recognize the CD44/OA3 receptor and to be

internalized rapidly by OVCAR-3 cells via receptor-mediated endocytosis. These results indicated that the chemical modifications used to create the Fab'/PEG construct do not interfere with this process and that internalization is actually enhanced somewhat compared to the native antibody.

### 2.4.3 Bispecific Fab'$_{OV\text{-}TL16}$-PEG-Fab'$_{anti\text{-}EGFR}$ (preliminary)

#### 2.4.3.1 Characterization

After the crosslinking with VS-PEG$_{5000}$-VS, the identity of the Fab'$_{OV\text{-}TL16}$-PEG-Fab'$_{anti\text{-}EGFR}$ construct was confirmed by SEC retention time, SDS-PAGE, and by MALDI-TOF spectroscopy. In MALDI-TOF spectra, the bispecific Fab'-PEG-Fab' construct was indicated by a peak centered around 102 kDa with a double ion peak at 54 kDa. A small extra peak at 59 kDa is likely the result of a contaminating, doubly conjugated Fab' fragment (Fab'-(PEG)$_2$). Although purified (Fab'$_{OV\text{-}TL16}$)-PEG-(Fab'$_{anti\text{-}EGFR}$) was obtained and isolated in this experiment, the total yield was very low (3%).

#### 2.4.3.2 Fluorescent Confocal Microscopy

Comprehensive kinetic and cell uptake experiments were limited due to the unavailability of a cell line that expressed both CD44/OA3 and EGFR. Uptake of OV-TL16 mAb by CD44$^+$ OVCAR-3 showed roughly the same pattern of punctate internal distribution and rate of internalization as seen previously for homospecific OV-TL16 Fab'-PEG-Fab'. Since OVCAR-3 cells do not overexpress EGFR, the intensity of anti-EGFR-TR seen in the cells was relatively low even at 24 h, although significantly higher than the background autofluorescence. The type of intracellular distribution was the same type of punctate seen for OV-TL16. In the cells incubated with bispecific (Fab'$_{OV\text{-}TL16}$)-

PEG-(Fab'$_{anti\text{-}EGFR}$), the distribution of intracellular staining is the same and the concentration of conjugate was significantly higher than that seen using anti-EGFR-TR.

## 2.5 Conclusion

The goal of this body of work described in this chapter was to investigate the utility of PEG dimerized antibody Fab' fragments for the selective targeting of cancer cells. Initial experiment found that OV-TL16 anti-CD44/OA3 Fab' fragments could be dimerized with maleimide-terminating PEGs at high yields and could be readily purified. The binding constants measured for OV-TL16 Fab'-PEG-Fab' was found to be biphasic and only moderately lower than that of the modified OV-TL16 IgG1. These conjugates were also found to be readily endocytosed by cultured ovarian carcinoma cells at concentrations and rates higher than unmodified IgG. Several attempts made to synthesize homospecific Fab'-PEG-Fab' using VS-PEG-VS and OV-TL16 and anti-EGFR Fab', however, produced yields that were insufficient for further study.

Difficulties generating high yields of stable UIC2 anti-P-pg Fab' fragments spurred the development of a novel and efficient method to produce highly purified Fab' fragments from IgG2a subtype antibodies. However, numerous subsequent attempts remained unsuccessful in creating stable Fab'-PEG-Fab' conjugates from the UIC2 hybridoma antibodies. The isolation of antifluorescein IgG2a type Fab' fragments from BDC1 and 4-4-2 hybridomas revealed that the difficulties with the UIC2 antibodies were particularly problematic for that hybridoma's antibodies. However, aggregation and crosslinking side products were a problem with the anti-HER2 and anti-EGFR monoclonal antibodies also.

Bispecific Fab'-PEG-Fab' conjugates were successfully produced using vinyl sulfone-terminated PEGs using IgG1 subtype mAbs, though at relatively low yields (~20%). Full characterization of these conjugates, however, was not feasible (at the time) due to the lack of availability of carcinoma cell lines that presented the CD44/OA3 tumor marker, while also over-expressing either EGFR or HER-2 receptor proteins.

The successful site-specific dimerization of OV-TL16 Fab' fragments showed the possible advantages of using chemical conjugation for antibody-based targeting. High binding kinetics to cell surface receptors, and high endocytic uptake rates for CD44/OA3 cells, indicated that the extended linker in the Fab'-PEG-Fab' construct resulted in kinetics at least equivalent to the unmodified OV-TL16 IgG antibody. It can be concluded that the chemical reactions to produce Fab' fragments and the crosslinking reactions did not damage the antigen binding activity of the fragments. Difficulty in reproducing these results for the other mAbs indicated the need to develop better techniques of antibody production, purification and storage, as well as new conjugation reaction methods that are site specific and preserve protein stability.

## 2.6 References


1. Omelyanenko V, Kopečková P, Gentry C, Shiah JG, & Kopeček J (1996) HPMA copolymer-anticancer drug-OV-TL16 antibody conjugates. 1. Influence of the method of synthesis on the binding affinity to OVCAR-3 ovarian carcinoma cells in vitro. *Journal of Drug Targeting* 3(5):357-373.

2. Říhová B, *et al.* (1997) HPMA-based biodegradable hydrogels containing different forms of doxorubicin. Antitumor effects and biocompatibility. *Annals of the New York Academy of Sciences* 831:57-71.

3. Říhová B (1997) Targeting of drugs to cell surface receptors. *Critical Reviews in Biotechnology* 17(2):149-169.

4. Hull EA, *et al.* (2014) Homogeneous bispecifics by disulfide bridging. *Bioconjugate Chemistry* 25(8):1395-1401.

5. Smith ME, *et al.* (2010) Protein modification, bioconjugation, and disulfide bridging using bromomaleimides. *Journal of the American Chemical Society* 132(6):1960-1965.

6. Cao Y & Suresh MR (1998) Bispecific antibodies as novel bioconjugates. *Bioconjugate Chemistry* 9(6):635-644.

7. Greaves M (2015) Evolutionary determinants of cancer. *Cancer Discovery* 5(8):806-820.

8. Merlo LMF & Maley CC (2010) The role of genetic diversity in cancer. *The Journal of Clinical Investigation* 120(2):401-403.

9. Rejmanová P, Kopeček J, Pohl J, Baudyš M, & Kostka V (1983) Polymers containing enzymatically degradable bonds, 8. Degradation of oligopeptide sequences in N-(2-hydroxypropyl)methacrylamide copolymers by bovine spleen cathepsin B. *Die Makromolekulare Chemie* 184(10):2009-2020.

10. Fowers KD, Callahan J, Byron P, & Kopeček J (2001) Preparation of Fab' from murine IgG2a for thiol reactive conjugation. *Journal of Drug Targeting* 9(4):281-294.

11. Mariani M, Camagna M, Tarditi L, & Seccamani E (1991) A new enzymatic method to obtain high-yield F(ab)2 suitable for clinical use from mouse IgGl. *Molecular Immunology* 28(1-2):69-77.

12. Yamaguchi Y, *et al.* (1995) Proteolytic fragmentation with high specificity of mouse immunoglobulin G. Mapping of proteolytic cleavage sites in the hinge region. *Journal of Immunological Methods* 181(2):259-267.

13. Francus T & Birshtein BK (1978) An $IgG_{2a}$-producing variant of an $IgG_{2b}$-producing mouse myeloma cell line. Structural studies on the Fc region of parent and variant heavy chans. *Biochemistry* 17:4324-4331.

14. Parham P (1983) On the fragmentation of monoclonal IgG1, IgG2a, and IgG2b from BALB/c mice. *The Journal of Immunology* 131(6):2895-2902.

15. Tsunasawa S, Masaki T, Hirose M, Soejima M, & Sakiyama F (1989) The primary structure and structural characteristics of Achromobacter lyticus protease I, a lysine-specific serine protease. *The Journal of Biological Chemistry* 264(7):3832-3839.

16. Hagmann ML, Kionka C, Schreiner M, & Schwer C (1998) Characterization of the $F(ab')_2$ fragment of a murine monoclonal antibody using capillary isoelectric focusing and electrospray ionization mass spectrometry. *Journal of Chromatography A* 816(1):49-58.

17. Indik ZK, *et al.* (1994) The high affinity Fc gamma receptor (CD64) induces phagocytosis in the absence of its cytoplasmic domain: The gamma subunit of Fc gamma RIIIA imparts phagocytic function to Fc gamma RI. *Experimental Hematology* 22(7):599-606.

18. Prasad L, Vandonselaar M, Lee JS, & Delbaere LT (1988) Structure determination of a monoclonal Fab fragment specific for histidine-containing protein of the phosphoenolpyruvate: Sugar phosphotransferase system of Escherichia coli. *The Journal of Biological Chemistry* 263(5):2571-2574.

19. Stewart GA & Stanworth DR (1975) The effect of acid treatment upon the susceptibility of rabbit IgG to proteolytic cleavage with various enzymes. *Immunochemistry* 12(8):713-721.

20. Eliasson M, Andersson R, Nygren PA, & Uhlen M (1991) Structural and functional analysis of the human IgG-Fab receptor activity of streptococcal protein G. *Molecular Immunology* 28(10):1055-1061.

21. Erntell M, Myhre EB, & Kronvall G (1985) Non-immune IgG F(ab')2 binding to group C and G streptococci is mediated by structures on gamma chains. *Scandinavian Journal of Immunology* 21(2):151-157.

22. Erntell M, Myhre EB, Sjobring U, & Bjorck L (1988) Streptococcal protein G has affinity for both Fab- and Fc-fragments of human IgG. *Molecular Immunology* 25(2):121-126.

23. Kranz DM, Herron JN, & Voss EW, Jr. (1982) Mechanisms of ligand binding by monoclonal anti-fluorescyl antibodies. *The Journal of Biological Chemistry* 257(12):6987-6995.

24. Nori A, Jensen KD, Tijerina M, Kopečková P, & Kopeček J (2003) Subcellular trafficking of HPMA copolymer-Tat conjugates in human ovarian carcinoma cells. *Journal of Controlled Release* 91(1-2):53-59.

25. Sakiyama F & Masaki T (1994) Lysyl endopeptidase of Achromobacter lyticus. *Methods in Enzymology* 244:126-137.

26. Zimmerman M, Patel G, & Patel Gay NJ (1976) A new fluorogenic substrate for chymotrypsin. *Analytical Biochemistry* 70(1):258-262.

27. Temponi M, Gold AM, & Ferrone S (1992) Binding parameters and idiotypic profile of the whole immunoglobulin and Fab' fragments of murine monoclonal antibody to distinct determinants of the human high molecular weight-melanoma associated antigen. *Cancer Research* 52(9):2497-2503.

28. Lu ZR, Kopečková P, & Kopeček J (1999) Polymerizable Fab' antibody fragments for targeting of anticancer drugs. *Nature Biotechnology* 17(11):1101-1104.

29. Khalili H, *et al.* (2013) Fab-PEG-Fab as a potential antibody mimetic. *Bioconjugate Chemistry* 24(11):1870-1882.

30. Khalili H, *et al.* (2016) An anti-TNF-alpha antibody mimetic to treat ocular inflammation. *Scientific Reports* 6:36905.

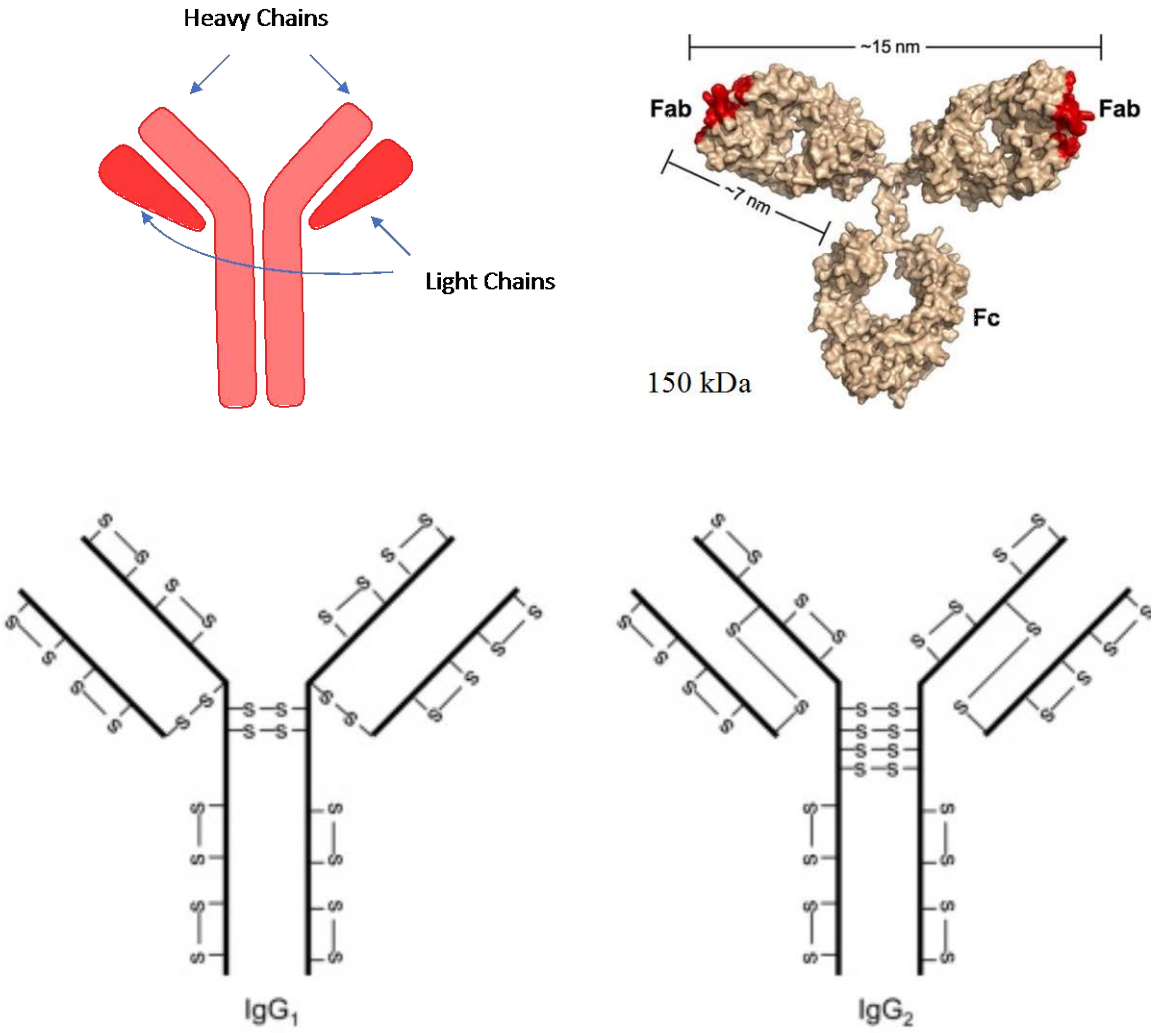


Figure 2.1. Depictions of the basic structure of the IgG protein. Lower half illustrates the differences in disulfide bridging between IgG1 and IgG2 isotype antibodies. (Adapted from Klein JS, Bjorkman PJ (2010) Few and far between: How HIV may be evading antibody avidity. *PLoS Pathog* 6 (5).)

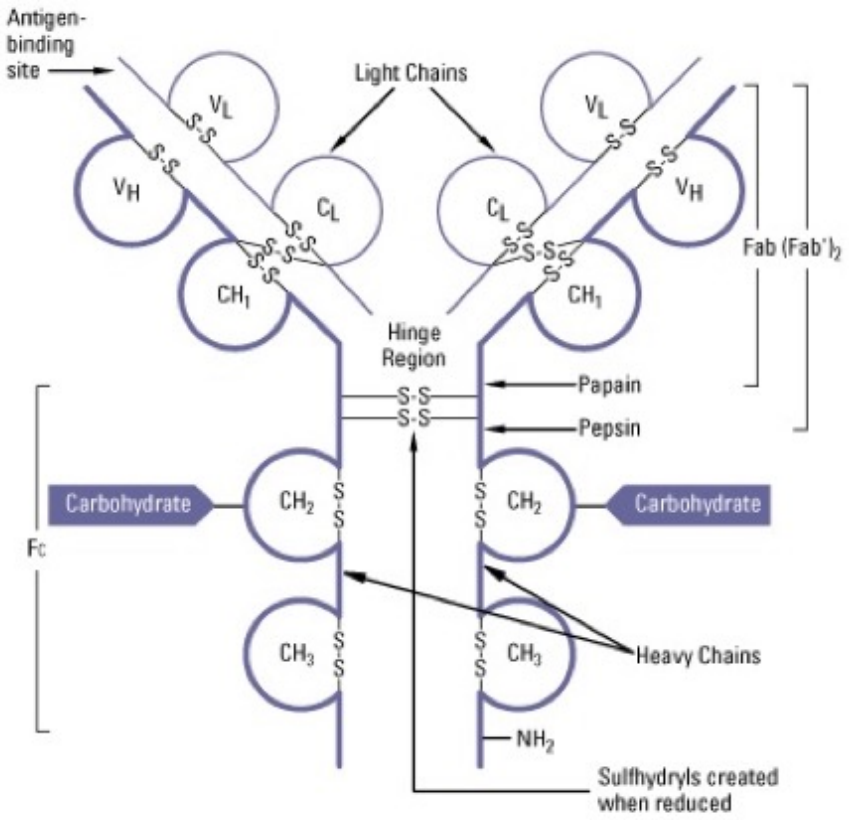


Figure 2.2. General structure of IgG1 antibody. Points of susceptibility in the hinge region to pepsin and papain are shown. Image adapted from ThermoFisher instruction manual for pepsin and papain.

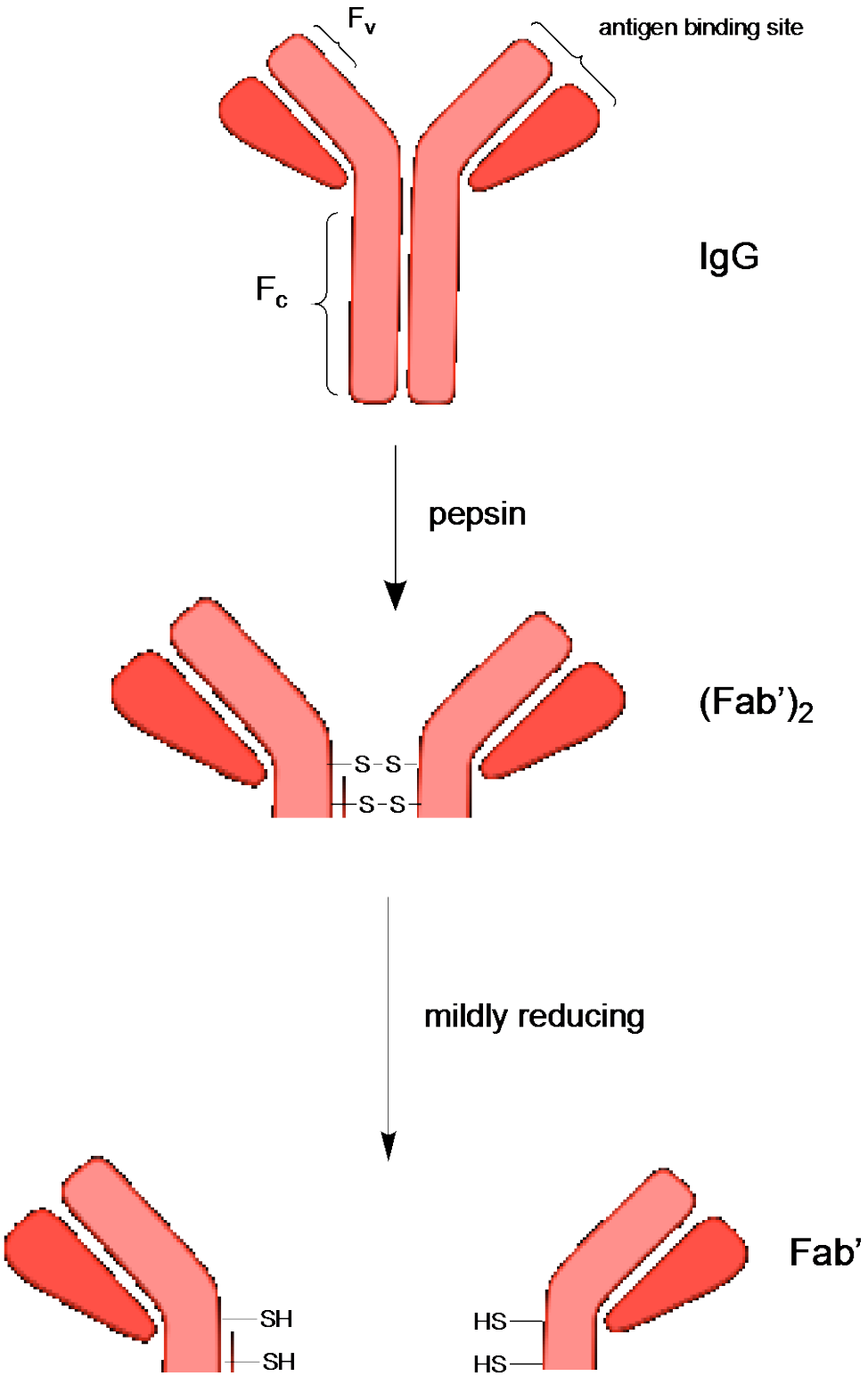


Figure 2.3. General scheme to produce Fab' fragments from IgG antibodies

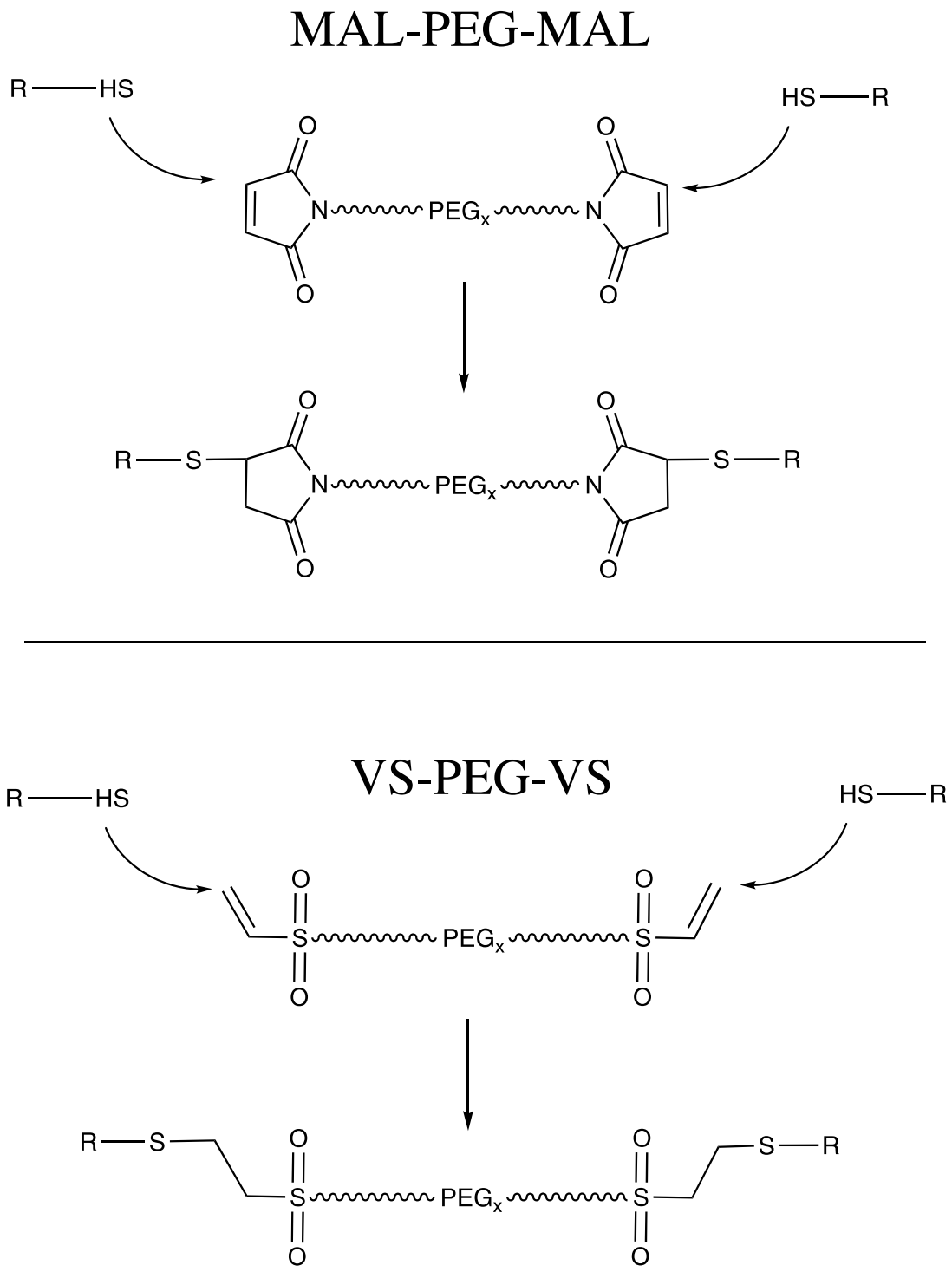


Figure 2.4. Two types of thiol-specific PEG crosslinkers used in study. Top frame: bismaleimide functionalized PEG crosslinking. Bottom frame: bisvinyl sulfone PEG crosslinking

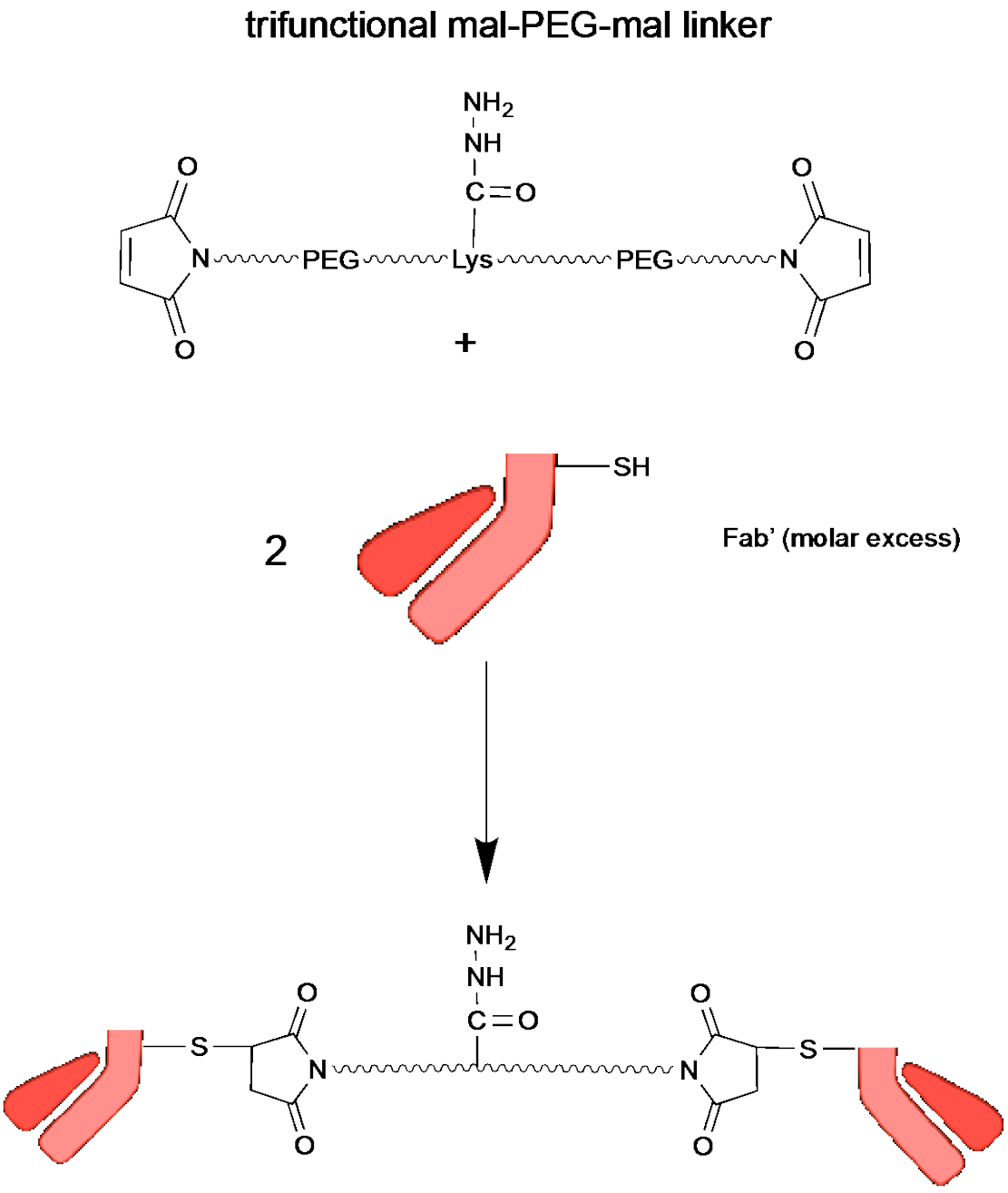


Figure 2.5. General method to dimerize homospecific Fab' fragments using a bismaleimide PEG crosslinker

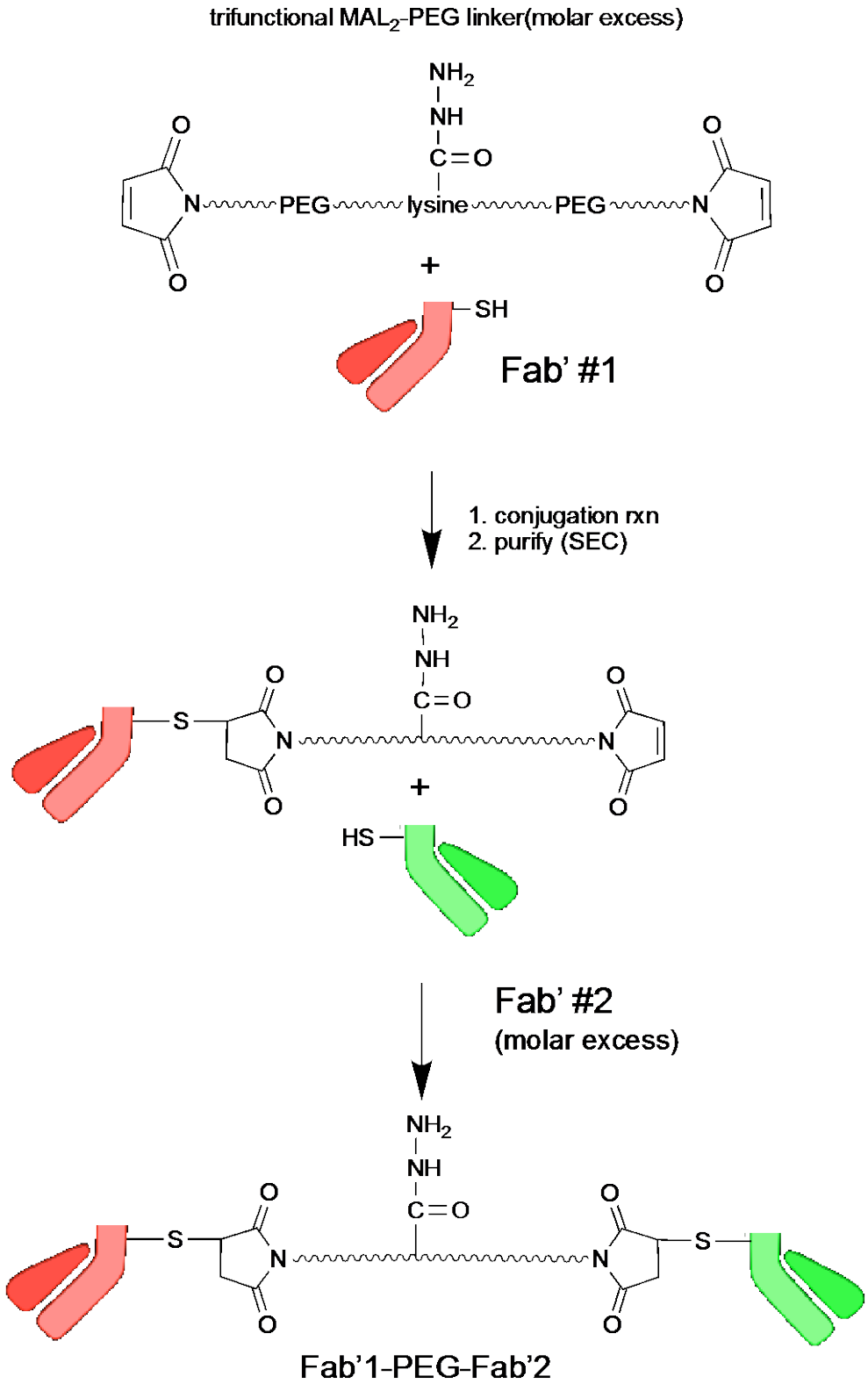


Figure 2.6. General method to dimerize bispecific Fab' fragments using a bismaleimide PEG crosslinker

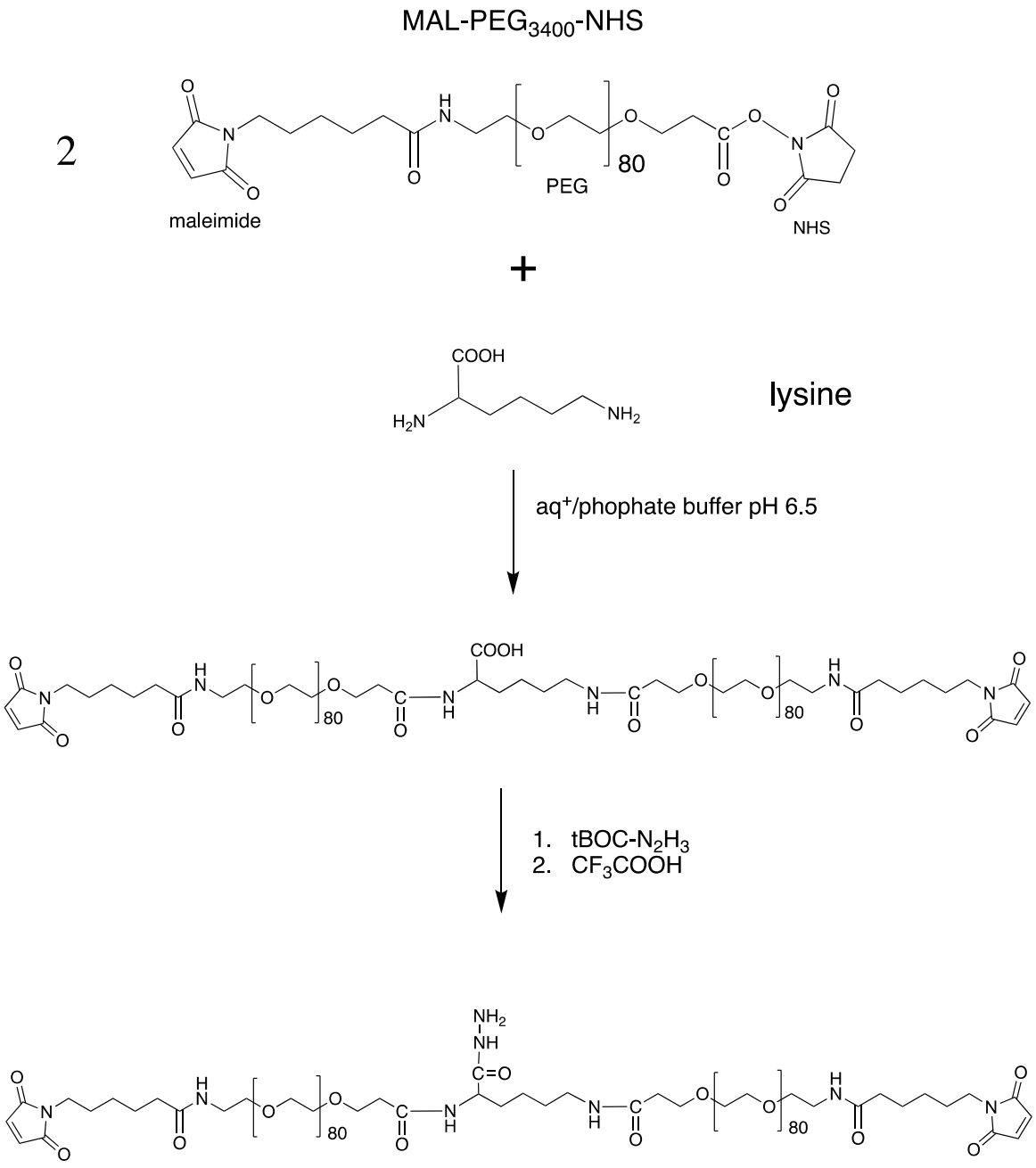


Figure 2.7. Scheme to produce hemitrifunctional linker for Fab' dimerization using heterobifunctional PEG linker coupled to lysine

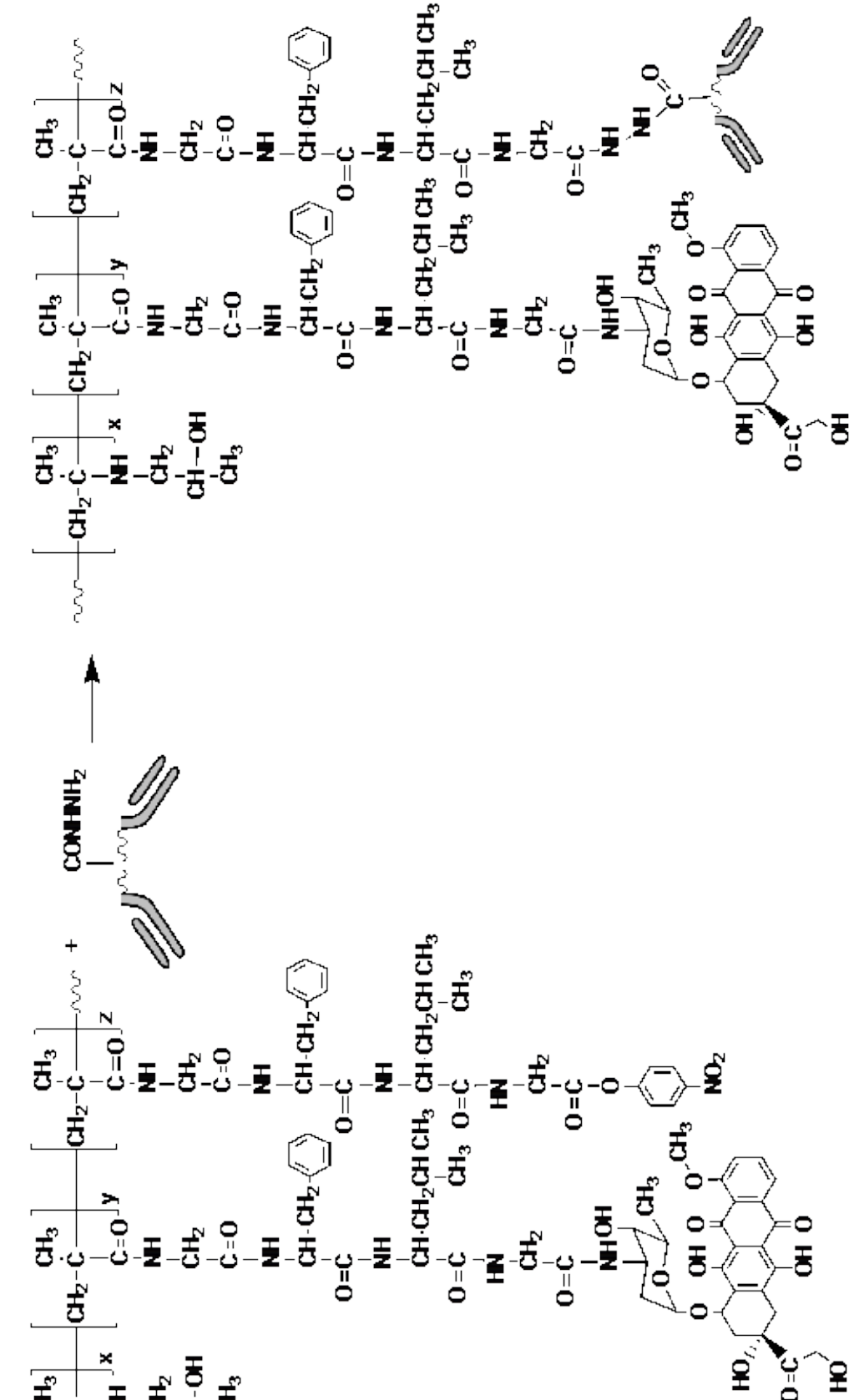

Figure 2.8. Schematic for the addition of Fab'-PEG-Fab' module to HPMA doxorubicin copolymer

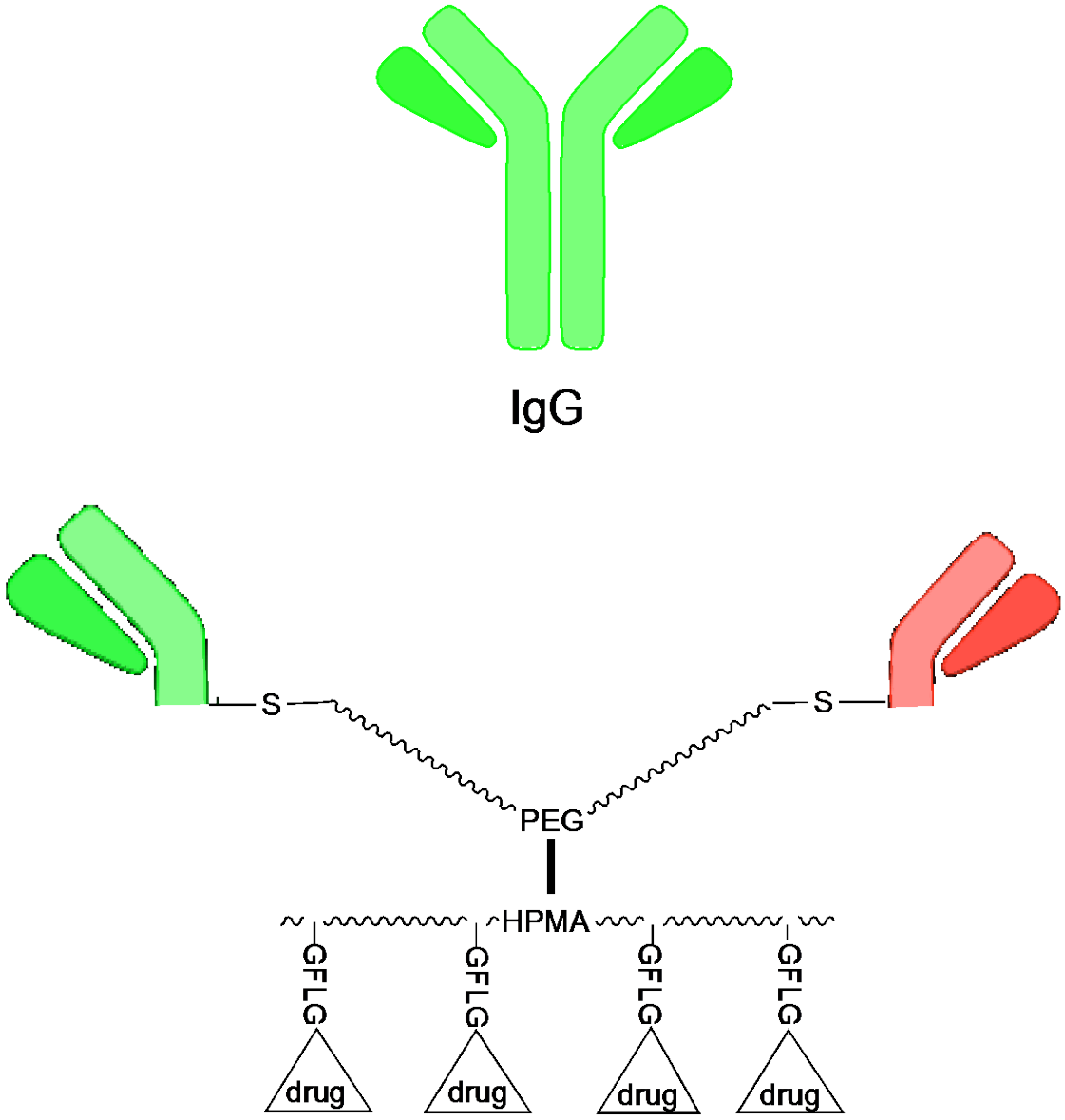


Figure 2.9. General structure for proposed HPMA drug conjugates targeted with bispecific Fab'-PEG-Fab'

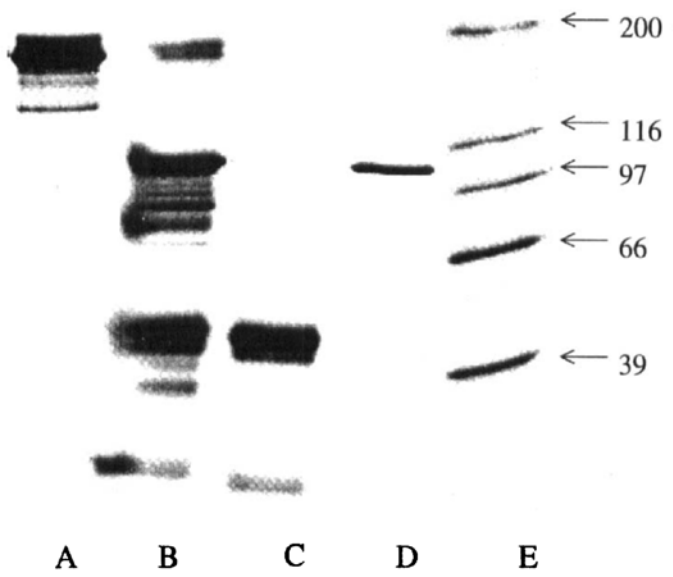


Figure 2.10. SDS-PAGE analysis of: **(A)** anti-P-gp IgG2a**, (B)** the digestion mixture of anti-P-gp IgG2a, (**C**) purified Fc fragment, (**D**) purified anti-P-gp $(Fab')_2$ fragment, (**E**) molecular weight ladder

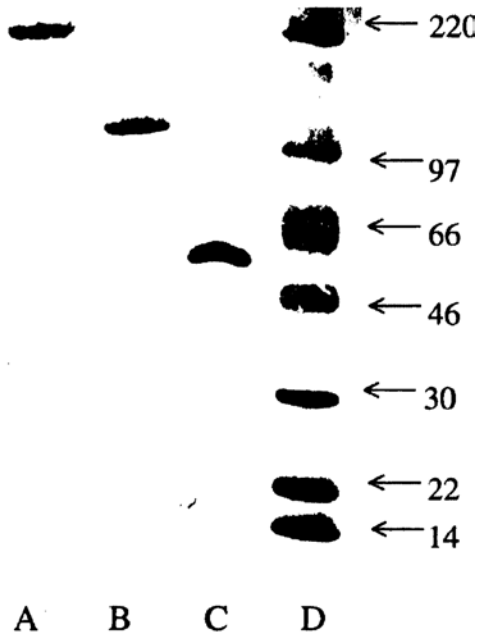


Figure 2.11. SDS-PAGE analysis of: **(A)** anti-fluorescyl BDC1 IgG2a**,**
**(B)** purified anti-P-gp $(Fab')_2$ fragment, (**C**) purified Fc fragment, (**D**) MW ladder

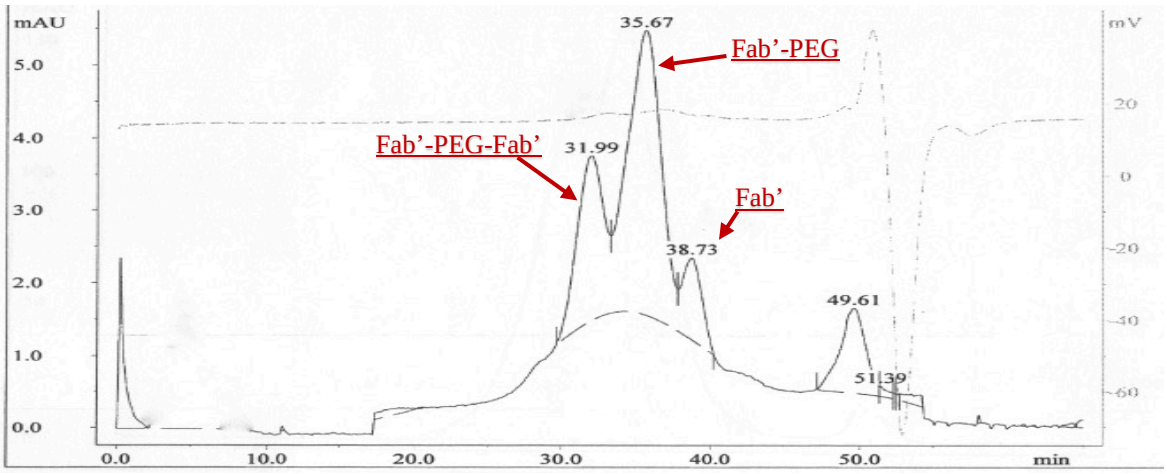


Figure 2.12. Analytical size exclusion chromatography (SEC Superdex 200) profile of OV-TL 16 Fab' conjugation reaction with MAL-PEG$_{3400}$-MAL crosslinker

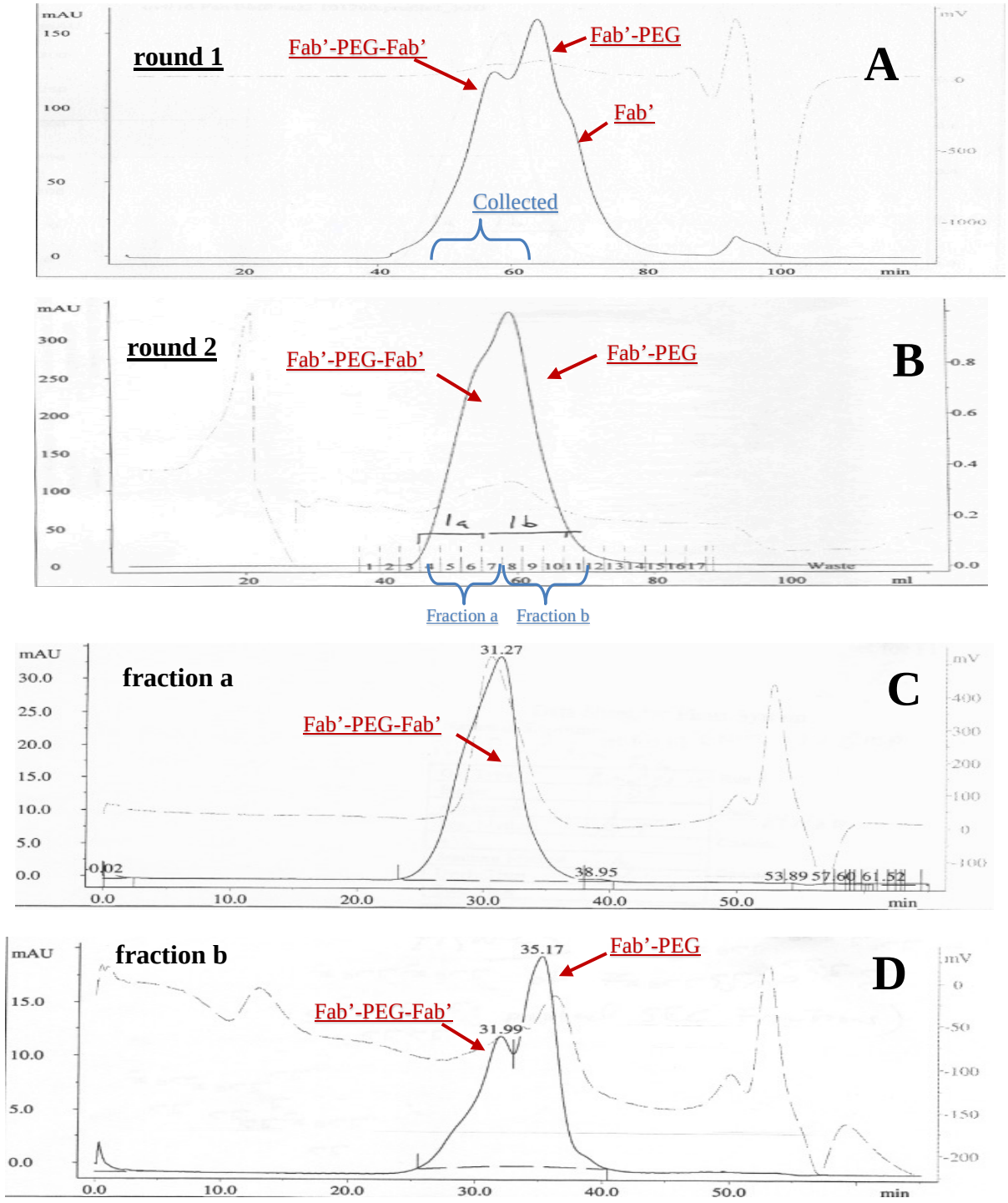


Figure 2.13. Size exclusion chromatography profiles for the purification of dimerized OV-TL 16 Fab'-PEG-Fab'. Profiles of the first and second rounds of preparative SEC are shown in panes **A** and **B**, respectively. Analytical SEC profiles of the indicated pooled fractions, "**a**" and "**b**", from the 2nd round of purification are shown in panes **C** and **D**, respectively. Fraction **a** contains purified dimerized OV-TL16 Fab'-PEG-Fab'

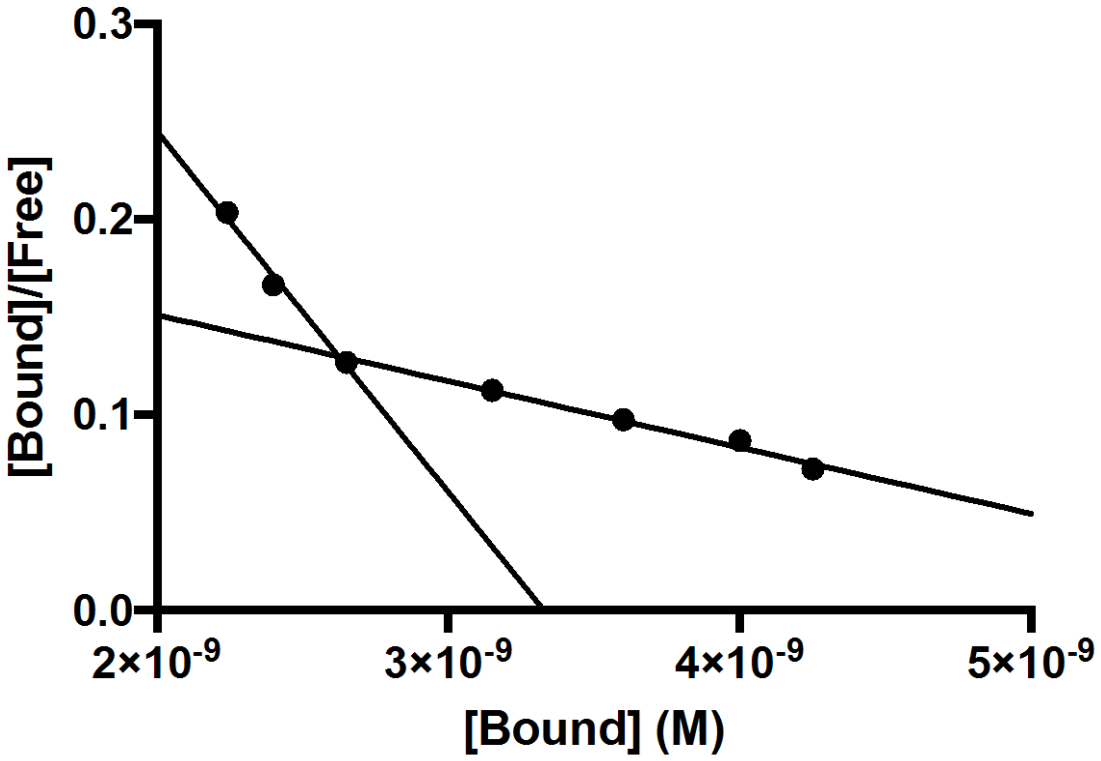


Figure 2.14. Scatchard plot analysis of OV-TL16 Fab'-PEG-Fab' binding kinetics to OVCAR-3 cells

Table 2.1. Summary of results of Scatchard analysis of OV-TL16 IgG, Fab', and Fab'-PEG-Fab' binding constant determinations

| OV-TL16 Antibody Species | $K_{D,ave}$ (nM) | $K_{D,high}$ (nM) | $K_{D,low}$ (nM) |
|---|---|---|---|
| **Fab'-PEG-Fab'** | 20±3 | 5.4.±0.6 | 30±2 |
| **IgG** | 2.0±0.2 | N/A | N/A |
| **Fab'** | 83±6 | N/A | N/A |

**OV-TL16 Fab'-PEG-Fab'-FITC** **OV-TL16-FITC IgG1**

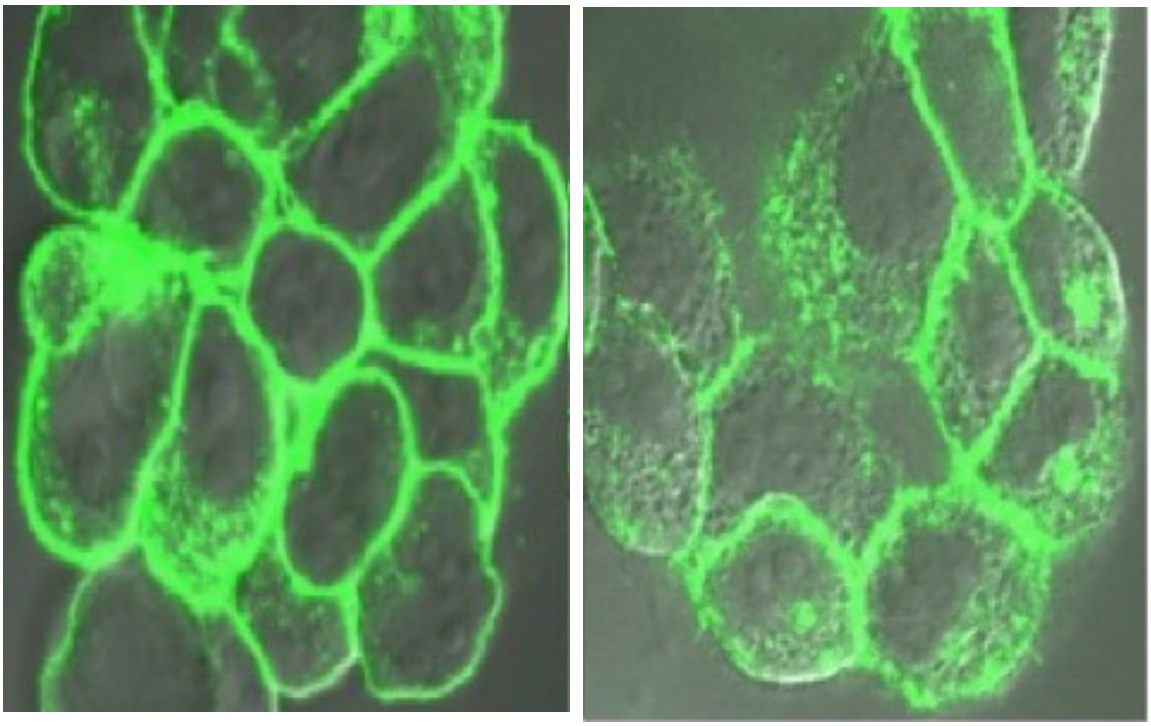

Figure 2.15. Results of confocal microscopy of OVCAR-3 cells incubated with Fab'-PEG-Fab'-FITC for 1 h (left), and OV-TL16-FITC antibody for 4 h (right)

# CHAPTER 3

# SEMITELECHELIC HPMA COPOLYMERS FUNCTIONALIZED WITH TRIPHENYLPHOSPHONIUM AS DRUG CARRIERS FOR MEMBRANE TRANSDUCTION AND MITOCHONDRIAL LOCALIZATION[1]

## 3.1 Abstract

Semitelechelic HPMA (*N*-(2-hydroxypropyl)methacrylamide) copolymers possessing a single terminal lipophilic triphenylphosphonium (TPP) cation and fluorescent labels were synthesized to determine how the attached cation affected cellular uptake and intracellular trafficking. In vitro mitochondrial uptake fluorescence quenching assays using isolated mouse liver mitochondria indicated that only lower molecular weight (<5 kDa) BODIPY® FL-labeled TPP-semitelechelic HPMA copolymers exhibited significant organelle localization or uptake. In vitro cellular uptake and intracellular trafficking was evaluated using cultured human ovarian carcinoma cells. Cells incubated with all types of TPP copolymers used in the study appeared to internalize the polymer by endocytosis only and all internalized copolymer was confined to the lysosomal

[1] This chapter is adapted with permission from: J. Callahan and J Kopeček. Semitelechelic HPMA Copolymers Functionalized with Triphenylphosphonium as Drug Carriers for Membrane Transduction and Mitochondrial Localization. *Biomacromolecules*. 2006 Aug; 7(8): 2347–2356. Copyright © 2006 American Chemical Society

compartment after 24 h. Endocytotic uptake of the TPP-HPMA copolymer conjugates was rapid, suggesting that they were internalized by adsorptive endocytosis, rather than fluid-phase pinocytosis. Semitelechelic copolymers microinjected into cultured cells indicated that the TPP moiety did not significantly localize the polymers to mitochondria.

## 3.2 Introduction

Synthetic polymers, such as HPMA copolymers, have been shown in recent years to be versatile tools to improve the efficacy of a wide array of conventional low-molecular weight drugs. When applied to the treatment of cancer, for example, polymeric carriers of anticancer drugs have been used to greatly enhance the biocompatibility, pharmacokinetics (1), nonimmunogenicity (2), and targetability (3-7) of these agents, while reducing their toxicity toward normal cells.

Because macromolecular therapeutics (polymer-drug conjugates) are not as freely diffusible as low molecular weight (LMW) drugs, their transport and biodistribution differ markedly from free drugs. Intravascular half-life, for instance, is greatly lengthened, particularly for polymer conjugates larger than the glomerular filtration cut-off. Drug concentrations in tumor tissue are increased due to the EPR (enhanced permeability and retention) effect as the result of high rates of leakage from the neovasculature of tumor tissue. Typically, cell uptake has been shown to occur via endocytosis, whereby high molecular weight molecules are typically trafficked to the lysosomal compartment, where nondegradable compounds remain. Drug activity in this case typically requires release of the drug from the carrier via hydrolyzable bonds. Obstacles that reduce the amount of drug delivered to target cells are created by the rate

of cellular internalization and/or lysosomal release. Efficacy is further limited by the problem of trafficking of bioactive agents to the subcellular compartment where the target's active site is located.

Plasma membrane transduction and delivery to the cytosol of synthetic polymers and biopolymers (such as nucleic acids) has recently been explored using cationic oligopeptides or CPPs (cell penetrating peptides). The CPP Tat peptide from the HIV-1 Tat protein has been used to deliver HPMA copolymers to the cytosol of cultured cells (8, 9). Both ANTP peptides from the antennapedia protein and Tat have been used to deliver antisense PNAs to the cytosol and nucleus to inhibit gene expression (10, 11).

Once macromolecules are delivered to the cytosol, several methods have been employed to traffic them to specific subcellular compartments such as the nucleus and mitochondria. Targeting constructs to affect nuclear and mitochondria targeting of synthetic and biological polymers have included nuclear targeting sequence (NLS) (12-18) and mitochondrial targeting sequence (MLS) (19, 20) peptide, respectively. In both cases, the peptide sequences take advantage of the endogenous nuclear or mitochondrial import machinery to deliver a conjugated, high-molecular weight cargo.

Nonpeptidic cationic functional groups have also been used as targeting moieties to penetrate the plasma membrane and to traffic conjugates to the mitochondrial compartment. These include rhodamine-123 (21, 22), oligoguanidinium (21, 23), and triphenylphosphonium (22-27). Notably, the experiments of Murphy et al. used terminally functionalized TPP to target antisense PNA into the mitochondria of isolated organelles and whole intact cells in vitro (28, 29). It was determined that TPP-PNA conjugates as large as 4 kDa were directly transduced through the plasma membrane,

trafficked through the cytosol, and passed through the inner and outer membranes of mitochondria in high concentrations.

Here, we have tested whether the lipophilic cationic moiety triphenylphosphonium (TPP) can be used to also traffic HPMA copolymer conjugates to the mitochondria of target cells. Semitelechelic HPMA polymers were synthesized using a thiol chain transfer agent containing TPP, thereby creating low-molecular weight polymers possessing single cation fixed on one terminus of the final polymer (TPP-HPMA) (30). Semitelechelic copolymers were then created using methacroylylated monomers containing either fluorescein or BODIPY® FL (4,4-difluoro-5,7-dimethyl-4-bora-3a,4a-diaza-s-indacene) to act as drug models and to allow for microscopic visualization of the polymers (Figure 3.1.). Cell uptake and intracellular trafficking of the copolymers was then characterized using cultured human ovarian carcinoma cells.

Ultimately, the ability to deliver macromolecular carriers to the cytoplasm with high efficiency and to control their intracellular trafficking will greatly widen the application and improve the efficacy of many drugs. This approach and internalization/intracellular trafficking model can be contrasted with the use of the polycationic polymer PEI (polyethyleneimine) to transport nucleic acids to the cytoplasm and, subsequently, the nucleus (31).

Mitochondrion malfunction is associated with many aspects of neuron degeneration, cancer, and aging (32). Mitochondria-targeting drug carriers could be used as effective vectors for anticancer drugs, as well as other drugs, that affect mitochondrion function, the apoptotic pathway, or other signal transduction factors localized in the mitochondria.

## 3.3 Experimental

### 3.3.1 Materials

Chemicals and solvents used were of reagent grade or better unless otherwise stated. Before syntheses, 4-bromo-1-butene (Sigma) and thiolacetic acid (Sigma) were freshly distilled under $N_2$. Triphenylphosphine (TPP, Sigma) was recrystallized from 95% ethanol. Diethyl ether was dried over $CaCl_2$ and stored over Na metal. Toluene was washed with 1/10 vol. cold concentrated $H_2SO_4$, then dried over $CaCl_2$ and stored over Na.

Nontelechelic copolymers of HPMA and methacryloylated fluorescein (MA-FITC) monomer were used as control and were prepared as described by Minko et al. previously (33). These HPMA-FITC copolymers were fractionated using size-exclusion chromatography to produce polymers of a narrow polydispersity.

### 3.3.2 Synthesis of the Chain Transfer Agent

### Thiobutyltriphenylphosphonium Bromide

Following the protocol by Burns et al., the thiol TBTP was generated by first synthesizing acylated TBTP (34). TBTP with a free thiol was generated as needed by removing the acyl protecting group using base hydrolysis. (Figure 3.2.)

#### 3.3.2.1 Synthesis of 4-Bromobutylthiolacetate (BBTA)

The precursor 4-bromobutylthiolacetate, was synthesized by reacting 36 mmol (2.8 g) of thiolacetic acid with 18 mmol (2.5 g) of 4-bromo-1-butene with 3.3 mg of AIBN (2, 2'-azobis-isobutyronitrile) at 40°C for 60 min under nitrogen (Figure 3.2.).

Water was removed from thiolacetic acid by distilling the liquid with phosphorous pentoxide. The crude product was extracted into $CHCl_3$, washed 3x with distilled $H_2O$, and dried overnight using $MgSO_4$. The solvent was then removed under vacuum and BBTA was purified by alumina chromatography using $CHCl_3$ as the mobile phase. The identity of BBTA was confirmed by TLC in $CHCl_3$, ESI-MS (electrospray ionization mass spectroscopy; m/z = 210.8), and $^1H$ NMR. The yield was 4.0 g (75%).

3.3.2.2 Acylated Thiolbutyltriphenylphosphonium Bromide (aTBTP)

Acylated thiolbutyltriphenylphosphonium bromide was synthesized by refluxing 4-bromobutyl thiolacetate (10.1 mmol, 1.5 ml) with triphenylphosphine (10.1 mmol, 2.7 g) in dry toluene (8 ml) for 2 h under nitrogen (Figure 3.2.). After cooling, the product was obtained as a viscous yellow liquid under a layer of toluene and white precipitate. The bottom solvent layer was washed with pentane followed by dry diethyl ether and dried under vacuum. Product identity and yield was determined using $^1H$-NMR, ESI MS and UV absorption spectra (Lambda 9 Perkin-Elmer spectrophotometer). The yield of acyl-protected TBTP was 1.1 g or 22%.

3.3.2.3 Thiobutyltriphenylphosphonium Bromide (TBTP)

Thiobutyltriphenylphosphonium bromide, the deprotected mercaptan used as a chain-transfer agent (Figure 3.2.), was prepared using a procedure modified from Burns et al. (34). Acylated TBTP was first dissolved in 95% ethanol. Then, 0.1 M NaOH was added and the solution was bubbled with argon for between 15 and 25 min. The solution was then neutralized by the addition of 90 mM HEPES buffer (pH 4.0). The solution

containing TBTP thiol was then added directly to the polymerization reactions.

### 3.3.3 Triphenylphosphonium-BODIPY® FL

As a control for the BODIPY-labeled HPMA copolymers in the isolated mitochondria assay, TBTP was conjugated to BODIPY® FL *N*-(2-aminoethyl) maleimide (Molecular Probes), as shown in Figure 3.3. Activated thiol TBTP was generated from acylated TBTP as described above immediately before the conjugation reaction. In a glass vial, 5.7 mg (12.1 μmol) of acylated TBTP was first deprotected by base hydrolysis and the activated thiol solution was then added to a solution of 4.5 mg (11.0 μmol) BODIPY FL *N*-(2-aminoethyl)maleimide dissolved in 1 ml of 1:1 DMF:$H_2O$ and left stirring at room temperature overnight. The reaction mixture was then dried by rotoevaporation.

The TPP-BODIPY conjugate was purified by preparative reverse-phase HPLC, using an analytical C18 RP column with UV (220 nm) and fluorescence detection (ex/em 480/518 nm). The column was run using a linear solvent gradient and solvent system consisting of buffer A = acetonitrile with 0.1% TFA, and buffer B = 0.1% TFA. The gradient was started at 30%/70% A/B and ended at 80%/20% A/B over 25 min. Fractions collected during the main elution absorbance/fluorescence peak were pooled and dried by rotoevaporation. A MALDI-TOF MS analysis of the purified product showed a single main product with a mass of 765.2, compared to 765 for the M+1 of the expected TPP-BODIPY conjugate. The final yield of product was 5.1 mg or 52.6%.

### 3.3.4 MA-GG-BODIPY® FL Monomer

Monomer incorporating the BODIPY® FL fluorescent dye was synthesized by reacting (11.3 mg, 3.0 nmol) of BODIPY® FL EDA (Molecular Probes) with MA- GG-ONp(35) (11.8 mg, 3.7 nmol) and a 1.2 molar excess (3.7 nmol) of N,N-diisopropylethylamine (DIPEA) in DMF (Figure 3.4.). After stirring for 4 h at room temperature, the product was purified on an LH-20 column and the fractions containing the product were pooled, dried, resuspended in water, and freeze-dried. The final yield of the bright orange product was 15.3 mg or 97% theoretical yield. ESI mass spectroscopy confirmed the product at mass 517 (M+1, m/z). $^{1}$H NMR (400 MHz, d6-DMSO) δ 8.24-7.84 (m, 4H, -NH-), 7.64-6.29 (m, 4H, Ar-H), 5.74 (s, $^{1}$H, - C=$CH_2$), 5.37 (s, $^{1}$H, - C=$CH_2$), 3.76-3.65 (m, 4H, CO-$CH_2$-NH), 3.45-3.10 (m, 8H, -$CH_2$-$CH_2$-), 2.46 (s, 3H, Ar-$CH_3$), 2.25 (s, $^{3}$H, Ar-CH3), 1.87 (s, 3H, $CH_3$-C=$CH_2$)

### 3.3.5 Semitelechelic HPMA Polymers: Synthesis and Characterization

Semitelechelic HPMA polymers possessing triphenylphosphonium as a terminal functional group were synthesized by free radical polymerization using TBTP as a chain transfer agent. All reactions used AIBN as the initiator. Ratios of initiator, monomers, and chain transfer agent used for the polymerization of semitelechelic polymers were roughly based on those used by Oupický et al. (36). In general, all polymerization reactions were performed with 0.8 M HPMA, $3x10^{-3}$ M AIBN and TBTP chain transfer agent concentrations ranging from $1x10^{-3}$ to $5x10^{-2}$ M. If fluorophore containing comonomers were included for the synthesis of copolymers, mole%s ranging from 0.5 to 5.0 were used, as stated below.

Reactions were typically performed at a scale of 1 ml. Before each reaction, the protecting acyl group of the chain transfer agent TBTP was removed to produce the free thiol, as described above.(34, 37) Methanol was used to dissolve all other reactants of the polymerization. After mixing, the reactant solution was bubbled with argon and sealed in a glass ampule. Polymerization reactions were done at 50°C for 24 h. When complete, the solutions were diluted 10x with distilled water and then dialyzed extensively against water using tubing with a molecular weight cut-off (MWCO) of 1 kDa for polymers ranging below 5 kDa, and a MWCO of 2 kDa for polymers ranging above 5 kDa. The samples were then freeze-dried to isolate the finished solid product.

### 3.3.6 Octanol : $H_2O$ Partition Coefficient Determinations

Approximately 1 mg of fluorescently-labeled HPMA copolymer was first dissolved in 500 µl of PBS (pH 7.4) in a 1.7 ml tube. An equal volume (500 µl) of 1-octanol was aliquotted to the tube and the sealed tube was mixed by shaking for at least 1 h. The tubes were then centrifuged at high speed for 1 min. The octanol layer was then removed and the concentration in each fraction was determined by fluorescent spectrophometry (ex/em = 480/518 nm; in/out slit widths = 10 nm). For this, standard curves of each polymer were created using both octanol-saturated PBS and PBS-saturated octanol.

### 3.3.7 Size-exclusion Chromatography

Size-exclusion chromatography (SEC) was used to determine the molecular weight distribution of the polymers. All samples were run on a Pharmacia FPLC System

equipped with UV and differential refractive index detectors (ÄKTA, Pharmacia) using either a Superdex 75 or Superose 6 HR10/30 analytical column in PBS (pH 7.3) calibrated with polyHPMA standards of a narrow polydispersity (Mw/Mn <1.1).

### 3.3.8 Mass Spectrometry

MALDI TOF mass spectra were determined using a Voyager-DETM STR Biospectrometry Workstation (Perseptive Biosystems, Framingham, MA). Polymer samples were spotted for analysis using a dried-droplet method. For each sample, ~1 mg of polymer sample was first dissolved in 400 μl of 50:50 water:acetonitrile/0.1% TFA solution. Fresh saturated solution of matrix material in the solvent system of 50:50 water:acetonitrile and 0.1% TFA solution was prepared by thoroughly mixing the matrix powder of either HABA (2,4-hydroxy-3,5-dimethoxyphenyl)acrylic acid) or sinapinic acid with 1 ml of solvent in a 1.7 ml tube, and then centrifuged to pellet the undissolved matrix. Then 5.0 μl of the supernatant matrix solution in a small plastic tube was taken and mixed thoroughly for a few seconds in a vortex mixer with the 5.0 μl of polymer sample. A 0.5-2 μl droplet of the resulting mixture was placed on the mass spectrometer's sample stage then the droplet was dried at room temperature.

### 3.3.9 TPP-HPMA-FITC Copolymers

Preliminary polymerizations were performed to characterize fluorescently labeled TPP-HPMA polymers. Initial copolymerizations used 0.5 mole% (4 mM) methacryloylated fluorescein (MA-FITC) monomer (38). In general, two different conditions were used consisting of either 7.5 or 12.5 mM TBTP chain transfer agent and

the same comonomer concentrations described for TPP-HPMA polymers above. During dialysis, the samples were centrifuged to remove precipitate that formed due to the high concentrations of MA-FITC and TBTP in the aqueous solution.

The molecular weights of the polymers were characterized by SEC using an analytical Superose 6 HR10/30 FPLC column. Due to the high polydispersity of the TPP-HPMA-FITC copolymers, they were further fractionated using a preparative Superdex 75 (HR16/60) column by FPLC. Fractions from the SEC column were subsequently pooled into 6 separate cohorts. These were then dialyzed extensively against water and freeze dried. The molecular weight distribution of each polymer fraction was then analyzed using SEC (Superose 6 HR10/30)) and MALDI-TOF MS.

### 3.3.10 TPP-HPMA-BODIPY® FL Copolymers

Semitelechelic polymers incorporating BODIPY monomer were synthesized using MA-GG-BODIPY® FL monomer and TBTP as a chain transfer agent and the general conditions described above. Copolymers with higher molecular weights (between 8 to 12 kDa) were produced using a TBTP concentration of 10 mM and a 0.1 mole% MA-GG-BODIPY® FL comonomer feed concentration. Low molecular weight copolymers were generated using either 0.5 mole% (4 mM) MA-GG-BODIPY® FL with 40 mM TBTP, or 1.0 mole% (8 mM) MA-GG-BODIPY® FL with 10 mM TBTP. Due to the low polydispersity of the BODIPY® FL-labeled polymers, no further purification or size fractionation was performed.

### 3.3.11 Polymers for Uptake and Localization Experiments

The semitelechelic polymers, synthesized to characterize mitochondrial and cellular uptake, were designed to test a range of parameters considered important to the mechanism of action of the cationic TPP moiety. In studies using TPP to enhance the uptake and localization of PNA the criteria cited to ensure activity were a molecular weight less than 4 kDa and a noncharged and relatively nonpolar macromolecular conjugate. For this reason, the semitelechelic polymers were synthesized of several types to investigate the physical requirements for activity. By varying the concentration of CTA used in polymerization, two classes of molecular weight distribution were created: a lower molecular weight class from 2-5 kDa, and a higher molecular weight class of 8-12 kDa. For both classes, semitelechelic copolymers were synthesized using fluorescent monomers possessing either fluorescein or BODIPY® FL. A summary of the polymers used in uptake and microinjection studies is shown in Table 3.1.

### 3.3.12 Uptake of TPP-HPMAs by Isolated Mitochondria

Uptake of the labeled polymers was measured by a fluorescence quenching assay using isolated mitochondria. Mouse liver mitochondria were suspended in solutions containing fluorescently labeled polymers, and quenching after the activation of mitochondrial electropotential was used to determine polymer uptake (39).

Free mitochondria were isolated from freshly removed mouse liver. For each series of experiments, the organ was washed with ~10 ml of isolation buffer (10 mM sucrose, 200 mM mannitol, 5 mM HEPES, 1 mM EGTA, 1 mg/ml BSA – pH 7.4). The liver was then homogenized using an Ultraturrax homogenizer with an S25N186 shearing

head. The liver was homogenized at low speed (8000 rpm) until tissue was dispersed and then at high speed (9500 rpm) two times for 15 sec.

To remove crude tissue debris, the homogenate was centrifuged at low speed (800 x g) for 10 min. The supernatant was then aliquotted into new tubes and centrifuged at high speed (10,000 x g) for 10 min. The pellets were then washed with fresh isolation buffer and recentrifuged for 10 min. The pellets were then suspended in ~1 ml of cold mitochondria uptake assay buffer (70 mM sucrose, 230 mM mannitol, 3 mM HEPES, 5 mM $KH_2PO_4$, 0.5μM rotenone – pH 7.4). The yield of mitochondria was calculated by total protein content using a standard microplate/Coomassie Blue assay.

An LS-55 luminescence spectrometer (Perkin-Elmer) was used to monitor the fluorescence of 2.5 ml sample solutions over time in a stirred sample cell warmed to 37°C. Polymer concentrations used were typically between 0.1 – 1 μg/ml. Solutions of ~1 μM MitoTrackerTM CM-$H_2$TMRos (Molecular Probes) and ~10 μg/ml TPP-BODIPY® FL were used as controls. Solutions testing unconjugated, free FITC, BODIPY® FL EDA, and non-telechelic HPMA-FITC (MW=10 kDa) were also run as controls. To test for the effect of bulk polymer on probe fluorescence, solutions containing 10 μg/ml TPP-BODIPY® FL and 10 μg/ml unlabeled pHPMA were run also.

For each incubation and fluorescence measurement, 0.5 mg of mouse liver mitochondria in 100 μl of uptake buffer was aliquotted to the glass cuvette. Shortly after, 100 μl of succinate solution buffered in 5 mM HEPES (pH 7.4) was added to activate the mitochondria to a final concentration of 5 mM. Finally, after 1-4 min, the decoupler FCCP was aliquotted in 100 μl to a concentration of 0.4 μM (40).

### 3.3.13 Whole Cell Incubation

Live cell, polymer uptake studies using scanning laser confocal fluorescence microscopy (Olympus Flowview with krypton/argon excitation lasers) were performed using OVCAR-3 and MDAH2774 ovarian carcinoma cells (ATCC) to determine if polymer was internalized and localized to mitochondria. Cells were cultured in media supplemented with 10% fetal bovine serum (HyClone Laboratories, Logan, UT) and 10 μg/ml insulin (HyClone) and 12.5 mM HEPES buffer (pH 7.4) under a humidified atmosphere at 37°C. OVCAR-3 cells were grown in RPMI media, and MDAH2774 ovarian carcinoma cells were grown in Leibovitz L-15 media (Sigma).

One day prior to each study, 50,000 to 100,000 cells were seeded on no. 1.5 glass-bottom 14 mm microwell dishes (MatTek Corp., Ashland, MA). For incubations, 2 ml of fresh media containing micromolar concentrations of TPP-HPMA polymer was added and the cell incubated for up to 24 h. Polymer concentrations were varied from 1 to 10 μM. However, 2 μM was used in most experiments. To visualize mitochondria, 100 mM MitoTrackerTM Orange CM-$H_2$TMRos was added to the media at least 1 h before microscopy. In some experiments, MitoTrackerTM was added after the cells had incubated with polymer. Before microscopy, the incubation media was replaced with fresh media and the cells were observed without ambient polymer to reduce background fluorescence. For microscopy, images were collected by combining dual-channel fluorescent and transmitted light using z-series slices in 0.2 μm steps. Image data were processed using ImageJ software.

### 3.3.14 Microinjection

Polymer localization from the cytosol was determined using microinjection. Fluorescently-labeled 0.5 mg/ml polymer/PBS solutions were directly introduced into the cytosol of plated MDAH2774 cells. Injections were performed using 0.5 μm glass needles equipped on an Eppendorf Transjector 5346 pressure injector and fixed to an Eppendorf 5171 micromanipulator arm. Pressures used varied from 50 to 200 HPa and extra care was taken to inject solutions as far from the cell nuclei as possible to avoid traumatizing the cell structure during injection. After injection, the media was replaced with fresh media containing 100 nM of MitoTrackerTM. The cells were then observed periodically for up to 24 h using laser scanning fluorescence confocal microscopy, as described above, to determine copolymer localization.

## 3.4 Results

### 3.4.1 Synthesis and Characterization of Semitelechelic TPP-HPMA Copolymers

In Figure 3.5., the average molecular weights of pHPMAs as a function of CTA concentration are summarized. The average molecular weights for two MA-FITC copolymers are also shown. There was a strong correlation between CTA concentration and the resulting polymer molecular weights.

When the data of these results are fitted into the Mayo equation (Equation 3.1.) (41):

$$1/DP_{n(end)} = 1/DP_{n,o} + C_s[S]/[M] \qquad \text{(Equation 3.1)}$$

where: $DP_{n(end)}$ and $DP_{n,0}$ are the number average degrees of polymerization with and without the chain-transfer agent S, respectively, [M] is the monomer concentration, and $C_s$ is the chain-transfer constant. If all polymers synthesized using the CTA TBTP are semitelechelic, and using the number average molecular weights derived from the SEC data, the calculated $C_s$ value was determined to be 0.84. Compared to previous data for other thiols used as CTAs, this result indicated that TBTP had a high efficiency of chain-transfer in the polymerization reaction (42).

UV-vis spectra of the semitelechelic polymers were determined using 1 mg/ml polymer sample solutions in water. The UV-vis spectra of the polymer samples indicated the incorporation of the TPP moiety based on its absorption maximum at 262 nm. MALDI-TOF mass spectra indicated that approximately 100% of the polymer chains possessing a single TPP moiety. Number average molecular weights of the polymer preparations were calculated using a molar absorptivity of $\varepsilon_{262nm} = 1650\ M^{-1}\ cm^{-1}$.

MALDI-TOF analyses of all preparations of semitelechelic TPP-HPMA showed a single series of molecular weights corresponding with the increments of increasing degrees of polymerization. As shown in Figure 3.6., the peak series corresponded well algebraically with m/z = 143.1 x *n*(HPMA) + 349.1 (TBTP), where *n* is the degree of polymerization. For copolymers incorporating MA-FITC, the MALDI spectra typically showed two series of peaks: one corresponding to $TPP_1$-(HPMA)*n* and another consistent with the empirical formula: m/z = 143.1 x *n* (HPMA) + 349.1 (TBTP) + 532 (MA-FITC). In Figure 3.7., the MALDI spectrum of SEC-fractionated semitelechelic copolymer synthesized using a 1% MA- FITC:HPMA mole ratio is shown. Here, only one peak series is evident and the masses correspond to semitelechelic copolymer where every

polymer possesses exactly one TBTP moiety and one MA-FITC monomer. The MALDI-TOF MS of semitelechelic copolymer synthesized with a 1% MA-GG-BODIPY®FL:HPMA feed mole ratio and 10 mM TBTP. (Figure 3.8.) Here, there are two series of peaks: one corresponding to TPP(1) - (HPMA)*n* and another consistent with the empirical formula: m/z = 143.1*n* (HPMA) + 349.1 (TBTP) + 517.4 (MA-GG-BODIPY® FL) SEC and MALDI-TOF MS analyses of the synthesized copolymers confirmed that all labeled polymer chains possessed exactly one TPP moiety and exactly one fluorophore pendant group.

Polymers were produced with narrow molecular weight distributions, which were predictably determined by the concentration of chain-transfer agent in the polymerization reaction. Overall, the TPP-HPMA copolymers produced for experimentation were synthesized within two molecular weight distributions: a lower molecular weight range of 2-4 kDa, and a higher molecular weight range of 8-16 kDa. When semitelechelic copolymers were produced using methacryloylated fluorescein monomer (MA-FITC), the average molecular weight of the polymer was found to be somewhat higher than predicted from the curve for semitelechelic TPP-HPMA, based on the concentration of chain-transfer agent. Before fractionation, the polydispersity of the FITC-labeled polymers was significantly higher than those determined for other semitelechelic polymers ($\mu$=1.4-1.8). The molecular weights of copolymers using the BODIPY® FL monomer MA-GG-BODIPY® FL were significantly lower than that predicted by the CTA concentration. In general, typical yields of TPP-HPMA were 25%, TPP-HPMA-FITC 10%, and TPP-HPMA-BODIPY® FL only 1%.

### 3.4.2 Partition Coefficients

The relative hydrophobicities of native pHPMA and semitelechelic TPP-HPMAs were found to range in values near those reported for PNAs.(43) The octanol:water partition coefficients determined for FITC-labeled and BODIPY® FL-labeled TPP-HPMA copolymers were found to be not significantly different from each other based on fluorophore type or molecular weight. The coefficients for TPP-HPMA copolymers all ranged from $3x10^{-3}$ to $1.5x10^{-2}$. The coefficients for nonsemitelechelic control HPMA-FITC polymers all were found to be approximately $5x10^{-2}$. These results can be compared to the coefficient for PNAs, which has been determined to be between $1x10^{-2}$ and $2x10^{-2}$.

### 3.4.3 Fluorescence Quenching Analyses with Isolated Mitochondria

Quenching studies using free mitochondria were performed with MitoTrackerTM CM-$H_2$TMRos and TPP-BODIPY® FL as positive controls for the assay. Shown in Figure 3.9. are typical examples of the timeline profiles obtained using TPP-BODIPY® FL control probe (Figure 3.9. A), and the copolymer TPP-HPMA-BODIPY® FL (Figure 3.9. B). In these examples, specific uptake/adsorption of the fluorescently labeled compounds is indicated by the quenching of fluorescence following the addition of succinate (S) and reactivation of mitochondrial membrane potential. Reversal of membrane potential and fluorophore uptake occurred after the addition of the inhibitor FCCP (F). The linear decrease of the fluorescent intensity before the addition of mitochondria, and increase seen after the addition of the succinate solution, are likely due to photobleaching of the fluorophores. For all probes and labeled copolymers, quenching occurred immediately after succinate addition and deflection of the fluorescence profile

reached equilibrium within 60 s. For each profile, the addition of the inhibitor was followed by a mirror image deflection profile that reached equilibrium in the same time frame as quenching. After correcting for appropriate dilution effects from the added activator and inhibitor solutions (3% – 4%), the magnitude of dequenching was calculated to be approximately of the same magnitude as quenching in each profile as a percentage of total fluorescent intensity. Profiles from the low molecular weight MitoTrackerTM and TPP-BODIPY® FL probes all showed smooth exponential transitions to equilibrium fluorescence after each step addition of solutions containing mitochondria, succinate, and FCCP. Using polymer solutions, however, these transitions were sometimes characterized by large fluctuations in intensity before reaching equilibrium. The profile for TPP-HPMA-BODIPY® FL-3kDa (Figure 3.9. B) displays one example.

Using the control TPP-BODIPY® FL probe, the average percentage of quenching/de-quenching was found to be about +/- 4% (Figure 3.9. A). Of the copolymer samples, only the profile of TPP-HPMA- BODIPY® FL-3 kDa possessed significant deflections from mitochondrial activation and inhibition, which were +/- 2% (Figure 3.9. B). The profile of the higher molecular weight copolymer TPP-HPMA- BODIPY® FL-12 kDa appeared to also have a quenching/de-quenching deflection. However, it was not significant (<1%). The profile of control HPMA-FITC-12 kDa possessed small decreases in fluorescent intensity consistent with dilution effects. None of the FITC-labeled semitelechelic TPP-HMPA-FITC copolymers had deflections significantly different from that of control HPMA-FITC. The presence of unlabeled polyHPMA-10 kDa in the assay had no significant effect on the profile of the TPP-BODIPY® FL probe (data not shown).

### 3.4.4 Cell Uptake and Localization Studies

Typical results from incubating cultured cells with fluorescently labeled polymers are shown in Figure 3.10. MDAH2774 cells incubated with TPP-HPMA copolymers in media showed only punctuate fluorescent staining for all types of polymers, regardless of time of incubation, cell type, or polymer concentration, fluorophore or molecular weight. No significant colocalization of polymer (green channel) with MitoTrackerTM (red channel) was observed for any of the polymer samples. In general, the semitelechelic TPP-HPMA copolymers showed a much more rapid degree of internalization compared to nonsemitelechelic HPMA-FITC control polymers. After 1 h, the amount of TPP-HPMA-BODIPY® FL internalized was roughly equivalent to that seen after 24 h using nontelechelic FITC-labeled control polymer. After 1 h the amount of internalized TPP-HPMA-FITC was significantly lower than that of TPP-HPMA-BODIPY® FL. No differences in the results occurred whether polymer or MitoTrackerTM was applied first to the cells.

MDAH2774 ovarian carcinoma cells microinjected with TPP-HPMA copolymer showed only diffuse fluorescent staining throughout the cytosol and nucleus for all sample types (Figures 3.11. A and 3.11. B). This was true for all types of polymer, regardless of time of incubation, fluorophore used, or molecular weight. In control injections, the diffusion of 10 kDa HPMA-FITC (Figure 3.11. C) was observed to not be significantly different than that seen using TPP-HPMA-FITC or TPP-HPMA-BODIPY® FL, and all appeared to enter the nuclei of the cells rapidly (< 15 min). No differences in the amount of label between the cytosol or nucleus was noticeable after approximately 30 min. When injecting 170 kDa HPMA-FITC, the polymer was largely excluded from the

nucleus for up to 8 h after injection (Figure 3.11. D). No differences in the results occurred whether polymer or MitoTrackerTM was applied first to the cells.

## 3.5 Discussion

### 3.5.1 Polymer Synthesis and Characterization

In characterizing the semitelechelic polymers in this study, there are several points and caveats that should be made. In general, all the MALDI-TOF MS analyses of the polymers indicated that a large majority of the polymerization products were semitelechelic and possessed exactly one TPP moiety per chain. In polymerizations using comonomers possessing a fluorophore, the product typically indicated that most common species incorporated no fluorophore while species possessing one fluorophore were a minority product. In evaluating the distribution of molecular weights, it should be noted that MALDI spectra have several biases due to the varying efficiencies of ionization of the different molecules that alter the results (44, 45). First, the polymers are polydisperse and the sensitivity of MALDI signals attenuates rapidly with increased molecular weight. For this reason, the molecular weight distribution of polymers derived from MALDI is heavily biased toward polymers with lower degrees of polymerization. This is especially true of polymers whose MWs range below 1 kDa as the ionizability of polymers grows exponentially higher as the degree of polymerization went below n=10. Conversely, it is difficult to collect MALDI signals for synthetic polymers with molecular weights greater than 15 kDa. In general, “reasonable” molecular weight distributions from MALDI analyses were only possible when the total ranges were between approximately 2 kDa and 12 kDa.

It is also possible that MALDI analysis overestimated the percentage of semitelechelic polymers compared to nontelechelic pHPMA. The addition of a single TPP moiety to the polymer greatly increases its efficiency of ionization compared to native pHPMA. If there was an order of magnitude difference in ionizability, it is possible that the assumed yield of semitelechelic polymer has been greatly overestimated in some of the calculations (44, 45).

These caveats aside, the MALDI-TOF MS spectra for TPP-HPMA were shown to be significantly more uniformly semitelechelic in contrast to previously synthesized semitelechelic polymers using thiol CTAs.(42) Previous analyses indicated that a significant portion of the polymers were terminated with AIBN adducts. This increased efficiency seen here may be the result of using lower concentrations of AIBN initiator and higher concentrations of CTA in the polymerizations (36).

The drawback of the concentration ratios used to produce this series of polymers, however, was low polymer yield. Typical yields of TPP-HPMA were 25%, TPP-HPMA-FITC 10%, and TPP-HPMA- BODIPY® FL only 1%. The very low yield of BODIPY copolymers, however, can be largely attributed to the radical scavenger activity of BODIPY (46). Fortunately, very little material was required to complete the studies described here.

### 3.5.2 Biological Activity

The use of lipophilic cations to target mitochondria is based on its physical properties. Trafficking to the mitochondria is a function of the attraction of the delocalized positive charge to the large electronegative transmembrane potential of the

mitochondria. Membrane transduction can occur since the lipophilic cation disrupts the membrane structure allowing the molecule to diffuse through the barrier, drawn by the transmembrane potential. In the case of the macromolecule PNA, it can be assumed that membrane destabilization is sufficient to drive the insertion of the linear conjugate through the lipid bilayer. Since PNA is a neutral molecule and relatively hydrophobic, the energy barrier required to move the rest of the molecule through the membrane would be low enough to be driven by the electrostatic interaction created by the cation. Here, we have tested this hypothesis with synthetic copolymers of HPMA.

The scenario for this hypothesized transmembrane transport mechanism suggested that the mitochondriotropic cation should be fixed to one terminus of a linear macromolecule. This was achieved for HPMA copolymers using a triphenylphosphonium alkyl thiol as a chain transfer agent. Radical chain polymerization with TBTP resulted in semitelechelic polymers that possessed single terminal TPP moiety on the polymer backbone. The other presumed physical requirements for mitochondrial targeting with lipophilic cations qualified that the conjugate possess a molecular weight less than 4 kDa and be otherwise electrically neutral and relatively nonpolar.

In this study, batches of TPP-HPMA copolymers were synthesized above and below 4 kDa by altering the concentration of CTA used in the polymerization. The requirement for conjugate neutrality was investigated using two different fluorophores in comonomers: fluorescein, which possesses a negative charge at physiological pH, and the lipophilic dye BODIPY® FL, which is uncharged. Using these probes, ionization state was investigated as a requirement for membrane transduction. The uptake studies using free isolated mitochondria indicated that TPP-modified HPMA polymers could be

trafficked to mitochondria in solution, but also showed that this partitioning was sensitive to the physical properties of the conjugate. In this qualitative analysis, only semitelechelic TPP-HPMA-BODIPY® FL with an average molecular weight below 5 kDa showed significant localization to mitochondria after the activation of membrane potential. Higher molecular weight BODIPY® FL copolymers above 10 kDa showed little if any localization and none of the FITC-labeled polymer yielded significant localization. Apparently, the TPP cation is only able to direct the movement of electrically neutral and very low molecular weight conjugates.

The fluorescence quenching results are not definitive, however, as they represent only a qualitative analysis of mitochondrial uptake. Fluorophore quenching can only indicate local concentration and does not yield information as to whether the probe is uptaken into the membranes of mitochondria or only absorbed to their surface. The significance of the degree of quenching of fluorophores conjugated to polymers is also questionable since the structure of the polymer around the fluorophore can have unpredictable effects on quenching/de-quenching. This issue may be responsible for the complex fluctuations of fluorescent intensity seen in the quenching profiles for the copolymers. Because of these uncertainties, localization studies using live cells should be considered more definitive on the effects of TPP conjugate.

The results of the cell incubation studies clearly showed that TPP-HPMA copolymers were not uptaken by the cells in the same manner as TPP-PNA. All internalization occurred by endocytosis and no evidence of endosomal release was noted after 24 h. Interestingly, different relative rates of internalization were noted for the different classes of copolymers. Compared to the nontelechelic HPMA-FITC polymer

control, the TPP semitelechelic polymers appeared to internalize significantly more quickly. This may simply be a function of their positive charge producing higher binding affinity to the plasma membrane. It is possible that the TPP moiety enhanced the amount of adsorption of the polymers and, thereby, greatly increased the rate of adsorptive endocytosis. Also, the BODIPY® FL-labeled polymers were internalized more rapidly than the FITC polymers. It can be hypothesized that the lack of negative charges on the BODIPY® FL polymers was the source of this difference.

The lack of plasma membrane penetration may simply be a consequence of some unknown physical requirement that is possessed by PNA, but is lacking in the HPMA copolymers. Membrane transduction may require some parameters of chemical make-up or molecular shape that have yet to be described. Another possibility is that TPP does not actually act to affect direct plasma membrane transduction by PNA, but rather enhances the uptake mechanism that occurs for unmodified PNA. Recent work describing the uptake of naked PNA has suggested that internalization occurs mainly by fluid-phase endocytosis followed by endosomal/lysosomal release to the cytosol (19). The role of TPP on the mechanism of cellular uptake of TPP-PNA may, therefore, be analogous to that proposed more recently for cell penetrating peptides, such as TAT, in high molecular weight conjugates (47). It is possible that TPP increases the rate by instead enhancing the rate of adsorptive endocytosis by increasing plasma membrane binding. TPP may also greatly increase the rate of endosomal release by disrupting vesicle structure after endocytosis. A combination of these effects is also possible.

More surprising were the results after polymer microinjection into the cytosol. None of the TPP polymers exhibited colocalization with mitochondria. Regardless of

molecular weight distributions or fluorophore type, all types of semitelechelic polymer were found to diffuse evenly throughout the cytosol and nuclei of the cells and to remain in that state after 24 h. These results are consistent, with respect to polymer distribution and time scale, with previous work where HPMA copolymers were microinjected into Hep G2 cells (48). Similar to the results described here, FITC-labeled HPMA copolymers with molecular weights of 23-25 kDa were found to enter the nuclei within 15 min of microinjection. However, in this study it was found that the copolymers partitioned largely into the nuclear compartment after 60 min. Here, the amount of LMW (< 20 kDa) control HPMA-FITC and TPP-HPMA copolymers of weights in the cytosol and nucleus remained roughly equivalent for up to 24 h. Meanwhile, the high molecular weight (170 kDa) HPMA-FITC control copolymer remained completely excluded from the nuclei. The similar results for semitelechelic and nontelechelic polymers demonstrated that the presence of the cationic TPP moiety had no significant effect on nuclear entry or nuclear accumulation of the copolymers.

One possibility for the absence of mitochondrial localization is that the movement restriction of HPMA polymers is much lower than that of PNA in cytoplasm. In the former case, the energetics of the electrostatic attraction of the TPP cation to the mitochondrial transmembrane potential may be insufficient to affect the free diffusion of the synthetic polymer in cytoplasm. Since PNA is a nucleic acid analog, its diffusion in cytoplasm may be restricted and guided by interactions with other nucleic acids and various proteins that are present in the cytosol. The formation of hybrid RNA:PNA duplexes, for example, may influence the intracellular fate of PNA in a manner not available to synthetic polymers in the cytosol (49). It may be significant that the

localization of TPP-HPMA copolymers was dependent on the type of fluorophore used. TPP-HPMA copolymers labeled with BODIPY® FL adsorbed readily to isolated mitochondria in vitro, whereas FITC-labeled copolymers showed insignificant adsorption. It is possible that the presence of the single negative charge on FITC was enough to significantly counteract the electrostatic force between the mitochondria and the TPP-copolymers. This suggests that driving force created by the lipophilic cation may be easily overwhelmed by the variety of other forces acting upon the polymeric carrier.

## 3.6 References


1. Seymour LW, Duncan R, Strohalm J, & Kopeček J (1987) Effect of molecular weight (Mw) of *N*-(2-hydroxypropyl)methacrylamide copolymers on body distribution and rate of excretion after subcutaneous, intraperitoneal, and intravenous administration to rats. *Journal of Biomedical Materials Research* 21(11):1341-1358.

2. Říhová B, Ulbrich K, Kopeček J, & Mancal P (1983) Immunogenicity of *N*-(2-hydroxypropyl) methacrylamide copolymers--potential hapten or drug carriers. *Folia Microbiologica* 28(3):217-227.

3. Kopeček J (1991) Targetable polymeric anticancer drugs. Temporal control of drug activity. *Annals of the New York Academy of Sciences* 618:335-344.

4. Lu ZR, Gao SQ, Kopečková P, & Kopeček J (2000) Synthesis of bioadhesive lectin-HPMA copolymer-cyclosporin conjugates. *Bioconjugate Chemistry* 11(1):3-7.

5. Omelyanenko V, Kopečková P, Gentry C, & Kopeček J (1998) Targetable HPMA copolymer-adriamycin conjugates. Recognition, internalization, and subcellular fate. *Journal of Controlled Release* 53(1-3):25-37.

6. Omelyanenko V, Gentry C, Kopečková P, & Kopeček J (1998) HPMA copolymer-anticancer drug-OV-TL16 antibody conjugates. II. Processing in epithelial ovarian carcinoma cells in vitro. *International Journal of Cancer* 75(4):600-608.

7. Xu JP, Ji J, Chen WD, & Shen JC (2005) Novel biomimetic polymersomes as polymer therapeutics for drug delivery. *Journal of Controlled Release* 107(3):502-512.

8. Nori A, Jensen KD, Tijerina M, Kopečková P, & Kopeček J (2003) Tat-conjugated synthetic macromolecules facilitate cytoplasmic drug delivery to human ovarian carcinoma cells. *Bioconjugate Chemistry* 14(1):44-50.

9. Jensen KD, Nori A, Tijerina M, Kopečková P, & Kopeček J (2003) Cytoplasmic delivery and nuclear targeting of synthetic macromolecules. *Journal of Controlled Release* 87(1-3):89-105.

10. Astriab-Fisher A, Sergueev D, Fisher M, Shaw BR, & Juliano RL (2002) Conjugates of antisense oligonucleotides with the Tat and antennapedia cell-penetrating peptides: Effects on cellular uptake, binding to target sequences, and biologic actions. *Pharmaceutical Research* 19(6):744-754.

11. Astriab-Fisher A, Sergueev DS, Fisher M, Shaw BR, & Juliano RL (2000) Antisense inhibition of P-glycoprotein expression using peptide-oligonucleotide conjugates. *Biochemical Pharmacology* 60(1):83-90.

12. Aronov O, *et al.* (2004) Nuclear localization signal-targeted poly(ethylene glycol) conjugates as potential carriers and nuclear localizing agents for carboplatin analogues. *Bioconjugate Chemistry* 15(4):814-823.

13. Braun K, *et al.* (2002) A biological transporter for the delivery of peptide nucleic acids (PNAs) to the nuclear compartment of living cells. *Journal of Molecular Biology* 318(2):237-243.

14. Frederickson R (1999) PNA-NLS delivers. *Nature Biotechnology* 17(8):739.

15. Kaihatsu K, Huffman KE, & Corey DR (2004) Intracellular uptake and inhibition of gene expression by PNAs and PNA-peptide conjugates. *Biochemistry* 43(45):14340-14347.

16. Nori A, Jensen KD, Tijerina M, Kopečková P, & Kopeček J (2003) Subcellular trafficking of HPMA copolymer-Tat conjugates in human ovarian carcinoma cells. *Journal of Controlled Release* 91(1-2):53-59.

17. van der Aa M, *et al.* (2005) Covalent attachment of an NLS-peptide to linear dna does not enhance transfection efficiency of cationic polymer based gene delivery systems. *Journal of Controlled Release* 101(1-3):395-397.

18. van der Aa MA, *et al.* (2005) An NLS peptide covalently linked to linear DNA does not enhance transfection efficiency of cationic polymer based gene delivery systems. *The Journal of Gene Medicine* 7(2):208-217.

19. Chinnery PF, *et al.* (1999) Peptide nucleic acid delivery to human mitochondria. *Gene Therapy* 6(12):1919-1928.

20. Szeto HH, Schiller PW, Zhao K, & Luo G (2005) Fluorescent dyes alter intracellular targeting and function of cell-penetrating tetrapeptides. *FASEB Journal : Official publication of the Federation of American Societies for Experimental Biology* 19(1):118-120.

21. Teicher BA, Holden SA, Jacobs JL, Abrams MJ, & Jones AG (1986) Intracellular distribution of a platinum-rhodamine 123 complex in cis-platinum sensitive and resistant human squamous carcinoma cell lines. *Biochemical Pharmacology* 35(19):3365-3369.

22. Teicher BA, Varshney A, Khandekar V, & Herman TS (1991) Effect of hypoxia and acidosis on the cytotoxicity of six metal(ligand)4(rhodamine-123)2 complexes at normal and hyperthermic temperatures. *International Journal of Hyperthermia : The Official Journal of European Society for Hyperthermic Oncology, North American Hyperthermia Group* 7(6):857-868.

23. Fernandez-Carneado J, *et al.* (2005) Highly efficient, nonpeptidic oligoguanidinium vectors that selectively internalize into mitochondria. *Journal of the American Chemical Society* 127(3):869-874.

24. Smith RA, Porteous CM, Coulter CV, & Murphy MP (1999) Selective targeting of an antioxidant to mitochondria. *European Journal of Biochemistry* 263(3):709-716.

25. Coulter CV, Kelso GF, Lin TK, Smith RA, & Murphy MP (2000) Mitochondrially targeted antioxidants and thiol reagents. *Free Radical Biology & Medicine* 28(10):1547-1554.

26. Kelso GF, *et al.* (2002) Prevention of mitochondrial oxidative damage using targeted antioxidants. *Annals of the New York Academy of Sciences* 959:263-274.

27. Smith RA, Kelso GF, James AM, & Murphy MP (2004) Targeting coenzyme Q derivatives to mitochondria. *Methods in Enzymology* 382:45-67.

28. Filipovska A, Eccles MR, Smith RA, & Murphy MP (2004) Delivery of antisense peptide nucleic acids (PNAs) to the cytosol by disulphide conjugation to a lipophilic cation. *FEBS Letters* 556(1-3):180-186.

29. Muratovska A, *et al.* (2001) Targeting peptide nucleic acid (PNA) oligomers to mitochondria within cells by conjugation to lipophilic cations: Implications for mitochondrial DNA replication, expression and disease. *Nucleic Acids Research* 29(9):1852-1863.

30. Kamei S & Kopeček J (1995) Prolonged blood circulation in rats of nanospheres surface-modified with semitelechelic poly[N-(2-hydroxypropyl)methacrylamide]. *Pharmaceutical Research* 12(5):663-668.

31. Erbacher P, *et al.* (2004) Genuine DNA/polyethylenimine (PEI) complexes improve transfection properties and cell survival. *Journal of Drug Targeting* 12(4):223-236.

32. Singh KK (2004) Mitochondrial dysfunction is a common phenotype in aging and cancer. *Annals of the New York Academy of Sciences* 1019:260-264.

33. Minko T, Kopečková P, & Kopeček J (2000) Efficacy of the chemotherapeutic action of HPMA copolymer-bound doxorubicin in a solid tumor model of ovarian carcinoma. *International Journal of Cancer* 86(1):108-117.

34. Burns RJ, Smith RA, & Murphy MP (1995) Synthesis and characterization of thiobutyltriphenylphosphonium bromide, a novel thiol reagent targeted to the mitochondrial matrix. *Archives of Biochemistry and Biophysics* 322(1):60-68.

35. Rejmanová P, Labský J, & Kopeček J (1977) Aminolyses of monomeric and polymeric 4-nitrophenyl esters of *N*-methacryloylamino acids. *Die Makromolekulare Chemie* 178:2159-2168.

36. Oupický D, Koňák Č, & Ulbrich K (1999) DNA complexes with block and graft copolymers of *N*-(2-hydroxypropyl)methacrylamide and 2-(trimethylammonio)ethyl methacrylate. *Journal of Biomaterials Science, Polymer Edition* 10(5):573-590.

37. Burns RJ & Murphy MP (1997) Labeling of mitochondrial proteins in living cells by the thiol probe thiobutyltriphenylphosphonium bromide. *Archives of Biochemistry and Biophysics* 339(1):33-39.

38. Omelyanenko V, Kopečková P, Gentry C, Shiah JG, & Kopeček J (1996) HPMA copolymer-anticancer drug-OV-TL16 antibody conjugates. 1. Influence of the method of synthesis on the binding affinity to OVCAR-3 ovarian carcinoma cells in vitro. *Journal of Drug Targeting* 3(5):357-373.

39. Torchilin VP, Khaw BA, & Weissig V (2002) Intracellular targets for DNA delivery: Nuclei and mitochondria. *Somatic Cell and Molecular Genetics* 27(1-6):49-64.

40. Davey GP, Tipton KF, & Murphy MP (1993) Use of an electrode selective for 1-methyl-4-phenylpyridinium (MPP+) to measure its uptake and accumulation by mitochondria. *Journal of Neural Transmission. Supplementum* 40:47-55.

41. Heitz W (1989) *Telechelics by radical polymerization reactions* (CRC Press, Boca Raton, FL).

42. Lu ZR, Kopečková P, Wu Z, & Kopeček J (1998) Functionalized semitelechelic poly[N-(2-hydroxypropyl)methacrylamide] for protein modification. *Bioconjugate Chemistry* 9(6):793-804.

43. Ardhammar M, Norden B, Nielsen PE, Malmstrom BG, & Wittung-Stafshede P (1999) In vitro membrane penetration of modified peptide nucleic acid (PNA). *Journal of Biomolecular Structure and Dynamics* 17(1):33-40.

44. Chen H & He M (2005) Quantitation of synthetic polymers using an internal standard by matrix-assisted laser desprption/ionization time-of-flight mass spectroscopy. *American Society for Mass Spectrometry* 16:100-106.

45. Zhang L-K, Rempel D, Pramanik BN, & Gross ML (2005) Accurate mass measurements by fourier transform mass spectrometry. *Mass Spectrometry Reviews* 24:286-309.

46. Makrigiorgos GM (1997) Detection of lipid peroxidation on erythrocytes using the excimer-forming property of a lipophilic BODIPY fluorescent dye. *Journal of Biochemical and Biophysical Methods* 35(1):23-35.

47. Brooks H, Lebleu B, & Vives E (2005) Tat peptide-mediated cellular delivery: Back to basics. *Advanced Drug Delivery Reviews* 57(4):559-577.

48. Jensen KD, Kopečková P, Bridge JH, & Kopeček J (2001) The cytoplasmic escape and nuclear accumulation of endocytosed and microinjected HPMA copolymers and a basic kinetic study in Hep G2 cells. *AAPS PharmSci* 3(4):E32.

49. Abibi A, Protozanova E, Demidov VV, & Frank-Kamenetskii MD (2004) Specific versus nonspecific binding of cationic PNAs to duplex DNA. *Biophysical Journal* 86(5):3070-3078.

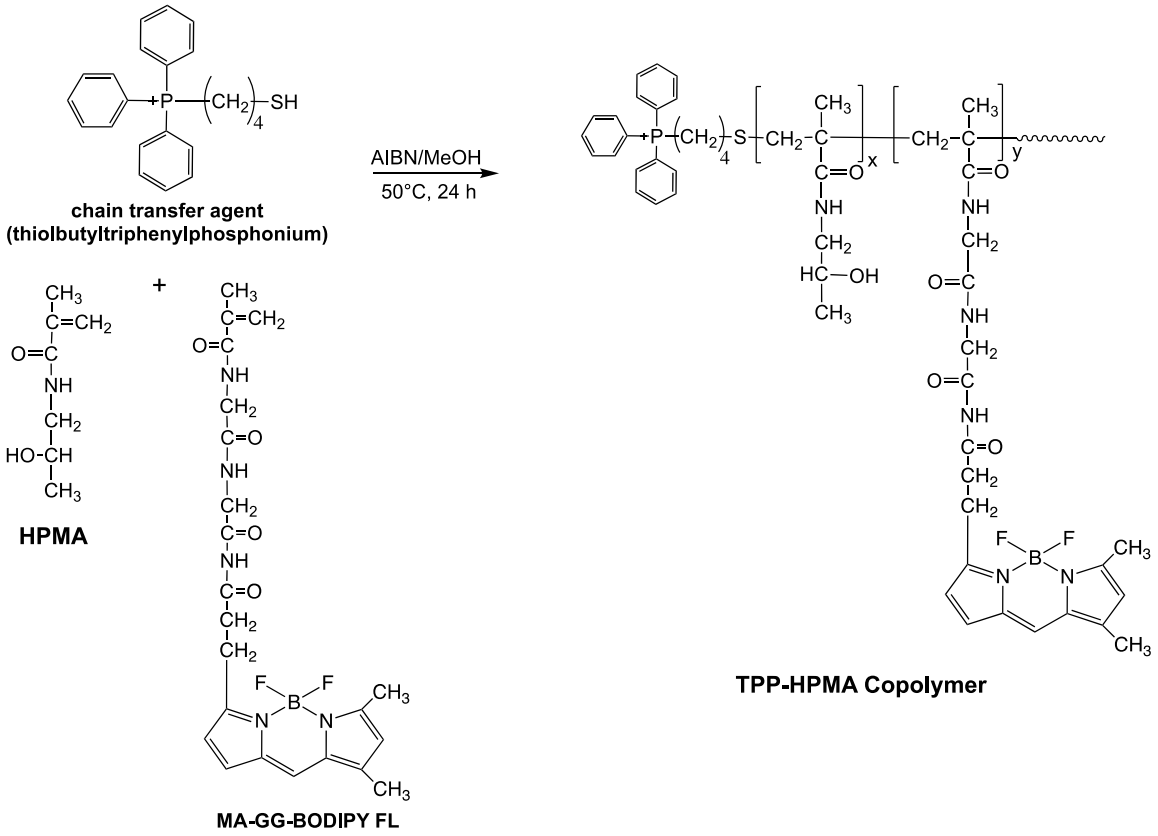


Figure 3.1. Synthetic scheme for TPP-functionalized semitelechelic HPMA copolymer incorporating the fluorescent moiety BODIPY® FL

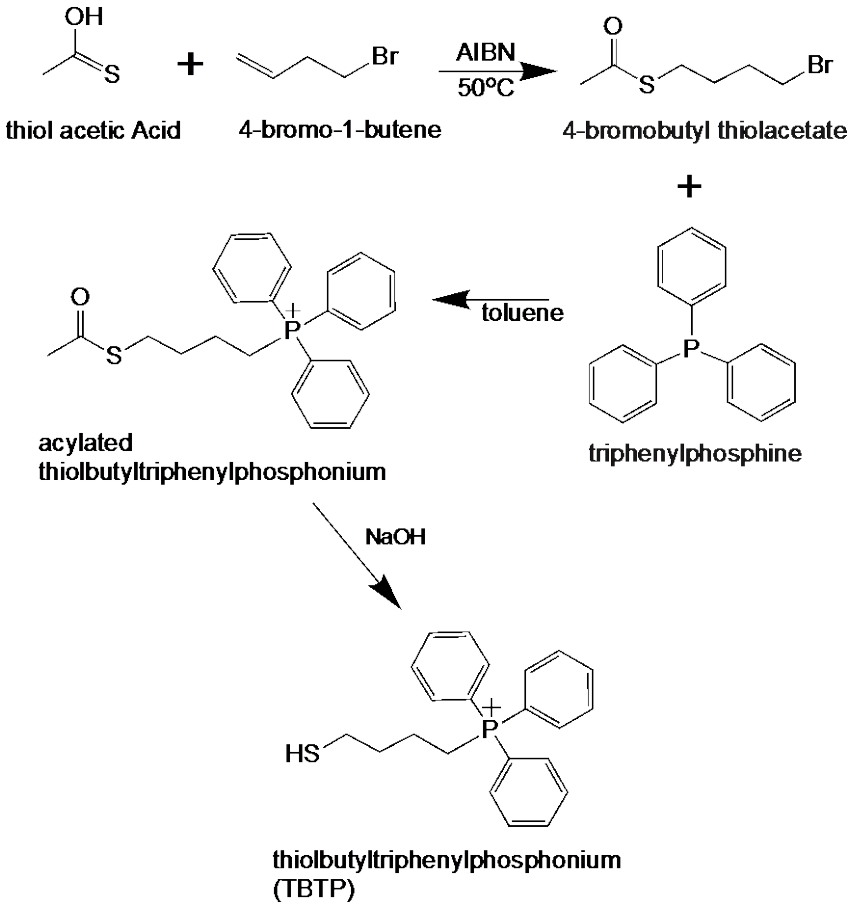


Figure 3.2 Synthesis of TPP chain transfer agent thiolbutyltriphenylphosphonium

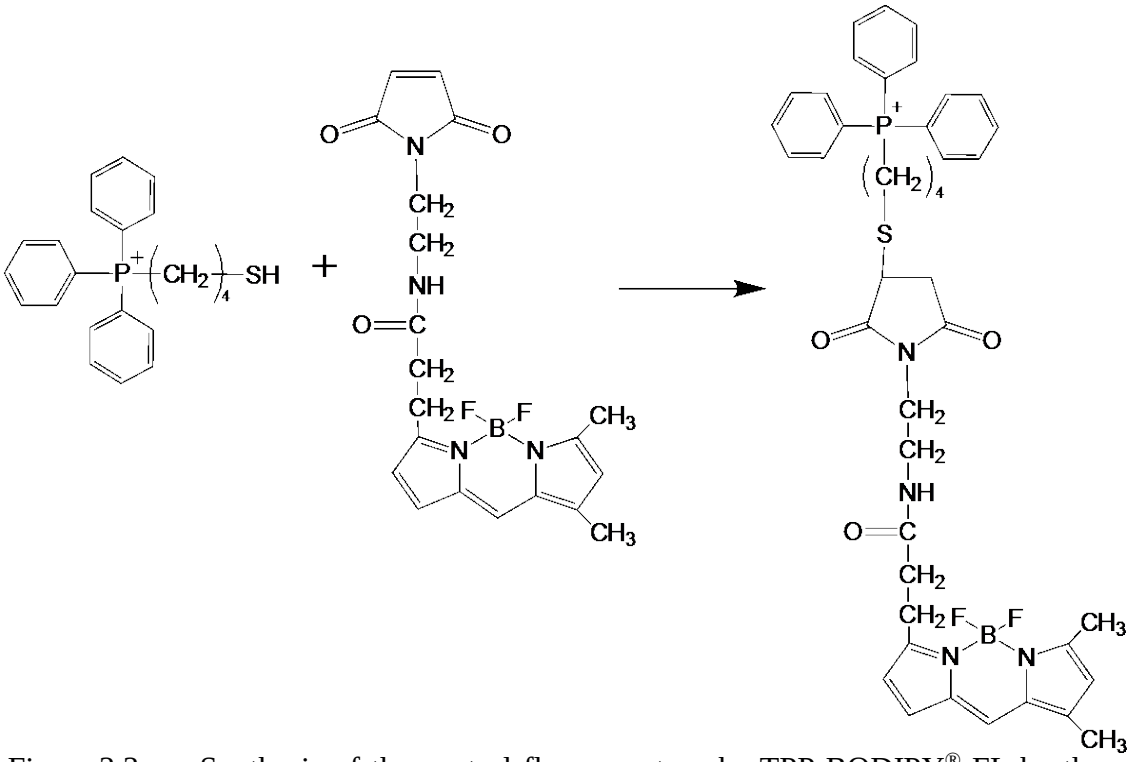

Figure 3.3. Synthesis of the control fluorescent probe TPP-BODIPY® FL by the conjugation of TBTP and BODIPY® FL N-(2-aminoethyl) maleimide

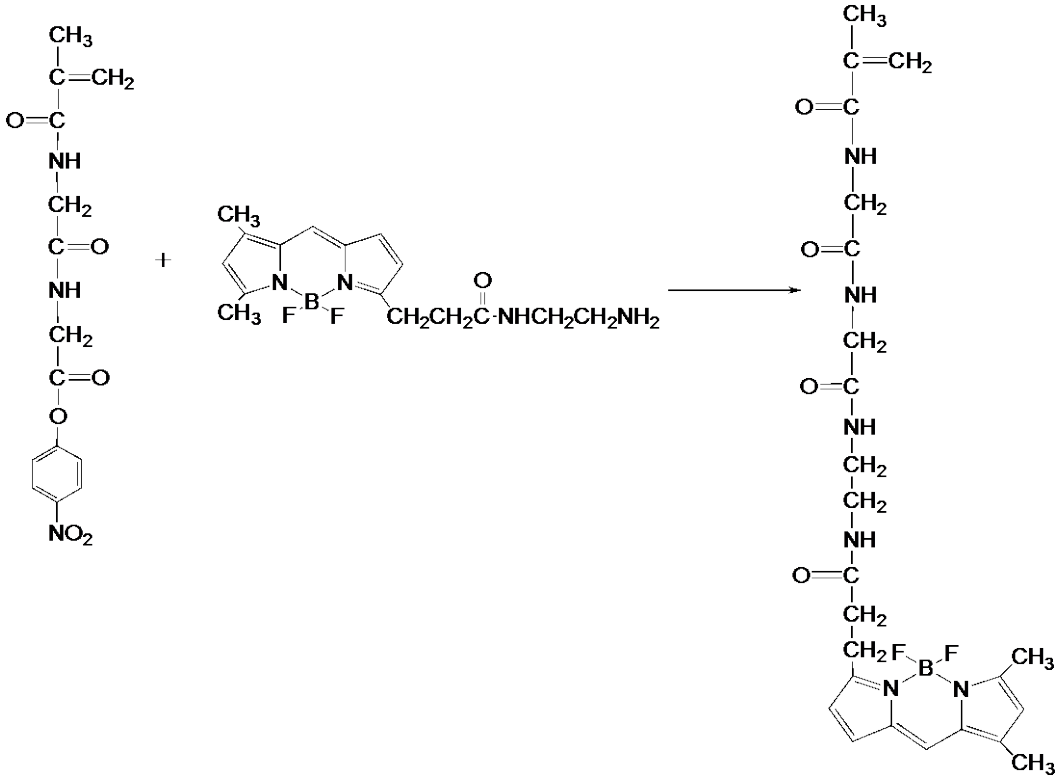

Figure 3.4. Synthetic scheme for the comonomer MA-GG-BODIPY® FL by the conjugation of BODIPY® FL EDA and MA-GG-ONp

Table 3.1 Summary of polymers used for mitochondrial uptake, cell incubation and microinjection studies

| polymer class | copolymers | $M_w$ average (kDa) | $M_W$ range (kDa) |
|---|---|---|---|
| semitelechelic TPP-HPMA | TPP-HPMA-FITC | ~4 | 2-5 |
| | | ~10 | 8-12 |
| | TPP-HPMA-BODIPY® FL | ~3 | 1-5 |
| | | ~12 | 10-15 |
| control pHPMA | HPMA-FITC | ~10 | 8-12 |
| | | ~170 | 150-210 |

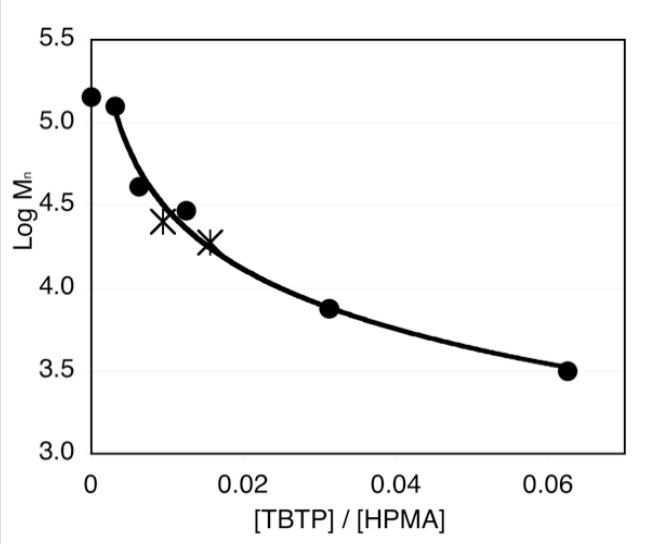


Figure 3.5. Summary of semitelechelic TPP-HPMA molecular weight vs. feed chain-transfer agent concentration to monomer concentration ratio. (●) The results for semitelechelic copolymer with MA-FITC are also shown (∗)

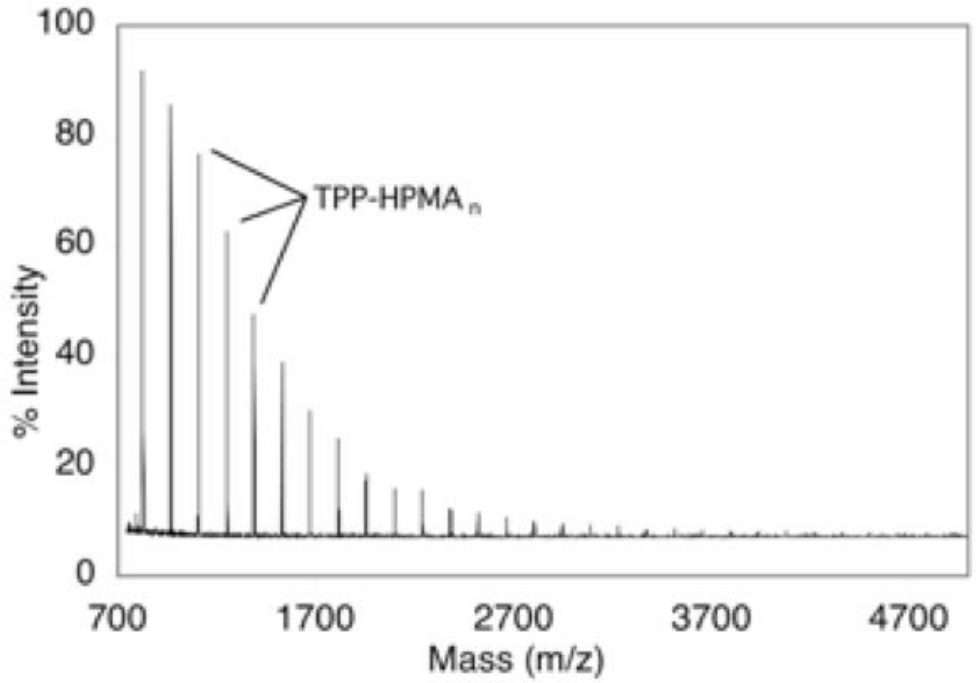


Figure 3.6. Typical MALDI-TOF mass spectrum of semitelechelic TPP-HPMA copolymer

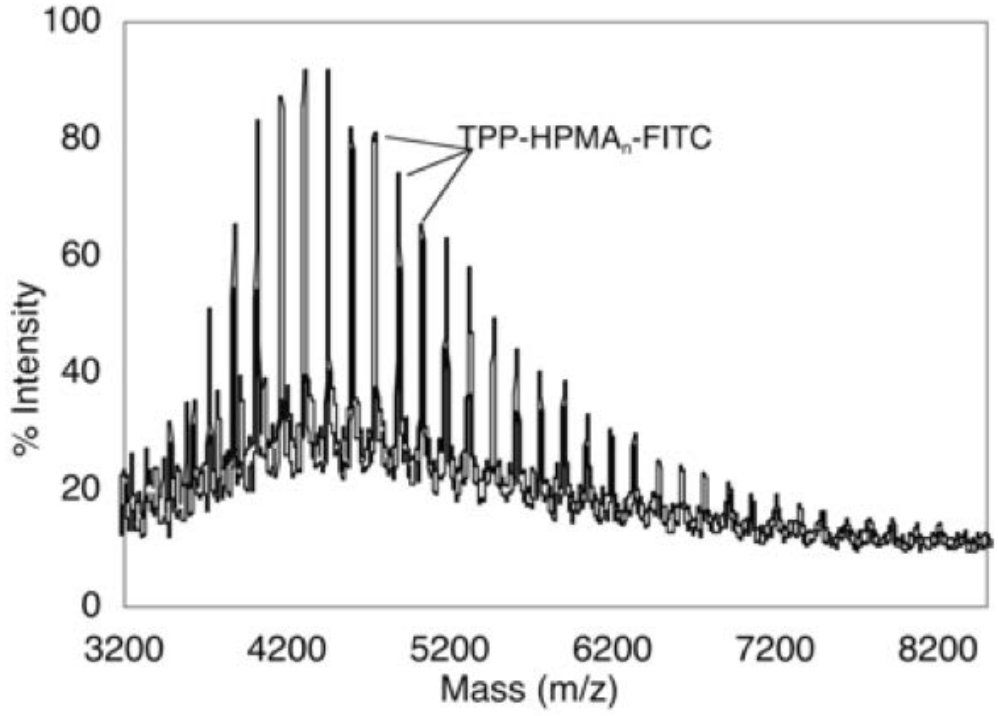


Figure 3.7. Typical MALDI-TOF mass spectrum of semitelechelic TPP-HPMA/MA-FITC copolymer

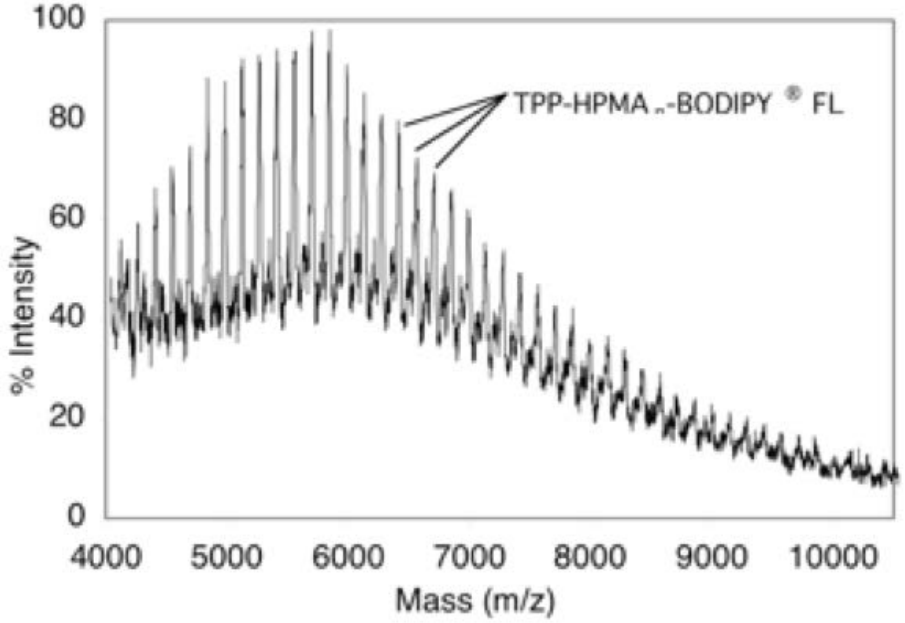


Figure 3.8. Typical MALDI-TOF mass spectrum of semitelechelic TPP-HPMA/MA-GG-BODIPY® FL copolymer

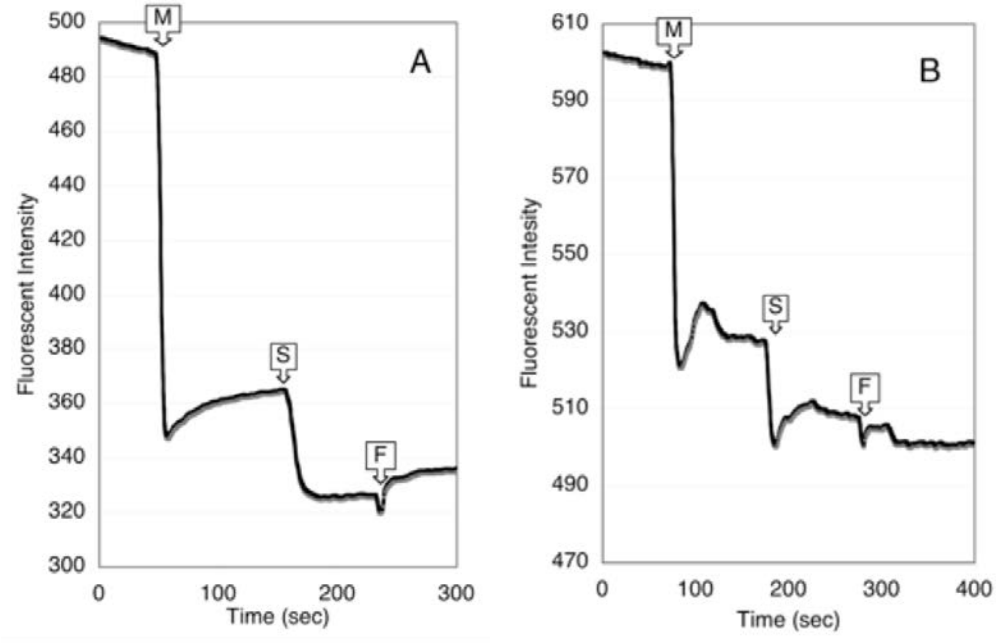


Figure 3.9. Timeline profiles of fluorescence quenching by mitochondria. Solution of TPP-BODIPY FL® control probe (**A**). Solution of semitelechelic copolymer TPP-HPMA-BODIPY FL® - 3 kDa (**B**). Points are indicated for the addition of mitochondria (M), the activator, succinate (S), and the inhibitor, FCCP (F)

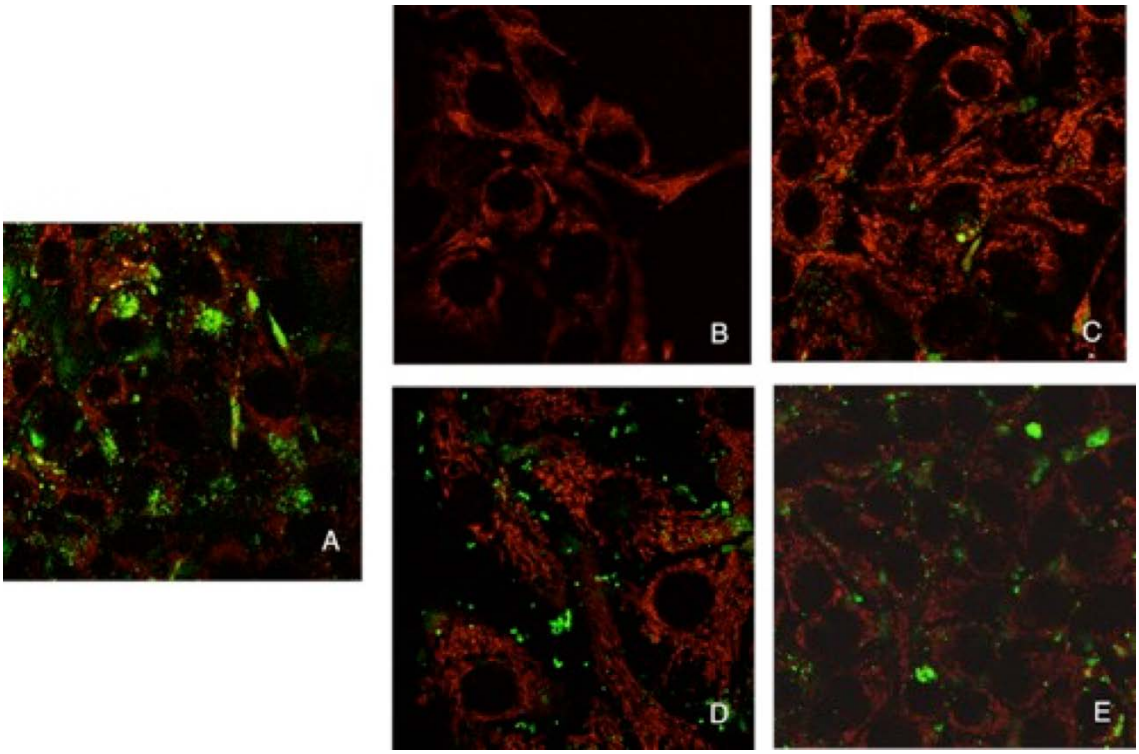


Figure 3.10. Confocal laser scanning fluorescent microscopy (40x mag.) of MDAH2774 ovarian carcinoma cells after incubation with fluorescently-labeled polymers. The red channel is Mitotracker™ Orange and the green channel is either FITC or BODIPY® FL. (A) Control polymer HPMA-FITC after 24 h incubation. (B-E): Semitelechelic TPP-HPMAs after 6 h incubations; (B) TPP-HPMA-FITC-4 kDa; (C) TPP-HPMA-FITC-12 kDa; (D) TPP-HPMA-BODIPY® FL-3 kDa; E: TPP-HPMA-BODIPY® F -12 kDa

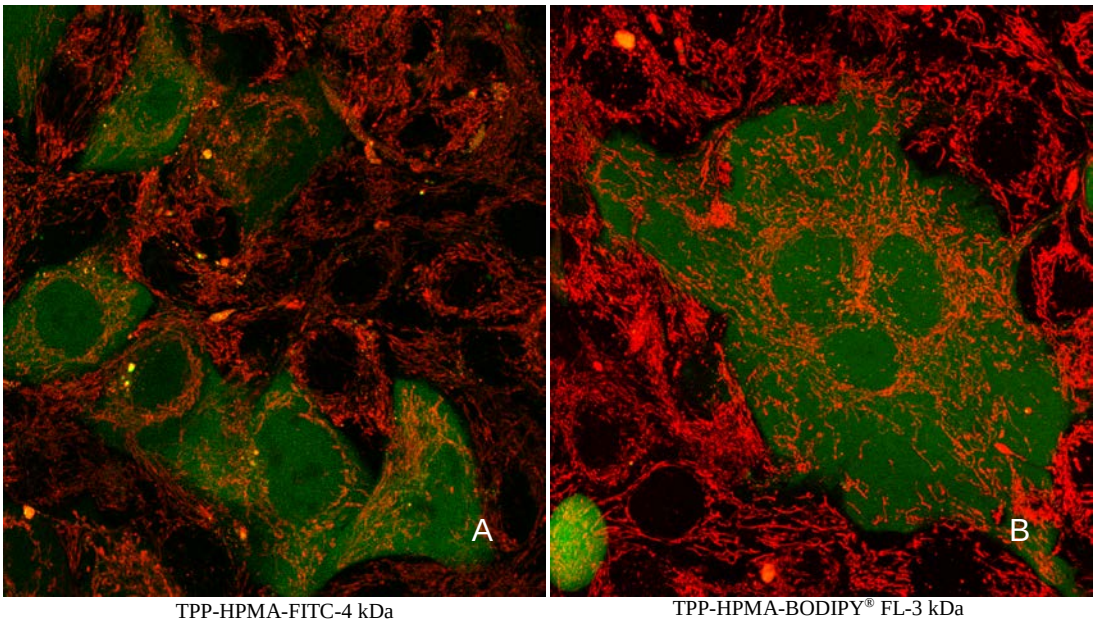


TPP-HPMA-FITC-4 kDa

TPP-HPMA-BODIPY® FL-3 kDa

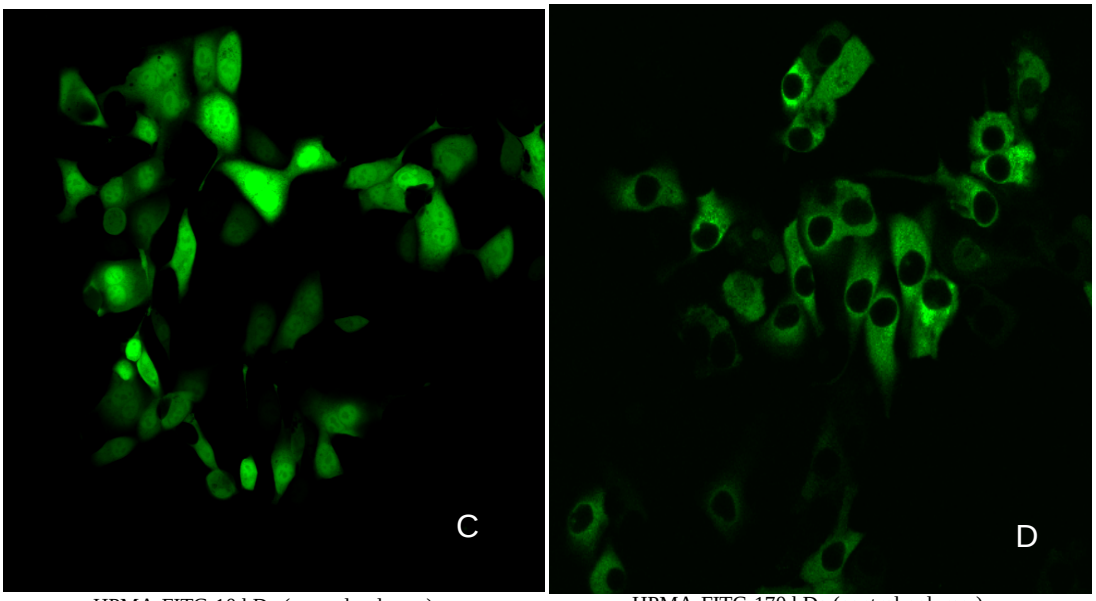


HPMA-FITC-10 kDa (control polymer)

HPMA-FITC-170 kDa (control polymer)

Figure 3.11 Confocal laser scanning fluorescent microscopy of MDAH2774 cells after microinjection with fluorescently-labeled polymers. The red channel is Mitotracker Orange and the green channel is either FITC or BODIPY® FL. **A**: Injection with TPP-HPMA-FITC-4 kDa and 24 h incubation at 37 °C. **B**: Injection with TPP-HPMA-BODIPY® FL-3 kDa and 24 h incubation. **C**: Injection with HPMA-FITC-10 kDa control and 20 min incubation. **D**: Injection with HPMA-FITC-170 kDa control and 6 h incubation

# CHAPTER 4

# INTRACELLULAR TRAFFICKING AND SUBCELLULAR DISTRIBUTION OF A LARGE ARRAY OF HPMA COPOLYMERS[1]

## 4.1 Abstract

The basic physicochemical properties that determine the distribution and fate of synthetic macromolecules in living cells were characterized using fluorescently labeled HPMA (*N*-(2-hydroxypropyl)methacrylamide) copolymers. Twelve different classes of water-soluble copolymers were created by incorporating eight different functionalized comonomers. These comonomers possessed functional groups with positive or negative charges, or contained short hydrophobic peptides. The copolymers were fractionated to create parallel "ladders" consisting of 10 fractions of narrow polydispersity with molecular weights ranging from 10 to 200 kDa. Polymer samples were added to the growth media of live cells and the resulting endocytosis and trafficking of the polymers was characterized and quantitated. All polymers were trafficked to the lysosomal compartment, but the kinetics and endocytotic pathway favored varied greatly due to comonomer chemical type

[1] This chapter is adapted with permission from: J. Callahan, P. Kopečková and J Kopeček. Intracellular Trafficking and Subcellular Distribution of a Large Array of HPMA Copolymers. *Biomacromolecules*. 2009 Jul 13; 10(7): 1704–1714. 

and the molecular weight of the copolymers. The intracellular distribution of polymers introduced directly into the cytoplasm was characterized for copolymer solutions microinjected into cultured ovarian carcinoma cells. Even the highest molecular weight HPMA copolymers were shown to quickly and evenly diffuse throughout the cytoplasm and remain excluded from membrane-bound organelles, regardless of composition. The exceptions were the strongly cationic copolymers, which demonstrated a pronounced localization to microtubules. For all copolymers, nuclear entry was consistent with passive transport through the nuclear pore complex (NPC). Nuclear uptake was shown to be largely dictated by the molecular weight of the copolymers. However, detailed kinetic analyses showed that nuclear import rates were moderately, but significantly, affected by differences in comonomer composition. HPMA copolymers containing amide-terminated phenylalanine-glycine (FG) sequences, analogous to those found in the NPC channel protein, demonstrated a potential to regulate import to the nuclear compartment. Kinetic analyses showed that 15 kDa copolymers containing GG**FG**, but not those containing GGL**FG**, peptide pendant groups altered the size-exclusion characteristics of NPC-mediated nuclear import.

## 4.2 Introduction

Water-soluble, synthetic polymers have been successfully used in a variety of applications to enhance the delivery and efficacy of therapeutic drugs, nucleic acids, peptides, and proteins. For example, polymeric anticancer drug carriers have been used to greatly enhance the biocompatibility (1, 2), pharmacokinetics (3, 4), nonimmunogenicity (2, 5), and cell targetability (6-10) of chemotherapeutic agents, while reducing their toxicity

toward normal tissues.

Typically, cell uptake of synthetic macromolecules occurs via endocytosis, whereby high molecular weight molecules are routed to the lysosomal compartment. Pharmaceutical activity necessitates the subsequent release of the active agent from the endocytotic vesicles. For polymer–low molecular weight drug conjugates, release of the drug from the polymeric carrier can be accomplished using hydrolyzable bonds. The delivery of intact macromolecules directly to the cytosol of target cells has been accomplished by a variety of methods that destabilize lipid membranes (11).

Once macromolecules are delivered to the cytosol, several methods may be employed to traffic them to specific subcellular compartments, such as the nucleus and mitochondria, to enhance their therapeutic efficacy. Nuclear and mitochondrial localization of macromolecules has been mediated by targeting peptides (12-15) or the lipophilic triphenylphosphonium (TPP) cation (16-18).

However, macromolecules (without subcellular targeting moieties) are typically excluded from entering membrane-limited organelles, such as mitochondria, lysosomes, the endoplasmic reticulum, in a nonspecific manner. The exception to this is the nucleus whose membrane possesses channels that allow the passive uptake of intermediate-sized macromolecules. The NPC (nuclear pore complex) of the nuclear envelope is composed of about 30 different nucleoporin proteins and is the conduit for both nuclear import and export of macromolecules, such as proteins and nucleic acids. In active transport, cargo as large as 40 nm possessing NLS (nuclear localization sequence) or NES (nuclear export sequence) signaling peptides are guided through the channel after binding to NTR (nuclear transport receptor) proteins (19). For smaller macromolecules below 10 nm, however,

NPCs have been shown to act as nonspecific pores that allow exchange between the nucleus and cytoplasm by diffusion (20). As a conduit for nonbiological macromolecules, the NPCs have been shown to transmit PEG-coated gold colloid particles 4–7 nm in diameter (21). In contrast, 27 and 39 nm PEG-gold particles and 25 nm quantum dot particles conjugated with NLS peptide sequences have been shown to require the active nuclear import mechanism for uptake by the nucleus (19, 21, 22).

Dynamic structural modeling of several of the nucleoporins in the core of the NPC has been used in an attempt to explain the dual size selection of active versus passive nuclear transport selection (23). The structure of several nucleoporins notably possesses natively unfolded domains containing hydrophobic FG (phenylalanylglycine) domains, consisting of FG, GLFG, and FXFG peptide repeats. Several different models have been debated to account for the dynamics of NPC transport. Ribbeck et al. have proposed that the FG domains form a polymer brush conformation in the NPC channel that excludes larger solutes by entropic hydrophobic repulsion (24, 25). Frey et al. have suggested that nucleoporins form an unstructured hydrogel mesh in the core of the NPC channel through reversible cross-links of FG peptide repeats that they possess (26, 27). Nuclear transport receptors have been shown to possess a number of hydrophobic regions that specifically bind to nucleoporins in their FG repeat regions and have been proposed to disassociate interchain cross-links. The pore proteins, thereby, form a 3-dimensional mesh with a simple molecular weight permeability cutoff when cross-linked. In this model of active transport, NTRs can open the nucleoporin mesh by “melting” the hydrogel structure and guide large macromolecules in or out of the nuclear compartment (28). Alternately, Melčák et al. proposed that the interface between the α-helical regions of nucleoporins selectively slide

circumferentially to dilate the NPC pore opening after NTR binding (29). More recently, several models of Nup structure have been proposed to account for transport in and out of the nucleus. This includes a diblock copolymer brush model (DCBM) that models FG nups as diblock polymers that form an unstructured "forest" of short and extended nup proteins that account for the different transport properties of the NPC (30). All these models emphasize the role of FG crosslinking in nup functionality, but the models envision the roles of the unstructured nucleoporin proteins in different configurations (31).

Nonetheless, relatively little is known about the chemical and physical forces that direct localization of macromolecules once in the cytosol. To help ascertain this basic understanding, we took advantage of a well-characterized and synthetically flexible polymer system to create an array of macromolecules with widely divergent chemical characteristics. Fluorescently labeled *N*-(2-hydroxypropyl)methacrylamide (HPMA) copolymers with a reproducible range of well-defined molecular weights were made using comonomers with a variety of charges and hydrophilicities in an attempt to reveal the physicochemical properties that guide the intracellular transport and distribution of synthetic macromolecules. The copolymers were fractionated into a series of polymers of narrow polydispersity and microinjected into the cytosol of cultured human ovarian carcinoma cells. Their fate was observed using fluorescence microscopy and other imaging methods. A variety of subcellular markers were simultaneously used to identify subcellular compartments within the cells to determine colocalization. Specific issues investigated included diffusion in the cytoplasm, relative rates of nuclear entry, binding to intracellular membranes and other structures, and sequestration by subcellular compartments.

Finally, HPMA copolymers containing FG (Phe-Gly) motifs were generated as an

attempt to modulate the kinetics of nuclear uptake of macromolecules. Their structure was based on recent theories describing the function of proteins of the NPC (nuclear pore complex) in the nuclear membrane that have been shown to regulate nuclear import and export of macromolecules.

## 4.3 Experimental Methods

### 4.3.1 Monomers

All chemicals and solvents used were of reagent grade or better unless otherwise stated. MAA (methacrylic acid), DEMA (2-(*N*,*N*-dimethylamino)ethyl methacrylate), and SEMA (2-sulfoethyl methacrylate) were purchased from PolySciences, Inc. HPMA (*N*-(2-hydroxypropyl)methacrylamide) (32) and MA-FITC (*N*-methacrylolyaminopropyl fluorescein thiourea) (33) were prepared as previously described. MATC (*N*-methacryloyloxyethyl trimethylammonium chloride) was prepared as described before by quaternization of DEMA with gaseous methylchloride in acetone (34). The peptide monomers *N*-methacryloylglycylglycine (MA-GG), *N*-methacryloylglycylphenylalanine (MA-GF), and *N*-methacryloylglycylphenylalanylleucylglycine (MA-GFLG) were prepared as described previously (35).

The amide-terminated monomers MA-GGFG-$NH_2$ (*N*-methacryloylglycylglycylphenylalanylglycine amide) and MA-GGLFG-$NH_2$ (*N*-methacryloylglycylglycylleucylphenylalanylglycine amide) were synthesized using standard Fmoc solid-phase peptide chemistry. On Rink Amide MBHA resin (Novabiochem), glycine and phenylalanine or glycine, phenylalanine, and leucine were sequentially attached. While still conjugated to the resin, the peptides were coupled to *N*-

methacryloylglycylglycine peptide (MA-GG). The completed monomers were then released using a TFA solution and precipitated in diethyl ether. The dried monomers were purified using RP-HPLC, and their mass verified using MALDI-TOF MS. The molecular masses for the two main ion peaks measured for MA-GGFG-$NH_2$ were 404.2 and 426.2, corresponding to calculated values 404.4 (M·H+) and 426.4 (M·Na+). The molecular mass of the main ion peak measured for MA-GGLFG-$NH_2$ was 539.3 versus a calculated value of 539.5 (M·Na+).

### 4.3.2 Polymer Chemistry

All copolymers used in this study were generated by radical chain polymerization using 0.60 wt % AIBN as the initiator. The feed mole ratios of all 12 copolymerizations and copolymer compositions are shown in Tables 4.1. and 4.2. The structure of monomers and copolymers is depicted in Figures 4.1. and 4.2. (For the sake of clarity, all polymers were named based on the concentration of feed comonomer rather than final content in the copolymers.) Methanol was used as the bulk solvent for all reactants of the polymerization in a total reaction volume of 5ml. To slightly lower the average molecular weight of each of the resulting copolymers, 0.078 wt % mercaptopropionic acid was added as a chain transfer agent. Before mixing with the other components of the polymerization reaction, some of the monomers were first dissolved in other solvents to ensure complete dissolution. The liquid monomer SEMA was diluted 1:10 with water to ensure miscibility with methanol during the polymerization reaction. The peptide monomers MA-GFLG, MA-GF, MA-GGFG-$NH_2$, and MA-GGLFG-$NH_2$ were dissolved in a minimum volume of DMSO (~2$\mu$L/mg) before addition to the reaction solution. The alkaline monomers DEMA and

MATC were dissolved in 0.05 N $HCl_{aq}$ to a monomer concentration of 250 mg/ml to acidify the final reaction solution.

After mixing, the polymerization solutions were bubbled with argon, sealed in a glass ampule, and then heated to 50°C for 24 h. When complete, the reactions were dried under vacuum and then redissolved in a minimum volume of methanol. The polymers were then separated from the unreacted monomers on an LH-20 column with methanol as the mobile phase. The eluted fractions containing the FITC-labeled product were then dried under vacuum, redissolved in a minimum amount of distilled water, and then freeze-dried to isolate the finished solid product. The final yields of all copolymers were between 75–85%.

### 4.3.3 Texas Red-labeled HPMA Copolymer

HPMA copolymers labeled with Texas Red (Table 4.2.) were synthesized in a two-step process, as previously described.(36) First, a copolymer of HPMA with *N*-(3-aminopropyl)methacrylamide (molar ratio 98:2) was synthesized by radical copolymerization. The copolymer contained 1.9 mol% of amine side chains; $M_W$ = 80000. In the second step, Texas Red was attached by the reaction of Texas Red succinimidyl ester (Molecular Probes) with amine groups of the copolymer. The purified product contained 1.6 mol% Texas Red, containing side chains as determined spectrophotometrically ($\varepsilon_{593\ nm}$ = 86000 $M^{-1}cm^{-1}$, PBS).

### 4.3.4 Copolymer Characterization

For all FITC-labeled copolymers, the content of MA-FITC monomer was determined by spectrometry using the absorbance at 495 nm ($\varepsilon_{495\ nm}$ = 80000 $M^{-1}cm^{-1}$) in 0.1 M borate buffer (pH 9). The content of peptide monomer in the six peptide-containing copolymers was determined by HPLC amino acid analysis (AAA) using phenylalanine as a reference. For this, 2–3 mg of peptide-containing copolymer was hydrolyzed in 0.2 ml of 6N HCl in a sealed glass ampule at 115°C for 16 h. The hydrolyzate was dried over NaOH pellets *in vacuo* and then dissolved in 0.5 ml of distilled $H_2O$. Before separation on a reverse phase Microsorb MV C18 column, the amino acids in the sample were derivatized with *o*-phthaldialdehyde (OPA). HPLC used a 10–90% gradient elution where solvent A was 0.05 M sodium acetate in 0.25% acetonitrile pH 6.0 and solvent B was 0.05 M sodium acetate in 70% acetonitrile. The HPLC fluorescence detector used the excitation at 229 nm and emission at 450 nm. The content of charged MAA, SEMA, and DEMA comonomers was determined using an automated TIM854 pH titration workstation (Titralab, Radiometer Analytical, Lyon, France) with a combined minitype electrode and either 0.05N NaOH or 0.05N HCl as a titration standard solution. Content of MATC was determined by potentiometric titration of chloride ions using a combined silver type electrode and 0.05 M $AgNO_3$ titration standard solution. The comonomer content and characterization of the copolymers are summarized in Tables 4.1. and 4.2.

Size-exclusion chromatography (SEC) was used to determine the molecular weight distribution of the polymers. All samples were run on an FPLC system (GE Healthcare) equipped with UV and differential refractive index detectors using a Superose 6 HR10/30 analytical column in PBS (pH 7.3) calibrated with pHPMA standards of a narrow

polydispersity ($M_w/M_n < 1.2$). To ensure accurate molecular weight calculations, polymer size was also calculated using dynamic light scattering in tandem with SEC. For this, d*n*/d*c* measurements were determined for each polymer with a DSP interferometric refractometer (OPTILAB, Wyatt Technology, Santa Barbara, CA) using standard polymer/PBS solutions. Molecular weight determinations were made using laser light scattering data (MINIDAWN, Wyatt Technology) and calculated using chromatographic software (ASTRA, Wyatt Technology).

### 4.3.5 Copolymer Fractionation

All 12 copolymers were further fractionated into a standard molecular weight "ladder" series using a preparative Superose 6 HR16/60 FPLC column. For each separation, 50 mg of polymer was loaded on to the column using PBS as the eluent and a flow rate of 1 ml/min. Fractions were collected using the same schedule for all copolymers, whereby 10 fractions of 5 ml each were taken during the 50 min window of polymer elution from the column. At least two 50 mg fractionations were performed for each copolymer. The corresponding fractions for each separation (labeled F1–F10 for fractions 1–10) were pooled, dialyzed extensively against water, and freeze-dried. The molecular weight distributions of the resulting polymer fractions were then characterized using a Superose 6 analytical SEC column. A summary of the molecular weight analyses for the fractions used in subsequent experiments is shown in Tables 4.1. and 4.2. Analyses of the content of comonomer for several randomly selected copolymer fractions were analyzed using pH titrations, AAA and AgCl titration to ensure that the mole fractions of the fractionated polymers were similar to the starting unfractionated polymers.

### 4.3.6 Cell Culture

MDAH2774 ovarian carcinoma cells (ATCC) were cultured in Lebowitz's L-15 media supplemented with 10% fetal bovine serum (HyClone Laboratories, Logan, UT) with 10 μg/ml insulin (HyClone) and 12.5 mM HEPES buffer (pH 7.4) under a humidified atmosphere at 37°C. All uptake experiments were performed in the presence of 10% FBS.

For static imaging studies, cells were seeded in No. 1.5 glass-bottom 14 mm microwell dishes (MatTek Corp., Ashland, MA). For time-lapse experiments, cells were seeded on 0.17 mm Delta T temperature-controlled microwell dishes (Bioptechs, Inc., Butler, PA).

In colocalization studies, fluorescent subcellular markers were used. For these, media containing the markers was added approximately 1 h before initial imaging, and fresh media was added to the microwell dishes immediately before imaging. To identify mitochondria, 100mM MitoTracker Orange CM-$H_2$TMRos (Molecular Probes) was added. To identify lysosomes, 50mM LysoTracker Red (Molecular Probes) was used.

### 4.3.7 Live Cell Imaging

Live cell polymer uptake studies were conducted using scanning laser confocal fluorescence microscopy (Olympus Flowview with krypton/argon excitation lasers). For static microscopy, images were collected by combining dual-channel fluorescent and transmitted light using z-series slices in 0.2 μm steps. Image data were processed using ImageJ software.

### 4.3.8 Incubation of MDAH Cells with Copolymers Dissolved in Media

As a control to determine the baseline mode of polymer internalization, MDAH ovarian carcinoma cells (ATCC) were incubated with each of the polymers in their incubation media. A single molecular weight fraction (fraction 9, all ranging in average molecular weights between 12–17 kDa) of each polymer type was used in a systematic study of uptake. Plated cells were incubated for 24 h in growth media containing 0.5 mg/ml polymer. Before imaging the media was replaced with fresh media. The cells were then imaged using confocal laser scanning microscopy (see Figure 4.2.).

More detailed uptake studies using the large polymer array were subsequently performed on C4-2 prostate carcinoma cells. (see Chapter 5) (37).

### 4.3.9 Microinjection

Fluorescently labeled 1.0 mg/ml polymer/PBS solutions were directly injected into the cytosol of plated MDAH2774 cells using 0.5 μm glass needles equipped on an Eppendorf Transjector 5346 pressure injector and fixed to an Eppendorf 5171 micromanipulator arm. Pressures used varied from 80 to 120 hPa and care was taken to inject solutions as far from the cell nuclei as possible to avoid causing physical trauma to the cells.

### 4.3.10 Intracellular Distribution of Copolymer Fractions

Following microinjection, MDAH2774 cells were observed periodically (every 10 or 15 min) for up to 48 h using laser scanning fluorescence confocal microscopy. For

detailed comparisons of the effect of molecular weight, every fraction from polymers 5% MAA-P, 5% GFLG-P, and 20% DEMA-P was used. The distribution of all types of polymers that were completely excluded from nuclei was characterized by injecting MDAH2774 cells with every F4 polymer, which all possessed molecular weights greater than 75 kDa. Cells were microinjected and then incubated at 37°C for 24 h. At 1 h before imaging, either LysoTracker Red or MitoTracker Orange (Molecular Probes) was added to the media. Immediately before imaging, the media was replaced with fresh media.

### 4.3.11 Rates of Nuclear Entry/Time Lapse Imaging

F7 (fraction 7) polymers of a uniform molecular weight ($M_W$ = 36 ± 6 kDa) of 5% comonomer polymers were selected. To quantify the rate of nuclear entry, time-lapse imaging was performed on MDAH2774 cells after microinjection. Each movie was started 10–15 min after polymer microinjection. Each frame of the movies represents 15 min (or 10 min in the case of polymers MAA-P, MATC-P, and GFLG-P) and they were collected until there was an apparent equilibrium between the nuclear vs. cytosolic concentrations. Laser power was set low (2–5%) to minimize bleaching during imaging. The image series used for measurement was of one confocal plane taken approximately midway through the nuclei or 2–4 $\mu$m above the coverslip surface. For quantification analysis, the image series was coded and the fluorescent image intensity data were collected by a blinded second party. Cells in the image series were numbered and tracked separately during the movie to account for cell migration and changes in cell shape. For each polymer, 5–9 cells in the series in the imaging frame were used in the analysis. Polymer concentrations in the nuclei and cytosol were measured by the image intensity of a 2 μm radii circular region in the

nuclei and the perinuclear cytosol of each cell. The regions used for measurement were manually moved during the series to account for cell movement. Nuclear entry time courses of each cell measured for each polymer were averaged and then curve-fitted by regression analysis using Equation 3.1 on SigmaPlot software to a three-parameter rising exponential function of the form:

$$R_{n/c} + R_0 + R_{eq} \times (1 - e^{-kt}) \qquad \text{(Equation 4.1)}$$

where $R_{n/c}$ is the ratio of the nuclear versus cytosol polymer concentration, $R_0$ is the fitted initial N/C ratio (to account for background fluorescence in measured values), $R_{eq}$ is the equilibrium concentration of polymer in the nucleus versus cytosol, and $k$ ($min^{-1}$) is the rate constant of nuclear uptake.

To evaluate statistically significant differences, the nuclear entry rate constants for all test polymers were compared to the rate constant calculated from control pHPMA-FITC using the two-tailed Student's *t* test. Differences in mean values were considered significant for P-values less than 0.05.

### 4.3.12 Fluorescence Recovery After Photobleaching (FRAP)

FRAP was performed on MDAH2774 cells after cytosolic microinjection of copolymers. In each study, polymer was injected 1–2 h before the bleaching experiment. Imaging was performed on a FV1000 Olympus confocal microscope with an independent light path and galvo SIM scanner (simultaneous image microscopy) image scanning system. An ~2 μm diameter spot was bleached for each microinjected cell using a 405 nm diode laser as the light source. Images before, during, and after bleaching were taken every ~0.6 s for several min. In some series, the bleaching laser was turned on continuously to

determine whether any copolymer was retained by components of the cell (i.e., FLIP, fluorescence loss in photobleaching).

#### 4.3.13 Coinjection of FG Peptide Copolymers and Nuclear Exclusion Markers

The FG containing polymers were generated to determine whether the peptide pendant groups affected the kinetics of nuclear entry via the NPC. For this, the FITC-labeled, fractionated copolymers were coinjected into MDAH2774 cells with fractionated Texas Red-labeled pHPMA (TR-P) as a marker for nuclear exclusion and uptake. For each coinjection, PBS solutions of 1mg/ml FITC test polymer and 1mg/ml TR-P marker polymer were injected into a field of cells. In separate regions of the same coverslip, the cells were injected with 1mg/ml solutions of either test polymer (green) or TR-P marker polymer (red) alone, to act as controls. Time-lapse confocal z-series imaging of the injected live cells was immediately initiated after injection. Images were collected using 488 nm and 543 nm lasers in sequence using the same settings for all three regions of injected cells.

## 4.4 Results and Discussion

### 4.4.1 Design and Characterization of an HPMA Copolymer Array

A large array of HPMA copolymers was synthesized by radical polymerization (Tables 4.1. and 4.2.). Eight different methacryloyl-functionalized comonomers were employed to confer different pendant functional groups to the resulting linear polymers (Figure 4.3.). For each copolymer, 1 mol% of MA-FITC (*N*-methacrylolyaminopropyl fluorescein thiourea) was incorporated for convenient visualization. Monomers with four

different types of charged groups were used: MAA (methacrylic acid), a weak acid; SEMA (2-sulfoethyl methacrylate), a strong acid; DEMA (*N*,*N*-dimethylaminoethyl methacrylate), a weak base; and MATC (*N*-methacryloyloxyethyl trimethylammonium chloride), a strong base. Four peptide-containing monomers were used to create relatively hydrophobic copolymers: *N*- methacryloylglycylphenylalanine (MA-GF), *N*-methacryloylglycylphenylalanylleucylglycine (MA-GFLG), *N*-methacryloylglycylglycylphenylalanylglycineamide (MA-GGFG-$NH_2$), and *N*-methacryloylglycylglycylleucylphenylalanylglycineamide (MA-GGLFG-$NH_2$). Fractionation using SEC provided 10 molecular weight fractions (F1–F10) each with a narrow polydispersity. The content of the comonomers in the resulting copolymers was typically 75–85% of the mol % of the feed concentration; however, for the sake of clarity, the feed comonomer concentrations were used for the nomenclature of the copolymers. For example, "5% GFLG-P" refers to the peptide copolymer resulting from the copolymerization of 5 mol% MA-GFLG, 94% HPMA, and 1% MA-FITC. SEC-fractionated copolymers were further designated by fractionation order and decreasing molecular weight. For example, the suffix in "5% GFLG-P-F7" refers to the seventh SEC fraction of copolymer 5% GFLG-P (Tables 4.1. and 4.2.).

The molecular weight profiles of the array copolymers from high (F4), midrange (F7), and low (F9) molecular weight fractions from the array copolymers used in later experiments were characterized by SEC. The middle range of fractions from F5 to F9 formed a molecular weight "ladder" of standard copolymer hydrodynamic sizes, as the differences in average molecular weight for fractions 5–9 from all the polymers had standard deviations less than ±6%. To illustrate, the average structure, and the SEC profiles

for the fractions collected from copolymer 5% MATC-P and 5% MAA-P are shown in Figures 4.4. and 4.5., respectively.

In summary, a two-dimensional array of HPMA copolymers was generated with 12 distinct chemical characteristics in one dimension, and a discrete sequence of five parallel molecular weights (10–80 kDa) in the other dimension.

### 4.4.2 Endocytosis and Subcellular Trafficking of Polymers from Media

Initial uptake studies showed that all copolymers when incubated with MDAH2774 ovarian carcinoma cells were internalized by endocytosis (Figure 4.5.). Punctate staining of all cells after incubation with all the polymers was consistent with lysosomal compartmentalization. It was also evident that the relative amount of polymer uptaken by the cationic polymers was consistent with adsorptive endocytosis and thereby showed the greatest amount of uptake. For no polymer was there evidence of any endosomal/lysosomal of polymer escape after 24 h.

### 4.4.3 Cytosolic Microinjection of HPMA Copolymers

The subcellular distribution of HPMA copolymers was characterized by pressure microinjecting copolymer solutions directly into the cytosol of cultured cells. For each species of copolymer, diffusion occurred rapidly throughout the cytosol after microinjection and had reached equilibrium within a few minutes required to collect images. The copolymers appeared to be excluded from all membrane-limited subcellular compartments, even after 24 h. The only notable shifts in intracellular distribution were observable in rates of nuclear entry. Here, differences were largely, but not entirely, a

function of molecular weight rather than the identity or initial concentration of comonomer. The lowest molecular weight polymers injected (i.e., the “F9” and “F10” fractions), with masses less than 25 kDa, immediately diffused throughout the nucleus after cytosolic injection (row **a** of Figure 4.6.). In contrast, the highest molecular weight polymers (>60–80 kDa; up to fraction “F5”) remained completely excluded from the nuclei, even after 24 h. (row **b** of Figure 4.6.). Polymer fractions in the intermediate molecular weights between 25–50 kDa entered the nuclear compartment in time frames that ranged from 15 min to 12 h. Subsequent experiments were designed to explore in detail the differences between polymers with respect to initial subcellular distribution and fate.

### 4.3.4 Short-term Intracellular Distribution

To evaluate polymer diffusion through the cytoplasm, FRAP (fluorescence recovery after photobleaching) experiments were performed on selected polymer samples using high-speed time-lapse imaging. When 2 μm regions of cytoplasm were bleached using a short burst from the laser, the diffusion of the surrounding polymer into the bleached area was very rapid and equilibrium was reestablished in less than 3 sec for all polymers types (Figure 4.7.).

Subsequent FLIP (fluorescence loss in photobleaching) experiments where laser bleaching was used for several minutes showed that all the polymers in the cell freely diffused to the bleached region within a few minutes. The only exception to this trend was observed when using copolymers possessing intermediate molecular weights (25–50 kDa) able to enter the nucleus but slowly over a period of hours. In these microinjected cells, the polymers disappeared from the cytoplasm within 2–3 min, but the copolymer in the nuclei

was retained and remained visible. Continued bleaching produced a very gradual decrease of polymer in the nuclei as the polymer slowly diffused out of the nuclear compartment and into the cytosol where it could quickly diffuse through the bleached region. The rapid and homogeneous diffusion of HPMA copolymers as large as 100 kDa throughout the cytoplasm is in good agreement with previous studies of the diffusion of biological macromolecules such as dextran and Ficoll (38-40). On the contrary, theories on the hydrogel nature of the cytoplasm seem not to hold based on these results (41).

The FLIP experiments using intermediate molecular weight (25–50 kDa) copolymers also confirmed that the only barriers to the free diffusion of most of the polymers were subcellular membrane structures. Furthermore, all the results, with respect to nuclear uptake and export, were consistent with simple size-limited unassisted diffusion through the nuclear pore complex (42, 43). Transport in and out of the nuclear compartment was thus symmetrical and consistent with the known properties of passive NPC transport, as opposed to active import or the result of disruption of the nuclear envelope.

### 4.3.5 Long-term Intracellular Distribution

The systematic analysis of the long-term fate of the copolymers used fractions with molecular weight averages greater than 80 kDa to avoid potential toxicity. This issue was illustrated in a time-lapse imaging of cells injected with the strongly cationic copolymer 20% MATC–P-F7, which showed the cells collapse and die immediately after the copolymer began to enter the nucleus of each cell, 1-3 h after microinjection.

Use of the organelle markers for mitochondria and lysosomes showed no colocalization using polymers of any of the 10 types studied here, even 24 h after

microinjection (data not shown). Further, the only cells that showed significant distributional nonhomogeneity in the cytoplasm were the highly cationic types, particularly 20% MATC-P. As shown in Figure 4.8, this polymer clearly localized to microtubules, as confirmed by colocalization with antitubulin antibodies. Much weaker microtubule localization was also noted for polymers 5% MATC-P and 20% DEMA-P. In each of these experiments, fluorescent staining of microtubules was a slow process and required several hours to become observable. Microtubule binding is consistent with the known cation-binding properties of tubulin proteins (44, 45).

Nuclear entry of copolymers was largely dictated by molecular weight rather than chemical composition. Copolymers with intermediate molecular weights between 25–50 kDa entered the nuclei, but slowly, over the course of 15 min to 24 h. The hydrodynamic diameters of charged HPMA copolymers in this mass range have been shown to be between 2–4 nm in free aqueous solution (34), a range consistent with passive diffusion through the NPC. Systematic time-lapse imaging was then performed on each type of copolymer using size fractions near the cutoff for entry. By using polymers near the nuclear uptake size limit, differences in the rate of nuclear uptake due to *chemical composition* might be characterized.

### 4.3.6 Kinetics of Nuclear Entry of Copolymers

The use of well-characterized synthetic macromolecules with well-controlled molecular size permitted to better characterize the passive transport characteristics of the NPC. Macromolecular size and shape of HPMA copolymers could be held constant while the chemical functional groups were altered. Because all the copolymers were charged and

relatively hydrophilic, they were all assumed to possess a similar extended, random coil structure in solution, given the presence of counterions. Small changes in import kinetics could be detected and attributed to surface chemical interactions apart from the dimensions of the macromolecules. To this end, time-lapse imaging of MDAH2774 cells after cytosolic injection was performed using all of the intermediate-sized F7 fractions of the 5% copolymers ($M_W$ = 36 ± 6 kDa) in the polymer array. This copolymer size range has been shown in preliminary studies to enter the nucleus in a time range of 1–6 h, a window convenient for reproducible image analyses. Samples from the time-lapse imaging are shown in Figure 4.9. for copolymer 5% GFLG-P-F7.

For comparison, fractionated pHPMA was used as a control. Imaging of the cells injected with control (neutral) homopolymers was taken rapidly (3 min/frame) to create a baseline with a minimized experimental error. Cells microinjected with HPMA copolymers were imaged using longer time intervals (10 or 15 min/frame). The time-lapse movies of the cells after microinjection of each of the six types of polymer revealed a large amount of both qualitative and quantitative data.

4.3.6.1 Observational Summary of Time-lapse Movies after Microinjection of Copolymers

- **5% SEMA-P (Strongly acidic):** Entry of the polymer into the nuclear is relatively quick, although not completely uniform. Maximum nuclear concentration is reached in 60 to 90 min. Rounding of the cells after injection suggests some toxicity to the cells.
- **5% MAA-P (Weakly acidic):** Entry of the polymer into the nucleus is relatively

quick, although the concentration in the nuclei never surpasses higher than half the starting concentration in the cytosol. The maximum nuclear concentration is reached in less than 30 min. Loss of adhesion and rounding of the cells after injection suggests some toxicity to the cells.

- **5% DEMA-P (Weakly basic):** Entry of the polymer into the nuclei is quick and very uniform. The maximum nuclear concentration is reached in less than 60 min for all cells. The cells remain well attached and spread during the time course indicating that the polymer is not significantly toxic.
- **5% and 20% MATC-P (Strongly Basic):** In each case, entry of the polymer into the nucleus was immediately followed by collapse of the nuclei and the whole cell. Nuclear entry appears to be dose-dependent as the cells with the lightest fluorescence exclude the polymer from their nuclei throughout the time of observation and never round or collapse. It may be hypothesized that the nuclear membrane is impermeable to the cationic polymer at low concentration, but destabilizes the membrane at higher concentrations allowing the polymer to quickly enter after that point. Nuclear entry is typically observable after 60 min for both comonomer concentrations. The polymer is toxic to the cell once in the nucleus at high enough concentration, perhaps due to condensation of genomic DNA.
- **5% GF-P (Peptide polymer):** Entry of the polymer into the nuclei was slow and not very uniform. The maximum nuclear concentration is reached doesn’t appear to be reached within 3-4 h and quantitation is complicated by the rounding of the cells during the time course. These results are most similar to those found using the 5% MAA polymer.

- **5% GFLG-P (Hydrophobic peptide polymer):** Entry of the polymer into the nuclei is slow and uniform. The maximum nuclear concentration doesn't appear to be reached within the 4 h of the time course. The cells remain attached and spread during the time course indicating that the polymer is not disruptive to the cell's structure. There appears to be some localization of the polymer to the perinuclear space and the nuclear membrane. This localization was not seen with higher molecular weight GFLG polymer so it cannot be identified as a specific localization to a subcellular compartment.

4.3.6.2 Nuclear Uptake Kinetics

In all cases, copolymer entry into the nucleus was consistent with first-order kinetics and the data were fit to rising exponential functions (Figure 4.10.). *P* values for calculated equilibrium N/ C (nuclear/cytoplasmic) ratios ($R_{eq}$) and import rate constants ($k$) were typically 0.001 or less. For all polymer types the final equilibrium ratios of nuclear versus cytoplasmic concentrations were less than unity, and ranged between 0.4 and 0.9. Since the polymers possessed some polydispersity and the average $M_W$ varied between polymer types, one possibility was that these differences in equilibrium concentration reflected a fixed molecular cutoff for polymer entry; however, there was no statistical correlation between polymer molecular weight distribution (SEC) and the equilibrium nuclear to cytosol concentration ratio (data not shown).

Overall, the calculated nuclear import rate constants and equilibrium nuclear concentration ratios were significantly different between some copolymer types. The calculated import rate constant ($k$) for the control pHPMA polymer was 0.0454 $min^{-1}$,

corresponding to a relatively rapid time (1–2 h) for uptake. The only two copolymers with statistically equivalent import rates were the two weakly charged copolymers 5% MAA-P and 5% DEMA-P, with similar rate constants. Forming another distinct group, the two strongly ionic copolymers and the hydrophobic 5% GF-P copolymer had import times which were significantly longer than the control pHPMA, between 2–3 h. Interestingly, the hydrophobic 5% GFLG-P peptide copolymer had the longest import requiring 4–5 h to reach equilibrium. In general, the kinetics of uptake of the different copolymers were found to be moderately, but significantly affected by their respective chemical characteristics. The weakly charged hydrophilic copolymers were found to possess uptake kinetics little different from the pHPMA control.

It can be concluded that the kinetics of nuclear entry of copolymers with different chemical compositions became distinguishable as the molecular weight of the polymers approached the size limit for passive diffusion through the NPC. It is possible that the hydration layer effects of the proteins and copolymers may have played a general role in transport rates. The “uncharged” pHPMA control polymer and weakly ionic copolymers had the fastest transport rates, and decreased charge in the hydrophobic environment of the pore may account for more free movement. The two strongly ionic copolymers had permanent charges, and repulsion from these charges may have created a barrier to transport by reducing partition into the hydrophobic NPC pore environment. It is also possible that the different copolymers may preferentially associate with proteins or other biological agents in the cell that may have greatly changed their hydrodynamic size or their relative affinity for the nucleoporins (Nups), the proteins that compose the internal structure of the NPC channel. Alternately, the slower transport rates for the peptide

copolymers may reflect a higher interaction between the polymers and Nups, where the higher hydrophobicity of the peptide copolymers produced a higher partition ratio into the nuclear channel, but a slower release rate from the interior side of the pore. The low release equilibrium into the nucleoplasm may have presented the rate-limiting step for nuclear entry of the peptide copolymers. Overall, nuclear import may have been optimized for the copolymers with minimal capacity for interaction with biological macromolecules.

#### 4.3.6.1 Nuclear Entry by FP Peptide Copolymers

The results of nuclear import kinetics using copolymers with GF and GFLG peptides, GF-P and GFLG-P, were of interest to recent work in modeling the dynamics of the structure of Nups to explain the dual size selection of active versus passive nuclear transport selection by the NPC. The structure of Nups is most notable due to the role natively unfolded domains play in controlling NPC transport kinetics (24-29, 46, 47). These unfolded domains are referred to as FG-regions due to their characteristic hydrophobic repeat peptide sequences containing FG, frequently including GLFG, and FXFG. It was by happenstance that two of the HPMA copolymers used in the initial cohort of samples in this study possessed similar (though inverted) peptide sequences, GF and GFLG. Furthermore, the average half-life of nuclear entry of the peptide copolymers (but not the molecular weight cutoff) was significantly higher, particularly for the GFLG copolymer. The overall pattern of the rate of nuclear entry was possibly merely a function of the relative hydrophobicity of these polymers. However, the slower import kinetics of the GFLG tetrapeptide copolymer were also suggestive that this polymer may be able to interact with proteins in the NPC channel in a specific manner that may resemble Nups or

the activity of the Nups- binding proteins responsible for active transport through the NPC (karyopherins). Subsequent experiments with an array of peptide-containing copolymers were designed to explore this possibility further.

### 4.3.7 Nuclear Transport Modulation with FG-peptide Copolymers

The 5% GGLFG-P and 5% GGFG-P (Table 4.2.) were selected to evaluate the potential of HPMA copolymers with FG motifs to modulate the kinetics of nuclear uptake. In these copolymers the FG sequence matched the correct sequence directionality of Nups and a spacer between the FG motif and the polymer backbone increased the accessibility for protein binding. Moreover, the peptide side chains were terminated with amides to remove the negative charge that would be directly adjacent to the putative binding sites.

In Figure 4.11. the calculated nuclear uptake half-lives and equilibrium nuclear/cytosol ratios, respectively, are shown for “F7” fractions of both copolymers after microinjection into the cytosol of MDAH2774 cells. The kinetic results showed that both copolymers displayed extended uptake half-lives similar to those measured for the 5% GFLG-P-F7 copolymer. In contrast, only the 5% GGFG-P-F7 copolymer yielded an equilibrium nuclear concentration significantly higher than that derived for control pHPMA. These results suggested that the rate of polymer transport through the NPC was affected by the overall hydrophobicity/hydrophilicity of the copolymers rather than by specific peptide interactions with nucleoporin proteins. The higher equilibrium nuclear concentration of the 5% GGFG-P-F7 copolymer, however, raised the possibility that this copolymer affected an increase in the molecular weight cutoff for diffusion through the NPC.

### 4.3.8 Polymer Coinjections

Because the peptide copolymers are presumed to interact directly with the nucleoporin cross-linking domains, general effects on NPC transport were evaluated using fractionated pHPMA labeled with Texas Red (TR-P) as nuclear exclusion marker (Table 4.2.).

For time-lapse imaging, FITC-labeled peptide copolymers were injected simultaneously into MDAH2774 cells with TR-P. As controls, separate regions of cells were injected with either the test or marker copolymers alone. When this approach was used, small changes in the kinetics of transport through the NPC affected by the peptide copolymers could be measured separately from the uptake kinetics of the peptide polymer itself. This precision in the experimental design and use of several types of controls were included to overcome several potential sources of experimental error. Pressure microinjection of high concentrations of the HPMA copolymers introduces several factors that may have interfered with the quantization of intracellular polymer concentrations over time. The injected cell's responses to the physical trauma of injection and the dispersal of copolymers may include direct damage to the nuclear membrane, mitosis in the cell, or other stresses that induce apoptosis or necrotic death. These can affect the structure of the nuclear envelope and obscure measurements of NPC-mediated nuclear uptake. For these reasons, data were collected from many separate cells and were used only from cells that remained morphologically stable and intact (alive) for the duration of time-lapse imaging. Cells that had very high initial concentrations or sudden increases in nuclear copolymer concentrations were excluded from data analysis.

Presuming that the FG peptide copolymers affect Nup cross-links and that this

interaction had a measurable effect on NPC transport, these changes were hypothesized to have several possible manifestations. One was that the copolymers might form their own cross-links with the Nups. If stably cross-linked, the polymers may have had the effect of blocking the NPC pore or tightening a putative hydrogel mesh structure. This may express itself as slowing the rate of pore transport or lowering the molecular weight cutoff of the channel. Alternately, the copolymers may have disrupted the Nup FG-domain cross-links or alter the dynamics of cross-linking. Given the hydrogel model of Nup structure (24, 26, 27), a phase transition in the pore structure may be affected similarly to the hypothesized mechanisms of active nuclear uptake by importin proteins. These changes may be expressed by increased uptake kinetics or a large increase in the size of macromolecules able to transit the NPC. Because it is known that the larger copolymers contained an increasing number of FG-peptides per polymer chain, different sizes of copolymer were anticipated to have different effects on transport, depending on the model of Nup structure.

Coinjections with the TR-P-F6 ($M_W$ = 45 kDa) marker polymer were performed to better evaluate whether the test copolymers increased the molecular weight cutoff of NPC transport. Because of its molecular weight distribution, TR-P-F6 was largely excluded from passive nuclear uptake for up to 12 h. Preliminary coinjections determined that noticeable increases in nuclear uptake only occurred when the lowest molecular weight fractions (F9) from each peptide copolymer were used. In addition, differences in marker polymer uptake only occurred when the peptide copolymer concentration was higher than a given threshold. For microinjections using 5% GGFG-P-F9 and 5% GGLFG-P-F9, it was found that polymer concentrations greater than 1 mg/ml were required given microinjection volumes less than 5–10% of the total cell volume, or an intracellular copolymer

concentration greater than 50–100 μg/ml.

In the final series of coinjection experiments, 5% GGFG–P-F9 ($M_W$ = 15 kDa) and 5% GGLFG-P-F9 ($M_W$ = 14 kDa) were each coinjected with TR-P-F6 marker polymer into MDAH2774 cells and then imaged for 8–12 h. Differences in the rate of nuclear uptake of the marker polymer were directly derived from a comparison of the coinjected cells and cells injected with the TR-P marker polymer alone. As shown in Figure 4.11., coinjection with 5% GGFG-P-F9 (but not 5% GGLFG-P) significantly increased the import rate constant and total equilibrium nuclear concentration of TR-P-F6 marker pHPMA compared to marker polymer alone. These results showed that the incorporation of the FG peptide motif onto HPMA copolymers had a small but measurable effect on the molecular size of solutes able to diffuse into the nuclei of nondividing cells. Although time to reach equilibrium was not increased significantly, the initial rate of uptake increased more than 3-fold, and the apparent molecular weight cutoff of the NPC channel was effectively increased by 20–30%.

The subtle variations in the kinetics of the different chemical types of copolymers near the molecular weight cutoff of passive nuclear uptake correlate well with the expected differences in binding to the hydrophobic domains of Nups. This observation is consistent with the repulsive exclusion models of NPC gating and passive transport (48, 49). It is also consistent with models of partitioning into the hydrophobic interior of the pore (50). However, more consensus between all of the competing models of NPC transport is required to fully interpret the meaning of these differences in transport (51-53). None of the FG-peptide copolymers dramatically increased the rate or the molecular weight limit of nuclear import in a manner that would suggest a complete phase transition of a putative

reversible Nup hydrogel. The importance of this is difficult to evaluate since the copolymers did not possess Nup binding sites analogous to those found on karyopherin proteins. Without a direct determination of the binding affinity between the copolymers and the Nups, it is difficult to evaluate the implications of unaltered uptake dynamics. The most striking result, however, was the shift in the molecular weight cutoff of nuclear uptake affected by low molecular copolymers containing GGFG peptides. This shift in NPC dynamics was significant, but was only seen using GGFG peptide and not with the GGLFG peptide polymer. It can be speculated why there was an observed difference in effects between the two peptides. One possibility is that the GGFG moieties weakly bound to FG-domain cross-links in a way that altered the dynamics of a putative Nup hydrogel structure, whereas GGLFG peptides would be expected to bind more strongly and not allow a rapid transfer of cross- links. These issues would be best resolved in future studies using copolymers created with more carefully controlled copolymer substitutions. For example, uniform low molecular weight polymers with exactly one, two, or more peptide groups would be useful to determine if the effects observed here were influenced by single vs. multimer binding to Nups. An essential preliminary to further this work would be to characterize the exact binding properties of a test polymer with Nup proteins in vitro before evaluating their effects in living cells.

## 4.4 Conclusions

HPMA copolymers were chosen for this series of experiments that exhibited a very wide range of chemical characteristics. This effectively served as a “copolymer library” to survey the basic interactions between synthetic polymers and living cells. All polymer

species were shown to be naturally uptaken by cells via endocytosis and are all ultimately trafficked to the lysosomal compartment.

HPMA copolymers directly microinjected into the cytosol of live cells proved to have very little interaction with any macromolecular component in the cell and were specifically excluded from all membrane-limited subcellular compartments, with exception of the nucleus. All copolymers rapidly and evenly diffused throughout the cytoplasmic compartment following microinjection, and the smallest copolymer fractions also rapidly diffused into the nucleus. After 24 h, most polymers freely diffused throughout the cell and remained at relatively equivalent concentrations where not membrane-limited, though variations were noted during time-lapse confocal live imaging. The exception to passive intracellular diffusion was the strongly cationic copolymer containing 20% MATC, a quaternary amine. This copolymer was found to exclusively localize to microtubules over a period of 2–12 h.

Nuclear entry from the cytoplasm was dictated by size-limited passive diffusion through the NPC. However, small but significant differences in rates of nuclear import were observed for polymers with sizes near the molecular weight exclusion limit as a function of the charge and hydrophobicity of the copolymers. HPMA copolymers containing peptides with Nup cross-linking sequences were found to exert a significant and specific, though modest, effect on the kinetics of NPC transport. It was found that low molecular copolymers possessing GGFG pendant groups (but not GGLFG peptides) increased the molecular weight threshold for passive uptake through the NPC channel. This was observed for the 5% GGFG copolymer itself and with coinjected polymer acting as a nuclear exclusion marker. It was hypothesized that interactions with the GGFG copolymer

may have altered the dynamics of Nup cross-linking in the NPC channel rather than affecting any general conformational transition in the proteins' structure. However, since the structure and function of Nup proteins in the nuclear pore is still an active area of debate (54), it is difficult to conclude whether the kinetics of FG-containing polymers were likely affecting FG-crosslinks due to the presence of their peptide pendant groups. However, more recent research has revealed that the Nup98 protein has a critical role in the exclusion of macromolecules through the NPC. Further, the Nup98 protein possesses terminal GLFG repeats whose interactions are critical for their function (55). As the structure/function relationships of Nup proteins are better modeled, the effect of the peptide copolymers used in this study may be better understood.

## 4.5 References


1. Kopeček J (1977) Soluble biomedical polymers. *Polimery W Medycynie* 7(3):191-221.

2. Říhová B, *et al.* (1989) Biocompatibility of *N*-(2-hydroxypropyl) methacrylamide copolymers containing adriamycin. Immunogenicity, and effect on haematopoietic stem cells in bone marrow in vivo and mouse splenocytes and human peripheral blood lymphocytes in vitro. *Biomaterials* 10(5):335-342.

3. Harris JM, Martin NE, & Modi M (2001) Pegylation: A novel process for modifying pharmacokinetics. *Clinical Pharmacokinetics* 40(7):539-551.

4. Seymour LW, Duncan R, Strohalm J, & Kopeček J (1987) Effect of molecular weight (Mw) of *N*-(2-hydroxypropyl)methacrylamide copolymers on body distribution and rate of excretion after subcutaneous, intraperitoneal, and intravenous administration to rats. *Journal of Biomedical Materials Research* 21(11):1341-1358.

5. Říhová B, Ulbrich K, Kopeček J, & Mancal P (1983) Immunogenicity of *N*-(2-hydroxypropyl) methacrylamide copolymers--potential hapten or drug carriers. *Folia Microbiologica* 28(3):217-227.

6. Cavallaro G, Licciardi M, Salmaso S, Caliceti P, & Gaetano G (2006) Folate-mediated targeting of polymeric conjugates of gemcitabine. *International Journal of Pharmaceutics* 307(2):258-269.

7. Forrest ML, Gabrielson N, & Pack DW (2005) Cyclodextrin-polyethylenimine conjugates for targeted in vitro gene delivery. *Biotechnology and Bioengineering* 89(4):416-423.

8. Kopeček J (1991) Targetable polymeric anticancer drugs. Temporal control of drug activity. *Annals of the New York Academy of Sciences* 618:335-344.

9. Nan A, Croft SL, Yardley V, & Ghandehari H (2004) Targetable water-soluble polymer-drug conjugates for the treatment of visceral leishmaniasis. *Journal of Controlled Release* 94(1):115-127.

10. Satchi-Fainaro R, Duncan R, & Barnes CM (2006) Polymer therapeutics for cancer: Current status and future challenges. *Polymer Therapeutics II*, eds Satchi-Fainaro R & Duncan R (Springer Berlin Heidelberg, Berlin, Heidelberg), pp 1-65.

11. Boussif O, *et al.* (1995) A versatile vector for gene and oligonucleotide transfer into cells in culture and in vivo: Polyethylenimine. *Proceedings of the National Academy of Sciences* 92(16):7297-7301.

12. Aronov O, *et al.* (2004) Nuclear localization signal-targeted poly(ethylene glycol) conjugates as potential carriers and nuclear localizing agents for carboplatin analogues. *Bioconjugate Chemistry* 15(4):814-823.

13. Chinnery PF, *et al.* (2000) Peptide nucleic acid and delivery to human mitochondria. *Gene Therapy* 7(9):813.

14. D'Souza GG, Boddapati SV, & Weissig V (2005) Mitochondrial leader sequence--plasmid DNA conjugates delivered into mammalian cells by DQAsomes co-localize with mitochondria. *Mitochondrion* 5(5):352-358.

15. Frederickson R (1999) PNA-NLS delivers. *Nature Biotechnology* 17(8):739.

16. Cuchelkar V, Kopečková P, & Kopeček J (2008) Novel HPMA copolymer-bound constructs for combined tumor and mitochondrial targeting. *Molecular Pharmaceutics*. 5(5):776-786.

17. Filipovska A, Eccles MR, Smith RA, & Murphy MP (2004) Delivery of antisense peptide nucleic acids (PNAs) to the cytosol by disulphide conjugation to a lipophilic cation. *FEBS Letters* 556(1-3):180-186.

18. Muratovska A, *et al.* (2001) Targeting peptide nucleic acid (PNA) oligomers to mitochondria within cells by conjugation to lipophilic cations: Implications for mitochondrial DNA replication, expression and disease. *Nucleic Acids Research* 29(9):1852-1863.

19. Pante N & Kann M (2002) Nuclear pore complex is able to transport macromolecules with diameters of about 39 nm. *Molecular Biology of the Cell* 13(2):425-434.

20. Paine PL, Moore LC, & Horowitz SB (1975) Nuclear envelope permeability. *Nature* 254(5496):109-114.

21. Feldherr CM & Akin D (1997) The location of the transport gate in the nuclear pore complex. *Journal of Cell Science* 110 (Pt 24):3065-3070.

22. Chen AA, Derfus AM, Khetani SR, & Bhatia SN (2005) Quantum dots to monitor RNAi delivery and improve gene silencing. *Nucleic Acids Research* 33(22):e190.

23. Krishnan VV, *et al.* (2008) Intramolecular cohesion of coils mediated by phenylalanine--glycine motifs in the natively unfolded domain of a nucleoporin. *PLoS Computational Biology* 4(8):e1000145.

24. Ribbeck K & Görlich D (2001) Kinetic analysis of translocation through nuclear pore complexes. *The EMBO Journal* 20(6):1320-1330.

25. Ribbeck K & Görlich D (2002) The permeability barrier of nuclear pore complexes appears to operate via hydrophobic exclusion. *The EMBO Journal* 21(11):2664-2671.

26. Frey S & Görlich D (2007) A saturated FG-repeat hydrogel can reproduce the permeability properties of nuclear pore complexes. *Cell* 130(3):512-523.

27. Frey S, Richter RP, & Görlich D (2006) FG-rich repeats of nuclear pore proteins form a three-dimensional meshwork with hydrogel-like properties. *Science (New York, N.Y.)* 314(5800):815-817.

28. Bickel T & Bruinsma R (2002) The nuclear pore complex mystery and anomalous diffusion in reversible gels. *Biophysical Journal* 83(6):3079-3087.

29. Melčák I, Hoelz A, & Blobel G (2007) Structure of Nup58/45 suggests flexible nuclear pore diameter by intermolecular sliding. *Science (New York, N.Y.)* 315(5819):1729-1732.

30. Ando D, *et al.* (2014) Nuclear pore complex protein sequences determine overall copolymer brush structure and function. *Biophysical Journal* 106(9):1997-2007.

31. Ando D & Gopinathan A (2017) Cooperative interactions between different classes of disordered proteins play a functional role in the nuclear pore complex of baker's yeast. *PloS One* 12(1):e0169455.

32. Kopeček JB, H. (1973) Poly[*N*-(2-hydroxypropyl)methacrylamide]. 1. Radical polymerization and copolymerization. *European Polymer Journal* 1(9):7–14.

33. Minko T, Kopečková P, & Kopeček J (2000) Efficacy of the chemotherapeutic action of HPMA copolymer-bound doxorubicin in a solid tumor model of ovarian carcinoma. *International Journal of Cancer* 86(1):108-117.

34. Koňák Č, Mrkvičková L, Nazarova O, Ulbrich K, & Seymour LW (1998) Formation of DNA complexes with diblock copolymers of poly(*N*-(2-hydroxypropyl) methacrylamide) and polycations. *Supramolecular Science* 5(1):67-74.

35. Ulbrich K, *et al.* (2000) Polymeric drugs based on conjugates of synthetic and natural macromolecules. I. Synthesis and physico-chemical characterisation. *Journal of Controlled Release* 64(1-3):63-79.

36. Minko T, Kopečková P, & Kopeček J (1999) Comparison of the anticancer effect of free and HPMA copolymer-bound adriamycin in human ovarian carcinoma cells. *Pharmaceutical Research* 16(7):986-996.

37. Liu J, *et al.* (2010) Endocytic uptake of a large array of HPMA copolymers: Elucidation into the dependence on the physicochemical characteristics. *Journal of Controlled Release* 143(1):71-79.

38. Gribbon P & Hardingham TE (1998) Macromolecular diffusion of biological polymers measured by confocal fluorescence recovery after photobleaching. *Biophysical Journal* 75(2):1032-1039.

39. Luby-Phelps K, *et al.* (1993) A novel fluorescence ratiometric method confirms the low solvent viscosity of the cytoplasm. *Biophysical Journal* 65(1):236-242.

40. Seksek O, Biwersi J, & Verkman AS (1997) Translational diffusion of macromolecule-sized solutes in cytoplasm and nucleus. *The Journal of Cell Biology* 138(1):131-142.

41. Pollack G (2001) *Cells, Gels, and the Engines of Life.* (Ebner, Seattle, WA).

42. Alber F, *et al.* (2007) The molecular architecture of the nuclear pore complex. *Nature* 450(7170):695-701.

43. Patel SS, Belmont BJ, Sante JM, & Rexach MF (2007) Natively unfolded nucleoporins gate protein diffusion across the nuclear pore complex. *Cell* 129(1):83-96.

44. Bhattacharyya B & Wolff J (1974) Thyroid tubulin: Purification and properties. *Biochemistry* 13(11):2364-2369.

45. Erickson HP & Voter WA (1976) Polycation-induced assembly of purified tubulin. *Proceedings of the National Academy of Sciences* 73(8):2813-2817.

46. Ben-Efraim I & Gerace L (2001) Gradient of increasing affinity of importin beta for nucleoporins along the pathway of nuclear import. *The Journal of Cell Biology* 152(2):411-417.

47. Pyhtila B & Rexach M (2003) A gradient of affinity for the karyopherin Kap95p along the yeast nuclear pore complex. *The Journal of Biological Chemistry* 278(43):42699-42709.

48. Lim RY, *et al.* (2006) Flexible phenylalanine-glycine nucleoporins as entropic barriers to nucleocytoplasmic transport. *Proceedings of the National Academy of Sciences* 103(25):9512-9517.

49. Rout MP, Aitchison JD, Magnasco MO, & Chait BT (2003) Virtual gating and nuclear transport: The hole picture. *Trends in Cell Biology* 13(12):622-628.

50. Macara IG (2001) Transport into and out of the nucleus. *Microbiology and Molecular Biology Reviews* 65(4):570-594.

51. Beck M & Medalia O (2008) Structural and functional insights into nucleocytoplasmic transport. *Histology and Histopathology* 23(8):1025-1033.

52. Dange T, Grunwald D, Grunwald A, Peters R, & Kubitscheck U (2008) Autonomy and robustness of translocation through the nuclear pore complex: A single-molecule study. *The Journal of Cell Biology* 183(1):77-86.

53. Yang W & Musser SM (2006) Nuclear import time and transport efficiency depend on importin beta concentration. *The Journal of Cell Biology* 174(7):951-961.

54. Wälde S & Kehlenbach RH (The part and the whole: Functions of nucleoporins in nucleocytoplasmic transport. *Trends in Cell Biology* 20(8):461-469.

55. Chatel G, Desai SH, Mattheyses AL, Powers MA, & Fahrenkrog B (2012) Domain topology of nucleoporin Nup98 within the nuclear pore complex. *Journal of Structural Biology* 177(1):81-89.

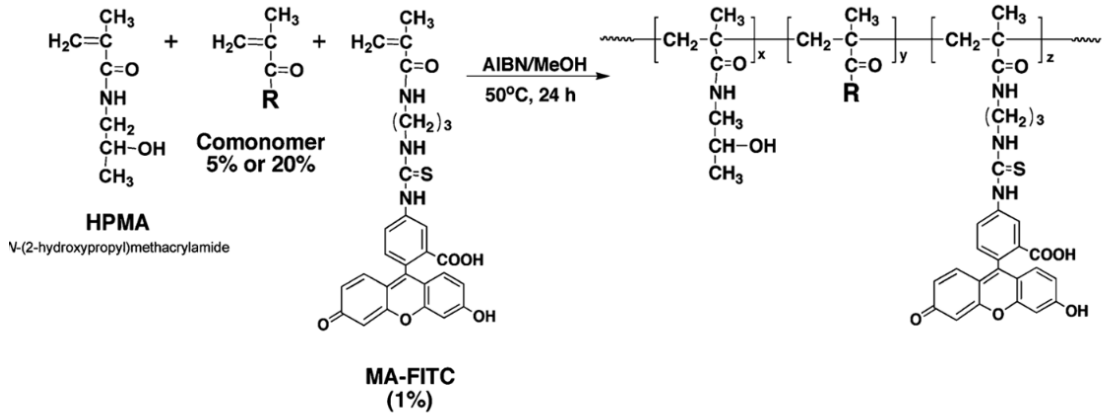


Figure 4.1. General synthetic scheme for HPMA copolymers

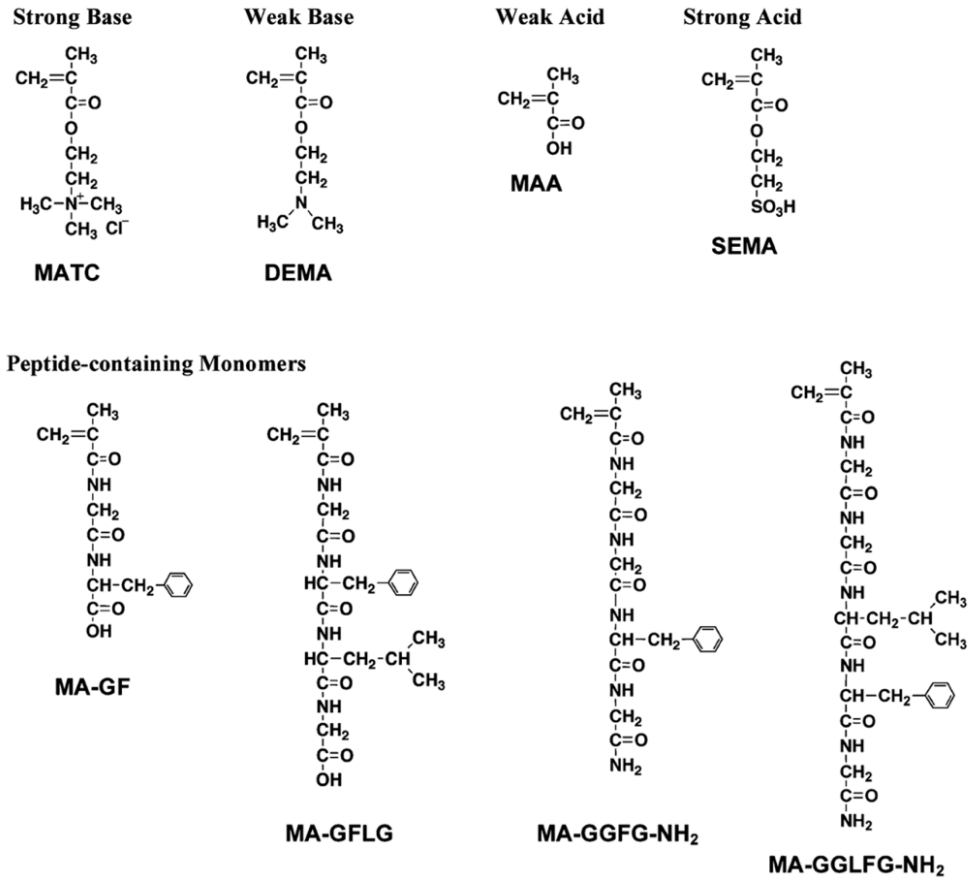


Figure 4.2. Structures of the monomers used to create the array of copolymers

Table 4.1. Characterization of microinjected HPMA copolymers.

| | | measured mole% in copolymer | | Unfractionated[c] | | | fractionation | | | | | | | | |
|---|---|---|---|---|---|---|---|---|---|---|---|---|---|---|---|
| | | | | | | | fraction 4 | | | fraction 7 | | | fraction 9 | | |
| polymer ID[a] | category | Mi | FITC[b] | $M_w$(kDa) | $M_n$(kDa) | $M_w/M_n$ | $M_w$ | $M_n$ | $M_w/M_n$ | $M_w$ | $M_n$ | $M_w/M_n$ | $M_w$ | $M_n$ | $M_w/M_n$ |
| 5% SEMA-P | strong acid | 3.9 | 0.78 | 41 | 27 | 1.5 | 125 | 106 | 1.2 | 30 | 27 | 1.1 | 14 | 13 | 1.1 |
| 20% SEMA-P | | 18.0 | 0.74 | 62 | 36 | 1.7 | 121 | 101 | 1.2 | 35 | 34 | 1.1 | 14 | 13 | 1.1 |
| 5% MAA-P | weak acid | 4.8 | 0.67 | 53 | 31 | 1.7 | 96 | 87 | 1.1 | 46 | 42 | 1.1 | 15 | 14 | 1.1 |
| 20% MAA-P | | 18.2 | 0.65 | 68 | 40 | 1.7 | 100 | 89 | 1.1 | 37 | 31 | 1.2 | 17 | 15 | 1.1 |
| 5% GF-P | peptides | 4.0 | 0.52 | 38 | 26 | 1.5 | 80 | 74 | 1.1 | 33 | 30 | 1.1 | 15 | 13 | 1.2 |
| 5% GFLG-P | | 4.6 | 0.59 | 41 | 26 | 1.6 | 111 | 95 | 1.2 | 43 | 38 | 1.1 | 15 | 13 | 1.2 |
| 5% DEMA-P | weak base | 4.7 | 0.59 | 44 | 32 | 1.4 | 81 | 77 | 1.1 | 29 | 26 | 1.1 | 16 | 15 | 1.1 |
| 20% DEMA-P | | 19.1 | 0.58 | 49 | 31 | 1.6 | 99 | 93 | 1.1 | 30 | 30 | 1.0 | 12 | 11 | 1.1 |
| 5% MATC-P | strong base | 4.4 | 0.55 | 53 | 31 | 1.7 | 105 | 96 | 1.1 | 37 | 30 | 1.2 | 15 | 14 | 1.1 |
| 20% MATC-P | | 16.5 | 0.58 | 50 | 30 | 1.7 | 103 | 93 | 1.1 | 40 | 34 | 1.2 | 16 | 13 | 1.2 |

Table 4.2. Characterization of FG-containing and exclusion marker HPMA copolymers

| | measured mole% in copolymer | | unfractionated[c] | | | fractionation | | | | | | | | |
|---|---|---|---|---|---|---|---|---|---|---|---|---|---|---|
| | | | | | | fraction 6 | | | fraction 7 | | | fraction 9 | | |
| polymer ID[a] | Mi | FITC[b] | $M_w$(kDa) | $M_n$(kDa) | $M_w/M_n$ | $M_w$ | $M_n$ | $M_w/M_n$ | $M_w$ | $M_n$ | $M_w/M_n$ | $M_w$ | $M_n$ | $M_w/M_n$ |
| 5% GGLFG-P | 2.8 | 0.66 | 40 | 26 | 1.5 | | | | 30 | 27 | 1.1 | 14 | 13 | 1.1 |
| 5% GGFG-P | 18.0 | 0.74 | 62 | 36 | 1.7 | | | | 26 | 24 | 1.1 | 15 | 13 | 1.1 |
| TR-P (Texas Red-labeled exclusion marker) | | | | | | 45 | 39 | 1.2 | 35 | 31 | 1.1 | | | |

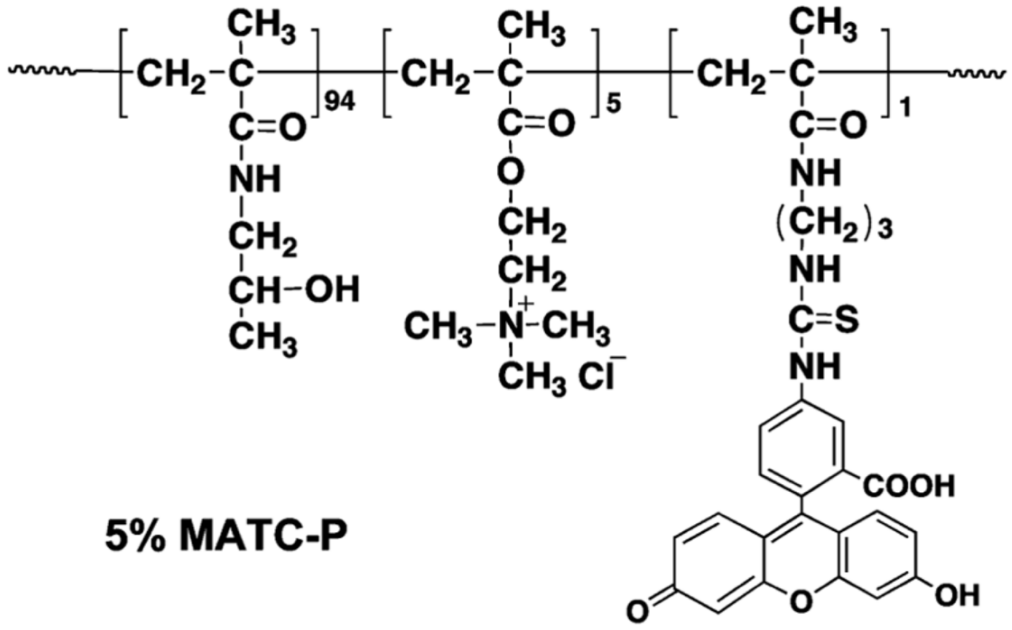


Figure 4.3. Example of the structure of an array HPMA copolymer.
5% MATC-P: HPMA, MATC, MA-FITC copolymer

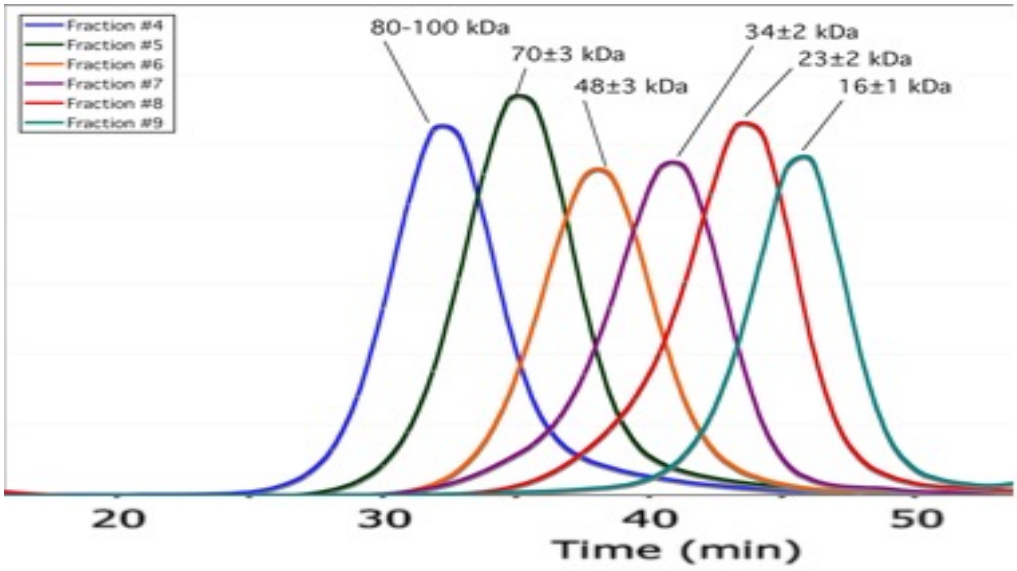


Figure 4.4. Size-exclusion chromatography profiles for fractionated 5% MAA-P with average Mw indicated for each fraction

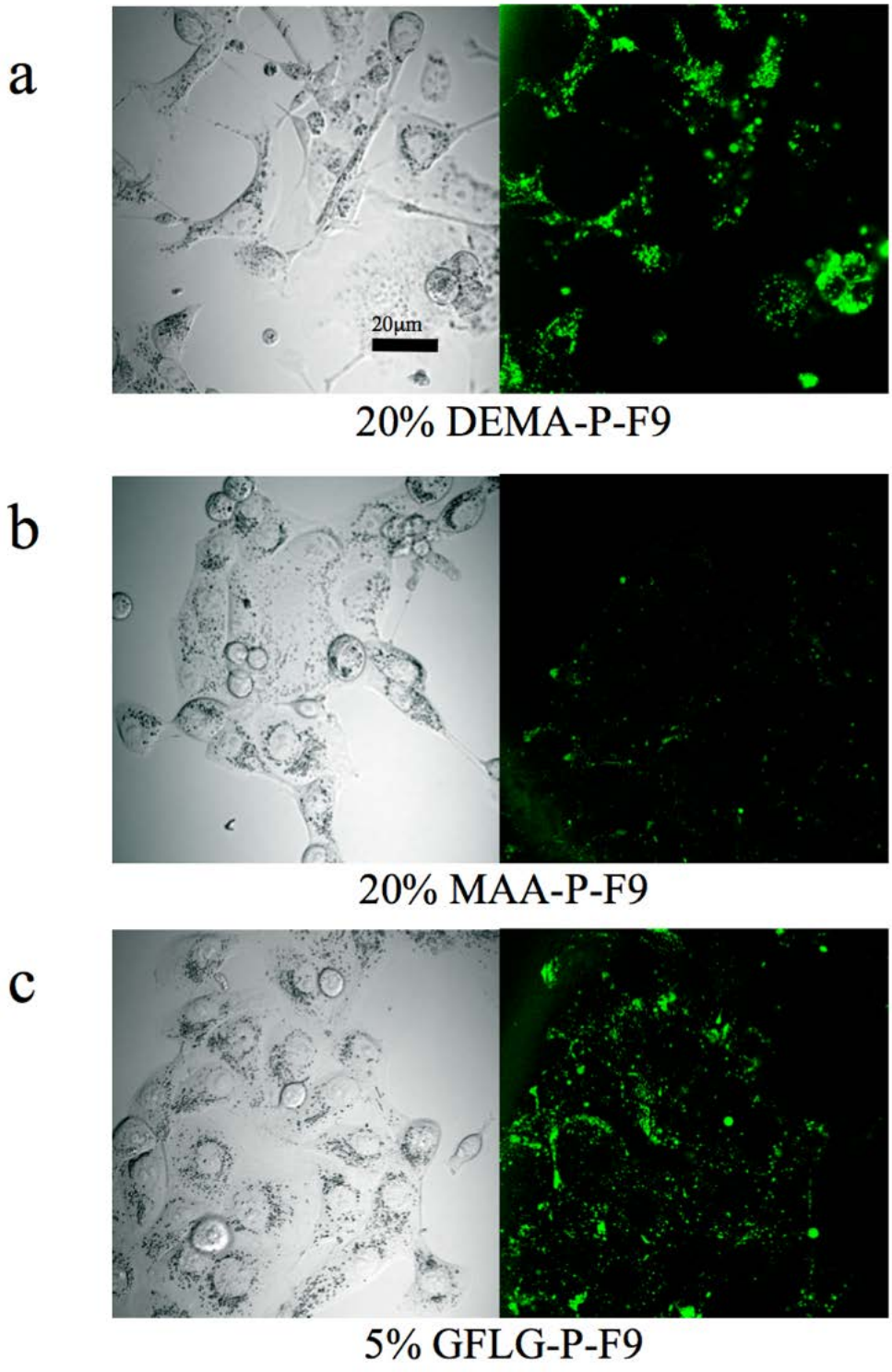


Figure 4.5. Confocal images of MDAH2774 after 24 h incubation with 0.5 mg/ml F9 fractions of HPMA copolymers. Examples shown are (a) 20% DEMA-P, (b) 20% MAA-P and (c) 5% GFLG-P

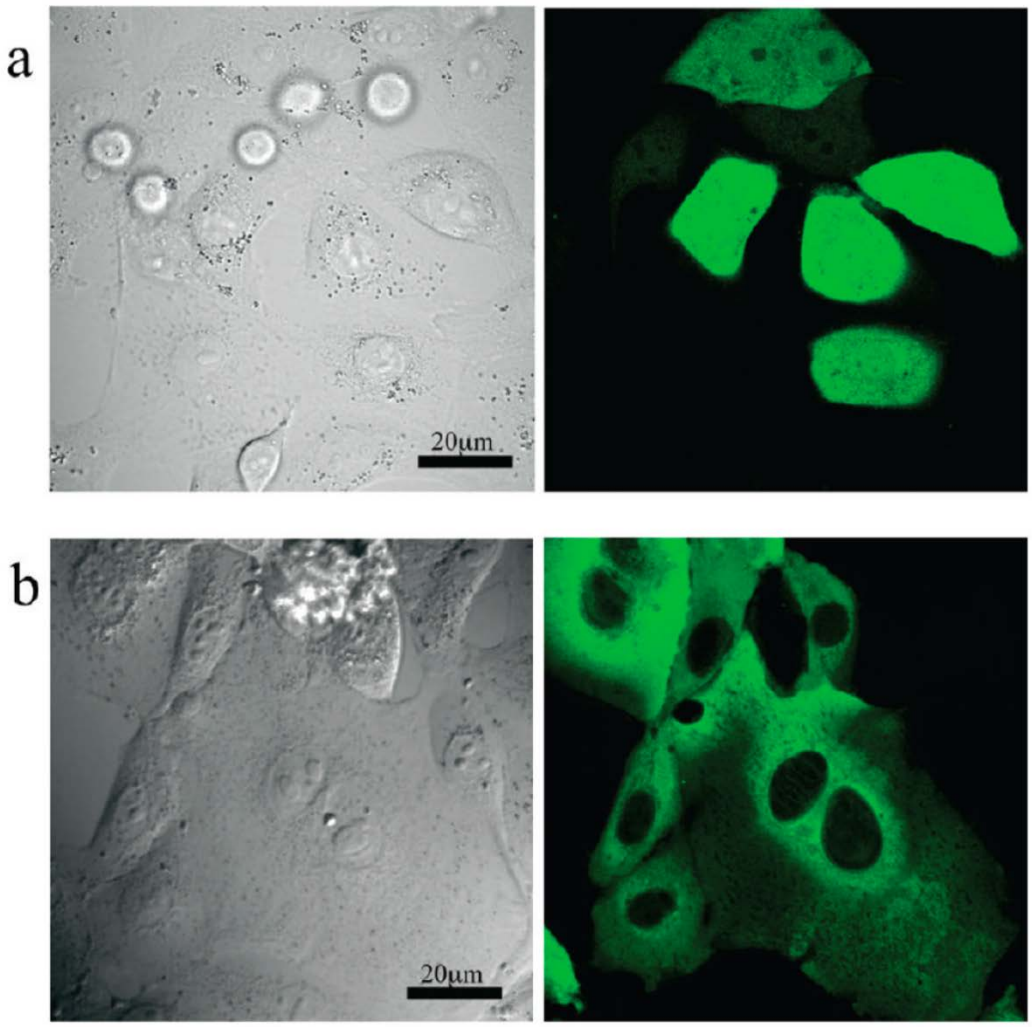


Figure 4.6. Typical images from confocal laser scanning fluorescent microscopy (40× mag.) of live MDAH2774 ovarian carcinoma cells after microinjection with FITC-labeled polymers. The transmitted images are on the left. On the right, images represent fluorescent FITC-labeled copolymer. (a) 20% MATC-P-F8 ($M_w$ = 23 kDa) 15 min after microinjection. Polymers under 25 kDa immediately dispersed in cytoplasm and nucleoplasm, but were excluded from other membrane-limited organelles. (b) 5% SEMA-P-F4 ($M_w$ = 125 kDa) 24 h after microinjection. Polymers over 75 kDa remain excluded from the nuclei and all membrane-limited organelles. All polymers except for 20% MATC-P remained evenly dispersed throughout the cytoplasm and excluded from subcellular structures, as demonstrated in this example

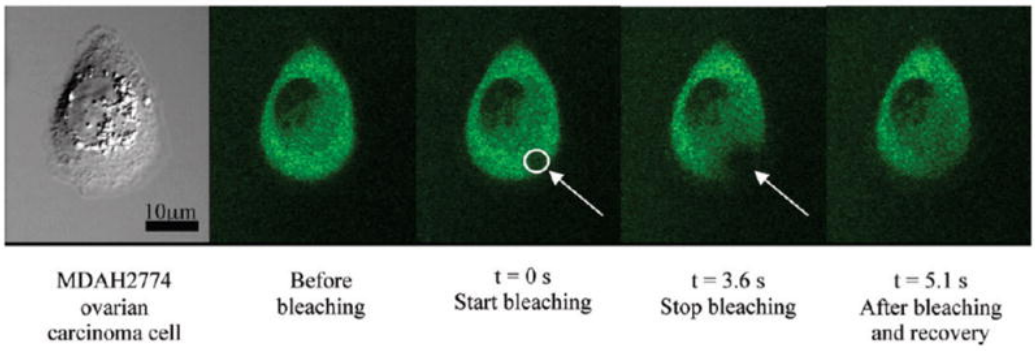


Figure 4.7. Example of time-lapse imaging from FRAP. Here, MDAH2774 cells were microinjected with copolymer 5% MAA-P-F4 ($M_w$ = 96 kDa) 2 h before the experiment. Area was bleached as indicated and cytosolic copolymer rediffused and restored equilibrium concentration within 3 s. The free diffusion in the cytoplasm of relatively high molecular weight copolymers was demonstrated

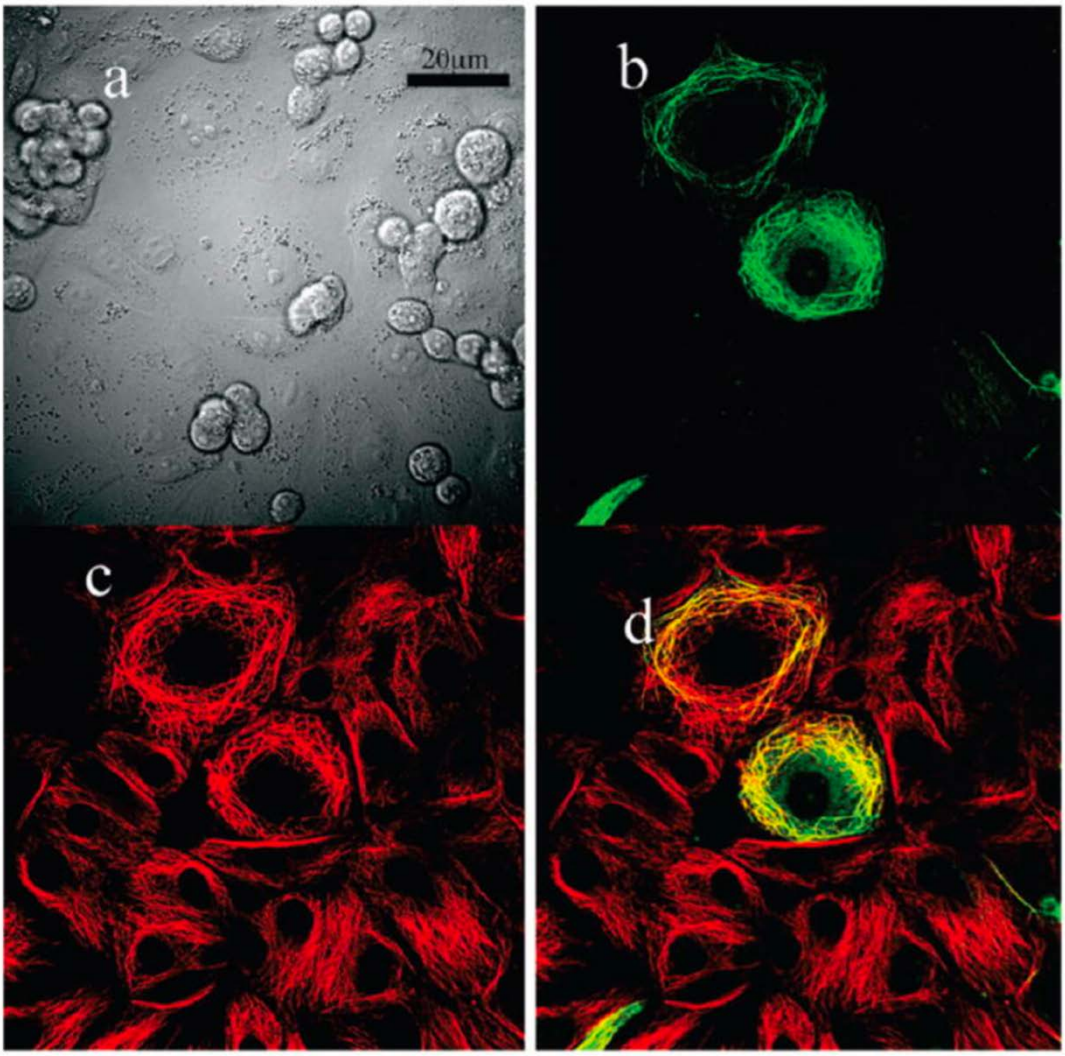


Figure 4.8. Typical images of fixed MDAH2774 cells after microinjection with strongly cationic copolymer 20% MATC-P-F4 ($M_w$ = 103 kDa), thereby demonstrating its localization on microtubules. Cells were microinjected with copolymer 24 h before fixation with 3% paraformaldehyde. Microtubules were labeled using E7 antitubulin primary antibody, which was visualized using a goat antimouse 555-Alexafluor secondary antibody. The transmitted image is shown in (a). The green channel (b) is from the FITC-labeled copolymer and the red channel (c) shows microtubule staining. Overlay fluorescent image (d) demonstrated microtubule colocalization with the copolymer although some inhibition of the antitubulin antibody was evident when injected cells were compared with noninjected cells

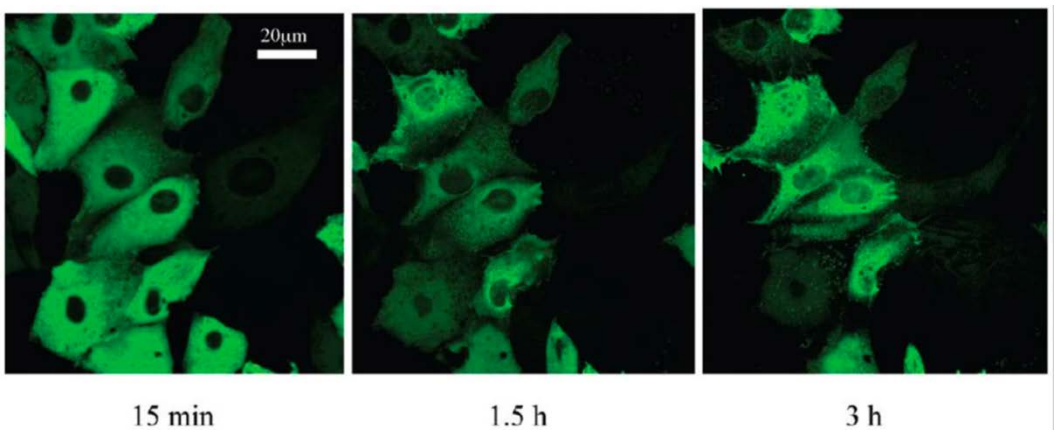


Figure 4.9. Time series of a single z-slice of MDAH2774 ovarian carcinoma cells microinjected with 5% GFLG-P-F7 ($M_w$ = 34 kDa; hydrophobic peptide) as a 1 mg/ml polymer solution in PBS. Green indicates HPMA copolymer and entry into the nuclei is shown over time

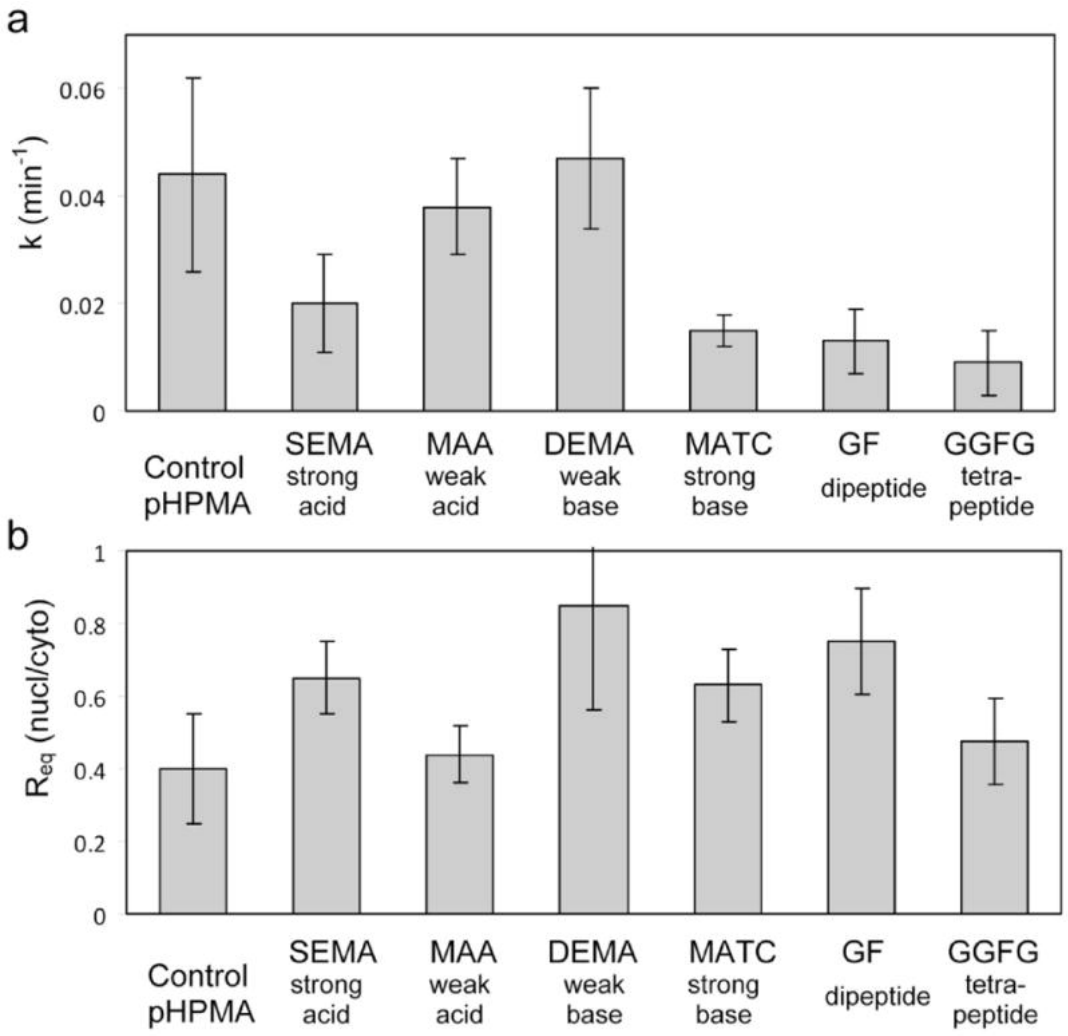


Figure 4.10. Nuclear uptake kinetics for copolymer injected cells (a) Nuclear uptake rate constants $k$ ($min^{-1}$) for 5% copolymers. (b) Equilibrium nuclear/cytosol polymer concentrations ($R_{eq}$) for each copolymer type. ($N$ = 5–9 cells). Error bars are standard errors (SE) for each calculated curve-fit

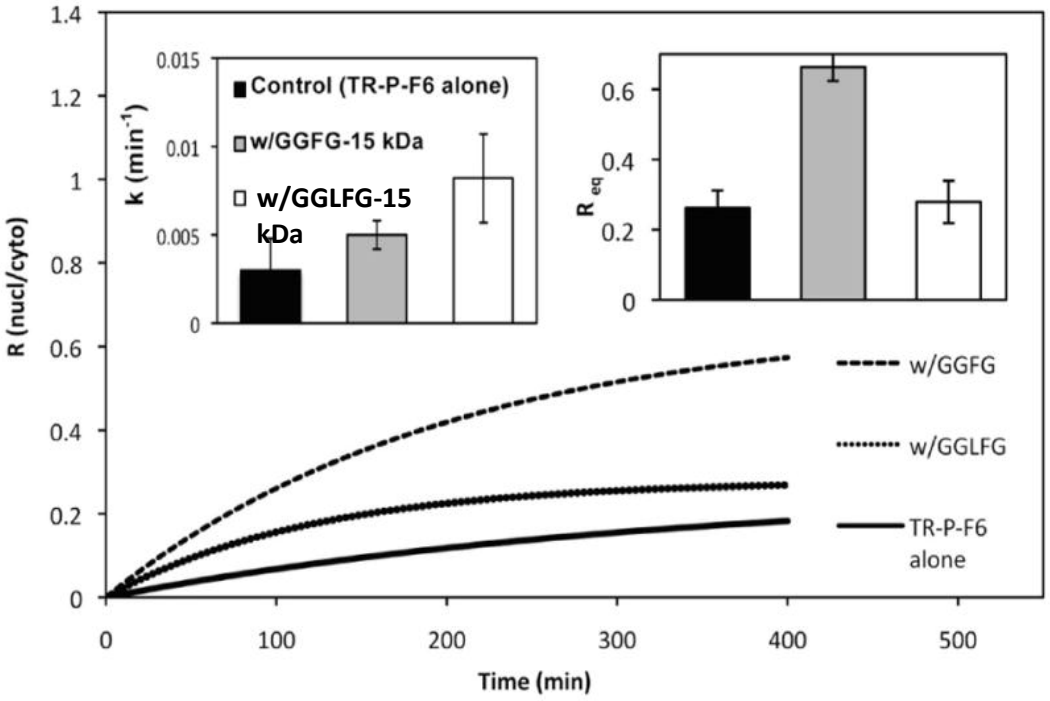


Figure 4.11. Summary of the nuclear uptake kinetics of co-microinjected TR-P-F6. Inset graph on the left shows the nuclear uptake rate constants $k$ ($min^{-1}$) and inset graph on the right shows the equilibrium nuclear/cytosol polymer concentrations ($R_{eq}$) for each copolymer type. Error bars in the inset are SE for each derivation

# CHAPTER 5

# AFTERWORD

## 5.1 Bispecific Fab' Conjugates for the Targeting of HPMA Copolymers

Despite a great deal of method development, no PEG dimerized Fab' constructs were synthesized suitable for conjugation to HPMA-drug conjugates. Only homospecific OV-TL16 (Fab')-PEG dimerization constructs were successfully made in yields that could be well characterized. All attempts to crosslink the UIC2 anti-P-gp, anti-EGFR, and HER-2 antibodies resulted in low yields due to protein degradation, chain disassociation, and the production of PEG side products. The refinement of Fab' production from IgG2a antibodies was successful for Fab' conjugation directly to activated HPMA copolymers (1), however, the UIC2 mAb proved to be too unstable for dimerization using PEG crosslinkers. Indeed, purified UIC2 $(Fab')_2$ fragments were found to significantly degrade and aggregated in storage at 4°C after just a few days. Some issues were by resolved the use of gentler reaction conditions by switching from bismaleimide to bisvinyl sulfone crosslinkers; however, this was not enough to produce sufficient yields for subsequent conjugation reactions.

In retrospect, it is not surprising that we encountered trouble with the stability of the UIC2 $(Fab')_2$ fragment. Indeed, in the field of therapeutic antibodies, finding methods to maintain the stability, colloidal stability, and activity of purified antibodies remains an

active area of development for mAbs and genetic engineered antibody constructs. It is now a well-known problem in antibody purification that high protein concentrations are prone to loss of material due to protein unfolding/denaturation, self-aggregation, intermolecular crosslinking, and colloidal stability (2).

"Stability engineering" of antibodies is a very active area of current research (3). This has been prompted by the greatly expanded industry of antibody products as therapeutics and the large number of production problems associated with purified antibodies and antibody products (4). Much of the work to modify antibody products is due to the difficultly of optimizing the structure, colloidal stability, binding constant, and effector functions of the proteins simultaneously. The genetic constructs are modified in many ways, with the most common being isotype switching where the constant domains of different isotypes of antibodies are swapped out (5).

For therapeutic and targeting purposes, Fab fragments from monoclonal IgG antibodies continue to be used extensively. The use of Fab' from reduced $(Fab')_2$ fragments has fallen out of favor due ongoing problems with low yields, disulfide scrambling and protein stability. Problems with Fab' fragments for use in synthetic chemistry have been associated with linker cyclization, protein aggregation and disulfide instability in the constant domains. One approach that has been successful in resolving the major problems with the use of Fab' fragments has the development of thiol-specific *bridging* moieties. These are bifunctional crosslinkers that effectively replace the disulfide bond with dithiol bonds connected by a short carbon spacer

As shown in Figure 5.1., these include dihalomaleimides and dithiolmaleimides (6, 7) and monosulfones (8-10). Compared to bimaleimide, bisiodoacetyl and bisvinyl sulfone

crosslinkers, these linkers can be attached *in situ* in a single reaction step and have much higher yields (11). The resulting crosslinking spacers are also much more stable than previous reaction products.

### 5.1.1 PEG Dimerized Fab' Fragments

Using PEG as a linker between two Fab fragments has continued to be developed and investigated as a potential stand-alone therapeutic. For example, Khali et al. have developed an efficient method of creating PEG dimerized Fab fragments, rather than Fab' fragments. The term "antibody mimetics" has been coined to describe their structure and function (12).

For a series of mAbs, the protein is digested with papain to produce free Fab fragments. These are then crosslinked using a PEG-di(monosulfone), a bis-thiol-specific conjugation dimerizer. Conjugation is accomplished by a sequence of addition–elimination reactions that has the net effect of inserting thiol ether bonds and a 3-carbon methylene bridge in the place of the terminal cysteine bridge of the Fab fragments. Due to the accessibility of the terminal disulfide bonds of the Fab fragment, this produces a very efficient, site-specific conjugation chemistry. The resulting conjugate is stabilized by replacing the cysteine disulfide bond at once *in situ* with a covalent spacer. This has been demonstrated to not only dimerize the Fab fragments via a PEG linker, but the resulting thiol ether bonds are more stable than the original disulfide bond. The PEG linkers used have ranged from 6-20 kDa. For later work, 20 kDa was chosen to duplicate the topography and hydrodynamic volume of unmodified whole IgG proteins as much as possible. This approach has been shown to increase the stability of the Fab fragments even compared to

unmodified IgG antibody proteins by preventing disassociation of the Fab light chain (13-15).

The binding kinetics of two of the Fab-PEG-Fab constructs was determined using surface plasma resonance. Constructs using the commercially available mAbs Bevacizumab (anti-VEGF-A) and Trastuzumab (anti-HER2/neu) were made. In both cases, the binding constants of the Fab-PEG-Fab construct were somewhat lower than the unmodified mAbs, but in both cases the $k_a$ constants were lower but the $k_d$ constants were much higher. These results are consistent with the binding constants measured for the homospecific OV-TL16 Fab'-PEG-Fab' studied here.

The same research group has created monospecific PEG linked IgG1 anti-TNF-$\alpha$ conjugate that is currently being used in animal testing for the treatment of uveitis, a non-infectious inflammatory disease of the eye (12). Their PEG dimerized Fab fragment (termed "$FpF_{infliximab}$") was created using Fab' fragments derived from the commercially available therapeutic mAb Infliximab, which is clinically approved for the treatment of inflammatory conditions such as rheumatoid arthritis, and is used off-label to treat uveitis. This application was chosen as it had previously been indicated that the Fc receptors in the eye cause the Infliximab mAb to be rapidly cleared.(16-19) In EAU (experimental autoimmune uveoretinitis) mice, it was found that $FpF_{infliximab}$ and Infliximab were equally effective in reducing the infiltration of CD45+ cells after a single injection before the peak of the disease.

### 5.1.2 Drug-free Therapeutic Polymers

More recent developments in macromolecular conjugates have incorporated the concept of oligomerization of cell receptors and Fab' targeting, and taken it in a novel direction to create a new class of drug-free therapeutics. Rather than dimerizing recognition motifs directly on the carrier, new systems have been successfully developed that use complementary paired conjugates that are able to induce conjugation and activation of cell surface receptor proteins *in situ* after binding to the cell surface. These use pairs of either antiparallel coiled-coils peptide sequences or complementary oligonucleotides

In these systems, a Fab' fragment is coupled to one sequence of the pair, and multiple copies of the complementary sequence are conjugated to an HPMA copolymer. The Fab' conjugate is applied first to prime the cells with one of the complementary pairs. Next, the polymer with the other complementary sequence is applied. Binding to the copolymer via the complementary pairs induces the interactions and activation of the targeted receptor protein. This approach has been successfully used to induce apoptosis in $CD20^+$ lymphoma cells.

This approach was used with anti-parallel coiled-coil peptide sequences and anti-CD20 Fab' fragments to create recognition pairs able to activate CD20 receptor proteins on lymphoma cells. When this system was used on Raji B cells, high levels of apoptosis were observed in vitro, and long-term survivors were observed in vivo in a lymphoma mice model (20, 21). A similar approach, using complementary morpholino nucleic acid analog oligomers as complementary recognition pairs, was shown to be even more effective. In these studies, Raji B cells were completely eradicated in a mouse model (22).

### 5.1.3 Bispecific Targeting for Cancer

Cancer treatments employing the general concept of bispecific targeting has expanded greatly since the time of this work. Using bispecific antibody constructs is now one of the most promising strategies for the treatment of cancer. Table 5.1. displays a selected list of bispecific antibody constructs that are undergoing clinical testing or have been approved for clinical use (23). All of the bispecific or multispecific antibody constructs that have reached clinical testing are the result of molecular biological techniques that engineered antibody domains.

## 5.2 Mitochondrial Targeting Using TPP

In retrospect, the inability of TPP-HPMA to achieve mitochondrial localization or plasma membrane transduction is not surprising given polymer molecular weights over 3 kDa. Only one paper in 2011 has reported the successful use of a single TPP moiety to traffic a PNA or any other macromolecule over 3 kDa, since the original 2001 paper by Murphy et al. (24). TPP is still used to target drugs to mitochondria; however, it has been found that uptake and localization of larger molecules requires multiple TPP moieties. The conjugates containing a single TPP moiety have used been used successfully to target small molecules, such as doxorubicin (25), MitoC, a derivative of ascorbic acid (26), and 1,8-naphthalimide, a fluorescent probe (27).

Large molecules and delivery of large payloads of LMW drugs have been successfully developed using TPP localization, but these have used nanoparticles that possess many TPP moieties on their surface. Polymeric micelles, liposomes and dendritic carriers used in these systems have components functionalized with TPP moieties which

are incorporated in the resulting complexes. They are termed “second generation” carriers for the targeting of mitochondria and are being developed as potential treatments for a range of diseases (28). For example, liposomes incorporating stearyltriphenylphosphonium bromide (STPP) were shown to localize encapsulated paclitaxel to mitochondria in OVCAR-3 cells (29). The liposome were prepared from mixed lipids consisting of lecithin (PC), cholesterol (Chol), and STPP at a molar ratio of PC:Chol:STPP = 65:15:2.

Mitochondriotropic dendrimers were created with branched poly(amidoamine) (PAMAM), PEI (poly(ethyleneimine)), and with oligolysine copolymers incorporating monomers functionalized with TPP (30-33). These were synthesized to possess surface termini functionalized with many triphenylphosphonium moieties. These have the potential to be an effective drug delivery system by encapsulating drugs or other bioactive molecules in their core or by conjugation on their surface.

After the results described here using semitelechelic TPP-HPMA, the lipophilic cation was used to increase the efficacy of a traditional lysosomotropic HPMA-drug copolymers. Cuchelkar et al. constructed HPMA copolymers containing monomers with TPP coupled to the photosensitizer drug $Mce_6$ (mesochlorin $e_6$), both linked by a degradable spacer to the copolymer backbone (34). TPP and $Mce_6$ were coupled via a 6-carbon spacer which was itself linked to the pendant group of a comonomer by a disulfide bond. An analogous copolymer was synthesized with BODIPY FL® in place of $Mce_6$ to track the location of the conjugate. When this copolymer was incubated with ovarian carcinoma cells, it was shown to be initially trafficked to lysosomes. After several hours, TPP-BODIPY FL® was observed to be released from lysosomes and localized to mitochondria. IC50 measurements, however, indicated that HPMA conjugate with TPP-

functionalized $Mce_6$ was only somewhat more effective at inhibiting the growth of ovarian carcinoma cells compared to HPMA-$Mec_6$ conjugate without TPP. It was also observed that the relative cytotoxicity of the TPP conjugate plateaued over time, and after 12 h, TPP targeted $Mce_6$ was only slightly more cytotoxic than HPMA-$Mce_6$ conjugates without TPP.

### 5.2.1 Conclusions on Mitochondrial Targeting with TPP

Targeting mitochondria remains a promising approach for the treatment of cancer and other diseases. However, the work here and the work of others has revealed some of the obstacles of using carriers targeting using lipophilic cations. This method of localizing to mitochondria is generally effective; however, the organelle has a complex structure with an inner and outer membrane and carriers do not necessarily partition into the needed area. It is also difficult to selectively release free drug in mitochondria as there are no effective enzymes or other obvious physio-chemical conditions that could be used for drug release. Others have found that TPP-conjugated carriers and TPP-drug conjugates are inactivated due to high binding to the inner mitochondria membrane (35, 36). Using cations also appears to be self-limiting since the binding of lipophilic cations progressively lowers the electronegativity of the mitochondria over time (37). This effect may explain the loss of cytotoxicity seen over time during growth inhibition studies. This may also be the source of nonspecific cytotoxicity that has been reported for some TPP-drug conjugates, particularly in the case of dendrimers (38).

## 5.3. Large Polymer Array

The large polymer array was designed to observe polymer-cell interactions in a systematic way that had never been explored before. When new, engineered materials are exposed to cells in vitro or in vivo, they often behave in unexpected ways. Cell binding, cell uptake, intracellular trafficking and distribution occur in unexpected ways. Comparing structurally parallel, but chemically diverse, HPMA copolymers provided us with an overview of how these materials behave similarly towards living cells, while noting some distinct differences.

### 5.3.1 Endocytosis[1]

After the experiments in Chapter 4, Lui et al. (39) used the same array of polymers to characterize their uptake and trafficking by endocytosis in more detail. To observe cell internalization, array polymers were added to the media of cultured C4-2 prostate carcinoma cells. Uptake concentrations were measured by flow cytometry, and endocytosis was characterized using confocal microscopy. A series of inhibitors were used to determine differences in the endocytotic pathways used by the different array copolymers.

#### 5.3.1.1 Uptake Measurements by Flow Cytometry

The C4-2 cells were seeded in 12-well plates at a density of $2.5 \times 10^5$ cells per well and incubated in medium for 1 day (37°C, 5% $CO_2$). Then cells were incubated with copolymers at 37°C for the indicated time periods. The concentration of copolymers used

[1] Parts of the following sections were adapted with permission from: J. Liu, H. Bauer, J. Callahan, P. Kopečková, H. Pan, J. Kopeček *Endocytic uptake of a large array of HPMA copolymers: Elucidation into the dependence on the physicochemical characteristics. Journal of Controlled Release*, 2010. **143**(1): p. 71-9. Copyright © 2009 Elsevier Inc

was 0.1 mg/ml in this type of study. After incubation, medium was removed. Cells were harvested and washed with PBS three times followed immediately by flow cytometry analysis. For each, $1.0 \times 10^4$ cells were processed and the mean fluorescence intensity was recorded for each sample.

Mean fluorescence intensity of each sample was converted into amount of copolymer taken up by the cells using flow cytometry and fluorescence plate reader. The fluorescence intensity of copolymers in cells was obtained from both flow cytometry analysis and fluorescence plate reader measurement. Meanwhile, the amount of FITC (ng) in the same sample was measured using the fluorescence plate reader. Hence, based on the content of FITC in each copolymer, the amount of copolymer in cells was derived.

5.3.1.2 Inhibition of Uptake Via Endocytic Pathways by Selective Inhibitors

Cells were preincubated in medium containing a selective chemical inhibitor of endocytic pathways for 30 min. Next, polymers were added in the presence of the inhibitor. Then cells were further incubated for fixed periods of time and harvested for flow cytometry. The inhibitors used, their concentrations, and pathways they inhibit are shown in Table 5.2.

5.3.1.3 Uptake of Polymers by C4-2 Cells

Subsequent, more detailed, analysis of the internalization of the array polymers using C4-2 cells revealed the differences in the endocytic pathways the copolymers followed. Fluid phase endocytosis is observed when membrane vesicles entrapping fluid containing macromolecules transport to late endosomes or lysosomes that accumulate in

perinuclear areas. Adsorptive endocytosis occurs when surrounding solutes associate with plasma membrane. In our studies, internalization of copolymers by cells was observed and captured under confocal microscope. For neutral pHPMA (P-FITC) and copolymers possessing weakly negatively charged groups (20% MAA-P), no internalization was detectable within 30 min incubation (Figure 5.1. A and E). The visible perinuclear localization of these copolymers was noticed after incubation for 4 h (Figure 5.1. B and F) and was more significant after prolonged incubation (Figure 5.1. C and G). For copolymers possessing strongly negatively charged groups (20% SEMA-P), perinuclear localization of copolymers only appeared after 12 h of incubation with cells (Figure 5.1. K). Unlike neutral or negatively charged copolymers, the copolymers possessing strongly positively charged groups (20% MATC-P) were seen to quickly (within 10 min) associate with the whole plasma membrane after exposure to cells (Fig. 5.1. Q), displaying characteristic adsorptive endocytosis. Subsequently, the membrane-associated pattern gradually disappeared and was replaced by an intracellular pattern, indicating that these membrane-associated copolymers were endocytosed into cells (Figure 5.1. S). The copolymers possessing weakly positively charged groups (20% DEMA-P) behaved similarly but less dramatically (Figure 5.1. M-O). In addition, P-FITC and HPMA copolymers containing different functional groups were found to colocalize with dextran 10 kDa, a fluid phase endocytosis marker (Figure 5.1. D, H, L, P and T). Hence, HPMA copolymers containing different charged groups were internalized into cells through different types of endocytosis. The neutral homopolymer and negatively charged copolymers were internalized into cells via fluid phase endocytosis, whereas positively charged copolymers were internalized by adsorptive endocytosis.

5.3.1.4. The Rate of Endocytic Uptake of HPMA Copolymers

Flow cytometry was used to quantify the endocytic uptake of copolymers possessing charged groups (Figure 5.2.) Mean fluorescence intensity of each sample was obtained and converted into amount of copolymer taken up by the cells. Positively charged copolymers, 20% MATC-P and 20% DEMA-P, were taken up much more efficiently than pHPMA (P-FITC) or copolymers containing negatively charged groups, 20% MAA-P and 20% SEMA-P. The uptake of copolymers containing negatively charged groups, 20% MAA-P and 20% SEMA-P, decreased when compared to P-FITC. Maximum uptake occurred with the strongly positively charged copolymer, 20% MATC-P, whereas least uptake took place with the strongly negatively charged copolymer, 20% SEMA-P; 5% MATC-P and 5% DEMA-P did not show significant increase in uptake, and 5% SEMA-P and 5% MAA-P did not show significant decrease of uptake compared to pHPMA (P-FITC), probably due to a low content of charged groups. Thus, the rate of uptake of HPMA copolymers was determined by the structure and content of the charged groups.

5.3.1.5 Effect of Molecular Weight on the Uptake of Charged Copolymers

The effect of molecular weight on the uptake of copolymers was evaluated by flow cytometry analysis. Copolymer fractions were incubated with cells and the uptake was measured. For pHPMA (P-FITC fractions) and negatively charged copolymers (20% MAA-P fractions), it was shown that the lower the molecular weight, the higher the uptake (Figure 5.4.). While there is little difference in the rate of uptake for small 20% DEMA copolymers, there was notable inflection point for copolymers larger than fraction F6 (MW = 60 kDa), and the uptake was 10-20 fold greater than pHPMA. In contrast, the uptake of

positively charged copolymers (20% DEMA-P fractions) decreased with decreasing molecular weight. These results suggest that uptake of HPMA copolymer containing charged groups is molecular weight dependent, but that the charge or charge density has a greater impact on endocytosis.

5.3.1.6 Summary of Results: Endocytosis of Array Copolymers

All copolymers, regardless of composition, charge or molecular weight, were internalized by endocytosis and all were ultimately trafficked to lysosomes, where they remained. Even the most strongly cationic HPMA copolymer used (20% MATC-P) was not observed to be capable of endosomal/lysosomal escape. Obvious differences in the rates and concentration of polymer internalized were noted, but the differences could all be (unsurprisingly) attributed to charge differences. Uptake was largely dictated by non-specific adsorption to the outer plasma membranes of the cells, yielding adsorptive endocytosis. Strongly positively charged polymers bound avidly, neutral and hydrophobic polymers bound weakly, and strongly negative polymers were repelled from the plasma membrane. This simple effect was reflected in differences in the preferred pathway of uptake: positively charged copolymers were shown to use micropinocytosis, as well as clathrin-mediated and dynamin-dependent endocytosis, weakly negatively charged copolymers employed the same pathways but to a lesser degree, whereas the strongly negatively charged copolymers were almost entirely uptaken by micropinocytosis.

These general results were all expected; however, the rates of adsorptive endocytosis for the strongly negative copolymers were also shown to be strongly dependent on charge density and molecular weight. While HPMA copolymers with a high content of

positively charged comonomer (20% MATC-P and 20% DEMA-P) were internalized at concentrations 10x-20x higher than the pHPMA control polymer, the 5% MATC-P and 5% DEMA-P copolymers were absorbed at rates only slightly higher than the control. Further, high molecular weight 20% DEMA-P copolymer fractions higher than 50 kDa are endocytosed to high concentrations, while 20% DEMA-P fractions lower than 50 kDa were internalized at concentrations no different than the control pHPMA. These results revealed inflection points where cell surface adsorption occurs; critical charge densities or zeta potentials that dictate whether adsorptive endocytosis of a nanoparticle will be the dominant uptake pathway.

Since adsorptive endocytosis is nonspecific, is it usually avoided in the design of drug delivery carriers. These results have helped inform others in the design of their constructs. Many drug delivery systems are meant to use a specific endocytic pathway and these results are frequently cited as an explanation for their choice of design (40-44).

### 5.3.2 Microinjection

Array polymers were also microinjected into the cytosol of MDAH2773 ovarian carcinoma cells. The distribution of the copolymers the cells was observed by time-lapse confocal microscopy and difference in kinetics of nuclear entry were calculated. Given the diverse chemical makeup of polymers, it was surprising how similarly all the polymers distributed throughout the cells. All copolymers initially diffused throughout the cytosol freely, rapidly and evenly. Low molecular weight fractions of the copolymer (MW = 11-15 kDa) immediately diffused throughout the cytosol and nucleus, while the largest copolymers remained excluded from the nucleus. When the cells were observed over the

next 24 h, only very subtle differences in their overall distributions were seen, which is remarkable considering how diverse their chemical makeup was. After several hours of observation, the only copolymers that didn't remain freely diffusable were the copolymers containing quaternary cations (MATC) which avidly bound to the microtubules in the cytosol. Furthermore, spot photobleaching (FRAP) of the copolymers in the cells confirmed that pHMPA remains freely diffused throughout the cell after 24 h. Sustained photobleaching showed that no copolymer was retained within any intercellular compartment or structure, including the nucleus. Weakly cationic copolymers were expected to preferably bind to organelle membranes or the inner lumen of the plasma membrane, but this was not observed.

5.3.2.1 Nuclear Entry

The subtle variations in the kinetics of the different chemical types of copolymers near the molecular weight cutoff of passive nuclear entry is consistent with the repulsive exclusion models of NPC gating and passive transport (45, 46). Again, given the broad range chemical characteristics of the different copolymers what was most striking was how similar all of them behaved. The only type that displayed significantly higher entry kinetics and a higher equilibrium nuclear concentration were the weakly basic MATC copolymers. For proteins, passive diffusion was considered to be limited in the 30-60 kDa, though more recently, it has been proposed that there is a "firm threshold" of 40 kDa for passive diffusion through the NPC (47), which is in good agreement with the results found for HPMA copolymers.

Four different FG-containing peptide copolymers were used to study the possible

interactions with the unstructured Nup proteins in the NPC. However, the differences in their entry kinetics remain difficult to interpret. At the time of this study, a simple" Nup hydrogel" model had been hypothesized to interpret the structure and function of the NPC. Nup proteins containing FG-repeats line the channel of the pore are unstructured (like synthetic polymers) and it is known from mutation studies that the hydrophobic interactions between FG-rich regions of the proteins are critical for NPC gating. In the past 10 years, however, competing models of nuclear have been proposed (Figure 5.5.) and the precise role of the Nup proteins remains an active topic of debate. Until a consensus on NPC function develops, the possible interplay between HPMA FG-peptide copolymers and gating into the nucleus will be difficult to interpret.

### 5.3.3 Other Work Citing Array Copolymers

All the observations and results using the large array represented preliminary survey of polymer-cell interactions and intracellular distribution due to charge and/or hydrophilicity/hydrophobicity, but they have proven useful for other groups developing various therapeutic nanoparticles. A review of non-PEG polymers used for therapeutic nanomedicines summarized the results for the array polymer study at length (48).

For example, recent work has used detailed computer modeling to describe the uptake and intracellular trafficking of gold nanoparticles used as radio-sensitizers for the treatment for cancer. Dobay et al. (2012) used the kinetics values determined in the polymer array study for the nuclear entry of 2-4 nm HPMA copolymers to approximate the kinetics of nuclear entry of 4 nm PEGylated gold nanoparticles (49). These results were

used to predict the concentration of gold nanoparticles in proximity of DNA in the nucleus to optimize dosing schedules before radiation treatments.

Zhong et al. (2016) developed an HPMA-drug conjugate for direct cytoplasmic delivery and nuclear targeting by incorporating a cationic MT (microtubule) targeting peptide sequence (50). They described their conjugate entering the cytosol using a non-endocytic microtubule pathway and accumulating in the nucleus. They referenced our array polymers, noting that awareness of nonspecific binding of polycationic HPMA copolymers to microtubules was important to the design of the conjugate.

## 5.4 Final Observations

Since this dissertation is being submitted 10 years after the work described was completed, an opportunity is presented to see the advances in our understanding of biology and our innovations in nanomedicines in a larger perspective.

For a polymer chemist developing nanomedicines, our increased knowledge of natural protein functions is a bit ironic when presented with the models that describe transport in and out of the nucleus through the NPC. All hypothesized simulations of the functioning of the unstructured Nup proteins use physio-chemical principles that had been developed long ago to describe the structure and function of synthetic polymers. The Nup proteins are now often referred to as “block copolymers” and the modelling of their structural transformations as hydrogels, or brush/comb conformations are directly borrowed from polymer physics. Indeed, the past decade has revealed that intrinsically disordered proteins (IDPs) and intrinsically disordered protein domains (IDR) account for over 30% of the entire proteome, and that IDPs and proteins with IDRs have critical roles

in a variety of cellular functions (51). In addition to transport through the nuclear pore, they have regulatory functions, a central role in the ordered assembly of macromolecular machines such as the ribosome, in organization of chromatin, in assembly and disassembly of microfilaments and microtubules, in binding and transport of small molecules, in the functioning of protein and RNA chaperones, and as flexible "entropic" linkers that separate functional protein domains (52-54). All along, Nature has been using the same properties of "synthetic' polymers that had originally been thought to be uniquely man-made.

From the other side, engineered materials for medical applications have become better and better refined to mimic biological structure and function. For example, one of the advantages of synthetic materials is that they resist enzymatic or chemical degradation in living systems. However, once their function has been completed, lack of polymer degradability can have toxic long-term consequences in vivo (55). For this reason, second-generation, biodegradable HPMA block copolymers have been developed that incorporate enzymatically degradable sequences in their backbone structure. These use a combination of RAFT (reverse addition-fragmentation chain transfer) polymerization and click reactions (alkyne-azide or thiol-ene) to add enzyme-degradable GFLG peptide sequences to the backbone of HPMA copolymer-drug conjugates (56). This approach has successfully been used to produce drug carriers for doxorubicin, paclitaxel, gemcitabine, and epirubicin for the treatment of ovarian cancer (57-60), and as a carrier for prostaglandin E1 for the treatment musculoskeletal disease (61).

The future development of nanomedicines will continue to be a promising approach to the treatment of many diseases as the human ability to manipulate the molecular structure of these constructs expands and refines. Emerging developments in

nanotechnology, imaging, proteomics, and genomics will inform us to new biological approaches, provide new tools to this technology, and produce an endless supply of new strategies to treat disease.

## 5.5 References


1. Fowers KD & Kopeček J (2012) Targeting of multidrug-resistant human ovarian carcinoma cells with anti-P-glycoprotein antibody conjugates. *Macromolecular Bioscience* 12(4):502-514.

2. Li W, *et al.* (2016) Antibody aggregation: Insights from sequence and structure. *Antibodies* 5(3):19.

3. Rouet R, Lowe D, & Christ D (2014) Stability engineering of the human antibody repertoire. *FEBS Letters* 588(2):269-277.

4. Geng SB, Cheung JK, Narasimhan C, Shameem M, & Tessier PM (2014) Improving monoclonal antibody selection and engineering using measurements of colloidal protein interactions. *Journal of Pharmaceutical Sciences* 103(11):3356-3363.

5. Ayyar BV, Arora S, & Ravi SS (2017) Optimizing antibody expression: The nuts and bolts. *Methods (San Diego, Calif.)* 116:51-62.

6. Hull EA, *et al.* (2014) Homogeneous bispecifics by disulfide bridging. *Bioconjugate Chemistry* 25(8):1395-1401.

7. Schumacher FF, *et al.* (2011) In situ maleimide bridging of disulfides and a new approach to protein PEGylation. *Bioconjugate Chemistry* 22(2):132-136.

8. Shaunak S, *et al.* (2006) Site-specific PEGylation of native disulfide bonds in therapeutic proteins. *Nature Chemical Biology* 2(6):312-313.

9. Balan S, *et al.* (2007) Site-specific PEGylation of protein disulfide bonds using a three-carbon bridge. *Bioconjugate Chemistry* 18(1):61-76.

10. Brocchini S, *et al.* (2006) PEGylation of native disulfide bonds in proteins. *Nature Protocols* 1(5):2241-2252.

11. Schumacher FF, *et al.* (2014) Next generation maleimides enable the controlled assembly of antibody-drug conjugates via native disulfide bond bridging. *Organic & Biomolecular Chemistry* 12(37):7261-7269.

12. Khalili H, *et al.* (2016) An anti-TNF-alpha antibody mimetic to treat ocular inflammation. *Scientific Reports* 6:36905.

13. Khalili H, Godwin A, Choi J-w, Lever R, & Brocchini S (2012) Comparative Binding of Disulfide-Bridged PEG-Fabs. *Bioconjugate Chemistry* 23(11):2262-2277.

14. Khalili H, *et al.* (2013) Fab-PEG-Fab as a potential antibody mimetic. *Bioconjugate Chemistry* 24(11):1870-1882.

15. Khalili H, Khaw PT, & Brocchini S (2016) Fc-fusion mimetics. *Biomaterials Science* 4(6):943-947.

16. Niu N, *et al.* (2011) Expression and distribution of immunoglobulin G and its receptors in an immune privileged site: The eye. *Cellular and Molecular Life Sciences* 68(14):2481-2492.

17. van Bilsen K, *et al.* (2011) The neonatal Fc receptor is expressed by human retinal pigment epithelial cells and is downregulated by tumour necrosis factor-alpha. *The British Journal of Ophthalmology* 95(6):864-868.

18. Heiduschka P, *et al.* (2007) Penetration of bevacizumab through the retina after intravitreal injection in the monkey. *Investigative Ophthalmology & Visual Science* 48(6):2814-2823.

19. Kim H, Robinson SB, & Csaky KG (2009) FcRn receptor-mediated pharmacokinetics of therapeutic IgG in the eye. *Molecular Vision* 15:2803-2812.

20. Wu K, Yang J, Liu J, & Kopeček J (2012) Coiled-coil based drug-free macromolecular therapeutics: In vivo efficacy. *Journal of Controlled Release* 157(1):126-131.

21. Zhang L, Fang Y, Yang J, & Kopeček J (2016) Drug-free macromolecular therapeutics: Impact of structure on induction of apoptosis in Raji B cells. *Journal of Controlled Release*.

22. Chu TW, Yang J, Zhang R, Sima M, & Kopeček J (2014) Cell surface self-assembly of hybrid nanoconjugates via oligonucleotide hybridization induces apoptosis. *ACS Nano* 8(1):719-730.

23. Kontermann RE & Brinkmann U (2015) Bispecific antibodies. *Drug Discovery Today* 20(7):838-847.

24. Lamla M, Seliger H, & Kaufmann D (2010) Differences in uptake, localization, and processing of PNAs modified by COX VIII pre-sequence peptide and by triphenylphoshonium cation into mitochondria of tumor cells. *Drug Delivery* 17(4):263-271.

25. Cui H, *et al.* (2017) Mitochondria and nucleus dual delivery system to overcome DOX resistance. *Molecular Pharmaceutics*.

26. Finichiu PG, *et al.* (2015) A mitochondria-targeted derivative of ascorbate: MitoC. *Free Radical Biology & Medicine* 89:668-678.

27. Huang S, *et al.* (2015) New photostable naphthalimide-based fluorescent probe for mitochondrial imaging and tracking. *Biosensors & Bioelectronics* 71:313-321.

28. Paleos CM, Tsiourvas D, & Sideratou Z (2016) Triphenylphosphonium decorated liposomes and dendritic polymers: Prospective second generation drug delivery systems for targeting mitochondria. *Molecular Pharmaceutics*. 13(7):2233-2241.

29. Solomon MA, Shah AA, & D'Souza GG (2013) In vitro assessment of the utility of stearyl triphenyl phosphonium modified liposomes in overcoming the resistance of ovarian carcinoma OVCAR-3 cells to paclitaxel. *Mitochondrion* 13(5):464-472.

30. Paleos CM, Tsiourvas D, Sideratou Z, & Tziveleka LA (2010) Drug delivery using multifunctional dendrimers and hyperbranched polymers. *Expert Opinion on Drug Delivery* 7(12):1387-1398.

31. Theodossiou TA, Sideratou Z, Tsiourvas D, & Paleos CM (2011) A novel mitotropic oligolysine nanocarrier: Targeted delivery of covalently bound D-Luciferin to cell mitochondria. *Mitochondrion* 11(6):982-986.

32. Biswas S, Dodwadkar NS, Piroyan A, & Torchilin VP (2012) Surface conjugation of triphenylphosphonium to target poly(amidoamine) dendrimers to mitochondria. *Biomaterials* 33(18):4773-4782.

33. Bielski ER, Zhong Q, Brown M, & da Rocha SR (2015) Effect of the conjugation density of triphenylphosphonium cation on the mitochondrial targeting of poly(amidoamine) dendrimers. *Molecular Pharmaceutics*. 12(8):3043-3053.

34. Cuchelkar V, Kopečková P, & Kopeček J (2008) Novel HPMA copolymer-bound constructs for combined tumor and mitochondrial targeting. *Molecular Pharmaceutics*.5(5):776-786.

35. Teller JK, Fahien LA, & Valdivia E (1990) Interactions among mitochondrial aspartate aminotransferase, malate dehydrogenase, and the inner mitochondrial membrane from heart, hepatoma, and liver. *The Journal of Biological Chemistry* 265(32):19486-19494.

36. Finichiu PG, *et al.* (2015) A mitochondria-targeted derivative of ascorbate: MitoC. *Free Radical Biology & Medicine* 89:668-678.

37. Guzman-Villanueva D MM, Nguyen HX, Weissig V (2015) Influence of triphenylphosphonium (TPP) cation hydrophobization with phospholipids on cellular toxicity and mitochondrial selectivity. *SOJ Pharmacy &Pharmaceutical Science,* 2(1), 1-9.

38. Modica-Napolitano JS & Weissig V (2015) Treatment strategies that enhance the efficacy and selectivity of mitochondria-targeted anticancer agents. *International Journal of Molecular Sciences* 16(8):17394-17421.

39. Liu J, *et al.* (2010) Endocytic uptake of a large array of HPMA copolymers: Elucidation into the dependence on the physicochemical characteristics. *Journal of Controlled Release* 143(1):71-79.

40. Aasen SN, *et al.* (2015) A novel nanoprobe for multimodal imaging is effectively incorporated into human melanoma metastatic cell lines. *International Journal of Molecular Sciences* 16(9):21658-21680.

41. Vandana M & Sahoo SK (2015) Synergistic activity of combination therapy with PEGylated pemetrexed and gemcitabine for an effective cancer treatment. *Eurorpean Journal of Pharmaceutics and Biopharmaceutics* 94:83-93.

42. Domínguez-Delgado CL, *et al.* (2014) Drug carrier systems using chitosan for non parenteral routes. *Pharmacology and Therapeutics*, ed Gowder SJT (InTech, Rijeka), p Ch. 10.

43. Vandana M & Sahoo SK (2012) Reduced folate carrier independent internalization of pegylated pemetrexed: A potential nanomedicinal approach for breast cancer therapy. *Molecular Pharmaceutics* 9(10):2828-2843.

44. Koschek K, Dathe M, & Rademann J (2013) Effects of charge and charge distribution on the cellular uptake of multivalent arginine-containing peptide-polymer conjugates. *Chembiochem : A European Journal of Chemical Biology* 14(15):1982-1990.

45. Lim RY, *et al.* (2006) Flexible phenylalanine-glycine nucleoporins as entropic barriers to nucleocytoplasmic transport. *Proceedings of the National Academy of Sciences* 103(25):9512-9517.

46. Rout MP, Aitchison JD, Magnasco MO, & Chait BT (2003) Virtual gating and nuclear transport: The hole picture. *Trends in Cell Biology* 13(12):622-628.

47. Schmidt HB & Gorlich D (2016) Transport selectivity of nuclear pores, phase separation, and membraneless organelles. *Trends in Biochemical Sciences* 41(1):46-61.

48. Barz M, Luxenhofer R, Zentel R, & Vicent MJ (2011) Overcoming the PEG-addiction: Well-defined alternatives to PEG, from structure-property relationships to better defined therapeutics. *Polymer Chemistry* 2(9):1900-1918.

49. Dobay MPD, Alberola AP, Mendoza ER, & Rädler JO (2012) Modeling nanoparticle uptake and intracellular distribution using stochastic process algebras. *Journal of Nanoparticle Research* 14(4):821.

50. Zhong J, *et al.* (2016) Direct cytoplasmic delivery and nuclear targeting delivery of HPMA-MT conjugates in a microtubules dependent fashion. *Molecular Pharmaceutics*. 13(9):3069-3079.

51. Liu Z & Huang Y (2014) Advantages of proteins being disordered. *Protein Science : A Publication of the Protein Society* 23(5):539-550.

52. Wright PE & Dyson HJ (2015) Intrinsically disordered proteins in cellular signaling and regulation. *Nature Reviews. Molecular Cell Biology* 16(1):18-29.

53. Dunker AK, Cortese MS, Romero P, Iakoucheva LM, & Uversky VN (2005) Flexible nets. The roles of intrinsic disorder in protein interaction networks. *The FEBS Journal* 272(20):5129-5148.

54. Uversky VN (2016) Dancing protein clouds: The strange biology and chaotic physics of intrinsically disordered proteins. *The Journal of Biological Chemistry* 291(13):6681-6688.

55. Conover C, Lejeune L, Linberg R, Shum K, & Shorr RG (1996) Transitional vacuole formation following a bolus infusion of PEG-hemoglobin in the rat. *Artificial Cells, Blood Substitutes, and Immobilization Biotechnology* 24(6):599-611.

56. Yang J & Kopeček J (2016) Design of smart HPMA copolymer-based nanomedicines. *Journal of Controlled Release* 240:9-23.

57. Pan H, Sima M, Yang J, & Kopecek J (2013) Synthesis of long-circulating, backbone degradable HPMA copolymer-doxorubicin conjugates and evaluation of molecular-weight-dependent antitumor efficacy. *Macromolecular Bioscience* 13(2):155-160.

58. Zhang R, *et al.* (2013) Synthesis and evaluation of a backbone biodegradable multiblock HPMA copolymer nanocarrier for the systemic delivery of paclitaxel. *Journal of Controlled Release* 166(1):66-74.

59. Zhang R, Yang J, Sima M, Zhou Y, & Kopeček J (2014) Sequential combination therapy of ovarian cancer with degradable N-(2-hydroxypropyl)methacrylamide copolymer paclitaxel and gemcitabine conjugates. *Proceedings of the National Academy of Sciences* 111(33):12181-12186.

60. Yang J, Zhang R, Radford DC, & Kopeček J (2015) FRET-trackable biodegradable HPMA copolymer-epirubicin conjugates for ovarian carcinoma therapy. *Journal of Controlled Release* 218:36-44.

61. Pan H, *et al.* (2013) Efficiency of high molecular weight backbone degradable HPMA copolymer–Prostaglandin E1 conjugate in promotion of bone formation in ovariectomized rats. *Biomaterials* 34(27):6528-6538.

62. Frey S, Richter RP, & Görlich D (2006) FG-rich repeats of nuclear pore proteins form a three-dimensional meshwork with hydrogel-like properties. *Science (New York, N.Y.)* 314(5800):815-817.

63. Peters R (2005) Translocation through the nuclear pore complex: Selectivity and speed by reduction-of-dimensionality. *Traffic (Copenhagen, Denmark)* 6(5):421-427.

64. Yamada J, *et al.* (2010) A bimodal distribution of two distinct categories of intrinsically disordered structures with separate functions in FG nucleoporins. *Molecular & Cellular Proteomics : MCP* 9(10):2205-2224.

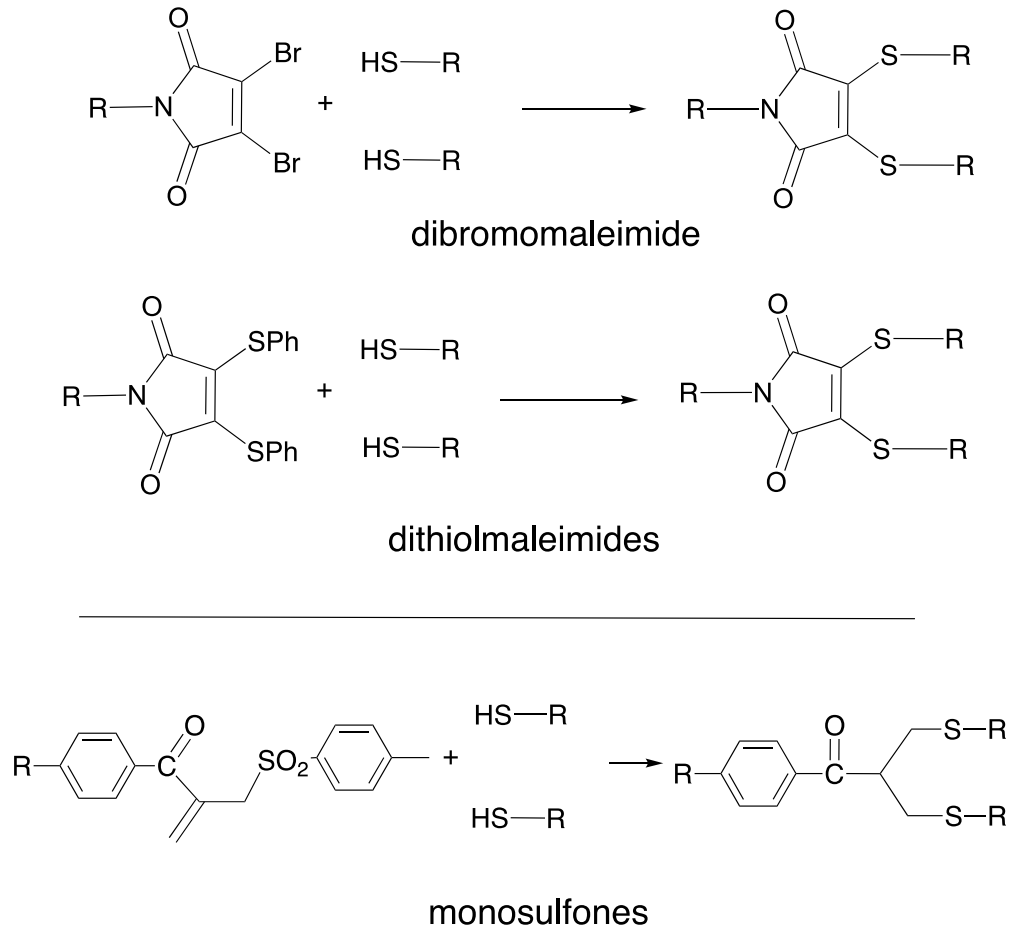


Figure 5.1 Structures and general reaction schemes for thiol-reactive disulfide bridging functional groups

Table 5.1. Selected list of bispecific antibody constructs that are undergoing clinical testing or have been approved for clinical use. (Adapted from Kontermann, RE & Brinkmann U (2015) Bispecific antibodies. *Drug Discovery Today* 20(7):838-847

| Name | Targets | Format | Indication | Status | Developed by |
|---|---|---|---|---|---|
| **Catumaxomab** | EPCAM + CD3 | TrioMab | Malignant ascites | Market | Fresenius Biotech (Trion) |
| "" | "" | "" | Ovary cancer | Phase 2 | |
| "" | "" | "" | Gastric cancer | Phase 2 | |
| "" | "" | "" | Epithelial cancer | Phase 1/2 | |
| **Lymphomun FBTA05** | CD20 + CD3 | TrioMab | BCL | Phase 1/2 | Fresenius Biotech (Trion) |
| **Ertumaxomab** | HER2-CD3 | TrioMab | Metastatic breast cancer | Phase 1 | Fresenius Biotech (Trion) |
| **Blinatumomab** | CD19 + CD3 | BiTE antibody | B cell ALL | Market | Amgen (Micromet) |
| "" | "" | "" | ALL relapsed refractory | Phase 2 | |
| "" | "" | "" | ALL pediatric | Phase 2 | |
| **MT111** | CEA + CD3 | BiTE antibody | Gastric cancer advanced adenocarcinoma | Phase 1b | Amgen (Micromet) |
| **MT112 BAY2010112** | PSMA + CD3 | BiTE antibody | Prostate cancer | Phase 1 | Bayer (Micromet) |
| **MT110 AMG 110** | EPCAM + CD3 | BiTE antibody | Colorectal cancer | Phase 1 | Amgen (Micromet) |
| "" | "" | "" | Lung and gastrointestinal cancer | Phase 1 | |
| **RG7221** | Angiopoietin 2 + VEGF | CrossMab | Colorectal cancer | Phase 2 | Roche |
| **RG6013** | FXI + FX | CLC-IgG | Hemophilia A | Phase 2 | Chugai (Roche group) |
| **RG7597** | HER1 + HER3 | DAF-IgG | Head and neck cancer, colorectal cancer | Phase 2 | Genentech (Roche group) |
| **RG7716** | Angiopoietin 2 + VEGF | CrossMab | Wet AMD | Phase 1 | Roche |
| **MM111** | HER2 + HER3 | scFv2-HSA | Advanced gastric and esophageal cancer | Phase 2 | Merrimack |
| **MM141** | IGF1R + HER3 | IgG-scFv | Advanced solid tumors | Phase 1 | Merrimack |
| **ABT122** | TNFalpha + IL17 | DVD-IgG | RA and inflammation | Phase 1/2 | Abbvie |
| **ABT981** | IL1a + IL1b | DVD-IgG | Osteoarthritis | Phase 1/2 | Abbott |
| **MGD006** | CD123 + CD3 | DART | AML | Phase 1 | Macrogenics and Servier |
| **MGD007** | GPA33 + CD3 | DART-Fc | Colorectal cancer | Phase 1 | MacroGenics and Servier |
| **BI1034020** | beta amyloid two epitopes | Bi-nanobody | Alzheimer's disease | Phase 1 | Ablynx (Boehringer Ingelheim) |
| **ALX0761** | IL17A + IL17F | Bi-nanobody | Inflammatory disease | Phase 1 | Ablynx (Merck Serono) |
| **SAR156597** | IL4 + IL13 | TBTI (DVD)-IgG | IPF | Phase 1 | Serono |
| **TF2** | CEA + hapten | D&L Fab3 | Colorectal cancer | Phase 1 | Immunomedics |
| **IL-17/IL-34 biAb** | IL23 + IL17 | scFv-Fc | Inflammatory and autoimmune disease | Phase 1 | BMS (Zymogenetics) |
| **AFM13** | CD30 + CD16 | TandAb | Hodgkin's disease | Phase 1 | Affimed |
| **AFM11** | CD19 + CD3 | TandAb | NonHodgkin's lymphoma | Phase 1 | Affimed |
| **LY3164530** | Her1 + cMET | orthoFab-IgG | Solid tumors | Phase 1 | Eli Lilly |
| **Removab** | EpCam × CD3 | Triomab quadroma | Malignant ascites | EU approval Apr. 23, 2009 | Trion Pharma, Neovii Biotecha |
| **Blincyto** | CD19 × CD3 | BiTE antibody | Acute lymphoblastic leukemia | FDA approval Dec. 3, 2014 | Amgen (Thousand Oaks, California) |
| **MCLA-128** | HER2 × HER3 | Bispecific antibody | Solid tumors | Phase 1/2 | Merus (Utrecht, the Netherlands) |
| **MEDI-565 (AMG-211)** | C-embryonic antigen × CD3 | BiTE antibody | Gastrointestinal adenocarcinoma | Phase 1 | AstraZeneca (London), Amgen |
| **REGN1979** | CD20 × CD3 | Bispecific antibody | Advanced malignancies | Phase 1 | Regeneron (Tarrytown, New York) |

Table 5.2. Endocytic pathway selective inhibitors and concentrations used

| Inhibitor | Concentration | Endocytic pathway |
|---|---|---|
| Chlorpromazine | 10 µM | Clathrin mediated endocytosis |
| Filipin | 2.5 µg/ml | Caveolae mediated endocytosis |
| Mevinolin | 10 µM | |
| Dynasore | 80 µM | Dynamin dependent endocytosis |
| Amiloride | 10 µM | Macropinocytosis |
| Wortmannin | 1 µM | |
| LY 294002 | 10 µM | |

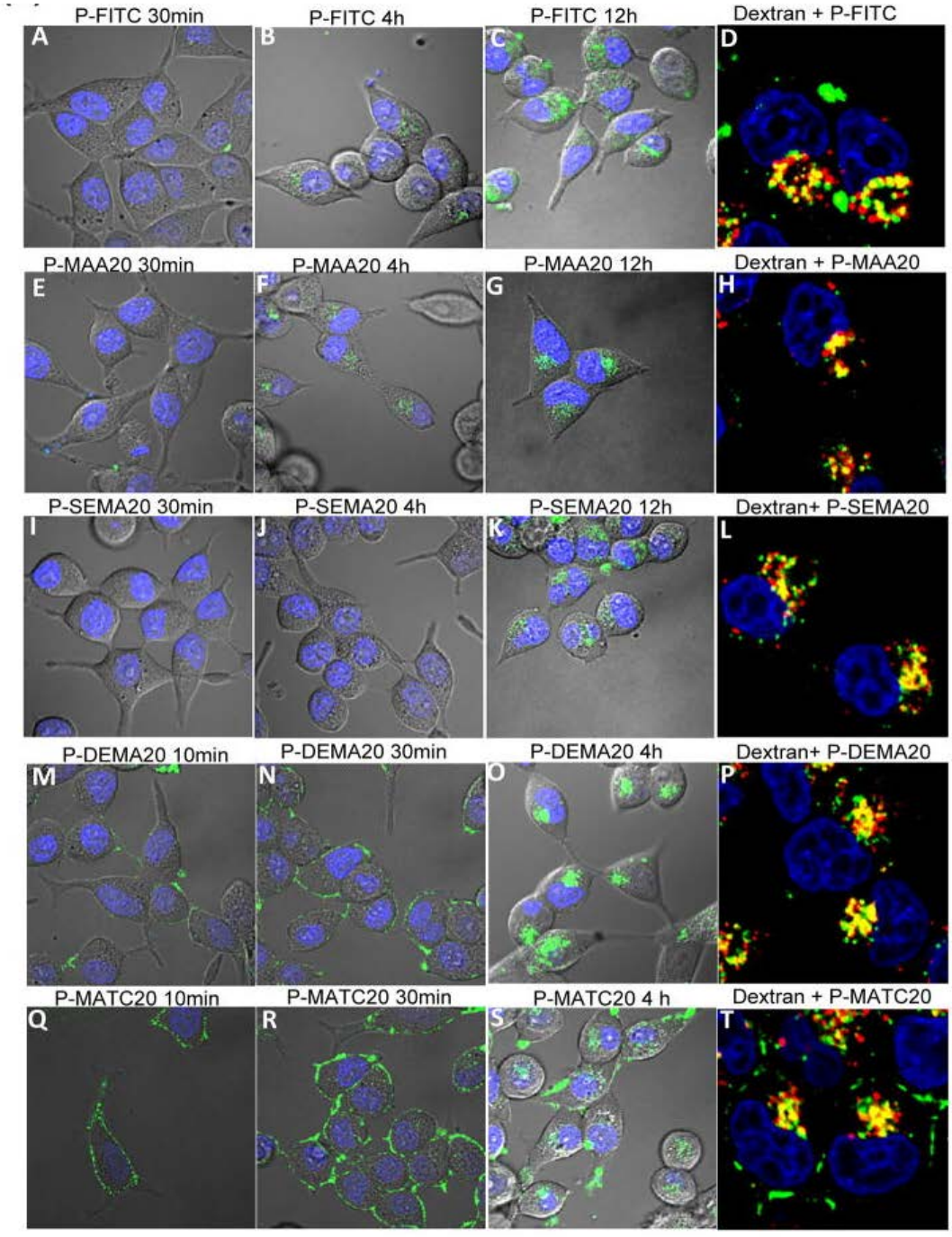


Figure 5.2. Endocytosis and quantification of uptake of HPMA copolymers. C4-2 cells were incubated with fraction 6 (F6) of indicated copolymers.

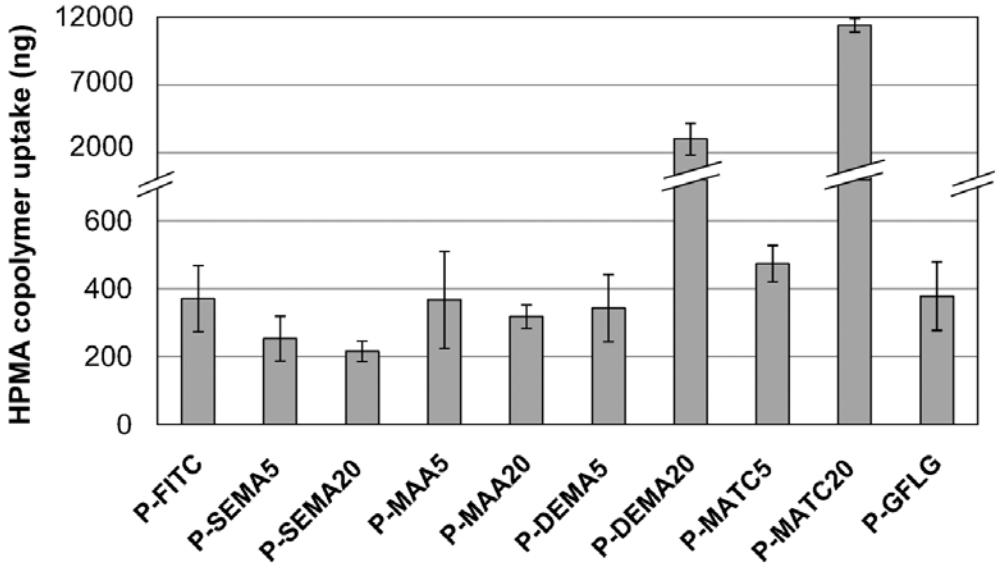


Figure 5.3. Quantification of uptake of copolymers by flow cytometry. Cells were incubated with F6 of copolymers for 12 h. The data shown are averages (±SD) of four separate experiments.

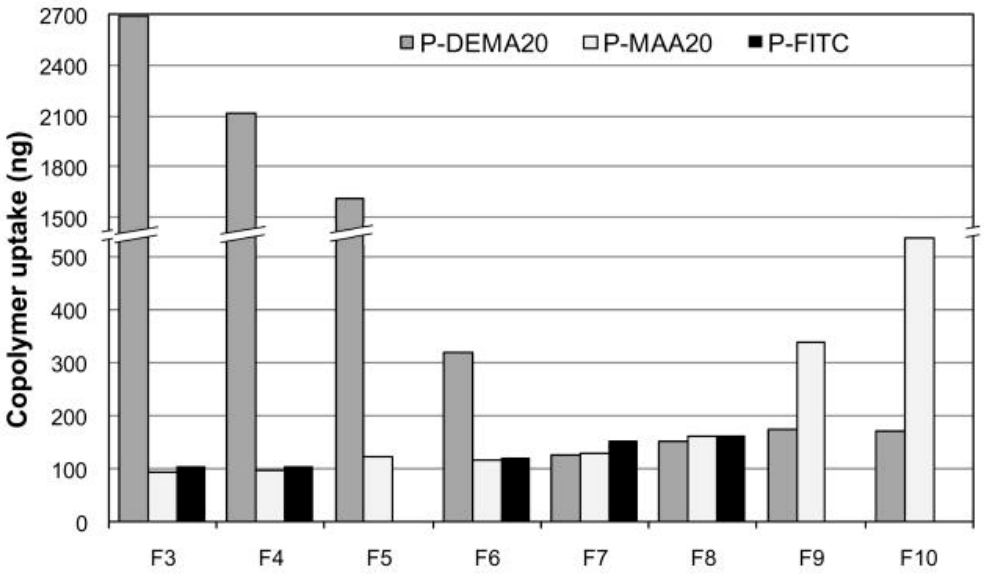


Figure 5.4. Molecular weight dependence of uptake of HPMA copolymers. Cells were incubated with medium containing 0.1 mg/ml of different fractions of P-FITC, 20%DEMA-P or 20%MAA-P for 12 h. After incubation, cells were harvested for flow cytometry analysis. The data shown are averages (±SD) of three separate experiments.

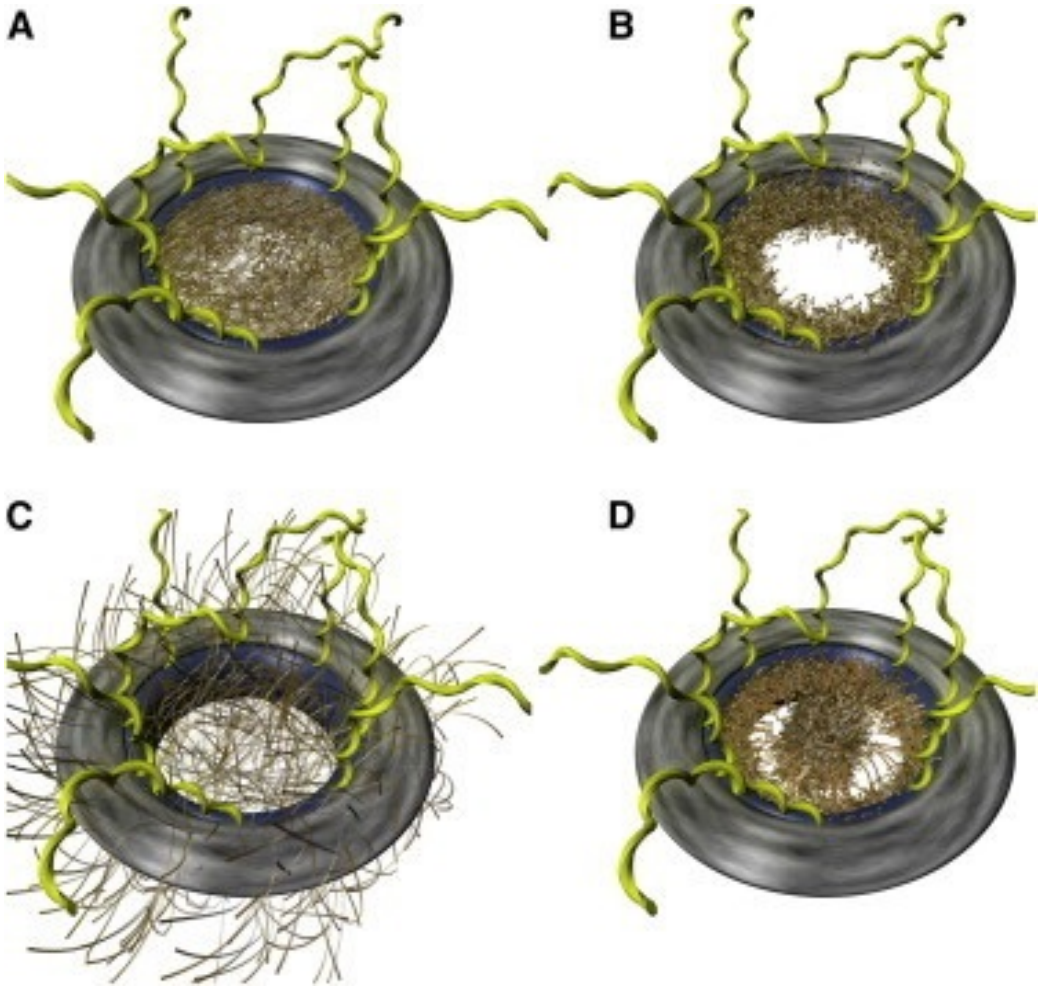


Figure 5.5. Illustration of NPC models (. Each NPC depicted spans the double lipid bilayer nuclear envelope, oriented such that the tops of the pores face the cytoplasm, while the bottoms of the pores face the nucleus. (*A*) FG nups form a hydrogel, which transport-factors and their cargo complexes transit by binding with FG motifs and temporarily disrupting cross-links in the FG nup meshwork.(62) (*B*) FG nups are collapsed and lie along the wall of the NPC, creating a surface to which transport-factors bind and diffuse along in a dimensionally reduced manner.(63) (*C*) FG nups form a polymer brush that binds transport factors (possibly collapsing in their presence) but excludes unwanted molecules that do not interact with the FG nups.(46) ((*D*) The di-block copolymer brush gate (DCBG) model individual FG nups can have collapsed coil gel-like regions and extended coil brushlike domains, resulting in a microphase separation of these domains within the NPC."(64) (Figure reproduced with permission from Ando D et al. (2014) Nuclear pore complex protein sequences determine overall copolymer brush structure and function. *Biophysical Journal* 106(9):1997-2007. Copyright © 2014 Biophysical Society. Elsevier Inc)